IRE Transactions

on ANTENNAS and PROPAGATION

Volume AP-6 **JULY, 1958** **Number 3**

Published Quarterly

TABLE OF CONTENTS

CONTRIBUTIONS

COMMUNICATIONS

PUBLISHED BY THE

ofessional Group on Antennas and Propagation

IRE TRANSACTIONS® PGAP IS A QUARTERLY PUBLICATION DEVOTED TO EXPERIMENTAL AND THEORETICAL PAPERS ON ANTENNAS AND WIRELESS PROPAGATION OF ELECTROMAGNETIC WAVES

MANUSCRIPTS should be submitted to John B. Smyth, Editor, Smyth Research Associates, 3555 Aero Court, San Diego 11, Calif. Manuscripts should be original typewritten copy, double spaced, plus one carbon copy. References should appear as footnotes and include author's name, title, journal, volume, initial and final page numbers, and date. Each paper must have a summary of not more than 200 words. News items concerning PGAP members and group activities should be sent to the News Editor, Mr. Arthur Dorne, Dorne and Margolin, Inc., 30 Sylvester Street, Westbury, L.I., N.Y.

ILLUSTRATIONS should be submitted as follows: All line drawings (graphs, charts, block diagrams, cutaways, etc.) should be inked uniformly and ready for reproduction. If commercially printed grids are used in graph drawings, author should be sure printer's ink is of a color that will reproduce. All halftone illustrations (photographs, wash, airbrush, or pencil renderings, etc.) should be clean and ready to reproduce. Photographs should be glossy prints. Call-outs or labels should be marked on a registered tissue overlay, not on the illustration itself. No illustration should be larger than 8 x 10 inches.

Copies can be purchased from
THE INSTITUTE OF RADIO ENGINEERS
1 East 79 St., New York 21, N.Y.

PRICE PER COPY: members of the Professional Group on Antennas and Propagation, $2.40; members of the IRE, $3.60; nonmembers, $7.20.

ANNUAL SUBSCRIPTION PRICE: PGAP members, included in PGAP fee of $4.00; IRE members, $8.50; Colleges and public libraries, $10.00; nonmembers, $17.00.

IRE TRANSACTIONS ON ANTENNAS AND PROPAGATION

Printed in U.S.A.

Entered as second-class matter, at the post office at Menasha, Wisconsin, under the act of August 24, 1912. Acceptance for mailing at a special rate of postage is provided for in the act of February 28, 1925, embodied in Paragraph 4, Section 412, P. L. & R., authorized October 26, 1927.

contributions

Maximum Gain of a Line Source Antenna if the Distribution Function is a Finite Fourier Series*

L. SOLYMAR†

Summary—If the highest permitted harmonics of the distribution function (this is the quantity of interest in practical application) and the supergain ratio are given, what is the maximum attainable gain? In this paper this optimum problem is solved through the introduction of n dimensional vectors and tensors and the result is obtained in closed form. For the case of two harmonics, numerical results are given. It is concluded that a small improvement in the specific gain is accompanied by a large change in the supergain ratio. The examination of the maximum of the specific gain, without auxiliary condition, leads to the conclusion that the addition of every harmonic increases the value of specific gain, but that the improvement is negligibly small until the number of harmonics becomes greater than the size of the aperture in wavelength. Using the method developed in this paper it is possible for any finite number of harmonics to calculate the optimum distribution function, but the computations become very lengthy as the number of harmonics increases.

List of Symbols

d = the size of the aperture in wavelengths.
$u = d \cos \theta$.
θ = the angle between the axis of the line source and the Fraunhofer zone point to be investigated.
$F(u)$ = the radiation pattern.
$g(p)$ = the distribution function.
$p = 2\pi x/d\lambda$.
x = the co-ordinate in the direction of the line source.
λ = the wavelength.
G_0 = the gain of a line source consisting of isotropic elements.
G_s = the specific gain.
γ = the supergain ratio.
n = the number of higher harmonics.
a_k = the coefficients of the Fourier series.
$\boldsymbol{a}$, $\boldsymbol{h}(u)$ = $n+1$ dimensional vectors.
$\boldsymbol{H}$, $\boldsymbol{A}$, $\boldsymbol{I}$ = $n+1$ dimensional tensors.
λ_1, λ_2 = Lagrange multipliers.
b_1, b_2, b, ϕ, A_1, A_2, A_3, B_1, B_2 = suitable chosen varibles.

Introduction

A LARGE number of different authors have dealt with the problem of line source antennae. There also exist optimum solutions for certain problems in connection with discrete radiators. The method is as follows.

* Manuscript received by the PGAP, December 10, 1957. This work was presented before the "Congrès International des Circuits et Antennes Hyperfrequences," October 1957, Paris, France.
† Standard Telecommun. Labs., Ltd., Enfield, Mddx., Eng.

A current distribution is sought which for a given number of point sources will produce 1) minimum main lobe width[1] for a given side lobe attenuation or 2) maximum gain[2] for a given tolerance sensitivity.

In the case of continuous line sources no optimum solution has yet been found. It has been proved that an arbitrary radiation pattern is realizable, *i.e.*, any gain and any side lobe attenuation.[3–5] However, if we allow certain restrictions in regard to the distribution function, then an optimum solution may be found. In the practical instance it is impracticable to realize more than a certain number of higher harmonics in the distribution function. We therefore put the distribution function in the form of finite Fourier series and look for the coefficients which, in the case of a given supergain ratio, will result in the highest gain.

At the present time there exists a gap between the case of the uniform distribution and that of the supergain distributions.

By the method outlined above it is possible to bridge this gap and to show that a small variation of the uniform distribution may result in a higher gain.

The Specific Gain and the Supergain Ratio

We have to start by investigating the gain of a line source. Taylor[6] has shown that, if the radiation of a line source is strongly directive, the gain may be expressed as the product of two factors. The first factor depends on the properties of the source element, the second factor is the gain which the entire antenna would have if the element factor were isotropic. If the beam is presumed to be broadside, the second factor is as follows.

$$G_0 = \frac{2d\,|\,F(o)\,|^2}{\int_{-d}^{d} |\,F(u)\,|^2 du} \tag{1}$$

where

d = the size of the aperture in wavelengths.
$u = d \cos\theta$
θ = the angle between the axis of the line source and the Fraunhofer zone point to be investigated (Fig. 1).
$F(u)$ = the radiation pattern.

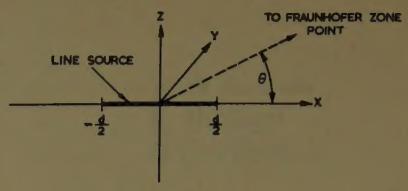

Fig. 1

Between the radiation pattern and the distribution function there is a Fourier-transform connection which may be expressed as follows.[6]

$$F(u) = \int_{-\pi}^{\pi} g(p) e^{iup} dp \tag{2}$$

where

$p = 2\pi x/d\lambda$.
x = the coordinate in the direction of the line source. (Fig. 1).
λ = the wavelength.

Our purpose is to compare different line sources on the basis of gain. For this purpose it is more convenient to investigate the specific gain (often called efficiency), $G_0/2d$, denoted by G_s.

If the size of the aperture is infinite it is easy to prove that $(G_0/2d)_\infty$ takes on its greatest possible value, namely unity, when $g(p)$ is uniform. Therefore, for any variation of the distribution $g(p)$, $(G_0/2d)_\infty$ must decrease. On this basis Taylor introduced the attribute of supergain ratio.[7]

$$\gamma = \frac{G_0/2d}{(G_0/2d)_\infty} = \frac{\int_{-\infty}^{\infty} |\,F(u)\,|^2 du}{\int_{-d}^{d} |\,F(u)\,|^2 du}. \tag{3}$$

Solution of the Optimum Problem

We now have the following problem. If we restrict the number of harmonics creating the $g(p)$ distribution function and prescribe the supergain ratio γ, what is the greatest possible value of the specific gain G_s?

In mathematical form, if[8]

$$g(p) = \sum_{k=0}^{n} a_k \cos kp, \tag{4}$$

how is it possible to choose the coefficients a_k so that

$$\gamma = \text{prescribed and } G_s = \text{Max?} \tag{5}$$

For solving this problem, we have to express our quantities by the help of the a_k.

[1] C. L. Dolph, "A current distribution for broadside arrays which optimizes the relationship between beamwidth and side-lobe level," Proc. IRE, vol. 34, p. 335–348; June, 1946.
[2] M. Uzsoky and L. Solymar, "Theory of super-directive linear arrays," *Atca Phys. Acad. Sci. Hung.*, vol. 6, pp. 185–206; 1956.
[3] H. J. Riblet, "Note on the maximum directivity of an antenna," Proc. IRE,v ol. 36, pp. 620–623; May, 1948.
[4] P. M. Woodward and J. D. Lawson, "The theoretical precision with which an arbitrary radiation pattern may be obtained from a source of finite size," *J. IEE*, vol. 95, pp. 363–369; September, 1948.
[5] R. Kovacs and L. Solymar, "Theory of aperture aerials based on the properties of entire functions of the exponential type," *Acta Phys. Acad. Sci. Hung.*, vol. 6, pp. 161–184; 1956.
[6] T. T. Taylor, "Design of line source antennas for narrow beamwidth and low side-lobes," IRE Trans. on Antennas and Propagation, vol. AP-3, pp. 16–28; January, 1955.
[7] We have to state that by some authors (for example, P. Aigrain in "Les antennes superdirectives," *L'onde Elec.*, vol. 32, pp. 51–54; February, 1952) the same quantity is proportional to Q, since it is connected with the stored energy.
[8] It is easy to show that we have the maximum gain if $g(p)$ is real and even.

The radiation pattern is

$$F(u) = \sum_{k=0}^{n} a_k \int_{-\pi}^{\pi} \cos kp e^{iup} dp$$

$$= 2 \sum_{k=0}^{n} a_k (-1)^k \frac{u \sin u\pi}{u^2 - k^2} . \quad (6)$$

For simplicity let us introduce the following $n+1$ dimensional vectors[9]

$$\boldsymbol{a} = (a_0, a_1 \cdots a_n)$$

$$\boldsymbol{h}(u) = \left\{ \frac{\sin u\pi}{u\pi}, -\frac{u \sin u\pi}{(u^2 - 1)\pi} \cdots (-1)^n \frac{u \sin u\pi}{(u^2 - n^2)\pi} \right\} . \quad (7)$$

Now we are in a position to express all our quantities with these vectors and two tensors derived from them. So we can write in this simplified form

$$F(u) = 2\pi \boldsymbol{a}\boldsymbol{h}(u) \quad (8)$$

and

$$G_s = \frac{\boldsymbol{aHa}}{\boldsymbol{aAa}} \quad \text{and} \quad \gamma = \frac{\boldsymbol{aa}}{\boldsymbol{aAa}}$$

where

$$\boldsymbol{H} = \boldsymbol{h}(0) \circ \boldsymbol{h}(0) \quad (9)$$

is the dyadic product of $\boldsymbol{h}(0)$ with itself,[10] and

$$\boldsymbol{A} = \int_{-d}^{d} \boldsymbol{h}(u) \circ \boldsymbol{h}(u) du. \quad (10)$$

$\boldsymbol{aAa}$ being proportional to the output, our problem is tantamount to finding the maximum of $\boldsymbol{aHa}$ in respect of $\boldsymbol{a}$, with prescribed $\boldsymbol{aa}$ and $\boldsymbol{aAa}$. The mathematical solution of this problem was obtained by Uzsoky and Solymar[2] in connection with linear arrays. Therefore we shall give only a brief summary below.

The finding of extrema can be reduced to the extremum problem.

$$\boldsymbol{aHa} + \lambda_1 \boldsymbol{aAa} + \lambda_2 \boldsymbol{aa} = \text{extr.} \quad (11)$$

where λ_1 and λ_2 are Lagrange multipliers. The variation of the function with respect to $\boldsymbol{a}$ is equated to zero, *i.e.*

$$\delta[\boldsymbol{aHa} + \lambda_1 \boldsymbol{aAa} + \lambda_2 \boldsymbol{aa}] = 0$$

$$[\boldsymbol{aH} + \lambda_1 \boldsymbol{aA} + \lambda_2 \boldsymbol{a}]\delta\boldsymbol{a} + \delta\boldsymbol{a}[\boldsymbol{Ha} + \lambda_1 \boldsymbol{Aa} + \lambda_2 \boldsymbol{a}]$$

$$= 2\delta\boldsymbol{a}[\boldsymbol{Ha} + \lambda_1 \boldsymbol{Aa} + \lambda_2 \boldsymbol{a}] = 0. \quad (12)$$

This expression must vanish for any variation of $\delta\boldsymbol{a}$, which is only possible if

$$\boldsymbol{Ha} + \lambda_1 \boldsymbol{Aa} + \lambda_2 \boldsymbol{a} = 0. \quad (13)$$

Rewriting $\boldsymbol{H} = \boldsymbol{h}(0) \circ \boldsymbol{h}(0)$, introducing the abbreviations

[9] We denote an n-dimensional vector with lower case bold face, and an n-dimensional tensor with capital bold face letters.

[10] The elements of the tensor $\boldsymbol{C} = \boldsymbol{a} \circ \boldsymbol{b}$ are defined by $C_{ik} = a_i b_k$.

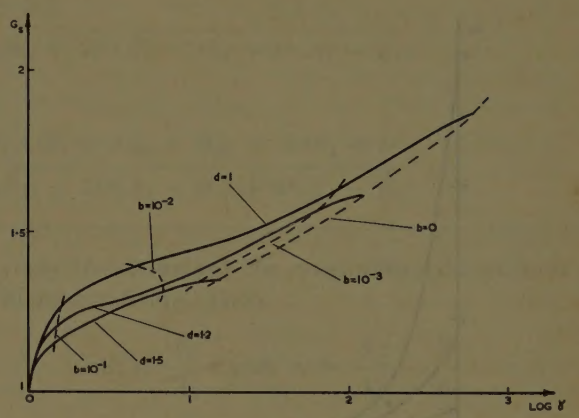

Fig. 2—Specific gain as a function of log γ, for $n=2$. ——— d=constant. – – – b=constant.

$$b_1 = -\frac{\lambda_1}{\boldsymbol{ah}(0)}, \qquad b_2 = -\frac{\lambda_2}{\boldsymbol{ah}(0)}, \quad (14)$$

and performing the necessary operations, we get

$$\boldsymbol{a} = (b_2 \boldsymbol{I} + b_1 \boldsymbol{A})^{-1} \boldsymbol{h}(0) \quad (15)$$

where $\boldsymbol{I}$ is the unit tensor.

So we get the optimum distribution. If we want to know further the value of the specific gain and that of the supergain ratio, we have to substitute $\boldsymbol{a}$ from (15) in (8).

Performing the operations and describing the results in a form which is more convenient for computation, we get

$$G_s^{-1} = \left\{ \frac{\partial \phi}{\partial b_1} \right\}_{b_2}$$

and

$$\gamma = \frac{\left\{ \frac{\partial \phi}{\partial b_2} \right\}_{b_1}}{\left\{ \frac{\partial \phi}{\partial b_1} \right\}_{b_2}} \quad (16)$$

where

$$1/\phi = \boldsymbol{h}(0)(b_2 \boldsymbol{I} + b\boldsymbol{A})^{-1} \boldsymbol{h}(0). \quad (17)$$

In the special case where $\lambda_2 = b_2 = 0$ we get the maximum gain without any auxiliary condition. Then

$$G = \boldsymbol{h}(0)\boldsymbol{A}^{-1}\boldsymbol{h}(0), \qquad \gamma = \frac{\boldsymbol{h}(0)\boldsymbol{A}^{-2}\boldsymbol{h}(0)}{\boldsymbol{h}(0)\boldsymbol{A}^{-1}\boldsymbol{h}(0)} . \quad (18)$$

For illustration we shall show several numerical results.

If $n=2$, *i.e.* two harmonics are taken into account, we draw on the (log γ, G_s) plane the $b_2/b_1 = b$ = const. and the d = const. curves.[11] (See Fig. 2.) We may see that a small improvement in G_s is accompanied by a large variation in γ. If one chooses the value of γ, and G_s, one may find the respective value of b_2/b_1 and d, by which

[11] The more detailed computations are seen in the Appendix.

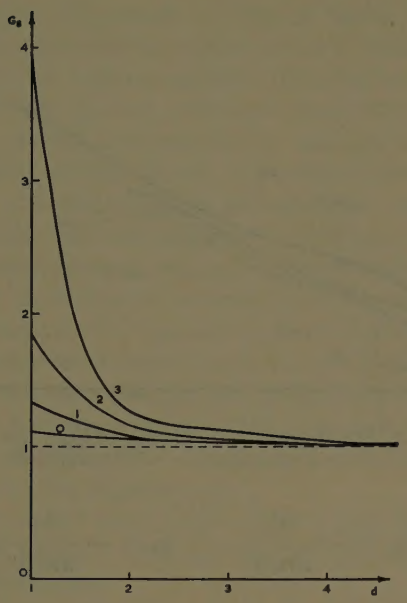

Fig. 3—The maximum of specific gain as the function of the aperture size in wavelengths for 0, 1, 2, and 3 harmonics.

the required distribution is known. By equations (16) we can construct these curves, also for higher n, but the numerical work grows very rapidly.

Now let us investigate the special case when we seek only the maximum gain. We show G_s (Fig. 3) as a function of d. It will be observed that when d attains the value n, the achievable improvement is small, and, as d increases, the value of G_s approximates that of the uniform distribution ($n=0$).

Finally there are shown in Table I for $n=2$ the coefficients of the harmonics (by normalization to $a_0=1$). Obviously as d increases, the coefficients of the first and second harmonics decrease.

TABLE I

d	a_0	a_1	a_2
1	1	0.775	17.324
2	1	−0.288	0.654
3	1	−0.084	0.096
4	1	−0.053	0.037

Conclusions

Based on the familiar formulas of the specific gain and supergain ratio the following optimum problem has been solved. If the number of the higher harmonics and the size of aperture in wavelength is given and the supergain ratio is prescribed, what is the maximum possible value of the specific gain? It is concluded that an essential improvement is attainable above the gain of the uniform distribution, but the practicability of this with increasing aperture sizes decreases. Without any general proof we state that, until the number of harmonics exceeds the size of the aperture in wavelengths the improvement is negligibly small, and, if d increases, to obtain the same specific gain n/d has to increase also.

Appendix

Here the computation of G_s and γ in the case of $n=2$ is shown. We have to compute at first ϕ, which by (17) is equal

$$\phi = [h(0)(b_2 I + b_1 A)^{-1} h(0)]^{-1}.$$

For this we need the expression of the tensor A and that of the vector $h(0)$. The elements of the A tensor by (10) are as follows:

$$A_{ik} = \int_{-d}^{d} h_i(u) h_k(u)\, du$$

$$= (-1)^{i+k} \int_{-d}^{d} \frac{u^2 \sin^2 u\pi}{(u^2 - k^2)(u^2 - i^2)}\, du$$

whence

$$A_{ik} = \frac{(-1)^{i+k}}{2(k^2 - i^2)\pi^2}\{ i\{ \mathrm{Cin}\,[2\pi(d+i)] - \mathrm{Cin}\,[2\pi(d-i)]\} - k\{ \mathrm{Cin}\,[2\pi(d+k)] - \mathrm{Cin}\,[2\pi(d-k)]\}\}$$

if $i \neq k$

$$A_{ii} = -\frac{1}{4i\pi^2}\{ \mathrm{Cin}\,[2\pi(d+i)] - \mathrm{Cin}\,[2\pi(d-i)]\} + \frac{1}{2\pi}\left\{ \mathrm{Si}\,[2\pi(d+i)] + \mathrm{Si}\,[2\pi(d-i)] - \frac{\sin^2 \pi d}{\pi} \frac{2d}{d^2 - 1}\right\} \text{ if } i \neq 0$$

$$A_{00} = \frac{2}{\pi}\left\{ \mathrm{Si}\, 2\pi d - \frac{\sin^2 \pi d}{\pi d}\right\},$$

where, by definition,

$$\mathrm{Cin}\, x = \int_0^x \frac{1 - \cos t}{t}\, dt, \qquad \mathrm{Si}\, x = \int_0^x \frac{\sin t}{t}\, dt.$$

The expression for the vector $h(0)$, will be very simple because, according to (7), all the elements are zero but the first. So the scalar product

$$h(0)(b_2 I + b_1 A)^{-1} h(0)$$

for $n=2$ will be

$$\begin{Bmatrix} 1 \\ 0 \\ 0 \end{Bmatrix} \begin{Bmatrix} b_2 + b_1 A_{00} & b_1 A_{01} & b_1 A_{02} \\ b_1 A_{10} & b_2 + b_1 A_{11} & b_1 A_{12} \\ b_1 A_{20} & b_1 A_{21} & b_2 + b_1 A_{22} \end{Bmatrix}^{-1} \begin{Bmatrix} 1 \\ 0 \\ 0 \end{Bmatrix} = \frac{|\, b_2 I + b_1 A\,|_{0,0}}{|\, b_2 I + b_1 A\,|} = \phi^{-1}$$

where $|\, b_2 I + b_1 A\,|$ is the determinant of the $b_2 I + b_1 A$ tensor, $|\, b_2 I + b_1 A\,|_{0,0}$ is the minor belonging to the element $b_2 I_{00} + b_1 A_{00}$. Getting the value of ϕ we can easily express G_s and γ by performing the differentiations according to (16). Then

$$G_s = \frac{[B_2 + bB_1 + b^2]^2}{A_3B_2 + 2bA_3B_1 + b^2(3A_3 - A_1B_2 + A_2B_1) + 2b^3(A_2 - B_2) + b^4(A_1 - B_1)}$$

and

$$\gamma = \frac{(A_2B_2 - A_3B_1) + 2b(A_1B_2 - A_3) + b^2(A_1B_1 + 3B_2 - A_2) + 2b^3B_1 + b^4}{A_3B_2 + 2bA_3B_1 + b^2(3A_3 - A_1B_2 + A_2B_1) + 2b^3(A_2 - B_2) + b^4(A_1 - B_1)}$$

where

$$A_3 = |\boldsymbol{A}|$$

$$A_2 = |\boldsymbol{A}|_{0,0} + |\boldsymbol{A}|_{1,1} + |\boldsymbol{A}|_{2,2}$$

$$A_1 = A_{11} + A_{22} + A_{33}$$

$$B_1 = A_{11} + A_{22}$$

$$B_2 = |\boldsymbol{A}|_{0,0}$$

$$b = \frac{b_2}{b_1}.$$

If $\lambda_2 = b_2 = b = 0$, we get the maximum gain without any auxiliary condition. Then

$$G_s = \frac{B_2}{A_3} \quad \text{and} \quad \gamma = \frac{A_2}{A_3} - \frac{B_1}{B_2}.$$

ACKNOWLEDGMENT

The author wishes to express his thanks to L. Lewin and Dr. A. E. Karbowiak of Standard Telecommunication Laboratories, Ltd., for a number of interesting discussions. Acknowledgment also is made to Standard Telecommunication Laboratories, Ltd., for facilities granted in the preparation of the manuscript and for permission to publish the paper.

On the Gain and Beamwidth of Directional Antennas*

ROGER F. HARRINGTON†

Summary—**A formula is given for the maximum gain of a class of antennas having fields expressible as a finite number of spherical wave functions. This maximum gain can be achieved for arbitrarily polarized radiation fields, and it can be related to antenna size by requiring the near fields to be small in magnitude. Also, the radiation field is in the form of a polynomial, so that patterns optimum in the Tchebycheff sense can be defined. Formulas for the relationship of beamwidth to sidelobe level are given.**

INTRODUCTION

IT has long been realized that a relationship exists between the size of a practical antenna system and the gain that can be achieved. On the other hand, there is no mathematical limit to the gain that can be obtained from currents confined to an arbitrarily small volume. However, if one looks at the field in the vicinity of a high-gain, small-size radiator, one finds extremely large field intensities. In a physical antenna, this would result in prohibitive heat loss. In an ideal lossless antenna, this would result in large energy densities, and thus in a "high Q" antenna. There is even some doubt that the required current distribution could be obtained in practice, since it is determined by the solution to a boundary value problem.

The problem is formulated in a manner similar to that used by Chu.[1] The field external to a sphere containing all sources can be expanded in terms of spherical wave functions

$$\psi_n = h_n^{(2)}(\beta r) f_n(\theta, \phi),$$

where n is an integer and $h_n^{(2)}$ is the spherical Hankel function. If ψ_n's up to $n = N$ are permitted, then the maximum gain obtained is

$$G = N^2 + 2N.$$

To relate this to antenna size, consider the magnitudes of the spherical Hankel functions. These are roughly sketched in Fig. 2. Note that for $\beta r > n$, the magnitude decreases very slowly, but for $\beta r < n$, it rises abruptly. Since the field components increase at least as rapidly as $|h_n|$, $\beta r = n$ is taken to be the point of "gradual cut-off." Assume that the antenna just fits into a sphere of

* Manuscript received by the PGAP, November 22, 1957; revised manuscript received March 13, 1958. This work was supported in part by Rome Air Dev. Ctr., Rome, N. Y.

† Dept. of Elec. Eng., Syracuse University, Syracuse, N. Y.

[1] L. J. Chu, "Physical limitations of omnidirectional antennas," *J. Appl. Phys.*, vol. 19, pp. 1163–1175; December, 1948.

radius R. At the surface of this sphere, all wave functions $n<\beta R$ remain small in magnitude, but those for $n>\beta R$ are large. Therefore it is postulated that wave functions $n>\beta R$ cannot be effectively used, and the "normal gain" of the antenna is

$$G = (\beta R)^2 + 2\beta R.$$

It is interesting to note that for large βR, the gain is $(\beta R)^2$, identical to the gain of a uniformly illuminated circular aperture of radius R.[2] The same conclusions can also be formulated in terms of the Q as defined by Chu.[1]

In addition to the gain relationship, one can also establish relationships between beamwidth and sidelobe level. Given a field constructed of spherical wave functions $n\leq N$, the field contains a polynomial of degree N in $\cos\eta$. A pattern optimum in the Tchebycheff sense is obtained by choosing this polynomial to be $T_N(a+b\cos\eta)$. This pattern has minimum beamwidth for a given sidelobe level, or vice versa. For large N, the beamwidths between half-power points on these optimum patterns are given by

$$BW = \frac{180\sqrt{2}}{\pi N}\sqrt{(\ln 2M)^2 - (\ln\sqrt{2}M)^2} \text{ degrees},$$

where M is the ratio of mainlobe field intensity to sidelobe field intensity. To interpret this in terms of antenna size, one sets $N=\beta R$ using the same reasoning as in the gain problem. The result is then called a "normal beamwidth," for it is not an absolute limit. Thus, the normal beamwidth of an antenna of maximum diameter $2R$ is

$$BW = \frac{180\sqrt{2}}{\pi\beta R}\sqrt{(\ln 2M)^2 - (\ln\sqrt{2}M)^2} \text{ degrees},$$

which is valid for large βR.

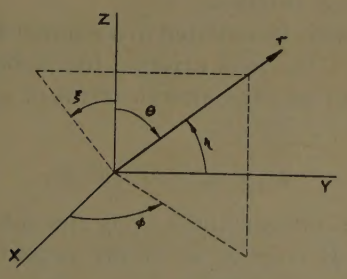

Fig. 1—Coordinate variables.

Derivation of Gain Formulas

Consider the coordinate variables as defined in Fig. 1. In a given direction θ, ϕ, the gain $G(\theta, \phi)$ of an antenna is defined as the ratio of the power radiated by an omnidirectional antenna to that radiated by the given antenna, assuming equal power densities in the given direction. This is summarized by

$$G(\theta,\phi) = \frac{4\pi r^2\sqrt{\epsilon/\mu}\,|\,E(\theta,\phi)\,|^2}{P}, \tag{1}$$

where E is the radiation field intensity and P the total power radiated. Throughout this paper, it is postulated that the coordinate axes are so oriented that the maximum field intensity is in the direction $\theta=\pi/2$, $\phi=0$. Henceforth when the term gain is used, it will mean $G(\pi/2, 0)$, and will be denoted simply by G.

Sets of formulas and their derivations for an arbitrary radiation field are found in the Appendix. Consider first the case of a ϕ-polarized field at $\theta=\pi/2$, $\phi=0$. This is obtained from (61) with $\alpha_{mn}=0$, $\hat{\alpha}_{mn}=\pi/2$, resulting in

$$E_\phi\left(\frac{\pi}{2}, 0\right) = \frac{e^{-j\beta r}}{\beta r}\sum_{m,n} j^{n-1}\left[A_{mn}P_n^{m\prime}(0) + \sqrt{\frac{\mu}{\epsilon}}\,mB_{mn}P_n^m(0)\right]. \tag{2}$$

The corresponding radiated power, (63), is

$$P = \frac{4\pi}{\beta^2}\sum_{m,n}\frac{1}{\epsilon_m}\left[\sqrt{\frac{\epsilon}{\mu}}\,|\,A_{mn}\,|^2 + \sqrt{\frac{\mu}{\epsilon}}\,|\,B_{mn}\,|^2\right]\cdot\frac{n(n+1)(n+m)!}{(2n+1)(n-m)!}. \tag{3}$$

The gain from (1) is therefore

$$G = \frac{\left|\sum j^n\left[A_{mn}P_n^{m\prime}(0) + \sqrt{\frac{\mu}{\epsilon}}\,mB_{mn}P_n^m(0)\right]\right|^2}{\sum\left[|\,A_{mn}\,|^2 + \frac{\mu}{\epsilon}\,|\,B_{mn}\,|^2\right]\frac{n(n+1)(n+m)!}{\epsilon_m(2n+1)(n-m)!}}. \tag{4}$$

It is found that[3]

$$P_n^m(0) = \begin{cases} j^{n-m}\dfrac{1\cdot3\cdot5\cdots(n+m-1)}{2\cdot4\cdot6\cdots(n-m)}, & n+m \text{ even}, \\ 0, & n+m \text{ odd} \end{cases}$$

$$P_n^{m\prime}(0) = \begin{cases} j^{n-m-1}\dfrac{1\cdot3\cdot5\cdots(n+m)}{2\cdot4\cdot6\cdots(n-m-1)}, & n+m \text{ odd}, \\ 0, & n+m \text{ even} \end{cases} \tag{5}$$

so that the numerator of (4) is unchanged by setting

$$A_{mn} = 0,\ n+m \text{ even} \qquad B_{mn} = 0,\ n+m \text{ odd}, \tag{6}$$

while the denominator is decreased. Furthermore, since the denominator depends only on the magnitude of A_{mn} and B_{mn}, one can adjust their phase to maximize the numerator. This is accomplished when all terms of the numerator add in-phase, which is the case for all terms real. Thus, define

[2] S. Silver, "Microwave Antenna Theory and Design," McGraw-Hill Book Co., Inc., New York, N. Y., p. 177; 1949.

[3] W. R. Smythe, "Static and Dynamic Electricity," McGraw-Hill Book Co., Inc., New York, N. Y., p. 153; 1950.

$$\Psi_{mn} = \begin{cases} |\, j^n P_n^{m\prime}(0)\,| = \dfrac{1\cdot 3\cdot 5\cdots(n+m)}{2\cdot 4\cdot 6\cdots(n-m+1)}, \\ \qquad\qquad n+m \text{ odd} \\ |\, j^n m P_n^m(0)\,| = m\dfrac{1\cdot 3\cdot 5\cdots(n+m-1)}{2\cdot 4\cdot 6\cdots(n-m)}, \\ \qquad\qquad n+m \text{ even}, \end{cases}$$

$$\Phi_{mn} = \frac{n(n+1)(n+m)!}{\epsilon_m(2n+1)(n-m)!},$$

$$a_{mn} = \begin{cases} |\, A_{mn}\,|, & n+m \text{ odd} \\ \sqrt{\dfrac{\mu}{\epsilon}}\,|\, B_{mn}\,|, & n+m \text{ even}. \end{cases} \tag{7}$$

All quantities are now real, and one can write (4) as

$$G = \frac{(\sum a_{mn}\Psi_{mn})^2}{\sum a_{mn}^2\Phi_{mn}}. \tag{8}$$

To maximize G, set $\partial G/\partial a_{ij}=0$ for all a_{ij}. The result is

$$G = \sum \Psi_{mn}^2/\Phi_{mn}. \tag{9}$$

This is the formula for the maximum gain using a given number of wave functions, assuming the field is ϕ-polarized along the beam axis.

To evaluate (9), sum first over m. For n given, m takes on values 0, 1, 2, $\cdots$, n, and the summation yields[4]

$$\sum_{m=0}^{n} \Psi_{mn}^2/\Phi_{mn} = 2n+1. \tag{10}$$

Restrict the allowable wave functions to $n \leq N$. The remaining summation over n in (9) then gives

$$G(N) = N^2 + 2N. \tag{11}$$

This is the maximum gain obtainable using wave functions up to $n=N$.

The case of a θ-polarized field along the beam axis is the dual problem to the above. The equations are all of the same form, obtained from the above by substituting $-H$ for E, ϵ for μ, μ for ϵ, B_{mn} for A_{mn}, and A_{mn} for B_{mn}. Of course, the result is the same, so that (11) also gives the maximum gain for a θ-polarized field along the beam axis.

Let us assume one does not wish to restrict the polarization. Maximizing the ϕ-polarized gain involves only A_{mn}, $n+m$ odd, and B_{mn}, $n+m$ even; maximizing the θ-polarized gain involves only the A_{mn}, $n+m$ even, and B_{mn}, $n+m$ odd. The gain formula for the general case is therefore of the form

$$G = \frac{(\sum a_{mn}\Psi_{mn})^2 + (\sum \hat{a}_{mn}\Psi_{mn})^2}{\sum (a_{mn}^2 + \hat{a}_{mn}^2)\Phi_{mn}}, \tag{12}$$

[4] This formula was established by actual summation up to $n=20$. The author has not obtained a general proof.

where the a_{mn} and $\hat{a}_{mn}$ are the coefficients pertaining to E_θ and E_ϕ, respectively. Setting $\partial G/\partial a_{ij}=0$, and $\partial G/\partial \hat{a}_{ij}=0$ for all ij, one again obtains (9). Thus, the same maximum gain formula (11) also applies to the case of arbitrary polarization along the beam axis.

It is not easy to obtain information concerning the radiation pattern and field polarization off the beam axis with the above formulation of the problem. To circumvent this difficulty, the alternate method of representing an arbitrary radiation field, given in the Appendix, can be used. It will be seen that the derivation of a maximum gain formula becomes simpler with this approach, but involves an approximation which is not valid for small N. (The error is 7 per cent for $N=3$, 1 per cent for $N=9$.)

Take the general formula for a radiation field θ-polarized everywhere, (68), and specialize to the case of a symmetric main beam. If $\sin\theta \doteq 1$ over the main beam, only the $m=0$ terms are left, and the radiation field is given by

$$E_\theta = -\sqrt{\frac{\mu}{\epsilon}}\,\frac{e^{-j\beta r}}{r}\sin\theta \sum_n j^n B_n P_n(\cos\eta) \tag{13}$$

where the angle η is as defined in Fig. 1. The power radiated by a field of the form of (13) is a complicated expression, for orthogonality of the wave functions is lost. However, since most of the power is radiated in the main beam ($\theta=\pi/2$), the total power calculated from (13) with $\sin\theta$ replaced by unity will be only slightly larger than the true power. Using this approximation, one obtains

$$\begin{aligned} P &= \sqrt{\frac{\epsilon}{\mu}}\int_0^{2\pi} d\xi \int_0^{\pi} d\eta r^2 \sin\eta\,|\, E_\theta\,|^2 \\ &\doteq 2\pi\sqrt{\frac{\mu}{\epsilon}}\sum_{m,n} j^{n-m} B_n B_m^* \int_0^{\pi} P_n(\cos\eta)P_m(\cos\eta)\sin\eta\, d\eta \\ &= 4\pi\sqrt{\frac{\mu}{\epsilon}}\sum_n |\, B_n\,|^2/(2n+1). \end{aligned} \tag{14}$$

The formula for gain, (1), thus becomes

$$G = \frac{|\sum j^n B_n P_n(1)\,|^2}{\sum |\, B_n\,|^2/(2n+1)}. \tag{15}$$

Again one can adjust the phases of the A_n to maximize the numerator. Let

$$\Psi_n = |\, j^n P_n(1)\,| = 1, \quad \Phi_n = 1/(2n+1), \quad a_n = |\, B_n\,| \tag{16}$$

and (15) can be written

$$G = \frac{(\sum a_n\Psi_n)^2}{\sum a_n^2\Phi_n} \tag{17}$$

which is the same form as (8). Maximization of the gain involves the same mathematical steps as in the first formulation, resulting in

$$G = \sum \Psi_n^2/\Phi_n = \sum (2n + 1). \tag{18}$$

Restricting allowable wave functions to $n \leq N$, one obtains for the summation

$$G(N) = N^2 + 2N + 1. \tag{19}$$

The difference between (19) and (11) arises from the inclusion of the $n=0$ term in the present formulation, which did not occur in the previous formulation. For large N, the two formulas are equivalent. The case of a field ϕ-polarized everywhere is the dual problem to the one just treated, so the result is the same, (19). The case of arbitrary polarization can be treated as in the first formulation, again resulting in (19). Thus, if the field is specified everywhere to have a given polarization, and the main lobe is to be symmetric, maximum gain can be achieved.

Relationship of Gain to Antenna Size

No mention has yet been made of the sources of the field. A given radiation field can be projected "backwards" toward the origin as far as desired.[5] If one stops at the sphere $r=R$, currents that produce the field can be determined according to the equivalence principle.[6] However, these currents are not unique; many distributions can be found giving the same field outside the sphere $r=R$. Evaluation of the field in the vicinity of the sphere $r=R$ involves the evaluation of a sum of terms of the form

$$\psi_n = h_n^{(2)}(\beta r) f_n(\theta, \phi). \tag{20}$$

A sketch of the magnitude of the spherical Hankel functions is given in Fig. 2. For βr large, these vary as

$$|h_n| \xrightarrow[\beta r \to \infty]{} (\beta r)^{-1/2} \tag{21}$$

and for βr small,

$$|h_n| \xrightarrow[\beta r \to 0]{} \frac{2}{\pi} \frac{(n-1)!\,2^{n-1}}{(\beta r)^{n+1}}. \tag{22}$$

The approximate point of transition between the slowly decreasing magnitude for large βr and the rapidly increasing magnitude for small βr is at $\beta r = n$. This is called the point of "gradual cutoff." Wave functions $n > \beta R$ give rise to prohibitively large fields at the antenna structure, and it is postulated that they cannot be used effectively. Another way of looking at this is to say that a wave function $n > \beta R$ having reasonable magnitude at the antenna structure will not be "felt" in the radiation field. An antenna is defined as having *normal gain* when it possesses the maximum gain possible using only wave functions $n \leq N = \beta R$. Thus, from (11), the normal gain of an antenna just fitting into a sphere of radius R is

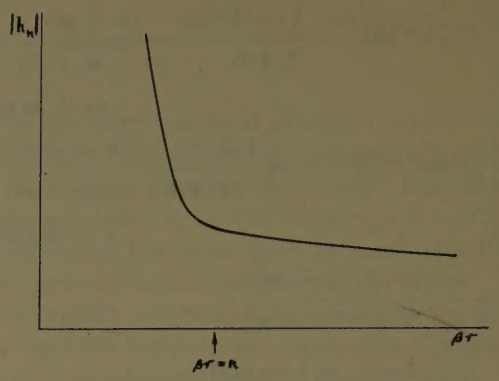

Fig. 2—Sketch of $|h_n^{(2)}(\beta r)|$.

$$G = (\beta R)^2 + 2\beta R \tag{23}$$

A distribution of currents confined to a sphere of radius R and giving rise to a greater gain is called a *supergain distribution.* Whether or not a supergain antenna is practical is a question that has not been answered satisfactorily. It is usually maintained that the large field intensities encountered would lead to prohibitive losses even if the proper current distributions could be obtained, and that supergain antennas are therefore impractical.

Beamwidth vs Sidelobe Level

The alternate formulation of the field given in the Appendix is best suited for considerations of the field pattern. For pencil beam antennas having a θ-polarized field, the radiation field is of the form

$$E_\theta = K(r) \sin\theta \sum b_n (\cos\eta)^n \tag{24}$$

where b_n are constants. Thus, using N harmonics, the radiation pattern is sin θ times a polynomial of degree N in cos η. Consider the plane $\theta = \pi/2$, in which the pattern is simply the polynomial. Let us suppose that the pattern is specified to be the Tchebycheff polynomial $T_N(x)$, defined as

$$T_N(x) = \begin{cases} \cos(N \cos^{-1} x), & x < 1 \\ \cosh(N \cosh^{-1} x), & x > 1. \end{cases} \tag{25}$$

scaled according to

$$x = a + b \cos\eta \tag{26}$$

so that a main beam and all possible sidelobes of equal amplitude fit within $-1 < \cos\eta < 1$. This is illustrated by Fig. 3. It is known from the theory of polynomials that no other polynomial of degree N can have either lower sidelobe levels with the same beamwidth to the first null, or a narrower beamwidth and the same sidelobe

[5] M. K. Hu, "Study of Near-Zone Fields of Large Aperture Antennas," Res. Inst., Syracuse University, Syracuse, N. Y., Final Report No. EE 282-574F1, sponsored by RACD Contract No. AF30(602)-928, part 1; April, 1957.

[6] S. Schelkunoff, "Electromagnetic Waves," D. Van Nostrand Co., Inc., New York, N. Y., p. 158; 1943.

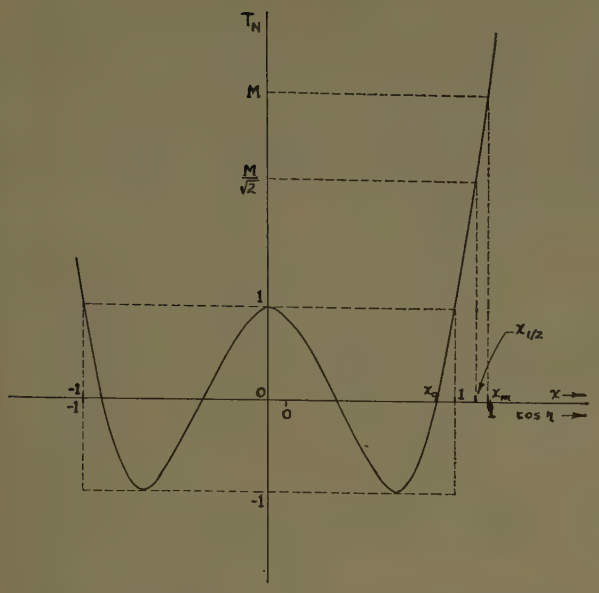

Fig. 3—Illustration of the use of $TN(x)$. ($N=4$ shown.)

levels.[7] In this sense, the Tchebycheff pattern is called *optimum*. The choice of the maximum value x_m of $T_N(x)$ to be included within the pattern $-1<\cos\eta<1$ determines the ratio of main beam level to sidelobe level.

The constants a and b of (26) are conveniently found from the points $x=-1$ and $x=x_m$, according to

$$-1 = a - b \qquad x_m = a + b \tag{27}$$

giving

$$a = \frac{x_m - 1}{2} \qquad b = \frac{x_m + 1}{2}. \tag{28}$$

Consideration will be restricted to 1) the ratio of maximum beam field to maximum sidelobe level, M, 2) the beamwidth between half power points, $BW_{1/2}$; 3) the beamwidth between first nulls, BW_0. If

$$M = E_{\text{beam max}}/E_{\text{sidelobe max}} \tag{29}$$

is chosen, it is evident from Fig. 3 that $TN(x_m)=M$, and from (25)

$$x_m = \cosh\left(\frac{1}{N}\cosh^{-1} M\right). \tag{30}$$

For $M>3$,

$$\cosh^{-1} M \doteq \ln 2M \tag{31}$$

to within 0.3 per cent. For $N>10\ln 2M$,

$$x_m \doteq 1 + \frac{1}{2N^2}(\ln 2M)^2 \tag{32}$$

the value of x_m-1 being correct to within 0.1 per cent. The value of $x_{1/2}$ can also be calculated with similar approximation to be

$$x_{1/2} \doteq 1 + \frac{1}{2N^2}(\ln \sqrt{2}M)^2. \tag{33}$$

From (25) it is evident that the first zero is

$$x_0 = \cos\frac{\pi}{2N} \tag{34}$$

and for $N>20/\pi$

$$x_0 \doteq 1 - \frac{\pi^2}{8N^2} \tag{35}$$

gives $1-x_0$ to within 0.1 per cent. These values of x must now be transformed to values of η. From (26) and (28) it follows that

$$\cos\eta = \frac{x-a}{b} = \frac{2x - x_m + 1}{x_m + 1}. \tag{36}$$

The value of $\sin\eta$ is given by

$$\sin\eta = \sqrt{1-\cos^2\eta} = \frac{2}{x_m+1}\sqrt{(x_m - x)(1+x)}. \tag{37}$$

For N large and $x=x_{1/2}$, x_0, one has $\eta\doteq\sin\eta$, $x_m+1\doteq 2$, $1+x_{1/2}\doteq 2$, and $1+x_0\doteq 2$, so

$$\eta_{1/2} \doteq \sin\eta_{1/2} \doteq \sqrt{2(x_m - x_{1/2})}$$
$$\eta_0 \doteq \sin\eta_0 \doteq \sqrt{2(x_m - x_0)}. \tag{38}$$

Finally, the beamwidths are twice the η's, so that substitution from (32,) (33), and (35 gives

$$2\eta_{1/2} \doteq \frac{\sqrt{2}}{N}\sqrt{(\ln 2M)^2 - (\ln\sqrt{2}M)^2}$$
$$2\eta_0 \doteq \frac{\sqrt{2}}{N}\sqrt{(\ln 2M)^2 + (\pi/2)^2}. \tag{39}$$

Thus, for large N, the optimum beamwidth between half power points is

$$BW_{1/2} \doteq \frac{180\sqrt{2}}{\pi N}\sqrt{(\ln 2M)^2 - (\ln\sqrt{2}M)^2}\ \text{degrees} \tag{40}$$

and the optimum beamwidth between first nulls is

$$BW_0 \doteq \frac{180\sqrt{2}}{\pi N}\sqrt{(\ln 2M)^2 + (\pi/2)^2}\ \text{degrees}. \tag{41}$$

These are the minimum beamwidths that can be obtained for the given sidelobe level, using N spherical wave functions.

To interpret these results in terms of antenna size, merely set $N=\beta R$, where R is the radius of the smallest sphere that can contain the antenna. These are then

[7] C. L. Dolph, "A current distribution for broadside arrays which optimizes the relationship between beam width and side-lobe level," Proc. IRE, vol. 34, pp. 335–348; June, 1946.

defined to be *normal beamwidths*, for it has not been proved that wavefunctions $n>\beta R$ cannot be used, but only that it is improbable that they can be used effectively. Thus, for large βR, the normal beamwidths for a given sidelobe level are given by

$$BW_{1/2} = \frac{180\sqrt{2}}{\pi\beta R}\sqrt{(\ln 2M)^2 - (\ln\sqrt{2}M)^2} \text{ degrees} \quad (42)$$

for half power points, and

$$BW_0 = \frac{180\sqrt{2}}{\pi\beta R}\sqrt{(\ln 2M)^2 + (\pi/2)^2} \text{ degrees} \quad (43)$$

for first nulls. To summarize these results, let

$$BW = A/(R/\lambda) \text{ degrees} \quad (44)$$

where $A_{1/2}$ and A_0, corresponding to $BW_{1/2}$ and BW_0, are given in Table I. For example, an antenna 10 wavelengths in diameter with sidelobe levels down 30 db has a normal beamwidth of 4.3 degrees between half power points and 11.5 degrees between first nulls.

TABLE I

Sidelobe level (db below max)	10	20	30	40	50	60
M	3.17	10	31.7	100	317	1000
$A_{1/2}$	14.0	18.3	21.5	24.5	27.1	28.8
A_0	31.4	43.8	57.3	71.4	85.5	100

Appendix

Expansion of a Field in Spherical Harmonics

In source-free empty space, the time-periodic field equations read

$$\nabla\times\boldsymbol{E} = -j\omega\mu\boldsymbol{H} \qquad \nabla\cdot\boldsymbol{E} = 0$$
$$\nabla\times\boldsymbol{H} = j\omega\epsilon\boldsymbol{E} \qquad \nabla\cdot\boldsymbol{H} = 0. \quad (45)$$

In view of the divergence relationships, all or part of $\boldsymbol{E}$ can be represented in terms of a vector potential $\boldsymbol{F}$, and all or part of $\boldsymbol{H}$, in terms of a vector potential $\boldsymbol{A}$. Let

$$\boldsymbol{E} = \boldsymbol{E}' + \boldsymbol{E}'' \qquad \boldsymbol{H} = \boldsymbol{H}' + \boldsymbol{H}'' \quad (46)$$

where

$$\boldsymbol{E}' = -\nabla\times\boldsymbol{F} \qquad \boldsymbol{H}'' = \nabla\times\boldsymbol{A}. \quad (47)$$

It then follows from (45) and (46) that

$$\boldsymbol{E} = \frac{1}{j\omega\epsilon}\nabla\times\nabla\times\boldsymbol{A} - \nabla\times\boldsymbol{F}$$

$$\boldsymbol{H} = \frac{1}{j\omega\mu}\nabla\times\nabla\times\boldsymbol{F} + \nabla\times\boldsymbol{A} \quad (48)$$

and $\boldsymbol{A}$ and $\boldsymbol{F}$ satisfy

$$\nabla\times\nabla\times\boldsymbol{F} - \beta^2\boldsymbol{F} = \nabla\Phi$$
$$\nabla\times\nabla\times\boldsymbol{A} - \beta^2\boldsymbol{A} = \nabla\hat{\Phi} \quad (49)$$

where Φ and $\hat{\Phi}$ are arbitrary scalars. Let the field be represented by $\boldsymbol{A}$ and $\boldsymbol{F}$ having only r components. (This is sufficient to represent an arbitrary field, but the proof will not be given here.) The $\boldsymbol{F}$ equation can then be separated into components, and the θ and ϕ component equations are

$$\frac{\partial^2 F_r}{\partial r\partial\theta} = \frac{\partial\Phi}{\partial\theta} \qquad \frac{\partial^2 F_r}{\partial r\partial\phi} = \frac{\partial\hat{\Phi}}{\partial\phi}. \quad (50)$$

Similar equations hold for A_r. These equations are satisfied identically if one sets

$$\Phi = \frac{\partial F_r}{\partial r} \qquad \hat{\Phi} = \frac{\partial A_r}{\partial r}. \quad (51)$$

The r-component equations for $\boldsymbol{A}$ and $\boldsymbol{F}$ then become

$$(\nabla^2 + \beta^2)(A_r/r) = 0 \qquad (\nabla^2 + \beta^2)(F_r/r) = 0. \quad (52)$$

Thus, both A_r and F_r are r times solutions to the scalar wave equation

$$\nabla^2\psi + \beta^2\psi = 0 \quad (53)$$

The elementary wave solutions to this which are applicable to the entire space external to a given sphere are

$$\psi_{mn} = h_n^{(2)}(\beta r)P_n^m(\cos\theta)\cos(m\phi + \alpha_{mn}). \quad (54)$$

Particular ψ's for F_r and A_r can be constructed of linear combinations of the elementary functions. Only integer values of m and n are permissible. Thus, the most general forms for $\boldsymbol{F}$ and $\boldsymbol{A}$ are

$$F_r = r\psi \qquad A_r = r\hat{\psi} \quad (55)$$

where

$$\psi = \sum_{m,n} A_{mn}h_n^{(2)}(\beta r)P_n^m(\cos\theta)\cos(m\phi + \alpha_{mn})$$
$$\hat{\psi} = \sum_{m,n} B_{mn}h_n^{(2)}(\beta r)P_n^m(\cos\theta)\cos(m\phi + \hat{\alpha}_{mn}). \quad (56)$$

The field components can now be evaluated in terms of the ψ's:

$$E_r = \frac{1}{j\omega\epsilon}\left(\frac{\partial^2}{\partial r^2} + \beta^2\right)(r\hat{\psi})$$

$$E_\theta = \frac{-1}{\sin\theta}\frac{\partial\psi}{\partial\phi} + \frac{1}{j\omega\epsilon r}\frac{\partial^2(r\hat{\psi})}{\partial r\partial\theta}$$

$$E_\phi = \frac{\partial\psi}{\partial\theta} + \frac{1}{j\omega\epsilon r\sin\theta}\frac{\partial^2(r\hat{\psi})}{\partial r\partial\phi}$$

$$H_r = \frac{1}{j\omega\mu}\left(\frac{\partial^2}{\partial r^2} + \beta^2\right)(r\psi)$$

$$H_\theta = \frac{1}{\sin\theta}\frac{\partial\psi}{\partial\phi} + \frac{1}{j\omega\mu r}\frac{\partial^2(r\psi)}{\partial r\partial\theta}$$

$$H_\phi = -\frac{\partial\hat{\psi}}{\partial\theta} + \frac{1}{j\omega\mu r\sin\theta}\frac{\partial^2(r\hat{\psi})}{\partial r\partial\phi}. \quad (57)$$

In the radiation field, the r components become negligible, and

$$E_\theta = \eta H_\phi, \quad E_\phi = -\eta H_\theta. \tag{58}$$

Thus, all pertinent information can be obtained from E_θ and E_ϕ. In general, these are found to be

$$E_\theta = \frac{1}{\sin\theta}\sum_{m,n} mA_{mn}h_n^{(2)}(\beta r)P_n^m(\cos\theta)\sin(m\phi+\alpha_{mn}) - \frac{\sin\theta}{j\omega\epsilon r}\sum_{m,n}B_{m,n}\frac{\partial}{\partial r}[rh_n^{(2)}(\beta r)]P_n^{m\prime}(\cos\theta)\cos(m\phi+\hat{\alpha}_{mn})$$

$$E_\phi = -\sin\theta\sum_{m,n}A_{mn}h_n^{(2)}(\beta r)P_n^{m\prime}(\cos\theta)\cos(m\phi+\alpha_{mn}) - \frac{1}{j\omega\epsilon r\sin\theta}\sum_{m,n}mB_{mn}\frac{\partial}{\sigma r}[rh_n^{(2)}(\beta r)]P_n^m(\cos\theta)\sin(m\phi+\hat{\alpha}_{mn}). \tag{59}$$

For βr large, the asymptotic form of the spherical Hankel function gives

$$h_n^{(2)}(\beta r) \xrightarrow[\beta r\to\infty]{} j^{n+1}\frac{e^{-j\beta r}}{\beta r}$$

$$\frac{\partial}{\partial r}[rh_n^{(2)}(\beta r)] \xrightarrow[\beta r\to\infty]{} j^n e^{-j\beta r}. \tag{60}$$

Thus, the radiation field can be written as

$$E_\theta = \frac{e^{-j\beta r}}{\beta r}\sum_{m,n} j^{n+1}\left[\frac{mA_{mn}}{\sin\theta}P_n^m(\cos\theta)\sin(m\phi+\alpha_{mn}) + \sqrt{\frac{\mu}{\epsilon}}\sin\theta B_{mn}P_n^{m\prime}(\cos\theta)\cos(m\phi+\hat{\alpha}_{mn})\right]$$

$$E_\phi = \frac{e^{-j\beta r}}{\beta r}\sum_{m,n} j^{n+1}\left[-\sin\theta A_{mn}P_n^{m\prime}(\cos\theta)\cos(m\phi+\alpha_{mn}) - \sqrt{\frac{\mu}{\epsilon}}\frac{mB_{mn}}{\sin\theta}P_n^m(\cos\theta)\sin(m\phi+\hat{\alpha}_{mn})\right]. \tag{61}$$

The power radiated by an arbitrary field is also of interest. In the radiation zone, the r component of the Poynting vector is

$$S_r = \sqrt{\frac{\epsilon}{\mu}}\,\boldsymbol{E}\cdot\boldsymbol{E}^* = \sqrt{\frac{\epsilon}{\mu}}\,(|E_\theta|^2 + |E_\phi|^2) \tag{62}$$

and the total power radiated is

$$P = \int_0^{2\pi} d\phi \int_0^\pi d\theta r^2 \sin\theta(|E_\theta|^2 + |E_\phi|^2)$$

$$= \frac{4\pi}{\beta^2}\sum_{m,n}\frac{1}{\epsilon_m}\left[\sqrt{\frac{\epsilon}{\mu}}\,|A_{mn}|^2 + \sqrt{\frac{\mu}{\epsilon}}\,|B_{mn}|^2\right]\cdot\frac{n(n+1)(n+m)!}{(2n+1)(n-m)!}. \tag{63}$$

The steps involved in (63) are rather involved, but follow the reasoning of Smythe.[8]

An alternate representation of the radiation field can be obtained. For this, one chooses

$$\Phi = \nabla\cdot\boldsymbol{F}, \qquad \hat{\Phi} = \nabla\cdot\boldsymbol{A} \tag{64}$$

instead of (51). Rectangular components of $\boldsymbol{F}$ and $\boldsymbol{A}$ then satisfy (53). $\boldsymbol{F}$ and $\boldsymbol{A}$ are chosen to have only z components, which have the general form

$$F_z = \sum_{m,n} A_{mn}h_n^{(2)}(\beta r)P_n^m(\cos\eta)\cos(m\xi+\alpha_{mn})$$

$$A_z = \sum_{m,n} B_{mn}h_n^{(2)}(\beta r)P_n^m(\cos\eta)\cos(m\xi+\hat{\alpha}_{mn}) \tag{65}$$

where η and ξ are as defined in Fig. 1. The η, ξ variables are chosen merely for more convenient representation of pencil beam antennas; the θ, ϕ variables could also be used. The general expression for the field is

$$\boldsymbol{E} = -\nabla\times\boldsymbol{F} - j\omega\mu\boldsymbol{A} + \frac{1}{j\omega\epsilon}\nabla(\nabla\cdot\boldsymbol{A})$$

$$\boldsymbol{H} = \nabla\times\boldsymbol{A} - j\omega\epsilon\boldsymbol{F} + \frac{1}{j\omega\mu}\nabla(\nabla\cdot\boldsymbol{F}) \tag{66}$$

for the choice (64). However, the radiation field can be found much more simply; it is given by

$$E_\phi \xrightarrow[\beta r\to\infty]{} -j\beta\sin\theta F_z$$

$$E_\theta \xrightarrow[\beta r\to\infty]{} j\omega\mu\sin\theta A_z. \tag{67}$$

Using the asymptotic formulas for the spherical Hankel function, (60), in the expressions for A_z and F_z, one finally obtains

$$E_\phi = \sin\theta\frac{e^{-j\beta r}}{r}\sum_{m,n} j^n A_{mn}P_n^m(\cos\eta)\cos(m\xi+\alpha_{mn})$$

$$E_\theta = -\sqrt{\frac{\mu}{\epsilon}}\sin\theta\frac{e^{-j\beta r}}{r}\sum_{m,n} j^n B_{mn}P_n^m(\cos\eta)\cos(m\xi+\hat{\alpha}_{mn}) \tag{68}$$

which applies only in the radiation zone. Note that when $F_z=0$, the field is everywhere ϕ-polarized, and when $A_z=0$, the field is everywhere θ-polarized. The $\boldsymbol{H}$ components are still given by (58).

[8] Smythe, *op. cit.*, p. 150.

Evaluating the Impedance Broadbanding Potential of Antennas*

A. VASSILIADIS AND R. L. TANNER†

Summary—**One of the principal concerns of the aircraft antenna designer is to determine whether an antenna having some known terminal impedance characteristics can be compensated to meet a specified, voltage standing-wave ratio (VSWR)-bandwidth relation. Alternatively, the problem may be to select from among possible antenna configurations that one which possesses the greatest impedance broadbanding potential.**

In this paper the problem is examined by means of modern circuit theory. Antenna impedances are approximated by rational algebraic fractions and the impedances represented by these functions are treated analytically to determine the VSWR-bandwidth relationship which may be obtained by optimum compensation. The functions that can be considered by the techniques developed are sufficiently complex to adequately represent the basic impedance characteristics obtained with typical airborne flush-mounted antennas over a frequency range that causes the dimensions of the antenna to vary between a small fraction of a wavelength and approximately a wavelength. Examples are given.

Introduction

An important problem in the design of antennas, especially aircraft antennas, is the determination of the maximum bandwidth possible for a specified antenna size and mode of radiation.

Pattern requirements restrict the number of possible feed configurations to those which excite modes giving approximations to the desired patterns. Within this restriction, however, the designer is faced with the necessity of choosing that particular configuration which offers the greatest promise for broadband impedance performance. The "raw" impedance characteristic of an antenna, which in practical antennas must almost always be obtained by measurement, does not provide a ready index to what might be described as the "broadbanding potential" of the antenna. The designer can find out how good the antenna is only by actually attempting broadband compensation. Even this is not a reliable index because the designer has no sure guide as to how to proceed in the design of a compensating network.

This paper describes a method by which antennas can be compared on the basis of an approximate quantitative criterion. A by-product of the process is an optimum lumped-element matching network, which, while seldom directly applicable to the compensation of the antennas, serves as a guide in the design of actual compensating networks.

The techniques employed in the theoretical consideration of the broadbanding problem are those developed in circuit synthesis theory. While powerful, these techniques are limited to the study of impedance functions that can be expressed analytically as rational algebraic functions. Such impedance functions are associated with lumped-element networks. Distributed systems, such as antennas, lead to much more complicated meromorphic functions, which, except in cases of almost trivial simplicity, cannot be explicitly expressed in analytical form, much less manipulated to investigate their broadbanding potential.

In order to treat the broadbanding problem analytically, therefore, we must first approximate the actual antenna impedance functions by rational algebraic fractions. This is equivalent to saying that we obtain lumped-element circuit representations for the antenna impedances. The lumped-element network which is the result of the approximation process then becomes the load which must be matched to a constant resistance generator for maximum power transfer over the frequency range of interest.

The matching of the impedance to the generator will require the design of a matching network which may be dissipative or nondissipative. In this application only lossless networks will be considered. The problem of impedance-matching limitations in the situation described has been considered by several investigators. The first of these was Bode [1], who treated the case of the simplest possible load network, a resistance paralleled by a capacitance, in connection with his investigation of wide-band amplifiers. The most general treatment, however, is that of Fano [2]. The method employed here is related to Fano's. By using simpler approximating functions and by obtaining the optimizing conditions in a different form, impedances of greater complexity can be practically treated.

The Approximation of the Antenna Impedances

Form of Approximating Function

Because of the distributed character of antennas it is evident that their input impedance must be expressed by a meromorphic function rather than by a rational algebraic function. The complex frequency plane representation of the admittance of a typical slot antenna, therefore, consists of an infinite set of alternating poles and zeros. Starting with a pole at the origin, the singularities fan out in conjugate pairs of zeros and poles moving away from the real and imaginary axes. The analogous case for dipole antennas must also be expressed by a meromorphic function. However, in this case a pole of impedance occurs at the origin. Thus the two cases are duals, and the same pole-zero structure applies to both. In the former it represents the admittance, while in the latter it shows the impedance.

On the real frequency axis the response is influenced

* Manuscript received by the PGAP, May 27, 1957; revised manuscript received, February 27, 1958. This work was supported by the U. S. Air Force under Contract AF 19(604)-1296.

† Stanford Res. Inst., Menlo Park, Calif.

most by the poles and zeros that are closest to the point considered, while the farther singularities contribute relatively little. This is especially true if the singularities are very close to the imaginary axis. The rational function that is used to approximate the antenna immitance in the low end of the spectrum, encompassing the first resonance, must have the pole-zero structure of the antenna immitance near the origin. As a first approximation, a satisfactory rational function will be of the form:

$$M(p) = \frac{C_1 p^2 + C_2 p + C_3}{p^3 + C_4 p^2 + C_5 p}, \tag{1}$$

where

$p = \sigma + jw$,

C_1 to C_5 are arbitrary constants.

This function consists of a pole at the origin, a pair of conjugate zeros, and a pair of conjugate poles. The basic requirement on this function is that it be "positive-real." In other words, we require a guarantee that this function represents a physical network.

A further requirement in this application is that the real part must be zero at zero frequency. It may be shown that this is true if $C_2C_5 = C_3C_4$. When the above conditions are satisfied, the rational function of (1) will result in the equivalent networks shown in Fig. 1(a) if the immitance represents the admittance of a slot antenna, and in the networks of Fig. 1(b) if the immitance function represents the impedance of a dipole antenna.

The evaluation of the constants C_1 and C_5 for a specific antenna must be chosen in such a manner that the antenna input immitance is approximated as closely as possible over an appreciable bandwidth.

Criterion and Methods of Approximation

In the actual approximation procedure the reflection coefficient is used. The reflection coefficient is defined as:

$$\rho(p) = \frac{1 - Y(p)}{1 + Y(p)} = \frac{Z(p) - 1}{Z(p) + 1}. \tag{2}$$

For the purpose of approximation, a least-square error criterion is used. The residual function R, of (3) is formed, where ρ^* is the actual measured antenna reflection coefficient, ρ is the approximating reflection coefficient,

$$R = \sum_{1}^{N} |\rho - \rho^*|^2, \tag{3}$$

and N is the number of points that are included in the approximation. This residual is the function that must be minimized by proper choice of the arbitrary constants C_1 to C_5 of the immitance function (1). In any procedure where R is minimized, the condition $C_2C_5 = C_3C_4$ must always be introduced.

A number of attempts have been made to adapt the approximation problem to solution by a high-speed computer, but these have been only moderately successful. The procedure that is used at present involves the use of two routines applied in sequence. The first routine, which essentially gives a rough approximation, depends for its solution on linear equations. The denominator of the residual function R is assumed independent of C_j. In this way the derivatives of R, with respect to the C_j, yield equations which are linear. These equations are used in conjunction with the side condition mentioned earlier and solution is obtained by an iterative procedure.

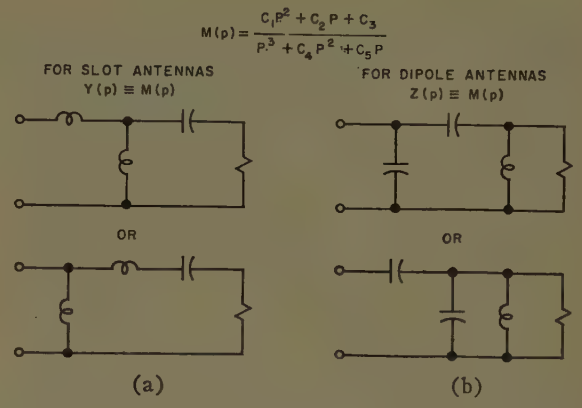

Fig. 1—The approximating function and its associated networks.

Although in some instances this procedure yields adequate results, the approximations in general are not satisfactory. This is due to the fact that the denominator was assumed independent of C_j's. The approximation obtained by the method outlined can usually be improved by the use of a technique devised by Hart and Motzkin [3]. In the Hart-Motzkin method the quantity R of (3) is considered as a function of the constants C_1 to C_5 and the gradient of R is calculated. The C_j's are then given an increment in the direction of the gradient and a new gradient is calculated. The weakest feature of this technique is in choosing the increment to be taken. If the increment is made too small, convergence is slow and the calculation becomes prohibitively expensive. If the increment is chosen too large the calculation may not converge.

The scheme that has been used is to pass a second degree curve through three points of different steps along the gradient direction computed at one of these points and then to take the position of the minimum as the point at which the next gradient is calculated.

Optimum Matching of Impedances

In general, a matching network is necessary when matching an arbitrary impedance to a generator with a constant internal resistance. The matching network is placed between the generator and the load as shown in Fig. 2.

It was shown by Darlington [4] that any impedance may be realized as a purely lossless network terminated in a single resistance. Thus the over-all network may be represented as in Fig. 3—two lossless networks in cas-

Fig. 2—Arbitrary load impedance with matching network.

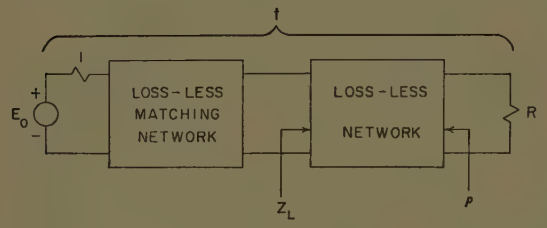

Fig. 3—Lossless matching network with Darlington representation of the load.

cade terminated by a resistance. It may be shown that with a lossless matching network it is impossible to obtain a perfect match over a range of frequencies. It is, of course, possible to obtain a perfect match at any number of points in a given frequency range. There is no guarantee, however, that between these points the match will be satisfactory, and in general it will not be. As will be shown later, we can obtain a perfect match at one point in a frequency band only by sacrificing performance elsewhere in the band.

To find a maximum bandwidth over which a given VSWR is possible with a given complexity of matching network, it is convenient to start from the over-all transfer coefficient. This is defined in terms of the per-unit power reaching the load as:

$$|t|^2 = \frac{P_L}{P_0} = 1 - |\rho|^2, \tag{4}$$

where

t = transfer coefficient,
P_L = power reaching the load resistance,
P_0 = available power.

For a load consisting of a paralleled resistance and capacitance, Bode [1] obtained the limiting criterion:

$$\int_0^\infty \ln\left|\frac{1}{\rho}\right| d\omega = \frac{\pi}{RC} - \pi \sum \lambda_i, \tag{5}$$

where ρ is the reflection coefficient of the over-all network, and λ_i are the real parts of the zeros of the reflection coefficient which occur in the right-half plane. The equation states that the area under the $ln|1/\rho|$ curve cannot exceed a value fixed by the value of the normalized capacitance. If there are zeros of the reflection coefficient in the right-half plane, the area will decrease accordingly.

It is therefore evident that the best possible match is obtained when the reflection coefficient is a constant $|P_m|$ over the desired bandwidth W and is unity elsewhere, as illustrated in Fig. 4.

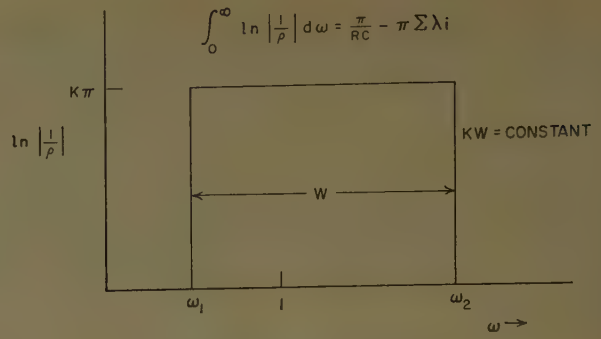

Fig. 4—Bode's criterion.

It follows that for finite networks the existence of a perfect match ($\rho = 0$) anywhere in the desired band represents a waste of area and leads to a poorer match at other points in the band.

Fano [2] extended the analysis to cover a general impedance and showed that, as the complexity of the impedance increases, additional restrictions in the form of simultaneous equations are imposed on the network. In order to obtain an optimum match, the reflection coefficient over a given bandwidth is minimized while at the same time satisfying the equations mentioned.

In the procedure employed in this paper, in order to obtain equations that are practical to solve, the loads are restricted to those whose zeros of transfer coefficient are located only at the origin and at infinity. This means that the load must have the form of a lossless ladder network terminated in a resistance. This restriction does not greatly hamper the approximation of antenna impedances by lumped-element networks.

As a further simplification, a Taylor, or maximally-flat approximation to the ideal transfer coefficient is used. For the band-pass case it is defined as:

$$|t|^2 = \frac{k^2 m^{2n}}{\left(\omega - \frac{1}{\omega}\right)^{2n} + m^{2n}}, \tag{6}$$

where

ω = normalized frequency,
m = normalized bandwidth,
k = amplitude constant,
n = degree of approximation.

From (6) the over-all reflection coefficient is obtained by using (4) and then selecting the left-half plane singularities. The over-all immittance is obtained using (2) expressed in terms of the bandwidth parameter m.

The form of the immittance function obtained may be expressed as:

$$M(\phi) = \frac{C_{00}\phi^\nu + C_{01}\phi^{\nu-1} + C_{02}\phi^{\nu-2} \cdots + C_{0\nu}}{C_{11}\phi^{\nu-1} + C_{12}\phi^{\nu-2} \cdots + C_{1\nu}}, \tag{7}$$

where ϕ is the complex frequency variable. The coefficients C_{ij} are functions of n, m, k, and a_i[5] (a_i represents all-pass sections that are introduced for added de-

grees of freedom. These are discussed later.) Depending on the order of the all-pass section which must be introduced, either $C_{0\nu}=0$, or $C_{1\nu}=0$.

This immittance represents either the admittance or the impedance of the over-all network looking into the load end of the network. A continued fraction expansion may be carried out on a function of this type. This method of obtaining the network represented by an immittance is well known in circuit synthesis [5], [6]. The form of the resulting expansion for the network used in the approximation of the antenna immittance would be:

$$M(\phi) = \psi_1\phi + \cfrac{1}{\psi_2\phi + \cfrac{1}{\cfrac{\psi_3}{\phi} + F(\phi)}}, \tag{8}$$

where $F(\phi)$ is the immittance of the remaining network. In this case it will be the matching network.

Thus the expansion is carried out until all the elements of the load have been removed starting from the load end of the over-all network. Using the recursion formulas for the continued fraction expansion, the element values of the load ψ_1, ψ_2, and ψ_3 may be expressed in terms of C_{ij}. The sequence of the elements for the network under consideration places the requirement that $C_{1\nu}=0$. This in turn restricts the order of the all-pass network to zero or an even number. Normalizing so that $C_{00}=1$, the following equations are obtained:

$$C_{11} = \frac{1}{\psi_1},$$

$$C_{02} - \psi_1 C_{13} = \frac{1}{\psi_1\psi_2},$$

$$\frac{C_{1,\nu-1}}{C_0} \leqq \left(\psi_2 + \frac{1}{\psi_3}\right), \tag{9}$$

for the top networks of Fig. 1(a) and (b). Similar equations are obtained for the bottom two networks.

If a dipole antenna is being considered, then:

$$\psi_1 = L_1, \qquad \psi_2 = C_1, \qquad \psi_3 = \frac{1}{C_2}.$$

Whereas if a slot antenna is being considered, then:

$$\psi_1 = \frac{1}{C_1}, \qquad \psi_2 = \frac{1}{L_1}, \qquad \psi_3 = L_2.$$

The inequality is due to the fact that the load network and the matching network may have a common zero of transmission. In other words, considering the matching of a slot antenna [which is approximated by the top network of Fig. 1(a)], this would mean that the matching network would have a series inductance for its first element.

In general, it is not possible to satisfy the three equations without introducing additional degrees of freedom, although under some circumstances the additional degrees of freedom are not necessary. These degrees of freedom are provided by the introduction into the matching network of the all-pass sections mentioned earlier. These all-pass sections result in zeros of reflection coefficient in the right-half plane. From the condition of (5) it is evident that maximum bandwidth is obtained by using a minimum number of these zeros.

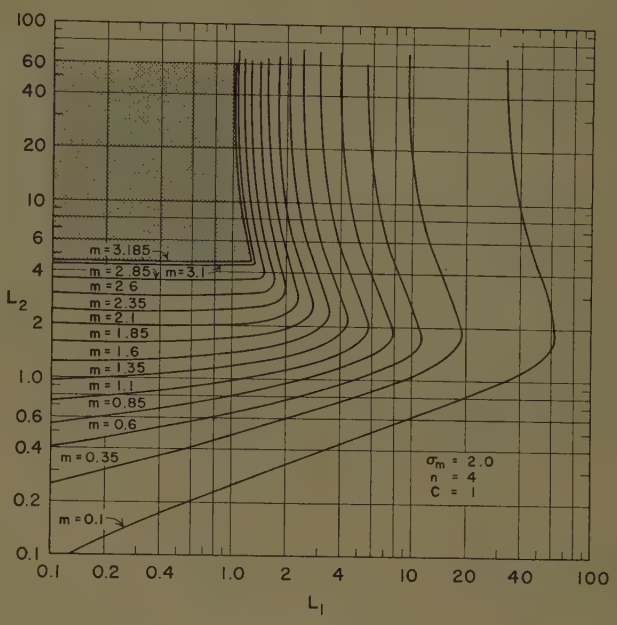

Fig. 5—Optimum curves for the approximating immittance.

Eq. (9) may also be used to compute optimum bandwidth curves by assuming parametric values for some of the variables involved, one of which is the normalized bandwidth. A sample series of curves is shown in Fig. 5, for a value of $\Psi_1 = C = 1$. There are two regions of realization. If the coordinates of a load fall in the shaded region, the value of the normalized bandwidth will be the limiting value of the boundary (in this case 3.185) and no all-pass section will be necessary. If the coordinates of load place it in the unshaded region, the value of m is given by the contour passing through the point. In this region a second-order all-pass section is necessary for optimum bandwidth.

Application to Practical Antennas

As an example of the application of the preceding theoretical results to practical antenna problems, consider the two slot antennas shown in Figs. 6 and 7. Both slots are backed by cavities 8 inches square by 2 inches deep; both slots are excited by balanced feeds and would have the patterns of a simple magnetic dipole. One of the slots is "end-loaded." The question might be asked whether this strategem results in a basic improvement of the impedance characteristic, and if so, how great is the improvement? The answer is not immediately apparent from the measured impedances, although it appears that the end loading does effect some improvement.

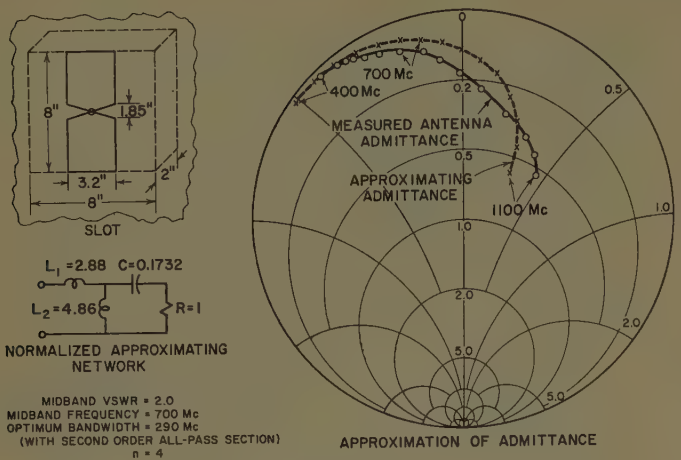

Fig. 6—Broad-band potential of slot antenna no. 1.

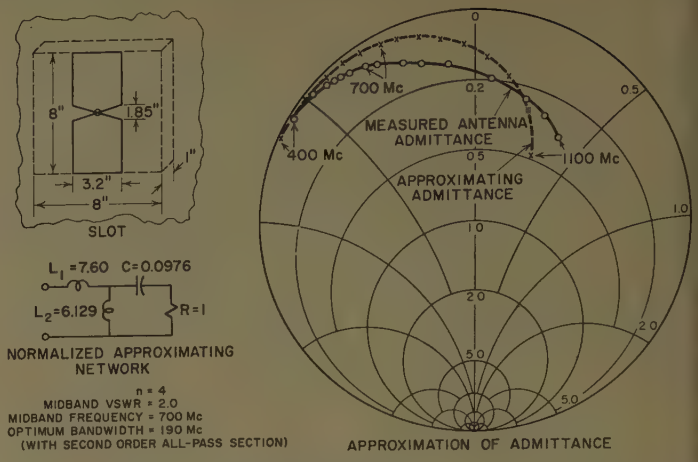

Fig. 8—Broad-band potential of slot antenna no. 3.

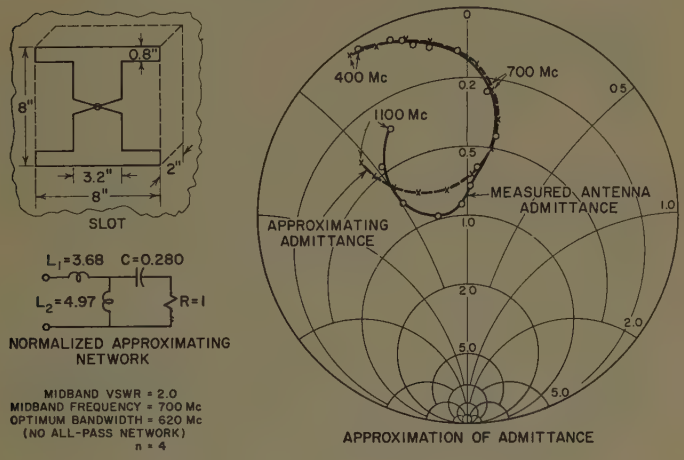

Fig. 7—Broad-band potential of slot antenna no. 2.

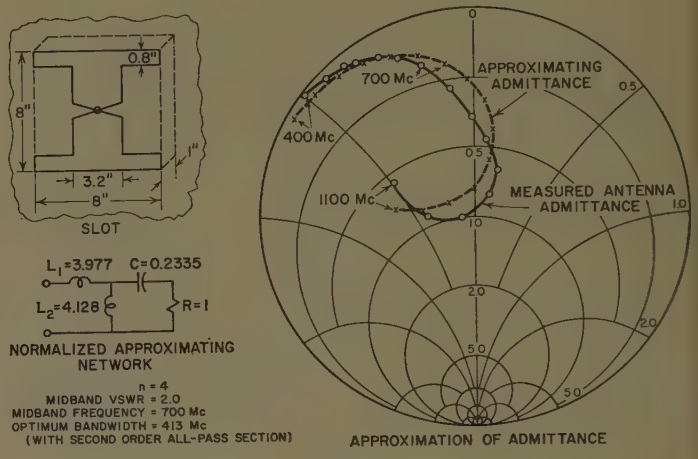

Fig. 9—Broad-band potential of slot antenna no. 4.

To investigate this question the impedances are approximated by the simple rational function described earlier. The approximating impedances are shown in the same diagrams as the measured impedances, and while the difference between the two curves is evident, particularly at the higher frequencies, the actual discrepancy in reflection coefficient is not great. It should be pointed out that by adding an additional pair of singularities to the approximating function the approximation could have been considerably improved. The lumped-constant circuits represented by the rational impedance functions are shown next to the impedance curves. Element values for both circuits are normalized with respect to a frequency, $f_0 = 7 \times 10^8$ cycles, which is taken as the center frequency in comparing the bandwidths.

Applying the methods outlined it was calculated that the slot without top loading had a fractional bandwidth, m/f_0, of 0.42 for a 2:1 VSWR. Moreover, the ideal matching network for this antenna contained an all-pass section, indicating that practical realization of a compensating circuit to achieve this bandwidth would be difficult. The end-loaded slot, on the other hand, gives a corresponding fractional bandwidth of 0.89, or more than twice as much, and the ideal matching circuit contains no all-pass section.

As a further example, the same slot antennas considered above are shown in Figs. 8 and 9. Here, however, the slots are backed by cavities 8 inches square by 1 inch deep; thus the effect of cavity depth may be observed by comparing the optimum bandwidth of similar slots.

Applying the methods outlined it was calculated that the slot without top-loading, Fig. 8, had an optimum fractional bandwidth of $m/f_0 = 0.27$ for a 2:1 VSWR compared with a value of 0.42 obtained with a 2-inch cavity. Furthermore an all-pass section is required in the matching network. Likewise, for the end-loaded slot, Fig. 9, an optimum bandwidth of $m/f_0 = 0.59$ was obtained compared to a value of 0.89 for the same slot with a 2-inch cavity. From these results we obtain an approximate quantitative measure of the effectiveness of increased cavity depth in improving the broadband characteristics of the antennas.

Conclusions

The examples just given illustrate the areas of usefulness of the theoretical methods described. It is evident, in view of the limited accuracy of the approximation to the antenna impedance, that the numerical results obtained cannot be realized with precision. Moreover, the theoretical bandwidths obtained repre-

sent the upper bound of what can be obtained in practice. Even with these limitations, however, it is evident that the results have considerable usefulness. With these results in hand we know, for example, that it would be foolish to search for a compensation scheme to match the first slot over a 2:1 bandwidth. Results of the type given also enable us to evaluate with considerable confidence the effects produced by such variations in antenna feed arrangement as the end loading of the slot.

Acknowledgment

The authors wish to acknowledge the contribution of J. A. Cochran in applying digital computation techniques to the approximation of antenna impedances.

Bibliography

[1] Bode, H. W. *Network Analysis and Feedback Amplifier Design*, New York: D. Van Nostrand Co., Inc., 1945.
[2] Fano, R. M. *Theoretical Limitations on the Broadband Matching of Arbitrary Impedances*, Cambridge: Massachusetts Institute of Technology, Research Laboratory of Electronics, Technical Report, No. 41, January, 1948.
[3] Hart, W. L., and Motzkin, T. S. "A Composite Newton-Raphson Gradient Method for the Solution of Systems of Equations," paper presented at Stanford University to the American Mathematics Society (April 30, 1955).
[4] Darlington, S. "Synthesis of Reactance 4-Poles," *Journal of Mathematics and Physics*, Vol. 18 (September, 1939), pp. 275–353.
[5] Vassiliadis, A. *Impedance Matching Limitations with Application to the Broadband Antenna Problem*, California: Stanford Research Institute Report, January, 1957.
[6] Guillemin, E. A. "A Summary of Modern Methods of Network Synthesis," in *Advances in Electronics*, New York: Academic Press Inc., Vol. 3, 1951.

Methods of Reducing Chromatic Aberration in Metal-Plate Microwave Lenses*

EDWARD K. PROCTOR†

Summary—**Microwave lenses of the waveguide type are subject to a pronounced degree of chromatic aberration because of the inherent dispersion of the waveguides. However, this aberration can be substantially eliminated over an appreciable bandwidth by making the lens of slot-loaded ridged waveguides with special properties. This type of lens design makes it possible to achieve additional benefits as well, such as improved scanning capability and elimination of discontinuities in the surfaces at the junction of adjacent "zones" or "steps." The ridged waveguides are periodically loaded by means of transverse slots in the ridges. The ridges may be relatively wide and hollow, or quite thin and solid. Additional desirable properties are obtainable by placing a relatively small strip of dielectric material above the ridge. Experimental data on the propagation characteristics of several of these structures and on the effect of varying such parameters as ridge height, slot width, slot depth, slot spacing, frequency, and size of dielectric strip are given.**

An analysis of the phase errors which result from changes in the operating frequency shows that the aberrations may conveniently be separated into one type in which the phase front from each zone of the lens is distorted, and a second independent type in which the desired phase relationship between the zones is destroyed. Methods of eliminating either or both of these types of aberration by suitable design of the ridged waveguides are described. In addition, it is shown how the ridged waveguides can conveniently be used to achieve "zoning" or "stepping" by changing the effective index of refraction, thereby eliminating discontinuities in the lens surfaces and avoiding the undesirable diffraction which would otherwise occur at the boundaries between adjacent zones. The superiority of this type of lens structure in wide-angle scanning applications is also discussed.

Numerical examples which illustrate the advantages of the loaded ridged waveguide lens are included.

* Manuscript received by the PGAP, October 7, 1957; revised manuscript received, March 27, 1958. The material presented here originally formed a portion of the "Final Engineering Report on Investigation of Variable Index of Refraction Lenses," September, 1952. The work was performed at the Sperry Gyroscope Co. under Signal Corps Contract No. DA 36-039-sc-15323.

† General Electric Microwave Lab., Palo Alto, Calif.

I. Introduction

MICROWAVE lenses of the waveguide type are subject to a pronounced degree of chromatic abberation (variation of focusing properties with change of frequency) because of the inherent dispersion of the waveguides of which the lens is comprised. This is readily apparent from the definition of the index of refraction for any waveguide of constant cross section,

$$n = \lambda_0/\lambda_g = [1 - (\lambda_0/\lambda_c)^2]^{1/2} \qquad (1)$$

in which λ_0 and λ_g are the wavelengths in space and in the waveguide, respectively, and λ_c is the cutoff wavelength of the waveguide. The surface contours of a lens are determined by the value of the index of refraction, so it is apparent that some defocusing will result if the operating wavelength is altered appreciably. In the design of optical lenses this difficulty is overcome by the use of compound lenses in which each of the several elements has a different amount of dispersion. It is therefore appropriate to inquire if analogous techniques can be used to advantage in the design of microwave lenses.

It is recognized, of course, that the class of artificial microwave dielectric materials, in which metallic or dielectric particles are placed in a supporting medium such as foamed polystyrene, generally have refractive indexes which vary only slightly over wide frequency ranges. However, these materials often have quite poor mechanical properties as compared to metal-plate lenses. It is desirable therefore, especially for military applications where good mechanical properties are essential, to overcome the difficulties caused by dispersion in a waveguide type lens.

In the ordinary type of waveguide lens mechanical tolerances and the rapid increase of dispersion near the cutoff wavelength make it impractical to achieve refractive indexes of much less than 0.5 or 0.6. Thus, in order to avoid excessive lens thickness at the outer edges, it is customary to zone the lens by introducing "steps" in one of the surfaces. The diffraction which inevitably occurs at these surface discontinuities evidently must upset the desired phase relations, and has been found to be a major cause of imperfect focusing and low aperture efficiency.

Another feature of ordinary waveguide lenses which sometimes limits performance, is that undesired, second-order reflected (or diffracted) waves can occur if the angle of incidence (or emergence) is improperly related to the spacing between adjacent plates of the lens. It can be shown that unless the wavelength, λ_0, the plate spacing, d, and the angle of incidence (or emergence), i, satisfy the inequality

$$\lambda_0/d > 1 + \sin i \qquad (2)$$

there will be a severe loss of power to the second-order reflected (or diffracted) waves. It should be noted, however, that decreasing the plate spacing, d, to satisfy (2) increases the amount of dispersion. It often happens that there is no reasonable compromise for practical values of i, especially in the case of scanning lenses.

The difficulties enumerated above led to consideration of periodic loading of waveguides in order to achieve indexes of refraction greater than unity, whose dispersion could be controlled in a desirable manner. It is apparent that with such waveguides it is possible to achieve the desired focusing action quite independently of the surface contours by varying the amount of loading from one waveguide to another. This makes it possible to choose the lens contours in such a manner that the wide-angle scanning properties of the lens are optimized. Methods of realizing this advantage are described in papers by Ruze,[1] and Proctor and Rees.[2] In addition, the desired zoning can be obtained by abrupt changes in the amount of loading, thereby avoiding undesirable discontinuities in the lens surfaces.

[1] J. Ruze, "Wide-angle metal-plate optics," PROC. IRE, vol. 38, pp. 53–59; January, 1950.

[2] E. K. Proctor and M. Rees, "Scanning lens design for minimum mean-square phase error," IRE TRANS. ON ANTENNAS AND PROPAGATION, vol. AP-5, pp. 348–355; October, 1957.

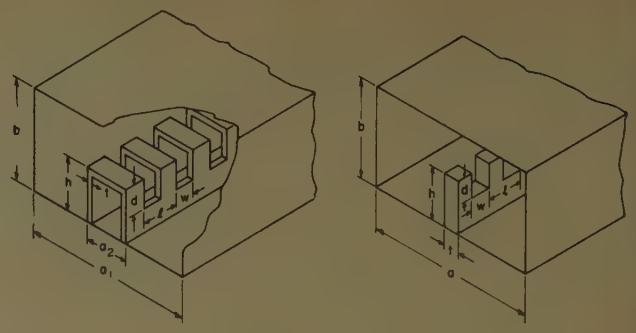

Fig. 1—Slot-loaded ridged waveguide. (a) Slotted-hollow-ridged waveguide. (b) Slotted-thin-ridged waveguide.

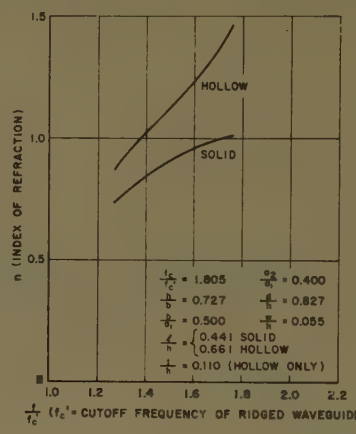

Fig. 2—Comparison of leaded hollow and solid-ridged waveguide.

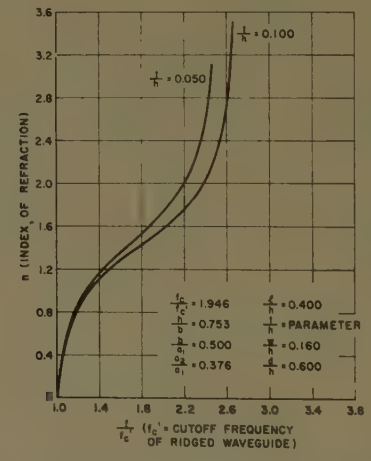

Fig. 3—Effect of varying ridge thickness in hollow-ridged waveguide.

II. Slot-Loaded Ridged Waveguides

Ridged waveguides have the desirable property that the outside dimensions may be made as small as desired without reaching a cutoff condition by choosing a ridge of appropriate size. Thus, a ridged waveguide lens can be made to satisfy (2) for any angle of incidence ($i \leq 90°$) without causing undue dispersion. In addition, it has been found that ridged waveguides may be loaded by means of slots in the ridges to achieve an interesting and useful variety of indexes of refraction. The two

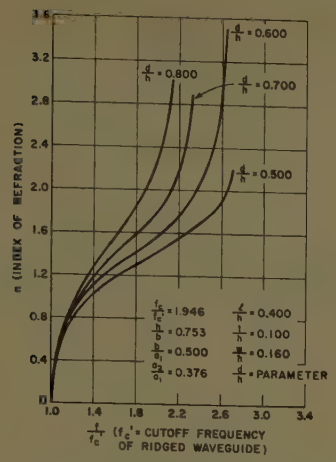

Fig. 4—Effect of varying slot depth in hollow-ridged waveguide.

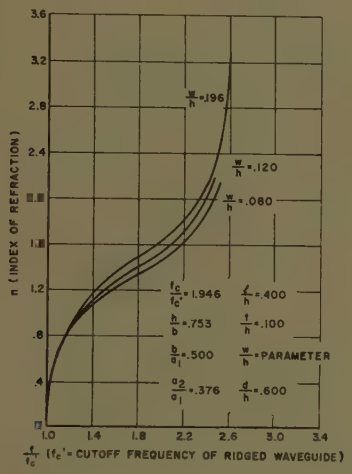

Fig. 5—Effect of varying slot width in hollow-ridged waveguide.

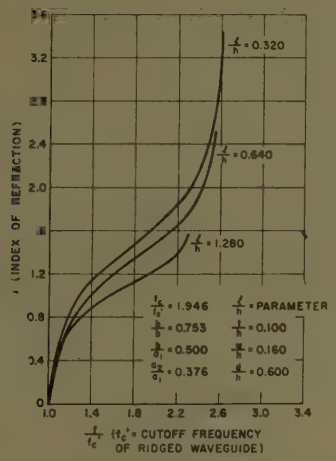

Fig. 6—Effect of varying slot spacing in hollow-ridged waveguide.

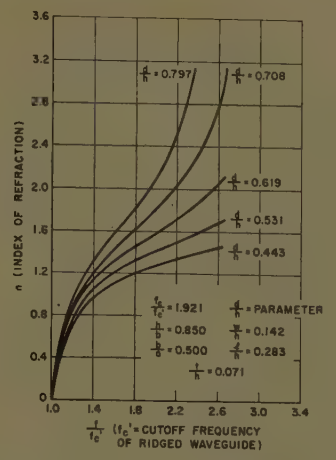

Fig. 7—Effect of varying slot depth in thin-ridged waveguide.

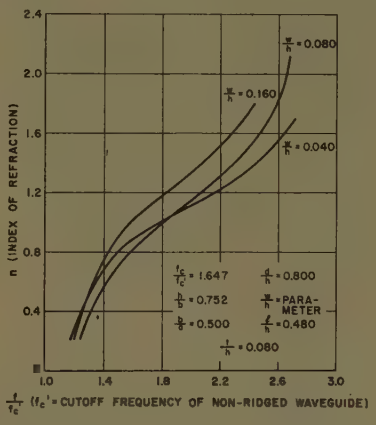

Fig. 8—Effect of varying slot width in thin-ridged waveguide.

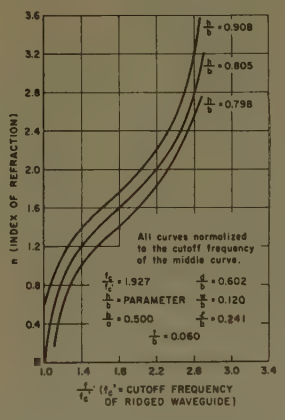

Fig. 9—Effect of varying ridge height in thin-ridged waveguide (all curves normalized).

most useful configurations and their pertinent dimensions are shown in Fig. 1. It should be noted in Fig. 1(a) that the ridge is hollow and has thin walls. The advantages of the hollow ridge as compared to an identical solid ridge are shown in Fig. 2, where it can be seen that identical slots produce a larger index of refraction in the hollow ridge. Fig. 3 shows that the index of refraction is increased as the ridge walls are made thinner. Figs. 4 through 6 show the effects of varying the slot depth, width, and spacing, respectively. Figs. 7 and 8 show the effects of changing the slot depth and width in the thin-ridged waveguide of Fig. 1(b), and Fig. 9 shows the effect of varying the ridge height.

Since the electric field in a ridged waveguide is most intense above the ridge, it was suspected that filling this space with a dielectric material would increase the index

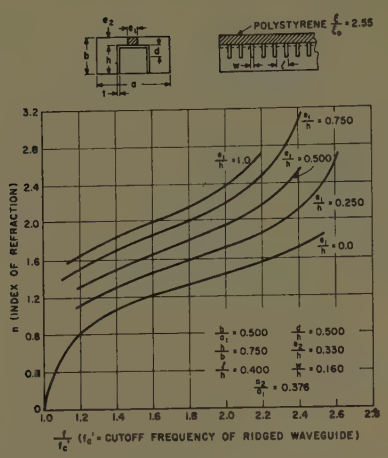

Fig. 10—Effect of dielectric placed on top of loaded hollow ridge.

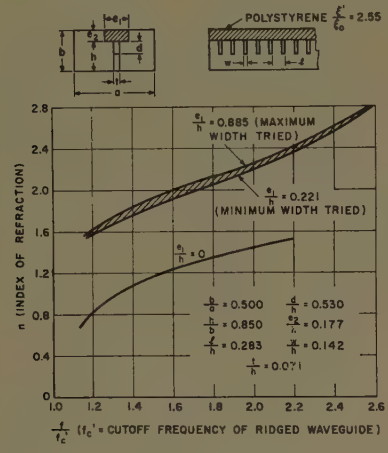

Fig. 11—Effect of dielectric placed on top of loaded thin ridge.

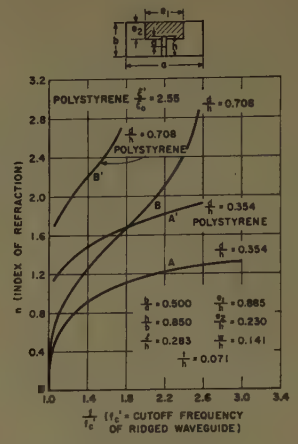

Fig. 12—Effect of dielectric placed on top of loaded ridge.

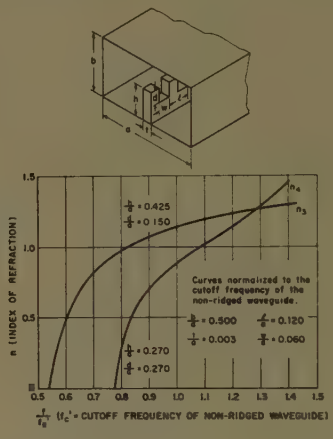

Fig. 13—Index of refraction curves for compensation of δ_d.

of refraction about as much as would result from completely filling the waveguide. Fig. 10 shows that this is indeed the case. In fact, for a dielectric strip of width equal to that of the ridge, the index of refraction is increased at some points by more than the square root of the dielectric constant of the added material. Furthermore, it can be seen that the value of the index of refraction can readily be altered by reducing the width of the dielectric strip. Similar results may be obtained by locating a strip of dielectric material above a thin-ridged waveguide, as shown in Fig. 11, but in this case the dependence of the index of refraction on the width of the strip is much less pronounced.

Finally, the effects of dielectric strips above slotted thin ridges of two different heights are demonstrated in Fig. 12. The curves, labeled A and B, which intersect each other will be of particular interest in the following discussion of reduction of chromatic aberration. Another pair of intersecting curves, obtained without dielectric loading, is shown in Fig. 13.

These curves demonstrate that values of index of refraction up to about three can be obtained quite readily. The slopes of these curves, which indicate the degree of dispersion, vary over quite a wide range and make it possible to design achromatic microwave lenses.

III. Analysis of Chromatic Aberration

The lens shown in Fig. 14 is of a completely general type in the sense that the equiphase surface which it is designed to produce, as well as the two lens surfaces, are completely arbitrary. No loss of generality is involved in the assumption of a point feed located at an arbitrary position. The lens is a special one because each waveguide of the lens is assumed to be divided into portions of lengths D_1 and D_2, having indexes of refraction n_1 and n_2, respectively, which can vary from cell to cell within the lens. The envelope of the boundary between these two regions is shown by a dashed line in Fig. 14. This assumption is not very restrictive in practice since the effective index of refraction, n, of a cell of length

$$D = D_1 + D_2 \tag{3a}$$

is determined by

$$nD = n_1D_1 + n_2D_2. \tag{3b}$$

For a given value of D, any desired value of n can be realized by infinitely many combinations of D_1, D_2, n_1, and n_2. As a matter of good engineering practice, one would ordinarily make n_1 as small as possible by using a non-loaded section of ridged waveguide and n_2 as large as possible by selecting one of the slot-loaded configurations of Figs. 4 through 13.

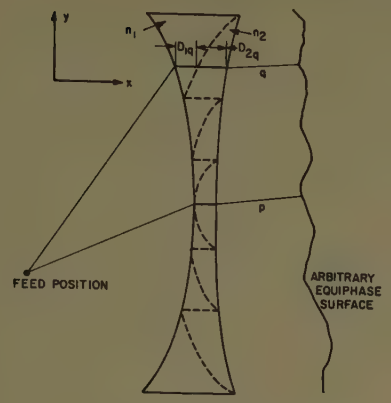

Fig. 14—Section of microwave lens.

Suppose that the lens has been designed to produce some arbitrary but specified equiphase surface which it is desired to maintain over some range of operating wavelengths. Such a design must specify, in accordance with criteria independent of the wavelength, the shapes of the two lens surfaces and the value of n for each cell. Hence, n and nD may be regarded as known quantities for each of the waveguides in the lens. However, among the infinitely many available choices of n_1, n_2, D_1, and D_2 there are some which minimize the amount of chromatic aberration.

Consider two arbitrary cells of the lens, p and q. The phase shifts from the feed point to the equiphase surface along the paths which pass through these cells must be equal, or, if the lens is zoned as shown in Fig. 13, they can differ only by an integer multiple, N, of 2π. In terms of equivalent path lengths these facts can be expressed by

$$(K_p + n_{1p}D_{1p} + n_{2p}D_{2p}) - (K_q + n_{1q}D_{1q} + n_{2q}D_{2q}) + N\lambda_0 = 0, \quad (4)$$

in which K_p and K_q are the space portions of the paths, and the other quantities are as indicated in Fig. 14. At a different wavelength, λ_0', the indexes of refraction have different values, n_1' and n_2', and the equiphase surface is in general distorted from its desired contour. The path-length error caused by the change in wavelength is given by

$$\delta = (K_p + n_{1p}'D_{1p} + n_{2p}'D_{2p}) - (K_q + n_{1q}'D_{1q} + n_{2q}'D_{2q}) + N\lambda_0'. \quad (5)$$

Subtracting (4) from (5) yields

$$\delta = D_{1p}\Delta n_{1p} + D_{2p}\Delta n_{2p} - D_{1q}\Delta n_{1q} - D_{2q}\Delta n_{2q} + N(\lambda_0' - \lambda_0) \quad (6)$$

in which $\Delta n = (n' - n)$ with appropriate subscripts. It can be seen that δ is composed of one part which is independent of N and of a second part which is independent of the change in index of refraction. Let

$$\delta_d = D_{1p}\Delta n_{1p} + D_{2p}\Delta n_{2p} - D_{1q}\Delta n_{1q} - D_{2q}\Delta n_{2q} \quad (7)$$

and

$$\delta_s = N(\lambda_0' - \lambda_0) \quad (8)$$

represent the contributions from dispersion and the "steps" or zones, respectively, and consider what can be done to eliminate each factor separately.

IV. Reduction of Chromatic Aberration Due to Dispersion

The path-length error attributable to dispersion alone is readily eliminated at the wavelength λ_0' by setting $\delta_d = 0$ in (7). This yields the expression

$$D_{1p}\Delta n_{1p} + D_{2p}\Delta n_{2p} = D_{1q}\Delta n_{1q} + D_{2q}\Delta n_{2q}. \quad (9)$$

Without loss of generality, cell p may be considered as a fixed reference cell which, for convenience, can be chosen as one of the several cells which has refractive index n_2 throughout its length. For this cell $D_{1p} = 0$ and its known length, D_{2p}, may be relabeled D_0. Rewriting (9) to incorporate these changes and recalling (3a) and (3b), there are only three equations to be satisfied for the qth cell, namely,

$$D_q = D_{1q} + D_{2q}, \quad (10)$$

$$n_q D_q = n_{1q}D_{1q} + n_{2q}D_{2q}, \quad (11)$$

and

$$D_{1q}\Delta n_{1q} = D_0\Delta n_{2p} - D_{2q}\Delta n_{2q}. \quad (12)$$

Since there are seven unknown quantities, D_{1q}, D_{2q}, n_{1q}, n_{2q}, Δn_{2p}, Δn_{1q}, and Δn_{2q}, it is possible to choose four of them arbitrarily.

From a practical engineering point of view, it is advantageous to choose particular values of n_{2q} and Δn_{2q} from one of the curves of Figs. 3 through 13 and use them for all cells of the lens in order to avoid having a different type of loading for each cell. This determines n_{2q}, Δn_{2q}, and Δn_{2p}. It is also convenient to obtain n_{1q} by using a nonloaded section of ridged waveguide. If this is done, both n_{1q} and Δn_{1q} are determined by the cutoff wavelength of the ridged waveguide in accordance with (1). Graphs relating cutoff wavelength to ridge size have been prepared by Cohn[3] and, more recently, by Hopfer.[4] This disposition of the fourth choice generally requires that the ridge height used for the nonloaded portion vary from cell to cell, but it does not appear possible to find an easier or simpler solution. The remaining quantities may be determined from (10)–(12).

V. Reduction of Chromatic Aberration Due to Zoning

The component of phase error due to the presence of zones or "steps" has been defined in (8) as

$$\delta_s = N(\lambda_0' - \lambda_0). \quad (8)$$

[3] S. B. Cohn, "Properties of ridge wave guide," Proc. IRE, vol. 35, pp. 783–788; August, 1947.
[4] S. Hopfer, "The design of ridged waveguides," IRE Trans. on Microwave Theory and Techniques, vol. MTT-3, pp. 20–29; October, 1955.

It is interesting to observe that this component is an inherent consequence of zoning and has nothing to do with the dispersion of the dielectric medium. The manner in which this phase error arises and an approach to its elimination are indicated in Fig. 15. For simplicity, a lens designed to generate a plane equiphase surface is considered. The solid lines in Fig. 15 indicate the relations between the segments of equiphase surfaces from different zones of the lens at the design wavelength, λ_0. Assuming that there is no dispersion in the lens, the thin dashed lines represent the actual conditions and the heavy dashed lines indicate the desired conditions at a longer wavelength, λ_0'. The important thing to note in Fig. 15 is that at the new wavelength, λ_0', the equiphase surfaces from adjacent zones are separated by the original wavelength, λ_0, instead of by λ_0' as is desired. Thus, the equiphase segment from zone 1 is in error by an amount $\delta_{s1}=(\lambda_0'-\lambda_0)$ and that from zone 2 by $\delta_{s2}=2(\lambda_0'-\lambda_0)$, in accordance with (8). For a ten per cent increase in wavelength and a lens having six zones, the result of the step phase error given by (8) would make the energy from the outermost zone a half wavelength out of phase with that from the central portion of the lens. This error can be partially compensated by refocusing the feed, but this is usually impossible or undesirable in practice and, in addition, produces other components of phase error within each zone. As an indication of the importance of δ_s, the author determined by experiment on a particular zoned lens that the gain at a wavelength differing from the design value by about five per cent could be increased by 1.5 to 2.0 db by refocusing the feed. Furthermore, the amount of refocusing required to maximize the gain was almost exactly the amount theoretically needed to bring the outer stepped portion back in phase with the center portion.

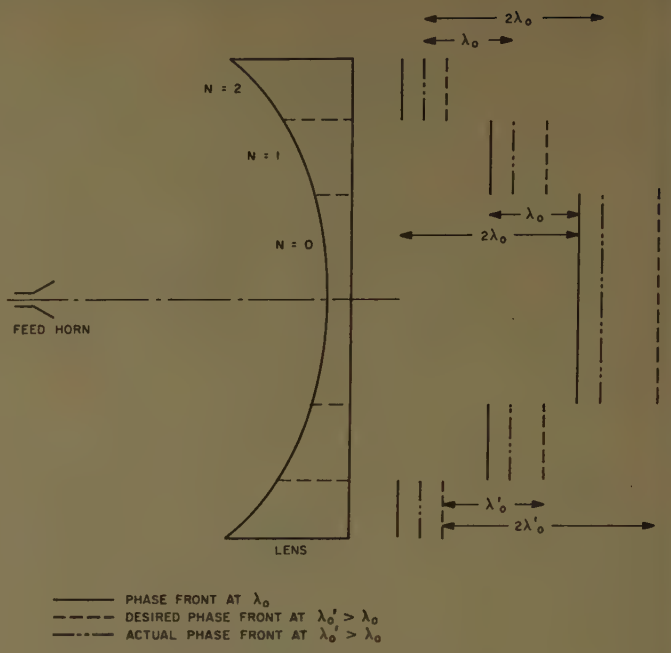

Fig. 15—Step phase errors for $\lambda_0'>\lambda_0$.

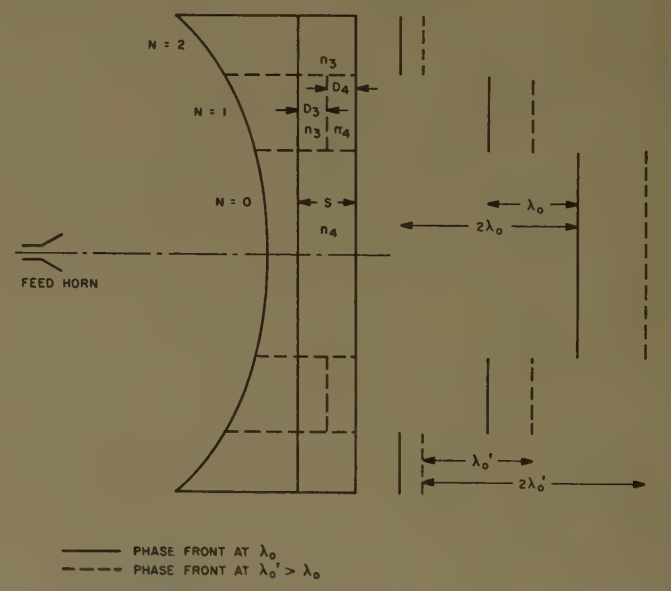

Fig. 16—Lens compensated for step phase errors.

The step phase error may be completely eliminated by adding a fixed length, S, to each waveguide, as indicated in Fig. 16. Let S be divided into portions of length D_3 and D_4 having refractive indexes n_3 and n_4 and such that

$$S = D_3 + D_4. \tag{13}$$

The lengths D_3 and D_4 may vary from one zone to another but not within a zone. The refractive indexes n_3 and n_4 are to have the same values in all zones. If $n_3=n_4$ at the design wavelength, λ_0, the net effect of the added section is to advance the equiphase surfaces from all zones by the uniform amount $n_3S=n_4S$. However, at a different wavelength, λ_0', where the refractive indexes have the values n_3' and n_4', with $n_3'\neq n_4'$, the equiphase surfaces will be advanced by amounts depending upon the values of $n_3'D_3$ and $n_4'D_4$. For zero step phase error at the wavelength λ_0', the equation

$$n_4'S - (n_3'D_3 + n_4'D_4) + \delta_s = 0 \tag{14}$$

must be satisfied. Substituting for δ_s from (8) and for D_4 from (13), (14) becomes

$$n_4'S - (n_3'D_3 + n_4'S - n_4'D_3) + N(\lambda_0' - \lambda_0) = 0, \tag{15}$$

which can be solved to yield

$$D_3 = \frac{N(\lambda_0 - \lambda_0')}{(n_4' - n_3')}. \tag{16}$$

For $N=0$, $D_3=0$ and $D_4=S$. For $N=N_{max}$, where N_{max} is the largest value of N for which compensation is desired,

$$D_3 = \frac{N_{max}(\lambda_0 - \lambda_0')}{(n_4' - n_3')} = S. \tag{17}$$

It is not essential that $n_3=n_4$ at the design wavelength, λ_0, provided the slopes are appropriately dif-

ferent, but a constant-thickness compensating section cannot be used unless $n_3=n_4$. In addition, if $n_3\neq n_4$, the design of the focusing portion of the lens is affected. Eq. (15) and the requirement that $n_3=n_4$ specify that the curves of n_3 and n_4 vs frequency must intersect with different slopes at the design wavelength, λ_0. The amounts of dispersion for n_3 and n_4 near the wavelength at which they intersect is not specifically determined, since $S=D_3+D_4$ can be chosen to fit the obtainable amounts of dispersion. Figs. 12 and 13 demonstrate that indexes of refraction which vary with frequency in the required manner can be obtained by suitable choices of loading methods. It should be possible to obtain a variety of desirable dispersion and cross-over characteristics by the methods described earlier.

VI. Alternative Method of Analysis

The preceding simple algebraic analysis leads to a clear understanding of the way in which chromatic aberration arises and points directly to effective engineering methods of overcoming the difficulties. Although the following alternative analysis does not lend itself as readily to a physical interpretation, it illuminates the subject from a slightly different point of view and may prove to be useful.

Consider Fig. 14 again and recall (4),

$$(K_p + n_{1p}D_{1p} + n_{2p}D_{2p}) - (K_q + n_{1q}D_{1q} + n_{2q}D_{2q}) + N\lambda_0 = 0. \quad (4)$$

As in the previous section, let $D_{1p}=0$, $D_{2p}=D_0$, $n_{2p}=n_{2q}=n_2$. Letting $K_q-K_p=\Delta K$, adding and subtracting the quantity n_2D_{1q}, and making use of the identity $D=D_{1q}+D_{2q}$, (4) becomes

$$n_2(D_0 - D) + D_{1q}(n_2 - n_{1q}) + N\lambda_0 - \Delta K = 0. \quad (18)$$

The desired achromatic property may be expressed as a requirement that the derivative of (18) with respect to λ_0 also be zero. Since n_{1q} and n_2 are the only quantities which depend upon the wavelength, the differentiation leads to

$$\frac{dn_2}{d\lambda_0}(D_0 - D) + D_{1q}\left[\frac{dn_2}{d\lambda_0} - \frac{dn_{1q}}{d\lambda_0}\right] + N = 0. \quad (19)$$

Since (18) and (19) must both be satisfied for an achromatic lens, they can be combined to eliminate D_{1q}. The resultant equation is

$$[\Delta K + n_2(D - D_0) - N\lambda_0]\left[\frac{dn_2}{d\lambda_0} - \frac{dn_{1q}}{d\lambda_0}\right] = \left[\frac{dn_2}{d\lambda_0}(D - D_0) - N\right](n_2 - n_{1q}). \quad (20)$$

The quantities ΔK, D, D_0, N, and λ_0 are presumed to be known. The remaining terms, n_{1q}, n_2, $dn_{1q}/d\lambda_0$, and $dn_2/d\lambda_0$, can be chosen to satisfy both the focusing requirements and the condition for achromaticity given by (20). If n_2 and $dn_2/d\lambda_0$ are chosen in any convenient manner, the additional requirement that n_{1q} be obtained from a nonloaded ridged waveguide suffices to determine the cutoff wavelength and hence the size of the nonloaded ridge. By using (1) and its derivative in (20) one can even obtain an explicit expression for the cutoff wavelength, but it is too unwieldy to be of much practical value.

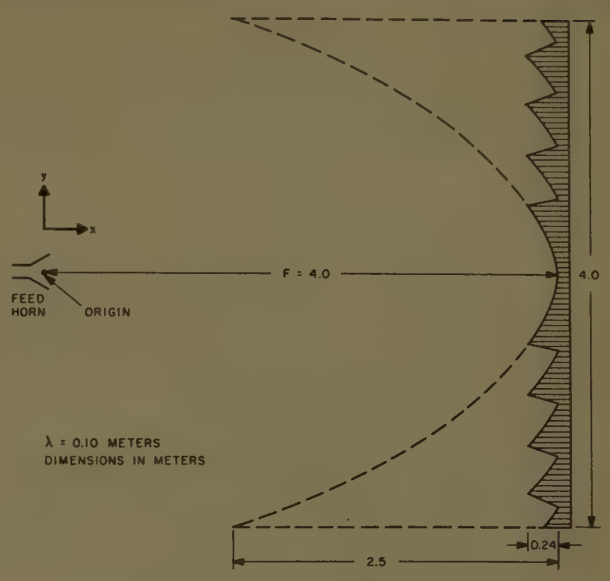

Fig. 17—Conventional waveguide lens.

There is very little of a general nature that can be obtained by further manipulation of (20). However, the equation shows that the components of phase error due to dispersion and to the presence of zones can be eliminated simultaneously in the focusing portion of the lens; it is not necessary to add a special section to compensate for the step phase errors if appropriate values of n_{1q}, n_2, $dn_{1q}/d\lambda_0$, and $dn_2/d\lambda_0$ are selected for each zone of the lens.

VII. Numerical Examples

Some simple numerical comparisons will serve to illustrate the advantages of the achromatic loaded ridged waveguide lens as compared to the conventional waveguide lens. For simplicity, the comparison will be made between two functionally similar "line-source" lenses designed to produce plane phase fronts. The conventional lens is shown in Fig. 17 and is taken to be a "constrained" lens; *i.e.*, the lens plates and the electric field are perpendicular to the plane of the figure so that all ray paths through the lens are of necessity parallel to the x axis.

For a point source located at the origin, the requirement of equal phase shifts along all ray paths through the lens may be expressed as

$$F = \sqrt{x^2 + y^2} + n(F - x) - N\lambda_0, \quad (21)$$

in which F is the focal length of the lens, n is the index of refraction given by (1), and x and y are the coordi-

nates of the envelope of the illuminated surface of the lens. Eq. (21) may be rearranged to yield

$$\frac{(x/F - n\alpha)^2}{\alpha^2} + \frac{(y/F)^2}{\alpha^2(1-n^2)} = 1 \tag{22}$$

with

$$\alpha = \left[\frac{1 - n + N\lambda_0/f}{1 - n^2}\right]. \tag{23}$$

It can be seen from (22) that each value of N determines an ellipse having one focus at the origin, and that all these ellipses have an eccentricity of $(1-n^2)$.

Consider now the special case of a 3000-mc lens having an aperture width of 40 wavelengths, a focal-length-to-aperture ratio of unity, and an index of refraction of $n=0.60$. If the lens is not zoned there will be no step phase errors and the illuminated surface will be as shown by the dotted lines in Fig. 17. By setting $N=0$ and $y=2$ meters in (22) and (23), the edge thickness of the lens is readily found to be 2.5 meters exclusive of the center thickness. If the lens is zoned as shown by the solid lines in Fig. 17, the horizontal distance from the center to the point at which the zone $N=0$ ends is 0.24 meter, and the thickness at the ends of the other zones is approximately the same. Over a 20 per cent bandwidth centered at 3000 mc the index of refraction, given by (1), varies from $n=0.458$ to $n=0.687$. The corresponding phase errors at the outside edges of the center zone may be determined from (7) and are 82.7° and 110.5°, respectively, at the upper and lower frequency extremes. Also, the lens contains four full zones and one partial zone. Setting $N=4$ in (8) results in a step phase error of 142.5° at either end of the frequency band. It is apparent that both the dispersion and the step phase errors are so large that the focusing properties of such a lens would deteriorate seriously at the extremities of a 20 per cent bandwidth.

For simplicity, the loaded lens chosen for comparison with the conventional lens is a lens of constant thickness as shown in Fig. 18. The wavelength, aperture width, and focal length have the same values as in the preceding example. The reference cell, p, is taken to be the center cell of the lens. As discussed earlier, it is advantageous to use the same value of n_2 in all cells of the lens. Since the lens is of constant thickness and $n_{2p}=n_{2q}=n_2$, (12) reduces to the simple requirement that

$$\Delta n_1 = \Delta n_2 \tag{24}$$

in order to eliminate δ_d. It is helpful to choose from among the many possible loading curves of Fig. 2 through Fig. 13 one which provides a large value of n_2 and a small value of Δn_2. The upper curve of Fig. 11 meets these requirements about as well as any. Anticipating the need for a pair of intersecting curves later

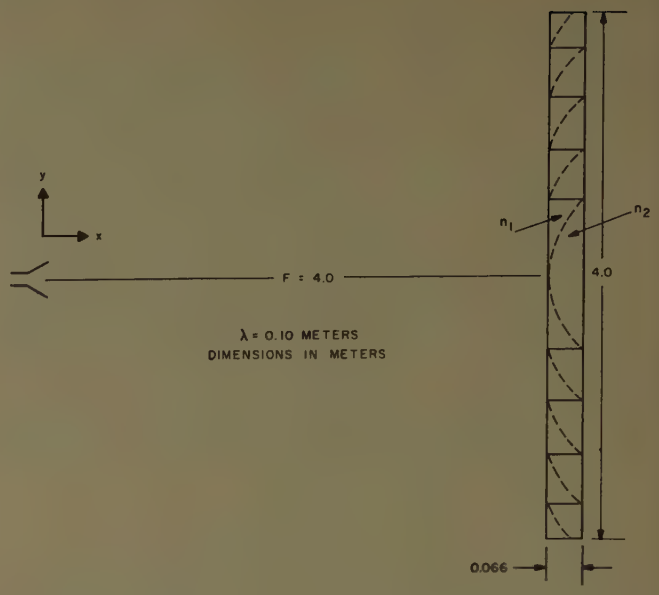

Fig. 18—Constant-thickness loaded lens.

on for elimination of δ_s, and noting that the cross-over point in Fig. 12 is at $f/f_c'=1.82$, it is necessary to choose $f/f_c'=1.82$ in Fig. 11 as the center frequency in order to have cells of the same size in both the focusing and step-compensating sections of the lens. This choice determines the cutoff frequency of the waveguide cells and hence all the physical dimensions, including the slot dimensions, as well as the values of Δn_2 for plus and minus 10 per cent changes in frequency. In the current example, the cutoff frequency is 1650 mc.

In selecting an index-of-refraction curve for n_1, it should be noted that the lens thickness is decreased as the difference between n_2 and n_1 is increased. This advantage, plus appreciable simplification of construction, may be realized by adopting a nonloaded section of ridged waveguide for n_1. In order to determine the cutoff frequency, and hence the required ridge height, which will cause the slope of n_1 to match the slope of n_2 as required by (22), it is helpful to plot the n_2 curve from Fig. 11 and the n_1 curve from (1) on separate graphs having logarithmic abscissas. The slopes may then be matched graphically by sliding the two graphs relative to each other and the ratio of cutoff frequencies is readily determined. For this example, a cutoff frequency of 2390 mc satisfies (24) as closely as is possible over the 20 per cent band.

The values of n_1, n_2, and (n_2-n_1) as determined by these choices are given in Table I.

TABLE I
VALUES OF INDEX OF REFRACTION

Frequency	2700	3000	3300
n_2	2.00	2.13	2.22
n_1	0.47	0.61	0.69
(n_2-n_1)	1.53	1.52	1.53

The lens thickness, D_0, may now be determined by observing that the differential phase shift for rays passing just above and below a zone boundary must be one wavelength. Hence, at the center frequency,

$$D_0(n_2 - n_1) = \lambda_0. \tag{25}$$

For the present example, $\lambda_0 = 0.10$ meter and $(n_2 - n_1) = 1.52$, so $D_0 = 0.0658$ meter. Since $D_{1p} = 0$, $D_{2p} = D_0$, and $D_{2q} = D_0 - D_{1q}$, (6) reduces to

$$\delta_d = D_{1q}(\Delta n_2 - \Delta n_1). \tag{26}$$

Since $D_{1q} \leq D_0$, the maximum value of δ_d occurs at the step boundaries. From the values in Table I, the maximum phase error due to dispersion is found to be 2.6° at either extremity of the 20 per cent frequency band.

It should be noted that the zoned conventional lens not only has from 32 to 42 times as much dispersion phase error, but is also over three times as thick. The step phase error of the loaded lens, however, will be just as large (142.5°) as that of the conventional lens unless remedial measures are used. Since there are only five zones, the simplest remedy is to eliminate the steps by making the lens five times as thick, resulting in a uniform thickness of 0.329 meter. This also multiplies the residual dispersion phase by five to yield a value of 13° at the band edges.

The step phase errors may also be reduced by adding a compensating section as described in Section IV. The values of n_3 and n_4 from Fig. 12 at the highest and lowest frequencies are given in Table II. From (16), using $N_{max} = 4$, the required thickness of the compensating section is found to be $S = 0.4$ meter. The total thickness of the lens is thus $S + D_0 = 0.466$ meter, which is somewhat greater than that of a nonzoned loaded lens. The thickness of the compensating section could be reduced by developing loading structures which provide curves that cross each other with a greater difference of slope.

TABLE II
VALUES OF n FOR COMPENSATING SECTION

Frequency	2700 mc	3300 mc
n_4	1.62	1.87
n_3	1.51	1.76
$(n_4 - n_3)$	0.11	0.11

VIII. Conclusions

The author would be the last to claim that the methods of designing and constructing microwave lenses described in this paper are as simple and elegant in practice as they appear to be in theory. There is no doubt that such lenses can be difficult to construct, and, for some applications, rather heavy and expensive. In addition, there are certain problems relating to impedance matching at the several interfaces which have not been considered in this paper. However, there are reasonable and practical ways of overcoming these difficulties which are described in a publication by Smedes.[5] His paper is especially noteworthy because it describes an extremely ingenious method of fabrication which overcomes many of the apparent difficulties. It also describes a means of reducing the surface reflections to acceptable levels. In addition, the paper provides excellent experimental confirmation of the predictions that a lens of this type would have superior focusing properties over a relatively wide band of frequencies and for a wide angle of scan.

[5] R. L. Smedes, "High efficiency microwave lens," 1956 IRE Convention Record, pt. 1, pp. 208–212.

Corrective Line Sources for Paraboloids*

C. J. SLETTEN†, R. B. MACK†, W. G. MAVROIDES†, AND H. M. JOHANSON†

Summary—By applying optical laws and ray tracing techniques to paraboloidal reflectors, it has been possible to derive the focusing and phasing criteria for obtaining wide angle performance of a paraboloidal microwave antenna system. Although this optics approach represents an approximation to the exact solutions, the experimental results indicate it is satisfactory for practical uses.

The analysis indicates the sections of the paraboloidal reflecting surface best suited to line source correction. The reflector peripheral contour which tends to minimize sidelobes has been indicated.

Two types of midpoint correctors are discussed. These will produce beams fanned in the elevation plane and well focused in the azimuth plane. Experimental results are presented from a midpoint corrector covering 60 degrees in elevation while maintaining well focused azimuth patterns over the entire elevation interval.

Several pencil beams may be produced using one reflector by placing ridge line correctors at the appropriate angles on the focusing surfaces.

* Manuscript received by the PGAP, July 3, 1957; revised manuscript received, March 10, 1958.

† Antenna Lab., Electronics Res. Directorate, Air Force Cambridge Res. Center, Air Res. and Dev. Command, Bedford, Mass.

I. Introduction

MICROWAVE antennas are frequently required to produce a beam that is narrow in one plane (usually azimuth) and fanned to a specific shape in the perpendicular (elevation) plane. The paraboloidal reflector is generally considered to be unsuitable for generating such complicated patterns because it is subject to large optical aberrations away from the geometric focus.

Upon analyzing the paraboloid one finds it is possible to correct for these aberrations by using line sources whose design is based on equations derived to find the elevation and azimuth focusing loci. Beams fanned to cover 60° in elevation, while still having good azimuth focusing characteristics, have been built. Also, several pencil beams in specified directions can be produced by using a reflector with off-axis correcting feeds.

In Section II of this paper the results of the analysis of the paraboloid are summed up and shown graphically. The engineering details for array and pillbox line-source feeds worked out from the optical results are described in Section III . Applications emphasize two new devices called *midpoint correctors* and *ridge-line correctors.*

II. Optical Theory of the Paraboloid

A. Analytical Approach

Although the paraboloidal reflector has been a leading design in microwave antennas since the beginning of radar, its wide-angle focusing properties have not been fully explored. This formulation of the optics of the paraboloid for specific application in microwave antenna design has been far from complete or exhaustive but it has revealed several characteristics of the reflector that are useful in pattern synthesis.

Diffraction theory, concisely expressed by Fourier transforms,[1] can be applied to predict pattern characteristics when geometric optic aberrations are small or absent, but not when the phase is substantially distorted. Improved computational techniques to speed the solution of patterns of a parabolic cylinder were reported by Allen.[2] Paraboloid patterns, however, present another magnitude of computational complexity.[3]

In order to use the Fourier transform method in reflector optics, the antenna is treated as a transmitter. A point source is assumed to be radiating at some position near the geometric focus. The preliminary step in determining the antenna pattern is to find the phase and amplitude on a convenient aperture plane through the use of geometric optics. This is not easy where a parabola or paraboloid is concerned, since it is difficult to express the phase distribution as an explicit function of the aperture coordinate. This is only the preliminary step, for these functions must then be summed over the aperture plane. A series derived from an approximate aperture phase function is discussed in Section II-B, 2.

Many features of the far-field pattern can be interpreted through optical analysis alone. From our analysis of radiation from a point source near the focus and reflected from the paraboloid, one can adduce which focusing regions are best. It was not until (see Section II-C), the reflector was analyzed as a receiving antenna, however, that continuity appeared in the picture of the focusing loci and the relative phase in different focal regions. The information obtained from analysis of the reflector as a receiving antenna has been most useful in beam synthesis.

B. The Paraboloid as a Transmitting Antenna

1) *Ray Analysis:* When a point source is placed at the geometric focus of a paraboloid, all the rays are reflected parallel with the axis of the paraboloid. When the source is off focus, the reflected wavefront has a characteristically cubic term, which shows up in the pattern aberration known as coma. If the source is displaced to a point $(0, y_0, z_0)$, one can write equations for the direction cosines of the reflected rays. To use zero as one of the source coordinates is permissible since a paraboloid is a surface of revolution. Results reported in this paper apply only to systems that are symmetric with respect to the yz plane, and not to those in which asymmetry exists because of source polarization or the use of asymmetric sections of the paraboloid. From the coordinates and ray directions in Fig. 1, we proceed to derive expressions for the direction cosines of the reflected rays as functions of the coordinates x, y, and z on the paraboloid, as follows.

The unit vector $\hat{S}_1$, for the distance (L_1) from the source to the reflector, measured along the incident ray, is

$$\hat{S}_1 = \frac{x}{L_1}\hat{\imath} + \frac{(y - y_0)}{L_1}\hat{\jmath} + \frac{(z - z_0)}{L_1}\hat{k}, \tag{1}$$

and

$$\hat{S}_1 = l_1\hat{\imath} + m_1\hat{\jmath} + n_1\hat{k},$$

where

$$L_1 = \sqrt{x^2 + (y - y_0)^2 + (z - z_0)^2}. \tag{2}$$

The unit vector along the outward normal is

$$\hat{\eta} = \frac{x\hat{\imath}}{\sqrt{x^2 + y^2 + 4F^2}} + \frac{y\hat{\jmath}}{\sqrt{x^2 + y^2 + 4F^2}} + \frac{2F\hat{k}}{\sqrt{x^2 + y^2 + 4F^2}} = l\hat{\imath} + m\hat{\jmath} + n\hat{k}, \tag{3}$$

[1] R. C. Spencer, "Fourier Integral Methods of Pattern Analysis," Mass. Inst. Tech., Cambridge, Mass., Rad. Lab. Rep. No. 762-1; 1946.

[2] C. C. Allen, "Antenna Pattern Calculation for Asymmetrical Aperture Distributions," Naval Res. Lab., Washington, D. C., Rep. No. 4043, p. 30; April, 1952.

[3] "Calculation of the Caustic Surface When the Reflecting Surface is a Paraboloid of Revolution and the Incoming Rays are Parallel," Parke Mathematical Labs., Concord, Mass., Study No. 3, Contract No. AF19(122)-484; February, 1952.

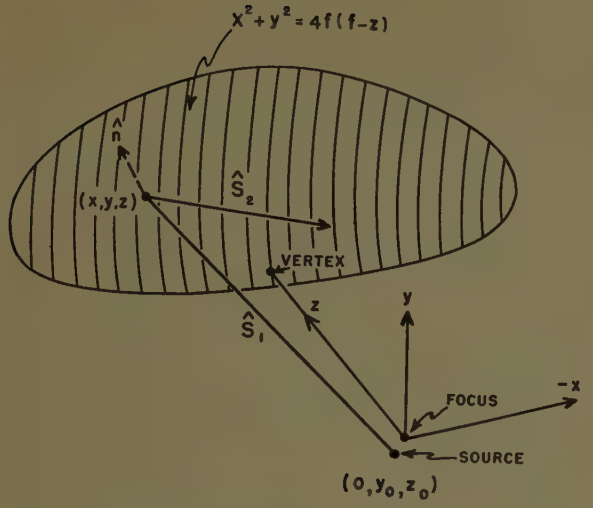

Fig. 1—Coordinate system for analyzing paraboloid as a transmitting antenna.

where F is the focal length. The vector formulation for Snell's law of reflection can be written

$$\hat{S}_2 = \hat{S}_1 - 2(\hat{\eta}\cdot\hat{S}_1)\hat{\eta} = l_2\hat{\imath} + m_2\hat{\jmath} + n_2\hat{k}, \tag{4}$$

and substituting for $\hat{S}_1$ and $\hat{\eta}$, we get

$$l_2 = l_1 - 2(ll_1 + mm_1 + nn_1)l, \tag{5a}$$

$$m_2 = m_1 - 2(ll_1 + mm_1 + nn_1)m, \tag{5b}$$

$$n_2 = n_1 - 2(ll_1 + mm_1 + nn_1)n; \tag{5c}$$

or, in terms of coordinates on the dish, the direction cosines of the reflected rays are

$$\cos\alpha_x = l_2 = \left[\frac{2Fz_0 + yy_0}{4F^2 - 2Fz}\right]\frac{x}{L_1}, \tag{6a}$$

$$\cos\alpha_y = m_2 = \left[\frac{2Fz_0 + yy_0}{4F^2 - 2Fz}\right]\frac{y}{L_1} - \frac{y_0}{L_1}, \tag{6b}$$

$$\cos\alpha_z = n_2 = \left[\frac{2Fz_0 + yy_0}{2F - z}\right]\frac{1}{L_1} + \frac{z - z_0 - 2F}{L_1}, \tag{6c}$$

$$\cos^2\alpha_x + \cos^2\alpha_y + \cos^2\alpha_z = 1.$$

It is therefore possible to make l_2 equal to zero, that is, to have no divergence of azimuth ray components, for one value of y only. This means that a strip across the reflector at a height y_m can be made free of azimuth ray deviation by placing source points along the line.

$$x_0 = 0,$$

$$z_0 = -\frac{y_0 y_m}{2F}. \tag{7}$$

This line lies in the yz plane and passes through the focus point (0, 0, 0) with a slope

$$\frac{z_0}{y_0} = -\frac{y_m}{2F}. \tag{8}$$

Also, from (6a) note that the azimuth components of reflected rays are always zero along the strip $x=0$. To find the feed coordinates $(0, y_0, z_0)$ for a beam that will have a minimum spread in the x or aximuth plane, the designer must first ascertain which azimuth strip y_m on the paraboloid section needs to be corrected. The correction strip is usually located where the reflector is widest in the x dimension, across a region of the dish maximally illuminated, and deviation of rays can be plotted on the reflector.[4] In this problem, geometric optics has an advantage over more refined studies because it serves to localize the region of the reflector causing pattern deterioration.

For example, with a symmetric reflector and the illumination strongest along a horizontal strip through the vertex, best azimuth patterns would be expected from sources along the y axis. For a reflector with center at $y=F/2$, the focal line would be inclined $14°2' = \tan^{-1} 1/4$ from the y axis, or at a slope parallel with the tangent to the reflector at the center of the y-correction strip. If sharp elevation patterns are required, the best focusing positions can be obtained from (6b). Since it is not possible to satisfy (6a) and (6b) simultaneously except at $(x_0=0, y_0=0, z_0=0)$ it is evident that the two planes have divergent regions of best focus, which is characteristic of astigmatic aberrations in lenses. This will be discussed further in Section II-C, 2.

2) *Phase Analysis:* According to diffraction theory, the radiated field is completely determined by the phase and amplitude distributions of current over an aperture. Determination of the far-field pattern involves surface integration of the currents over the aperture; unfortunately, exact integration can be accomplished only in the simpler cases. Certain characteristics of the patterns can, however, be inferred directly from known theory if the aperture phase function can be expanded in a power series in terms of the aperture coordinates.

Some information confirming ray analysis can be obtained by considering an approximate phase function, but this is most accurate for small values of y_0 and z_0. If we assume that the reflected rays are parallel to the z axis, the function

$$\psi = L_1 + z - 2 \tag{9}$$

represents the relative distance from a point source to the reflector and back to the plane $z=0$.

When ψ is developed in a double MacLaurin series in terms of the coordinates x and y, we get the following series:

$$\begin{aligned}\psi(x,y) = {} & \psi(0,0) + \psi_x(0,0)x + \psi_y(0,0)y \\ & + \tfrac{1}{2}[\psi_{xx}(0,0)x^2 + 2\psi_{xy}(0,0)xy + \psi_{yy}(0,0)y^2] \\ & + \tfrac{1}{6}[\psi_{xxx}(0,0)x^3 + 3\psi_{xxy}(0,0)x^2y \\ & + 3\psi_{xyy}(0,0)y^2x + \psi_{yyy}(0,0)y^3] + \cdots.\end{aligned} \tag{10}$$

[4] S. Silver, "Microwave Antenna Theory and Design," M.I.T. Rad. Lab. Ser., McGraw-Hill Book Co., Inc., New York, N. Y., vol. 12; 1949.

When these derivatives are calculated and evaluated at $x=0$, $y=0$, we note that $\psi_x(0, 0)$, $\psi_{xy}(0, 0)$, $\psi_{xxx}(0, 0)$, and $\psi_{yyx}(0, 0)$ are all zero. Hence, the power series out to the cubic terms is

$$\psi = \psi(0,0) + \psi_y(0,0)y + \frac{\psi_{yy}(0,0)}{2}y^2 + \frac{\psi_{yyy}(0,0)}{2}y^3 + \frac{\psi_{xx}(0,0) + y\psi_{xxy}(0,0)}{2}x^2;$$

$$\psi(0,0) = \sqrt{y_0^2 + (1-z_0)^2} - 1;$$

$$\psi_y(0,0) = -\frac{y_0}{\sqrt{y_0^2 + (1-z_0)^2}};$$

$$\psi_{yy}(0,0) = \left\{\frac{1+z_0}{2[y_0^2 + (1-z_0)^2]^{1/2}} - \frac{1}{2} - \frac{y_0^2}{[y_0^2 + (1-z_0)^2]^{3/2}}\right\};$$

$$\psi_{yyy}(0,0) = \left\{\frac{3/2(y_0 + z_0y_0)}{[y_0^2 + (1-z_0)^2]^{3/2}} - \frac{3y_0^3}{[y_0^2 + (1-z_0)^2]^{5/2}}\right\};$$

$$\psi_{xx}(0,0) = \left\{\frac{1/2(1+z_0)}{[y_0^2 + (1-z_0)^2]^{1/2}} - \frac{1}{2}\right\}, \text{ or } y_0^2 = \psi z_0;$$

$$\psi_{xxy}(0,0) = \left\{\frac{y_0(1+z_0)}{2[y_0^2 + (1-z_0)^2]^{3/2}}\right\}. \tag{11}$$

All coordinates are normalized to unity focal length.

The coefficients in the power series are functions of y_0 and z_0. Of course, all terms vanish when $y_0=0$, and $z_0=0$ when a plane wave is generated across the aperture. The coefficient $\psi_y(0, 0)$ represents a linear tilting of the beam. The coefficient of x^2 is of paramount interest to us as it represents the functional relation of y_0 and z_0 for zero azimuth defocusing. This term indicates again that perfect azimuth focusing can be achieved for only one value of y. In Fig. 2 we plotted the coefficient

$$\psi_{xx}(0, 0) + \psi_{xxy}(0, 0)y_m = 0 \tag{12}$$

for $y_m=\frac{1}{2}$ and $y_m=0$. Note that these loci are tangent to the straight lines obtained by ray analysis in the limit of small values of y_0 and z_0. If we assume that the center of the dish $x=0$, $y=y_m$ is most heavily illuminated, the term $\psi_{yy}(0, 0)$, usually considered the elevation defocusing factor, and the term $\psi_{yyy}(0, 0)$, the elevation coma factor, can be combined to find feed positions (values of y_0 and z_0) for best elevation patterns.

The advantages of this formulation are 1) phase errors are identified with terms familiar to optical designers, and 2) the phase function ψ is in a form usable for attempting pattern calculations with integrals of the form:

$$E = \iint e^{jk\psi} e^{jk[x \sin\alpha + y \sin\beta]} dxdy. \tag{13}$$

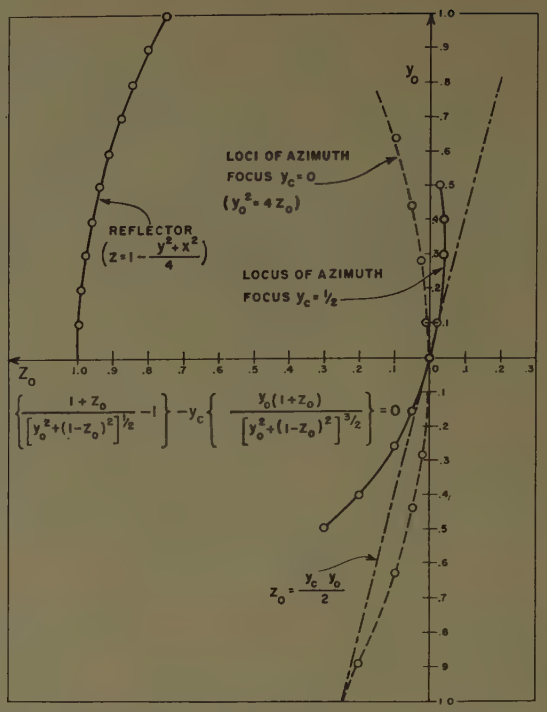

Fig. 2—Locus of feed positions giving rise to zero azimuth defocusing for $y_m=0$ and $y_m=0.5$.

3) *Estimated Power Plot from Ray Analysis:* Still another analysis can be used to determine the pattern deterioration due to errors of geometric optics. When a source is placed at a point near the focus with coordinates $(0, y_0, z_0)$, the reflected rays diverge over a range of angles. The direction cosines of the reflected rays are given in (6a) and (6b). If we specialize (6b) to the two-dimensional cylindrical case, that is, let x equal zero, we obtain

$$\cos\alpha_y = \left[\frac{2Fz_0 + yy_0}{4F^2 - 2Fz}\right]\frac{y}{L_1} - \frac{y_0}{L_1}, \tag{14}$$

where

$$L_1 = \sqrt{(y-y_0)^2 + (z-z_0)^2}. \tag{15}$$

Assuming the primary illumination from a uniform line source to be nearly constant across the aperture, if we define the function P as the total power incident between the ordinates y_a and y on the reflector, per unit length in the x direction, we have

$$P = K(y - y_a). \tag{16}$$

Differentiated with respect to the direction angle α_y, (16) becomes

$$\frac{dP}{d\alpha_y} = K\frac{dy}{d\alpha_y}. \tag{17}$$

Note that $dP/d\alpha_y$, evaluated at any particular angle α_y, is a measure of the energy radiated in the α_y direction. Substituting (14) into (17),

$$\frac{dP}{d\alpha_y} = \frac{K \tan \alpha_y}{\left[\dfrac{4Fz_0 + 2yy_0}{4Fz_0y + y_0(y^2 - 4F^2)} - \dfrac{2y}{y^2 - 4F^2} - \dfrac{(y - y_0) - (z - z_0)(y/2F)}{(y - y_0)^2 + (z - z_0)^2}\right]} \tag{18}$$

where

$$\tan \alpha_y = \frac{4F[(F - z)(z - z_0 - 3F) + yy_0 - F(F - z_0)]}{4Fz_0y + y_0(y^2 - 4F^2)}.$$

With a source at the focus ($y_0 = z_0 = 0$), $(dP/d\alpha_y) \to \infty$. This means that all the power across the aperture is concentrated in the direction $\alpha_y = 0$. When the source moves to a point (y_0, z_0), the function $dy/d\alpha_y = KdP/d\alpha_y$ still goes to infinity at some value of y. The best patterns may be expected if y_0 and z_0 are adjusted so that

$$\left.\frac{d\alpha_y}{dy}\right|_{y_m} = 0, \tag{19}$$

where y_m is the center of the aperture.

For a symmetric parabolic cylinder, the vertex should be the center of illumination; in other words, the condition required would be fulfilled by

$$\left.\frac{d\alpha_y}{dy}\right|_{y=0} = 0. \tag{20}$$

From (18) we see

$$\left.\frac{d\alpha_y}{dy}\right|_{y=0} = \cot \alpha \left[-\frac{z_0}{Fy_0} + \frac{y_0}{(F - z_0)^2 + y_0^2}\right] = 0, \tag{21}$$

which yields the condition

$$y_0^2 = z_0(F - z_0). \tag{22}$$

This optimum elevation focusing curve for a line source feeding a parabolic cylinder is a circle of radius $F/2$, its center at (0, 0, $F/2$), and its circumference described through the focus and the vertex. The function

$$\frac{dP}{d\alpha_y} = f(\alpha_y) \tag{23}$$

can be plotted and a crude pattern obtained. So long as the angular "spread" of the pattern is less than the beamwidth determined by diffraction, little trouble need be anticipated from optical errors.

C. The Paraboloid as a Receiving Antenna

The preceding analyses are inadequate for predicting what combination of point sources will produce a required pattern. Solution of the synthesis problem is better approached through consideration of the power and phase distributions in the focal region when a plane wave is incident on the reflector. We can then see where to place absorbers (or radiating elements when transmitting) to recombine the power dispersed over the focal region. It is fortunate that there are regions of high ray density; on the azimuth focusing surfaces, these regions of high density can be approximated by straight lines.

1) *Ray Analysis:* When a plane wave is incident on a paraboloid, the reflected rays converge toward the focal region; the highest ray density is found on the caustic surfaces.[3,5,6] The astigmatic[7] surface corresponding to best elevation focusing is contained in the general caustic solution and discussed in the following section.

Assume that a plane wave, parallel to the x axis but tilted with respect to the y axis, is incident on the paraboloidal reflector. Unit vectors along incoming rays (see Fig. 3, next page) are

$$\hat{S}_0 = 0 - \sin\theta\hat{j} + \cos\theta\hat{k}. \tag{24}$$

The unit exterior normal to the reflector is again (3)

$$\hat{\eta} = \frac{x\hat{i} + y\hat{j} + 2F\hat{k}}{\sqrt{x^2 + y^2 + 4F^2}}. \tag{25}$$

Snell's law gives

$$\hat{S}_1 = \hat{S}_0 - 2(\hat{\eta} \cdot \hat{S}_0)\hat{\eta}. \tag{26}$$

The direction cosines of the reflected rays are

$$l_1 = \frac{2(y \sin\theta - 2F \cos\theta)x}{x^2 + y^2 + 4F^2}, \tag{27}$$

$$m_1 = -\sin\theta + \frac{2(y \sin\theta - 2F \cos\theta)y}{x^2 + y^2 + 4F^2}, \tag{28}$$

and

$$n_1 = \cos\theta + \frac{2(y \sin\theta - 2F \cos\theta)2F}{x^2 + y^2 + 4F^2}. \tag{29}$$

We can find where these rays pierce any plane; the highest density of intersecting rays, or in-phase rays, is in the yz plane.

Since $x_0 = 0$ is the yz plane, and since the reflected rays are straight lines, we can write

$$\frac{x_0 - x}{l_1} = \frac{y_0 - y}{m_1} = \frac{z_0 - z}{n_1} = -\frac{x}{l_1}. \tag{30}$$

We can solve for y_0 and z_0, thus defining the locus of ray interception in the yz plane, and obtain a parametric set in terms of the xyz coordinates of the dish:

[5] "Calculations of the Caustic Surface of a Paraboloid of Revolution for an Incoming Plane Wave of Twenty Degrees Incidence," Parke Mathematical Labs., Concord, Mass., Rep. No. 7, Contract No. AF19(604)-263; May, 1952.

[6] "Reflection on the Vertical Symmetry Plane for Incoming Parallel Rays at −10 degrees with the Axis of a Paraboloid of Revolution," Parke Mathematical Labs., Concord, Mass., Rep. No. 3, Contract No. AF19(604)-263; August, 1952.

[7] This use of "astigmatic" surface does not agree with optic definitions. Our terminology defines this surface on the basis of single plane waves, whereas in optics the astigmatic surface focuses one dimension for a large number of plane waves.

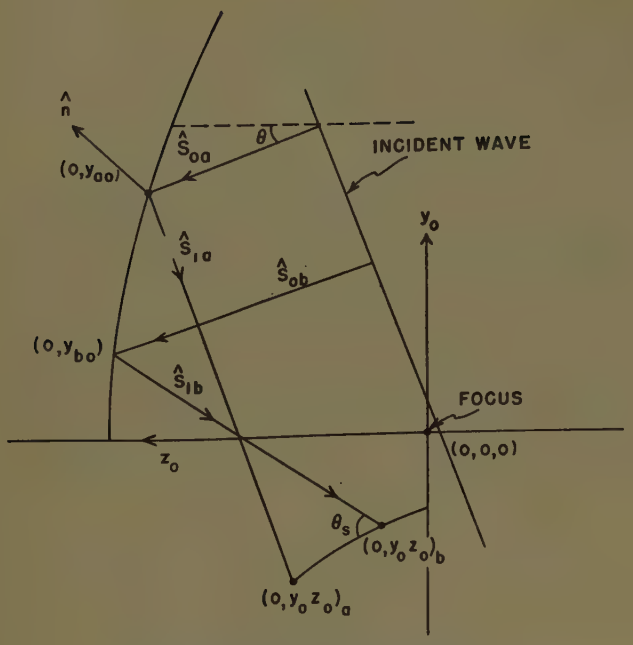

Fig. 3—Coordinate system for analyzing paraboloid as a receiving antenna.

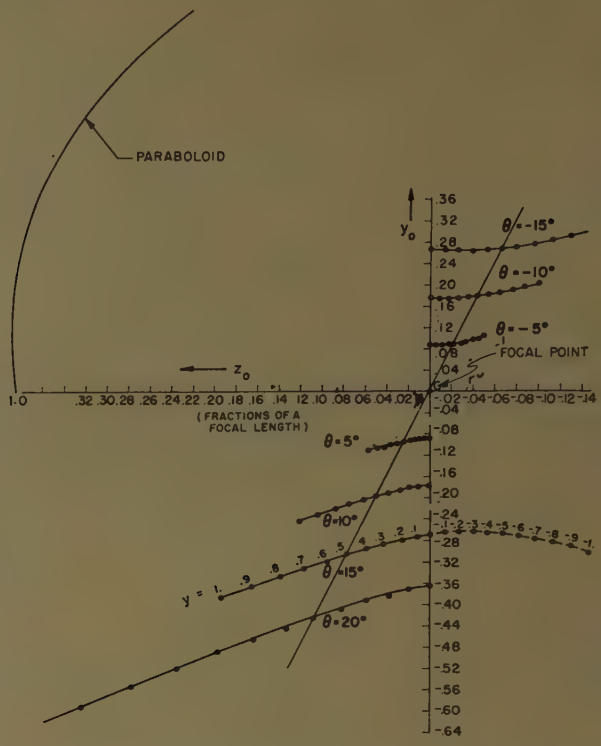

Fig. 4—Loci of best azimuth focus (ridge lines) for plane waves incident upon the reflector at various elevation angles θ. Note each circled point is related to a definite point on the reflector center line ($x=0$), starting from the $y_m=0$ point falling on the vertical axis. The ridge line at $\theta=15$ degrees is for a complete paraboloidal reflector; the others are for paraboloidal reflectors in the region $y\geq 0$ only.

$$y_0 = -\frac{\sin\theta(x^2+y^2+4F^2)}{4F\cos\theta - 2y\sin\theta}, \tag{31}$$

$$z_0 = \frac{\cos\theta(x^2+y^2+4F^2)}{4F\cos\theta - 2y\sin\theta} - 2F + z. \tag{32}$$

In Fig. 4, the locus of ray interception for various tilt angles θ has been plotted for the limit when $x\to 0$. Note that all rays do not intercept a line but that the ray density is highest in the limit as $x\to 0$. These astigmatic lines are the best for azimuth focus at elevation angles θ and are referred to in the remainder of this report as ridge lines.

2) *The Relation of Azimuth and Elevation Focusing Loci to the Complete Caustic:* The Parke Mathematical Laboratories[5,6] have computed the envelope that includes all rays reflected from a cut parabola for 20 degrees and -10 degrees incidence. The general equations for the caustic surface are:

$$z_0 = z - \left[1 - \frac{(2f-z)(\cos\theta)}{2f\cos\theta + y\sin\theta}\right]B \tag{33}$$

$$x_0 = x - \frac{x}{2f}B \tag{34}$$

$$y_0 = y - \left[\frac{y}{2f} - \frac{(2f-z)(\sin\theta)}{2f\cos\theta + y\sin\theta}\right]B \tag{35}$$

where

$$B = 2f - z + \cos\theta\,(z\cos\theta + y\sin\theta) \pm (2f-z)(-\sin\theta)\left[1 - \frac{(z\cos\theta + y\sin\theta)^2}{2f-z}\right]^{1/2}. \tag{36}$$

The alternate use of the positive and negative signs in B of (33)–(35) leads to two focusing surfaces. One of these surfaces is related to azimuth focusing and one to elevation focusing.

We will limit our attention to a narrow strip of the reflector in the yz plane, $x=0$, and use a unit focal length, $f=1$. Let

$$\frac{z\cos\theta + y\sin\theta}{z-2} = \sin(\delta - \theta) \tag{37}$$

and

$$\cos\delta = \frac{-y}{z-2}, \quad \text{then} \quad \sin\delta = \frac{z}{z-2}. \tag{38}$$

Choosing the positive sign in B of (33) and (35) gives

$$\frac{y_0}{z_0} = -\frac{2}{y} \tag{39}$$

which is the straight line azimuth focus discussed in Section II-B.

Choosing the negative sign in B of (33) and (35) leads to the second focusing surface. This is a circle given by

$$z_0^2 + y_0^2 - (1 - 3y^2/4)z_0 + \frac{y(y^2-12)}{8}y_0 = 0 \tag{40}$$

with its center at

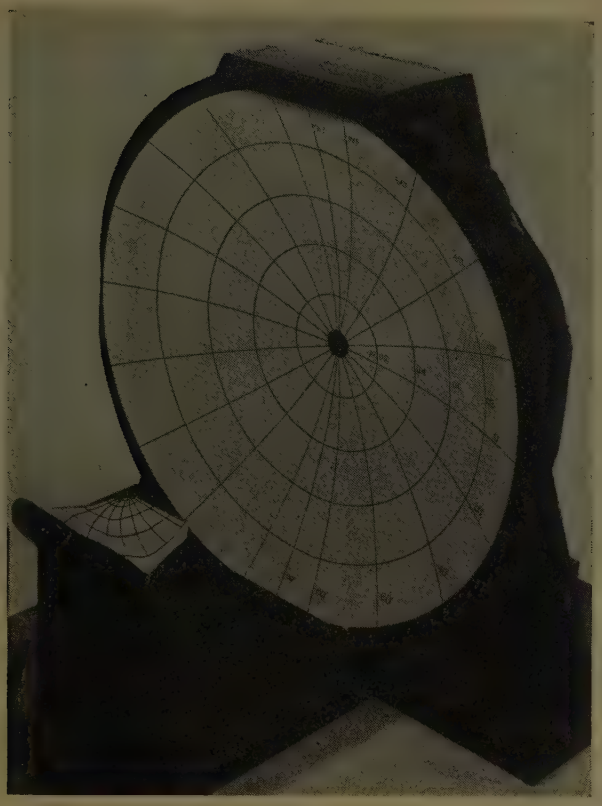

Fig. 5—Azimuth caustic surface of a paraboloidal reflector for an incoming plane wave at $\theta = 20$ degree incidence.

$$z_0 = \frac{4 - 3y^2}{8} \tag{41}$$

$$y_0 = -\frac{y(y^2 - 12)}{16}. \tag{42}$$

The complete azimuth caustic and its relation to the reflector is shown in Fig. 5. The loci of azimuth and elevation focus for a number of correction points ($y = y_m$) on the reflector are plotted in Fig. 6. For each corrected point (y_m) on the reflector, the azimuth and elevation focus loci are represented by a straight line and a circle, respectively. Note that for all correction points except $y_m = 0$, the elevation and azimuth loci intersect at two points, one at the true focus and one at some secondary focus.

On substitution of (37) and (38) into the quantity B in (33)–(35),

$$B = 2[1 + \sin\theta(y\cos\theta - z\sin\theta)]$$

for the negative sign; (43)

$$B = 2 \quad \text{for the positive sign.} \tag{44}$$

The expression for astigmatism is therefore

$$A = 2\sin\theta(y\cos\theta - z\sin\theta) \tag{45}$$

and for zero astigmatism it is

$$\tan\theta = \frac{y}{z}. \tag{46}$$

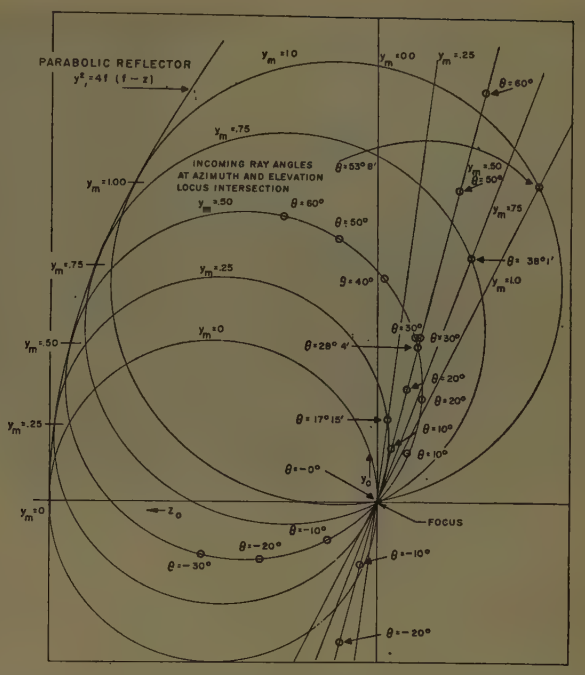

Fig. 6—Elevation and azimuth focusing loci for various correction points y_m and various angles of incidence. Note elevation focus is denoted by circles and azimuth focus by straight lines.

This relation, (46), will give the elevation angle of the secondary focus. For example, if the correction point on the reflector is chosen to be $y = y_m = 0.50$, then $z = 0.9375$, and $\theta = 28°4'$.

Consider, in Fig. 6, a typical correction point, $y_m = 0.75$. Below focus, the circle and straight line rapidly diverge; above focus, the straight line is near the circle between the true focus and the secondary focus. This means that with an array made to lie along the azimuth focus line for negative y values (below focus) the beams are sharp in azimuth but badly defocused in elevation. Therefore, extending the array below focus results in loss of gain. If the array is extended above focus, the two loci are closer together between the two focal points and accordingly there is less elevation defocusing over this region. Consequently, in the region between the two focal points, there is less rapid loss of gain. For example, the secondary focus occurs $38°1'$ for a correction point of $y_m = 0.75$. Better gain over this elevation interval can be expected if the primary feed is built to lie above focus. Such construction also makes a more compact physical unit. Although the primary feed then extends across the reflector aperture, no serious shadowing has been noted on models built to operate at $\lambda = 3.2$ cm and $\lambda = 1.25$ cm.

3) *Experimental Verification of Ridge Lines:* Once the locus of the azimuth curves or ridge lines is known, it is possible to construct a line source incorporating the proper phase and radiating elements that will coherently absorb the power for one elevation tilt angle θ, but the collection of power with a line source can never be com-

Fig. 7—Paraboloid mirror used for optical verification of the ridge lines.

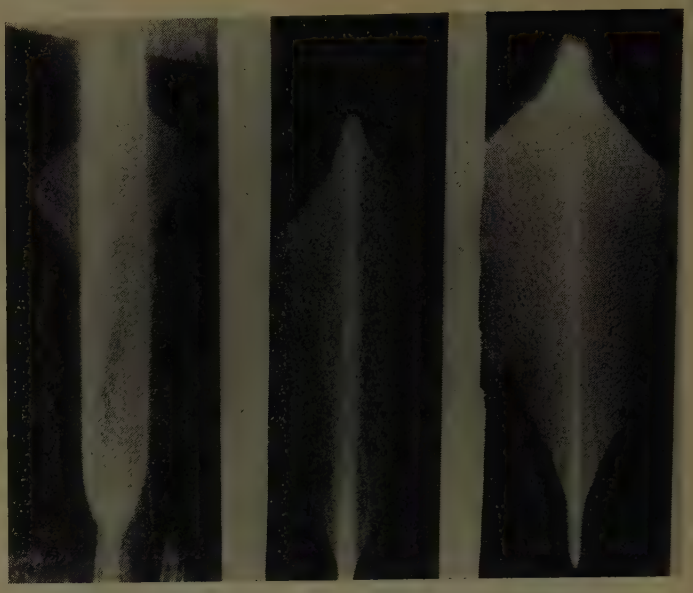

Fig. 8—Ridge lines obtained using a paraboloidal mirror and distant light source at 20 degree incidence.

plete except at the focus. Depending on the ratio of the focal length to the diameter of the reflector, however—and large F/D ratios give better results—patterns not greatly inferior to those obtained with a horn at the focus can be obtained if a suitable power taper is put on a phased line source. This type of correction is similar to the one made on a spherical reflector[8] and its value was confirmed in two types of experiments we conducted. In the first method a polished Alzac paraboloidal optical reflector, the bottom half covered with a light-absorbing cloth was used (see Fig. 7). The incoming plane wave from a distant light source was at a 20 degree tilt to the axis of the paraboloid. Photographs on film exposed along an astigmatic locus show a bright line corresponding to the elongated image of a light source at infinity. Prints of three exposures on photographic film in the holder seen in position in Fig. 7 are shown in Fig. 8. These illustrate, from left to right, that the image line becomes brighter and sharper as the film is moved into the line corresponding to $\theta = 20$ degrees (see Fig. 4).

In the other experiment to show the presence of sharp astigmatic lines, a slotted waveguide built to fit a curve of Fig. 4 was used. This line source was designed for the 15 degree elevation angle at X band. The phase along this astigmatic line was computed by determining the length of the path from the line to the incident plane wave. The geometry is shown in Fig. 9. Only those rays lying in the plane containing the reflector axis and corrector are considered since other rays that are intercepted by the corrector will tend to be in phase. From Snell's law

$$2\beta = \alpha_1 - \alpha_0; \tag{47}$$

and from Fig. 9

$$\tan 2\beta = \frac{y}{F - z} \tag{48}$$

[8] R. C. Spencer, C. J. Sletten, and J. E. Walsh, "Correction of Spherical Aberration by a Phased Line Source," AF Cambridge Res. Labs., Cambridge, Mass., Rep. No. E5069; May, 1951.

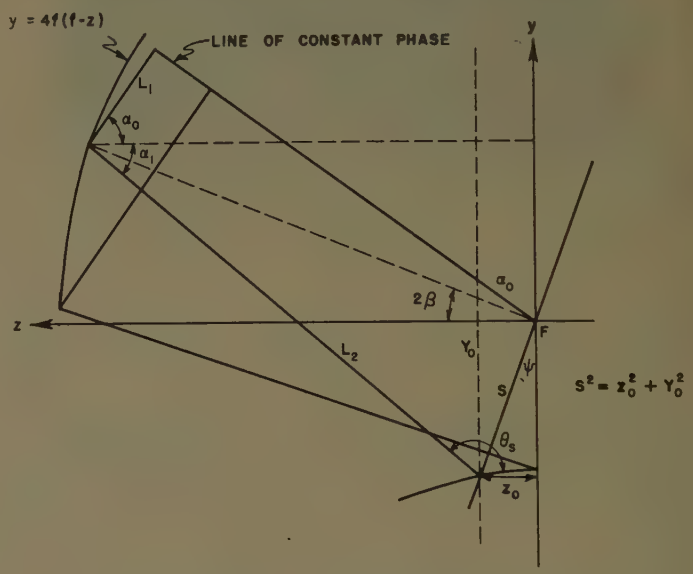

Fig. 9—Geometry for designing a ridge line corrector.

where F is the focal length; we get

$$\cos \alpha_1 = \frac{F - z - z_0}{L_2} \tag{49}$$

where L_2 is the length of the reflected ray. Then

$$L_2 = \frac{F - z - z_0}{\cos \alpha_1}; \cos \alpha_0 = \frac{L_1}{F - z - y \tan \alpha_0} \tag{50}$$

$$L_1 = \cos \alpha_0 (F - z - y \tan \alpha_0), \tag{51}$$

where L_1 is the length of the incident ray from the reflector to the plane of constant phase. Therefore $L = L_1 + L_2$ is the total length of the path from the feed line to the equiphase front.

If we notice that each point (y_0, z_0) on the ridge lines in Fig. 4 is connected to a definite point (y, z) on the paraboloid by (31) and (32), we now have L, the path length or phase, as a function of

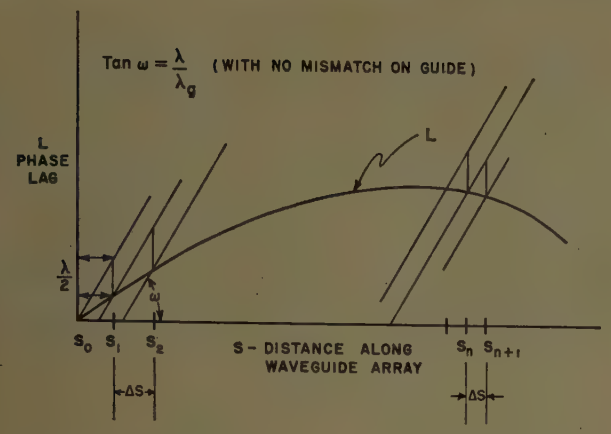

Fig. 10—Graphical construction for computing the longitudinal spacings of the radiating elements on a ridge line corrector.

$$S = \sqrt{y_0^2 + z_0^2} \tag{52}$$

along the guide. Plotting L against S enables us to find the longitudinal spacing ΔS between radiators with 180 degree phase reversal. The type of construction shown in Fig. 10 can be used to approximate the phase distribution on the line source.

An alternative procedure is to measure the angle η that the rays make with line segments S on the astigmatic line and then integrate the differential expression $dL/dS = \cos \eta$ to yield the phase function $L(S)$. The function $L(S)$ can then be approximated by an array with element-spacing obtained by the method indicated in Fig. 10.

Power radiated along such an array was computed to be proportional to ray density with power arbitrarily tapered at the ends of the line source.

Patterns obtained with a small horn directed at the center of the dish from its location at the point corresponding to $y = 0.5\ F$ on the 15 degree astigmatic curve, and patterns obtained with the astigmatic line source corrector, are compared in Fig. 11(a) and 11(b). The corrector produces a much better elevation pattern and an increase in gain of about 4 db, the azimuth beamwidths in both types are comparable, but the azimuth sidelobers are lower with the corrector. It should be possible to distrbiute such line source correctors in a paraboloid when multiple pencil beams are required.

D. Influence of Reflector Shape on Pattern Characteristics

1) *Method of Analysis:* A paraboloidal reflector with an elliptical periphery was analyzed to determine the influence of reflector shape and contour upon the pattern. This elliptical contour is considered to be nearly optimum and is used in several existing systems. The main objectives were 1) to locate the section of the surface where correction would be most expedient, and 2) to help decide on the optimum reflector contour.

The method used was to trace incoming rays reflected from the periphery of the reflector onto the plane containing the best azimuth focusing line and the x axis,

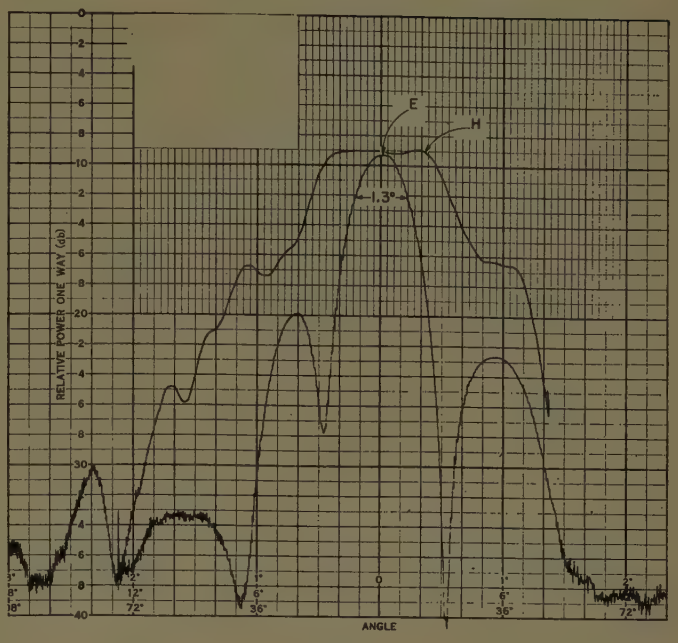

(a)

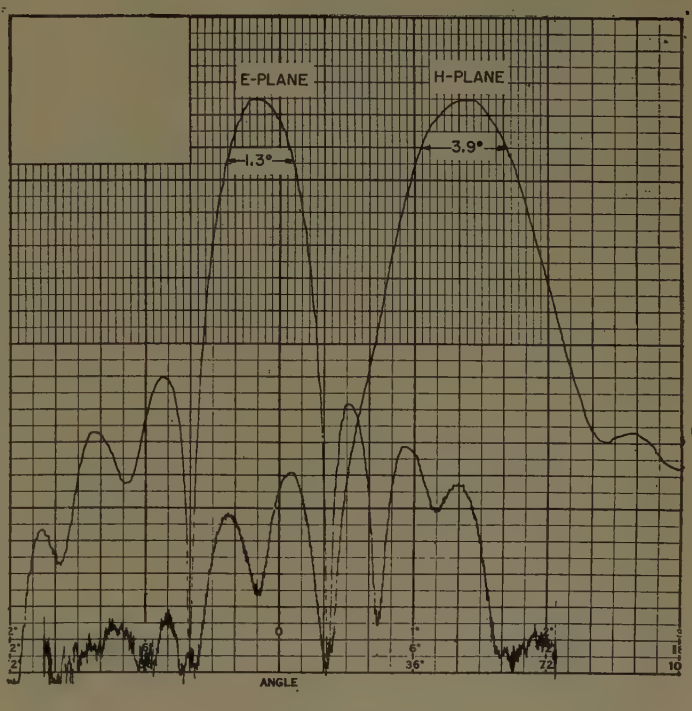

(b)

Fig. 11—(a) Azimuth (E plane) and elevation (H plane) patterns obtained using a small horn located at the point corresponding to $y_m = 0.5\ F$ on the 15 degree ridge line. (b) Patterns obtained with a ridge line corrector designed to correct $y_m = 0.5\ F$ for $\theta = 15$ degrees.

by the procedures discussed in Section II-C, 1. By (8) the slope of this plane is

$$\frac{z_0}{y_0} = \frac{-y_m}{2F} = \tan \psi. \tag{53}$$

By considering the density of rays projected onto this plane it is possible to determine which sections of the reflector have the poorest focusing properties.

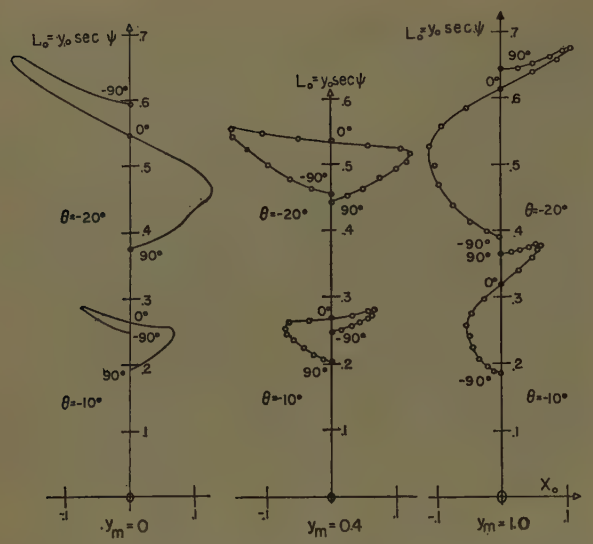

Fig. 12—Projections of reflector peripheral rays on the plane containing the line of azimuth focus for negative θ.

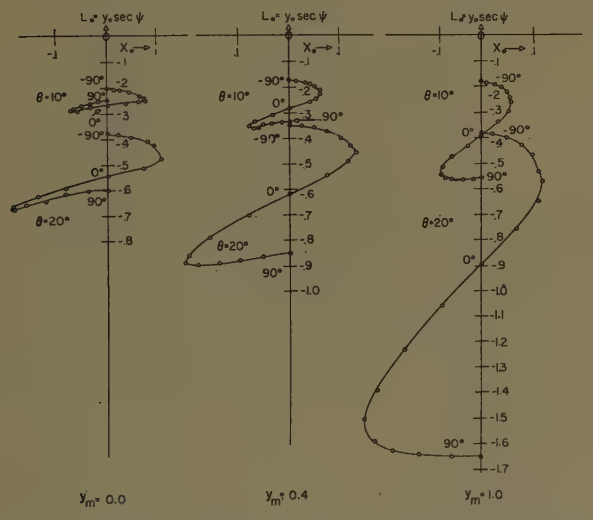

Fig. 13—Projections of reflector peripheral rays on the plane containing the line of azimuth focus for positive θ.

2) *Interpretation of Ray Studies:* The projections of the peripheral rays on the plane containing the appropriate azimuth focus line are shown in Figs. 12 and 13 for correction points $y_m = 0$, 0.4, 1.0, and incident ray angles $\theta = \pm 10$ degrees, ± 20 degrees. Curves for negative θ are shown in Fig. 12 and curves for positive θ in Fig. 13. The negative values of θ arise when the correcting line source is extended above focus across the reflector aperture, as indicated in Fig. 4. The positive values of θ occur when the correcting line source extends below focus. The curves in Figs. 12 and 13 are symmetrical about the y axis (for clarity, only one-half of each curve is shown). Each circle on the curves corresponds to a definite position on the reflector periphery (Fig. 14). The points on the curves corresponding to $\alpha = 0$ degree, ± 90 degrees are indicated.

Consider the curves for negative θ (Fig. 12). This above-focus location for the correcting line source affords an important advantage in that the spread of the rays in the L_0 direction is comparatively small. The azimuth focusing, indicated by the spreading in the x_0 direction, improves as y_m is increased. At the corrected strip $y = y_m$, x_0 is, of course, zero. The largest errors in the x_0 direction arise from those sections of the reflector that are below the corrected strips. Because of this, the reflector surface should have its midpoint high above the vertex. If possible, the reflector contour should be trimmed on the lower side (the side nearest the vertex) for values of α between -30 degrees and -60 degrees (see Fig. 14). Choosing too large a value of y_m must, however, be avoided because the line source should be close enough to the reflector to prevent spillover losses.

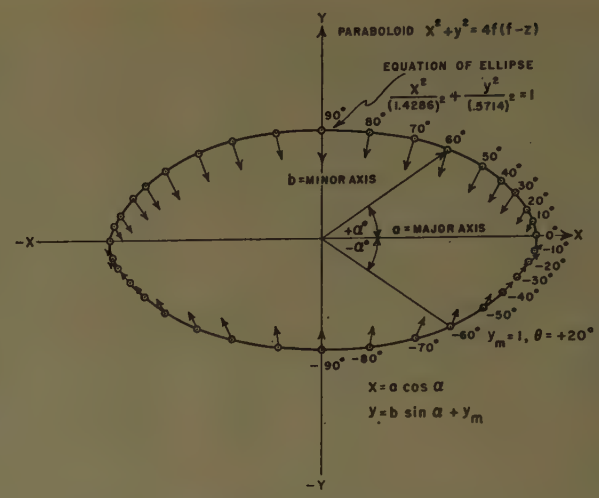

Fig. 14—Relation of projected rays to points on the reflector periphery.

When the correcting line source is placed below focus the variations in the L_0 direction are very large. The pattern is distorted in elevation but the smallest errors originate in those sections of the reflector that are below the midline. This is in contrast to the results obtained with line sources lying above focus. The best area for the midpoint of the reflector surface would now be near or below the vertex. The contour of the reflector should now be trimmed on top for values of α between $+30$ degrees and $+60$ degrees.

III. Design of Midpoint Correctors for Beam Shaping

The preceding analysis indicates that a beam, fanned in the elevation plane and well focused in the azimuth plane, can be obtained by placing a feeding array along the indicated straight line for azimuth focusing, and directing the array energy at the corresponding strip on the reflector. A number of satisfactory systems have been designed using these principles. The feeding arrays for these systems have been designed to lie both above and below the focus, but all of the arrays corrected the $y = f/2$ (f = focal length) strip on the reflector. Thus, these arrays are called "midpoint correctors." The reflectors used were all off-axis sections of paraboloids with f/D ratio in elevation of about 1 and $\frac{1}{3}$ in azimuth.

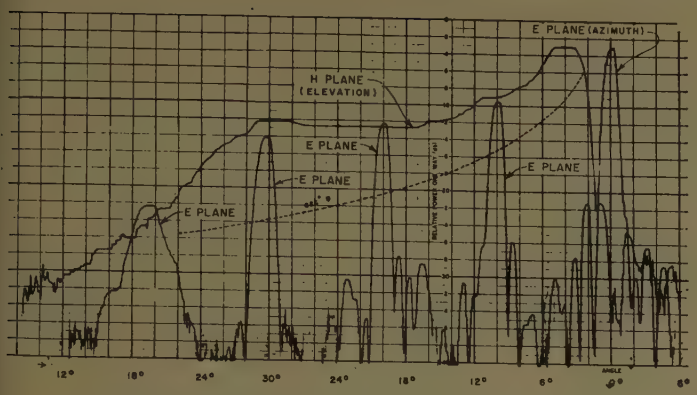

Fig. 15—Patterns obtained with a correcting line source (slot array) placed below focus $\lambda = 3.2$ cm.

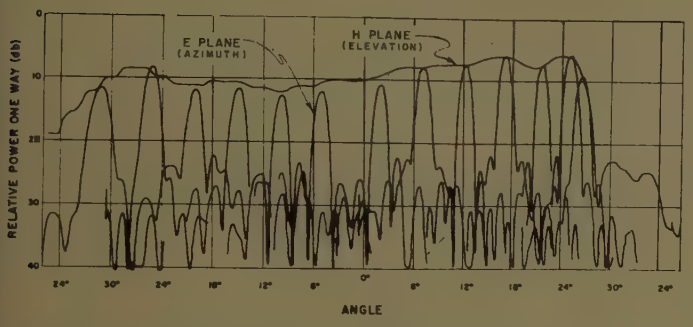

Fig. 16— Patterns obtained with a correcting line source (slot array) extending above focus $\lambda = 3.14$ cm.

Two types of phased line sources have been used as midpoint correctors: 1) longitudinal shunt slots in rectangular waveguide, and 2) continuously radiating pillboxes. Waveguide slot arrays extending below the focus have been built to provide up to 40 degrees of $\csc^2$ elevation coverage, with azimuth beamwidths everywhere less than 1.5 degrees, and sidelobes everywhere lower than 15 db (Fig. 15). An array built to lie above the focus provided approximate $\csc^2$ coverage over a 60 degree elevation sector, with azimuth beamwidths all less than 1.5 degrees, and sidelobes all lower than -13 db (Fig. 16).

A. Longitudinal Shunt Slot Arrays

The phase and amplitude distributions can be independently controlled on a longitudinal shunt slot array. The amplitude is controlled by the transverse displacements of the slots from the waveguide center line, and the phase is controlled by the longitudinal positions of the slots.

If the total radiation from the array is to focus on one horizontal strip y_m of the reflector, the electrical distances from the input terminal of the array through any slot to the point y_m must be equal. The geometry for computing these paths is illustrated in Fig. 17.

Note that the azimuth focus line along which the array should lie is parallel to the tangent of the reflector at the correction point. Computations are simplified if we normalize all lengths in terms of $R = 1.0303\,f$, the distance from the focal line to y_m.

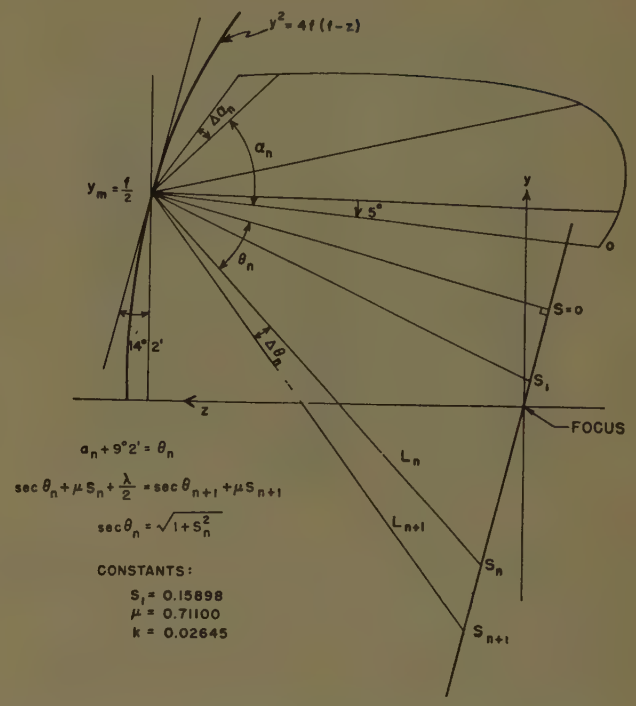

Fig. 17—Geometry for determining the phase distribution of a mid-point corrector.

With 180 degree phase reversal between the slots, the equation for the normalized coordinates S_n of the center of a slot n is given by the iterative relation:

$$L_n + \mu(S_n - S_{n+1}) + k + L_{n+1}. \qquad (54)$$

Hence,

$$(1 + S_n^2)^{1/2} + \mu S_n + k = (1 + S_{n+1}^2)^{1/2} + \mu S_{n+1}. \qquad (55)$$

Letting

$$D_n = (1 + S_{n+1}^2)^{1/2} + \mu S_{n+1} = (1 + S_n^2)^{1/2} + \mu S_n + k \qquad (56)$$

where

$$\mu = \frac{\lambda_a}{\lambda_g} \quad \text{and} \quad k = \frac{\lambda_a}{2R} \qquad (57)$$

then

$$S_{n+1} = \frac{\mu D_n - (\mu^2 - 1 + D_n^2)^{1/2}}{\mu^2 - 1}$$

$$[\text{Note: } D_{n+1} = D_n + k]. \qquad (58)$$

The longitudinal spacings of the slots are thus fixed by the required phase distribution; the transverse displacements can now be used to control the amplitude distribution. As a first approximation of obtaining a $\csc^2\theta$ power pattern in elevation, notice that the power radiated in ΔS along the array will appear in the internal $\Delta\alpha$ as shown in Fig. 17. Thus if the slots are equally spaced, all that is necessary is for each slot to radiate a fraction of the input power proportional to $\csc^2\alpha_n$. The

Fig. 18—Slot arrays designed to operate at about $\lambda = 3.20$ cm.

longitudinal slot spacing actually decreases toward the end of the array farthest from the focus. If we do not compensate for this the result is a gradual increase in the power radiated off focus. However, this increase in radiated power is approximately balanced by the loss of gain due to elevation defocusing as the slots are placed farther away from focus.

Let the required powers radiated by each slot be $P_0, P_1, P_2, \cdots, P_N$ where N is the slot number from the feeding terminal. Then the coupling coefficient is

$$K_n = \frac{WP_n}{1 - W\sum_{n=0}^{n-1} P_i} \tag{59}$$

where

$$W = \frac{1 - g}{\sum_{n=0}^{N} P_n} \tag{60}$$

and g represents the fraction of power fed to the end of the array.

The drop per slot is

$$\text{db} = 10 \log \left[\frac{1}{1 - K_n}\right]. \tag{61}$$

The actual displacement can now be found from either theoretical or experimental coupling curves.[4,9] Some of the slot arrays are shown in Fig. 18.

When the first slot in the array is not near the focal point, it is difficult to obtain a sharp elevation pattern near the horizon. One method of accomplishing this is to use a lightly coupled parasitic slot out of phase with the first slot in the main array.

B. Continuously Radiating Pillboxes

The limited band-pass and power breakdown characteristics of slots are often serious disadvantages. If the lack of good amplitude control and an increase in the size of the primary feed are not disadvantages, a continuously radiating pillbox structure is a useful substitute for slotted waveguide arrays.

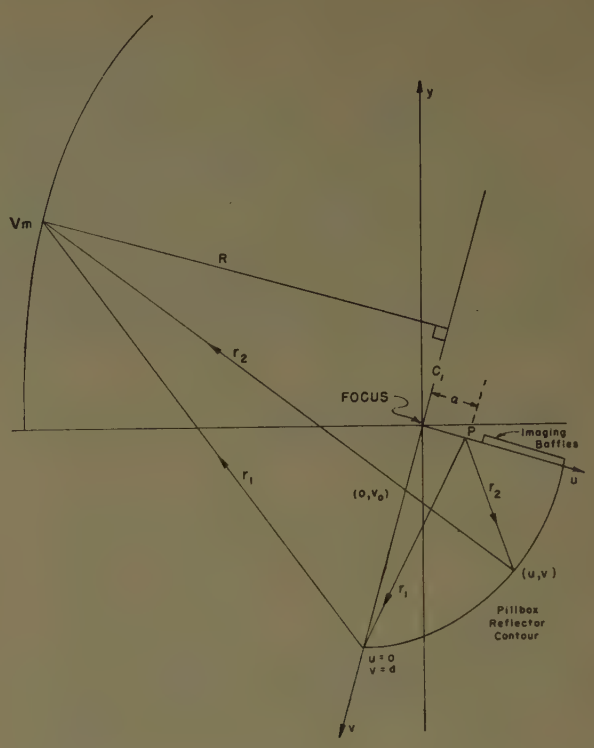

Fig. 19—Geometry for computing pillbox midpoint corrector.

The parametric equations of a pillbox reflector that will produce a phase function $\delta(v_0)$ along the pillbox aperture are found by using mathematical envelopes.[10] (See Fig. 19.)

The criteria for designing a pillbox midpoint corrector is to place its aperture along the azimuth focus line corresponding to y_m and to focus all the energy at y_m (see Fig. 19). The path length inside the pillbox from the feed point P, to the pillbox reflector contour, to a point on the pillbox aperture v_0, is:

$$\mu[(u - a)^2 + v^2]^{1/2} + \mu[u^2 + (v_0 - v)^2]^{1/2} = -\delta + C_1 \tag{62}$$

where μ is the ratio between the phase velocity in the pillbox and the phase velocity in air, δ is the phase lead required at v_0, and C_1 is an arbitrary constant that permits the curve to be shifted according to the coverage desired. Eq. (62) is an ellipse, with P at one focus and v_0 at the other. The envelope of the family of ellipses generated by assigning values to v_0 is the locus of the required reflector.

To find the equation of the reflector, first differentiate (62) with respect to v_0. Thus,

$$\frac{\mu(v_0 - v)}{[u^2 + (v_0 - v)^2]^{1/2}} = \frac{d(-\delta)}{dv_0} \tag{63}$$

[9] W. H. Watson, "The Physical Principles of Waveguide Transmission and Antenna Systems," Clarendon Press, Oxford, Eng.; 1947.

[10] K. S. Kelleher, "Analysis of Antenna Wavefronts," Naval Res. Lab., Washington, D. C., Rep. No. R-3329; July, 1948.

It is usually easier to eliminate either u or v and get $v=v(v_0)$ and $u=u(v_0)$ as parametric equations, so we let

$$f_1 = \frac{-\delta(v_0) + C_1}{\mu} \tag{64}$$

$$f_2 = \frac{d[-\delta(v_0)]}{\mu dv_0} \tag{65}$$

where f_1 and f_2 are functions of v_0 only. By simultaneous solution of (62) and (63) u can be eliminated to get

$$v = \frac{\dfrac{f_1^2 + v_0^2 - a^2}{2} + v_0\left[\dfrac{a(1-f_2^2)^{1/2}}{f_2} - \dfrac{f_1}{f_2}\right]}{v_0 - \dfrac{f_1}{f_2} + \dfrac{a(1-f_2^2)^{1/2}}{f_2}}, \tag{66}$$

u can be computed from

$$u = (v_0 - v)\frac{(1-f_2^2)^{1/2}}{f_2}. \tag{67}$$

For TEM propagation ($\mu=1$) the aperture can be flared without changing the focus of the pillbox from the point y_m. Where $\mu \neq 1$, however, flaring will change the characteristics of pillbox patterns in both planes. Metal imaging baffles can be used to modify the directivity of the horn used as a point source. Patterns obtained with this type of feeding system are shown in Fig. 20.

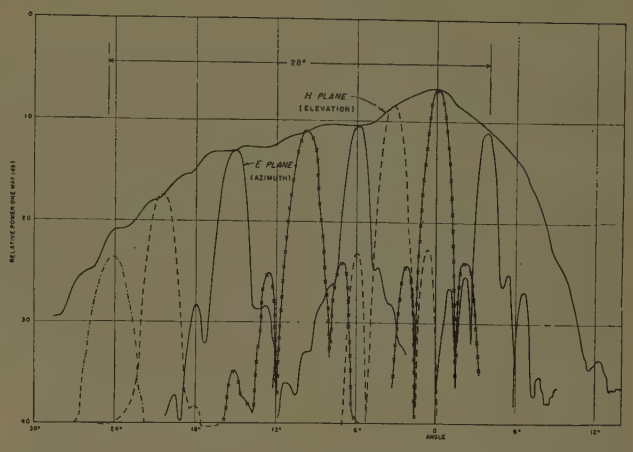

Fig. 20—Patterns obtained using a pillbox midpoint corrector.

Antenna Evaluation Methods*

W. S. LUCKE†

Summary—**Shannon's formula for channel capacity in terms of bandwidth and signal-to-noise ratio is used in a proposed method of antenna evaluation as a weighting function for averaging antenna patterns and impedances over space and frequency. This method is particularly applicable to situations where antennas with widely different characteristics are being compared for similar applications over relatively large bandwidths in which the characteristics of each antenna are subject to wide variation. The evaluation method based upon the Shannon formula is compared with others such as the "antenna-system-efficiency" and "minimum-level" methods.**

THIS paper and a companion one by Moore[1] present results of an investigation into antenna evaluation methods which was conducted at Stanford Research Institute during 1949–1953. The purpose of this review is to give wider circulation to the information that was developed and to provide a comparison with the ideas presented in another paper by Blass.[2]

This paper summarizes a report in which traditional concepts of antenna evaluation were examined and a new method, based upon Shannon's work, was presented. Moore summarizes a comparison of several antenna evaluation methods as applied to a specific antenna problem: namely, the HF aircraft-antenna system.

This investigation[3] is of a method for the evaluation of antenna systems that give a quantitative answer to the question of how well an antenna system meets the requirements of its application. This method is particularly directed at the problem of evaluating for a particular application several antennas that have widely varying patterns and impedances and that are difficult to compare directly. This problem is a common one in the selection of proper aircraft antennas for relatively wide-band usage in the lower frequency bands. For example, in the HF frequency band proposed antenna types may consist of the fixed-wire, tail-cap, wing-cap,

* Manuscript received by the PGAP, July 10, 1957.
† Weapons Systems Lab., Stanford Res. Inst., Menlo Park, Calif.
[1] E. J. Moore, "Performance evaluation of HF aircraft antenna system," this issue, p. 254.
[2] J. Blass, "A method for evaluating antennas," IRE TRANS. ON ANTENNAS AND PROPAGATION, vol. AP-6, pp. 95–96; January, 1958.
[3] W. S. Lucke, "An Antenna Evaluation Method," Stanford Res Inst., Menlo Park, Calif., Tech. Rep. 17, Contract AF 19(122)78, 1951. This research was supported by Air Force Cambridge Res. Center.

or wing-root types. These types have quite different patterns and different impedance variations over the 2–25 mc band, but all are capable of fulfilling the requirements of the application. However, in measuring or comparing these capabilities for a particular application, such as the aircraft HF requirement, or in evaluating the performance of a new type of antenna, one is confronted with a vast quantity of impedance data, radiation patterns, and matching network calculations. Although these data are essential to a description of the system, their bulk usually discourages the engineer who attempts more than a qualitative evaluation. Study of evaluation methods that reduce the bulk of the data to a small amount of more useful information has been undertaken in the past. However, the lack of universal acceptance of the results obtained has prompted a re-examination of the problem from a new point of view.

Two evaluation methods that have met with some acceptance, and are, therefore, to be compared with any new solution, are the "antenna-system-efficiency"[4] and the "minimum-level" or "pattern-distribution-function"[5] methods of evaluation. The antenna-system-efficiency method is based on the premise that the usefulness of a transmitting antenna system is directly proportional to the ratio of the power radiated into the prescribed sector (with prescribed polarization) to the power input of the antenna system. The minimum-level method is based on the assumption that the effectiveness of a transmitting antenna is measured by the portion of the prescribed sector over which the signal amplitude (of prescribed polarization) is above a minimum level. This level is determined through considerations of the signal power of the transmitter and the noise properties of the receiver.

The system-efficiency and minimum-level evaluations have been accepted because their application has yielded results that are in reasonable agreement with qualitative evaluations based upon operational experience. There are, however, some defects in both procedures. These are principally results of the manner in which the amplitudes of the field distribution are weighted. The system-efficiency method is based on the assumption that the usefulness of an antenna for communication between two points increases in direct proportion to the percentage of total power which is transmitted between the points. This is unrealistic, since it is well-known that at high signal-to-noise levels the increase is not linear. Furthermore, at low signal-to-noise levels there exists a threshold in some types of circuits (*e.g.*, voice) below which the circuit is unusable. These levels should therefore have vanishing weight. The use of the minimum-level definition overcomes some of these objections by establishing a discontinuity in the weighting function, giving no weight to lesser signals and uniform weight to greater signals. This, too, is an artificial criterion since it is well-known that the merit of an antenna varies in a smoother fashion with signal level.

The antenna evaluation method presented here is based upon a communication-theory approach to the problem. As the fundamental premise, it is assumed that the effectiveness of an antenna is measured by its effect upon the information-transmission capabilities of the communication circuit in which it is an element. An appropriate measure is the "capacity" of the communication system, defined as the maximum possible rate of transmission of information. The results of Shannon[6,7] and others who have expounded a general theory of communication and have given expressions for the rates of transmission of information are thus applicable to the problem.

As a first step, it is presumed that the object of the analysis is the evaluation of the performance of an antenna system relative to the performance of other antennas that might be used in the same circuit. It is therefore assumed that all other components of the circuit are independent of the antenna. For example, the generator of the signal and the receiving system are assumed to have properties that are independent of the antenna systems. If transmitting antennas are being compared, the receiving antenna is assumed to have fixed properties, and vice versa. The relative coordinates and attitudes of the transmitting and receiving antennas are assumed to be governed by a probability function that is a quantitative expression of the probability of communication as a function of their coordinates and attitudes. Having made these assumptions, it is possible, through the use of Shannon's results, to calculate the capacity of the circuit averaged over coordinates and attitudes, in accordance with the probability function. It follows from the fundamental premise of this analysis that the average capacity is a direct measure of antenna effectiveness.

Shannon gives the following expression for the capacity, C, for transmission of information:

$$C = W \log_2\left(1 + \frac{S}{N}\right) \tag{1}$$

in which S and N are signal and noise-power densities assumed to be uniform in the frequency band W (cycles per second) and vanishing outside. The base-2 logarithm assures that the capacity is the number of bits per second that can be transmitted without error when they are properly encoded into signals having the assumed power spectrum. It is impossible to transmit without error at a greater rate than given by C, in (1). Systems in present use do not achieve the maximum rate possible because of limitations in the coding and decoding processes. Studies have shown, however, that the maxi-

[4] J. V. N. Granger, "Systems considerations in aircraft antenna design," IRE TRANS. ON AIRBORNE ELECTRONICS, vol. AE-1, pp. 1–12; December, 1951.

[5] A. Ellis, "Study of External Navigation Antennas on Lockheed Constellation Aircraft," Airborne Instr. Lab., Mineola, N. Y., Rep. 726–IT; August, 1949.

[6] C. E. Shannon, "A mathematical theory of communications," *Bell Sys. Tech. J.*, vol. 27, pp. 379–423, July, 1948; pp. 623–656, October, 1948.

[7] C. E. Shannon, "Communication in the presence of noise," PROC. IRE, vol. 37, pp. 10–21; January, 1949.

mum rates of nonideal circuits bear a direct relationship to the capacity. Therefore, the effect of the antenna system upon the rate of communication with nonideal coding systems may be measured by its effect upon the capacity of the system.

An extension of (1) for the capacity, when the signal, $S(f)$, and the noise, $N(f)$, powers are functions of the frequency, f, is given by

$$C = \int_0^\infty \log_2 \left[1 + \frac{S(f)}{N(f)}\right] df. \tag{2}$$

Eqs. (1) and (2) may be applied to the evaluation of antennas by expressing the signal-to-noise ratio at the output of the receiver in terms of other parameters of the communication circuit. An assumed uniform signal and noise spectrum in the band W leads to

$$C(r, \theta, \phi) = W \log_2 [1 + R(r, \theta, \phi)] \tag{3}$$

in which $C(r, \theta, \phi)$ is the capacity for transmission of information, and r, θ, ϕ are spherical coordinates of the receiver relative to the transmitter. The term $R(r, \theta, \phi)$ is the signal-to-noise ratio at the output of the receiver and is a function of r, θ, ϕ and of the parameters of the circuit. The effectiveness of an antenna system is measured by the value of $C(r, \theta, \phi)$ averaged over all possible values of the relative coordinates. This is given by

$$\overline{C} = \int_v p(r, \theta, \phi) C(r, \theta, \phi) dv \tag{4}$$

in which $p(r, \theta, \phi)\, dv$ represents the probability of communication to the volume dv with relative coordinates r, θ, ϕ, and the integration is performed over all space. The probability function satisfies the relation

$$\int_v p(r, \theta, \phi) dv = 1. \tag{5}$$

Application of (2) leads to

$$\overline{C} = \int_v \int_0^\infty p(r, \theta, \phi) \log_2 [1 + R(r, \theta, \phi)] df dv \tag{6}$$

in which R and p may be dependent upon the frequency.

An implication of (4) and (6) is that the effectiveness of an antenna in communicating between two points is a logarithmic function of the signal-to-noise ratio. This weighting function is to be compared with the weighting functions of the antenna-system-efficiency and minimum-level methods of evaluation previously described. It should be remarked that the logarithmic weighting function is rigorously applicable to an ideal system only; it is, thus, not strictly applicable to systems in present use, although comparison with the other weighting functions shows much agreement.

In many applications of this evaluation method it is possible to reduce the complexity of (4) and (6). For example, assume that the communication circuit is in free space, so that

$$R(r, \theta, \phi) = \frac{\eta_t \eta_r P G_t G_r \lambda^2}{16\pi^2 r^2 k T F W} \tag{7}$$

in which η_t and η_r are the efficiencies of the transmitting and receiving antenna matching networks; P is the signal power-input density (watts/cycles) to the transmitting antenna system; G_t and G_r are the directive gains of transmitting and receiving antennas; F is the noise figure of the receiver; k is Boltzmann's constant; T is the absolute temperature; and W is the bandwidth of the system.

As a generalized form for both transmitting and receiving antennas, R may be expressed as

$$R(r, \theta, \phi) = \frac{K \eta G(\theta, \phi)}{r^2} \tag{8}$$

in which K is a constant, and therefore

$$\overline{C} = W \int p(r, \theta, \phi) \log \left[1 + \frac{K \eta G(\theta, \phi)}{r^2}\right] dv. \tag{9}$$

Under these conditions the integration over the radial coordinate may be performed independently of other integrations. It is also possible to determine the optimum $G(\theta, \phi)$ that maximizes $\overline{C}$ for a particular $p(r, \theta, \phi)$. When $p(r, \theta, \phi)$ is a constant between limiting values of θ and ϕ and vanishing outside, it may be shown that the optimum $G(\theta, \phi)$ is also a constant between these limits and vanishing outside.

Another possible simplification is the comparison of antennas for a fixed value of r. This leads to a modified form

$$\overline{C}' = W \int\int p(\theta, \phi) \log \left[1 + \frac{K\eta}{r^2} G(\theta, \phi)\right] \sin \theta d\theta d\phi \tag{10}$$

in which $p(\theta, \phi)$ is subject to the condition

$$\int\int p(\theta, \phi) \sin \theta d\theta d\phi = 1. \tag{11}$$

Under these conditions it is possible to determine the optimum pattern $G_0(\theta, \phi)$ that yields a maximum value of $\overline{C}'$. It is given by

$$G_0(\theta, \phi) = \frac{r^2}{K\eta} \left\{ p(\theta, \phi) \left[\int\int \sin \theta d\theta d\phi + \frac{K\eta}{r^2} \right] - 1 \right\} \tag{12}$$

in which the limits of integration are those between which $p(\theta, \phi)$ is nonvanishing.

In the comparison of antennas for communication circuits operating at low signal-to-noise ratios, the complexity of the formula for $\overline{C}'$ is considerably reduced. If the approximation

$$\log (1 + X) = X \qquad X \ll 1$$

is employed, (10) reduces to

$$\overline{C}' = \frac{WK\eta}{r^2} \int\int p(\theta, \phi) G(\theta, \phi) \sin \theta d\theta d\phi. \tag{13}$$

In this form the average capacity is proportional to the average power available in the communication circuit.

This form is equivalent to the antenna-system-efficiency criterion for a uniform probability function within a prescribed angular sector. Since only uniform probability functions have been considered in past use of the antenna-system-efficiency method, it should be noted that an extension of this evaluation method to the use of nonuniform probability functions should lead to a result similar to (13).

Thus the concept of using the Shannon formula as a weighting function for antenna evaluation was evolved. In another paper by the author,[3] this method was applied to the evaluation of a particular antenna system and compared with results obtained for the antenna-system efficiency and minimum-level evaluation methods.

ACKNOWLEDGMENT

The author wishes to acknowledge the contribution of Dr. J. V. N. Granger to this work. Under Dr. Granger's leadership a favorable environment for this type of research was created. Alternate criticism and encouragement coupled with constant searching enquiry on his part helped to produce worthwhile results, of which this paper is only one of several.

Performance Evaluation of HF Aircraft Antenna Systems*

ERNEST J. MOORE†

Summary—**Many antennas, especially for aircraft application, must radiate into large sectors and operate over wide bands of frequency. At the same time, means of pattern control are often limited. In order to evaluate the performance of such antennas, several antenna-rating schemes have been proposed in the past. This paper[1] is concerned with the evaluation of HF aircraft antennas used for long-range voice ground-to-air and air-to-ground communications. The different antenna evaluation methods are compared theoretically for consistency among themselves. It is shown that they all lead to essentially identical relative ratings of different antennas used on the same aircraft. Furthermore, these ratings can be related to articulation scores, operationally the most significant parameter of voice-communication circuits. Since all the rating schemes investigated lead to about the same results, the simplest of these, namely the radiation pattern efficiency, appears to be the most suitable measure of effectiveness of HF aircraft antennas. The conclusions reached were verified through computations on radiation patterns obtained from model measurements.**

INTRODUCTION

IN a companion paper Lucke[2] has described a method of antenna evaluation based on the average information capacity of the channel of which the antenna forms a part. Other evaluation methods somewhat simpler in application have been used in the past. In particular, the radiation-pattern distribution function (or minimum-level criterion) has been used by Ellis[3] for rating various proposed UHF or VHF antennas for aircraft application, and Granger has defined a "radiation-pattern efficiency"[4] for the evaluation of HF aircraft antennas.

The purpose of this paper is to compare these different methods of antenna evaluation when they are applied to the aircraft-liaison antenna. This antenna is used for long-range air to-ground and ground-to-air communications in the HF range. Since voice transmissions are used almost exclusively over such circuits at the present time, the number of words correctly identified at the receiver appears to be an operationally more significant measure of circuit effectiveness than the information transmission rate. Such a measure, when obtained under suitably controlled conditions, is called the articulation score.[5] It will be shown that articulation scores and information rate lead to essentially the same results when evaluating antennas for this application. These two measures, in turn, are closely related to the radiation pattern efficiency and the minimum level criterion.

In order to compare the various proposed methods of antenna evaluation, an analysis was made of the radiation patterns of different HF antennas on several aircraft. The performance ratings obtained for a given antenna, by the use of the different measures, were then compared as to the consistency of the results obtained. A study was also made of the changes of the ratings caused by varying some of the parameters of the evaluation schemes. It was found that all of the proposed methods of antenna evaluation lead to essentially equal

* Manuscript received by the PGAP, July 10, 1957. The work was supported by the Antenna Section, Commun. and Navig. Lab., Wright Air Dev. Ctr.

† Systems Evaluation Group, Weapons Systems Lab., Stanford Res. Inst., Menlo Park, Calif.

[1] This paper consists essentially of Appendix B of the following report: E. J. Moore, "Performance Specification and Evaluation of Liaison Antennas," Stanford Res. Inst., Menlo Park, Calif., Final Rep. Task III, SRI Project 606, Contract AF 33(616)83; November, 1953.

[2] W. S. Lucke, "Antenna evaluation methods," this issue, p. 251.

[3] A. R. Ellis, "Study of External Navigation Antennas on Lockheed Constellation Aircraft," Airborne Instr. Lab., Mineola, N. Y., Rep. No. 726-II; August, 1949.

[4] J. V. N. Granger, "Systems considerations in aircraft antenna design," IRE TRANS. ON AIRBORNE ELECTRONICS, vol. AE-1, pp. 1–12; December, 1951.

[5] See, for instance, G. H. Miller, "Language and Communication," McGraw-Hill Book Co., Inc., New York, N. Y., 1951.

results. This fact not only makes it possible to rate antennas by the most convenient method, but also leads to an interpretation of the ratings in terms of articulation scores which are considered here as a primary measure of system performance. It was also found that some of the parameters required in computing the ratings can be varied over considerable ranges before changing the relative standing of different antennas on the same aircraft. It is often difficult to determine the appropriate magnitude of such parameters, especially where sky-wave propagation is involved. This analysis shows that exact knowledge of these factors is not required for the determination of the relative merit of several proposed antenna systems.

Average Information Capacity as a Measure of Antenna Performance

Lucke[2] has proposed a "factor of merit" for antenna systems given by the average information capacity of the circuit of which the antenna forms a part, the average being taken over all situations under which communication links may take place. Let ζ stand for the aggregate of all the variables on which the signal-to-noise ratio, $S/N(\zeta)$, at the receiving end of the link, depends. For the air-to-ground liaison system, these variables are the antenna-radiation patterns, the transmitted power, and the atmospheric noise, as well as time, place, distance, and frequency of transmission. The variable ζ is distributed with a probability density, $p(\zeta)$. The average information capacity of the circuit, per unit bandwidth, is given by

$$\overline{C} = \int p(\zeta) \log_2 \left[1 + \left(\frac{S}{N}(\zeta) \right) \right] d\zeta, \qquad (1)$$

where the integration has to be carried out over the volume for which $p(\zeta)$ is defined, *i.e.*, for the volume for which

$$\int p(\zeta) d\zeta = 1.$$

Extensive numerical work is required to compute the average information capacity for even the simplest case. For sky-wave transmission, where the signal-to-noise ratio depends on a large number of variables, use of such a factor is very cumbersome indeed, since changes in both signal level and noise enter the factor in a complicated manner. Such changes may be due to mismatching of the antennas, variations in ionospheric absorption, or use of different transmitters, as well as to changes in the orientation of the transmission path with respect to the aircraft. It is therefore of interest to examine (1) for possible simplifications.

If the signal-to-noise ratio is always less than unity, we have approximately

$$\overline{C} = 1.44 \int p(\zeta) \left[\frac{S}{N}(\zeta) - \frac{S^2}{N}(\zeta) + \cdots d \right] \zeta. \qquad (2)$$

The first term in this expansion can itself be used as a factor of merit and has been discussed elsewhere.[6]

The approximation of (2) breaks down for signal-to-noise ratios larger than unity. In general, however, (1) may be written as follows:

$$\overline{C} = \log_2 \left[1 + \left(\frac{\overline{S}}{N} \right) \right] + p(\zeta) \log_2 \left[1 + \frac{\frac{S}{N}(\zeta) - \left(\frac{\overline{S}}{N} \right)}{1 + \left(\frac{\overline{S}}{N} \right)} \right] d\zeta,$$

where the bar indicates average values, *i.e.*,

$$\frac{\overline{S}}{N} = \int p(\zeta) \frac{S}{N}(\zeta) d\zeta. \qquad (3)$$

Now assume that the deviation of the signal-to-noise ratio from its average value is small compared to the average value, *i.e.*,

$$\frac{\left(\frac{\overline{S}}{N} \right)^2 - \left(\frac{\overline{S}}{N} \right)^2}{1 + \left(\frac{\overline{S}}{N} \right)} \ll 1.$$

Expanding the logarithmic term and carrying out the integration, the average information capacity is found to be

$$\overline{C} \cong \log_2 \left[1 + \left(\frac{\overline{S}}{N} \right) \right] - 0.72 \frac{\left(\frac{\overline{S}}{N} \right)^2 - \left(\frac{\overline{S}}{N} \right)^2}{\left[1 + \left(\frac{\overline{S}}{N} \right) \right]^2}. \qquad (4)$$

To test the validity of this approximation, the operations required by (1) and (4) were performed on some radiation patterns of HF antennas on a C-54 aircraft. The noise, N, and the function, $p(\zeta)$, were taken to be constant for these computations. The integrations were carried out over all directions in azimuth about the aircraft antenna, using various slices of the radiation patterns of 10° width in elevation. Separate computations were made for several values of noise power, the smallest noise power considered differing from the largest by about 20 db. In the mean, the average information capacity evaluated by the use of (4) differed from the value computed from (1) by only 0.4 per cent. The maximum error among the thirty cases considered was 3 per cent. Using the first term of (4) only, *i.e.*, letting

$$\overline{C} \cong \log_2 \left[1 + \left(\frac{\overline{S}}{N} \right) \right], \qquad (5)$$

[6] E. J. Moore, "Factor of merit for aircraft antenna systems for the frequency range from 3 to 30 mc," IRE Trans. on Antennas and Propagation, vol. AP-3, pp. 67–74; August, 1952.

the average error was 8 per cent with a maximum error of 14 per cent. It appears, therefore, that (5), which depends only on the average signal-to-noise ratio, may be used as an approximation to the average information capacity. It should be noted that as long as this approximation is satisfied, use of the average signal-to-noise ratio as a measure of antenna performance will lead to the same rank order in the comparison of several antennas as that obtained from use of the average information capacity. The radiation-pattern efficiency which will be discussed presently is also closely related to the average signal-to-noise ratio.

The Useful Solid Angle Sector

A complete discussion of all factors required in the computation of the performance measures is outside the scope of this paper. It can be shown, however, that when comparing the relative merit of various proposed antenna systems, much of the detailed consideration of ionospheric transmission can be neglected without altering the relative standing of antenna systems. Therefore, before proceeding with a discussion of other performance measures, certain simplifications will now be introduced which limit the number of variables to those directly related to the antennas. The evaluation factors will then be expressed in terms of radiation patterns and antenna impedance alone. Only the case of transmission from the aircraft to a ground station will be considered, because differences in antenna systems can be shown to have relatively little effect on reception on the aircraft.[1]

In order to arrive at these simplifications, variations in ionospheric conditions must largely be ignored. Noise will be considered constant for any particular case; it will then play the role of a parameter of the various performance measures. The only changes in signal strength considered are those due to variations in antenna patterns that occur because of changes in the direction of transmission with respect to the aircraft. For a constant heading of the aircraft with respect to the ground station, the signal-to-noise ratio is then fixed. To take account of the true variations in signal-to-noise ratio, its distribution in time should also be considered. However, measurements show these distributions to be stationary about their mean value, so that conclusions reached on the basis of a single value of this ratio are representative of those obtained by the use of the entire distribution.

These assumptions physically correspond to replacing the actual ionosphere by a perfectly reflecting layer at a fixed height, supporting a single transmission mode only. Other properties of sky-wave transmission are, however, retained. Since, in general, sky-wave signals are randomly polarized, the signal power is proportional to the total power density at the receiver. The power density per unit solid angle, $P(\Omega)$, about the aircraft antenna is given in terms of the antenna-gain function and the total transmitted power, P_t, by:

$$P(\Omega) = P_t \frac{G(\Omega)}{4\pi} . \tag{6}$$

If $G_1(\Omega)$ and $G_2(\Omega)$ are the gains in any two perpendicular directions of polarization, the power gain of interest here is given by

$$G(\Omega) = G_1(\Omega) + G_2(\Omega). \tag{7}$$

Gains are usually determined for polarization in the θ and ϕ directions of a spherical coordinate system about the aircraft.

The direction of the transmission path, with respect to the aircraft, depends on the relative location of aircraft and ground station. A consideration of all possible directions of transmission leads to a probability distribution expressing the likelihood that a given solid angle sector about the aircraft will contain the transmission path. Since this function is not readily obtainable in practice, the probability density is here taken as a constant over a solid angle sector, Ω_u, considered to be useful for transmission; no communications are assumed to take place in directions outside this sector. The extent of the useful sector is not well-defined. However, examination of the performance measures as a function of this sector shows that this lack of precise knowledge does not significantly influence antenna ratings.

Antenna-performance measures have so far been discussed largely in terms of the antenna radiation patterns. The antenna impedance is another important function of the antenna. It is directly related to the maximum obtainable efficiency of the matching circuit which transforms the antenna impedance to that of the transmission line connecting the transmitter and antenna. Ohmic losses in the transmission line, matching circuit, and the antenna itself, as well as power lost due to incomplete matching, reduce the total available transmitter power, P_t, in (5). Such losses may therefore be included as a constant fractional multiplier of the gain function. In the following discussion, the gain is to be understood to contain this loss factor unless explicitly stated otherwise.

The Voice Intelligibility Index

Articulation scores as observed over the liaison system not only provide a readily measurable performance rating for the circuit but they also have a more direct operational significance than the information capacity. The articulation score has therefore been proposed here as the basic measure for the comparison of antenna systems. It may be noted that the articulation score is a function of the amount of information received by the listeners. However, the articulation score cannot be taken as a direct measure of the amount of information in the speech wave.[5]

The measured relationship between signal-to-noise ratio and articulation scores is shown in Fig. 1. Since,

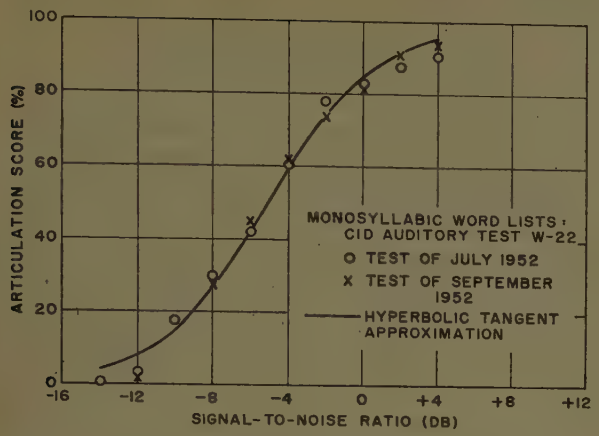

Fig. 1—Articulation scores as a function of signal-to-noise ratio in white noise.

for the constant noise which is assumed here, the signal-to-noise ratio is directly proportional to the antenna gain, the latter could be transformed into articulation scores, provided the constant of proportionality were known. A measure of antenna effectiveness called "voice intelligibility index" can then be obtained by averaging articulation scores over the useful solid angle sector, Ω_u. In practice, the constant of proportionality between gain and the signal-to-noise ratio is a function of time, since signal-to-noise ratios vary with ionospheric conditions. The position of the gain on the signal-to-noise ratio scale therefore also varies with time. As discussed earlier, these time functions are ignored here, and the relative position of gain and signal-to-noise ratio is regarded as a parameter. The term "voice intelligibility index" was chosen in order to make clear the distinction between this measure and true articulation scores which depend on the changes of both signal and noise.

For the sake of simplicity, a linear approximation is used for the relation between articulation score and signal-to-noise ratio shown in Fig. 1. Let g denote the gain function in decibels, *i.e.*,

$$g = 10 \log_{10} G(\Omega), \tag{8}$$

and let y be the threshold value, *i.e.*, that value of g for which the articulation score is zero. If d is the range in gain from zero per cent articulation score to 100 per cent articulation score (about 15 db as seen from Fig. 1), then the articulation score is given by

$$\begin{aligned} A(g, y) &= 0 && g < y \\ A(g, y) &= 100 \frac{g - y}{d} && y < g < y + d \\ A(g, y) &= 100 && g > y. \end{aligned} \tag{9}$$

The threshold level, y, is a parameter, as previously discussed. The voice intelligibility index, $I(y)$, is then given by the following integral:

$$I(y) = \frac{1}{\Omega_u} \int_{\Omega_u} A(g, y) d\Omega. \tag{10}$$

The voice intelligibility index in the form of (10) may be regarded as an average of the function $A(g, y)$ over the solid angle sector, Ω_u. If $p(g)dg$ is the fraction of all values of g occurring in Ω for which the gain, g, lies between the following limits:

$$g < g_1 < g + dg$$

the voice intelligibility index may be written in the equivalent form

$$I(y) = \int_{-\infty}^{+\infty} A(g, y) p(g) dg \tag{11}$$

which is an average over the gain, instead of an average over the solid angle. Substituting for $A(g, y)$ in (11), it is found that after some reductions,

$$I(y) = \frac{100}{d} \int_{y}^{y+d} \Phi(g > u) du \tag{12}$$

where $\Phi(g, u)$ is the fraction of all values of g within Ω_u, which exceeds u decibels, *i.e.*

$$\Phi(g > u) = \int_{u}^{\infty} p(x) dx. \tag{13}$$

One essential difference between the voice intelligibility index and the performance measure based on average information capacity is the way in which changes in transmitted power affect the ratings. For the voice intelligibility index, the loss in power due to ohmic losses anywhere in the system can be taken account of through a shift of the function $I(y)$, in the direction of the g axis, by an amount equal to the power-transfer efficiency expressed in decibels. The index can, therefore, be calculated on the basis of the radiation patterns alone. The loss in power through the system is later included in the rating by a simple shift in origin of the g coordinate.

It was shown earlier that the average information capacity of the liaison system is closely related to the average signal-to-noise ratio, provided these ratios are not too widely scattered from their mean. This condition was shown to be satisfied by aircraft antenna radiation patterns in the high-frequency range. It will now be shown that a similar relationship exists between the voice intelligibility index and the average signal-to-noise ratio. For this purpose, the useful angular sector is divided into three regions:

Ω_1 over which $g < y$

Ω_2 over which $y < g < y + d$

Ω_3 over which $g > y + d$

corresponding to the three ranges over which the function $A(g, y)$ of (9) is continuous and where, of course,

$$\Omega_1 + \Omega_2 + \Omega_3 = \Omega_u.$$

If the average gain is taken over the sector Ω_2 rather than over the entire useful sector, the voice intelligibility index is found from (10) to be given, approximately, by

$$I(y) = 100 \frac{\Omega_3}{\Omega_u} + \frac{100}{d} \frac{\Omega_2}{\Omega_u} 10 \log_{10} \overline{G} - y] - \frac{217}{d} \frac{\Omega_2}{\Omega_u} \frac{\overline{G^2} - \overline{G}^2}{\overline{G^2}}. \quad (14)$$

The last term of this equation has already been shown to be small for HF aircraft-antenna radiation patterns. If it is further assumed that the noise is such that almost the entire pattern within the useful solid sector lies within the range $y<g<y+d$, *i.e.*,

$$\frac{\Omega_1 + \Omega_3}{\Omega_u} \ll 1,$$

then the voice intelligibility index is given by the following approximate expression

$$I(y) \cong \frac{100}{d} (\bar{g} - y) \quad (15)$$

where

$$\bar{g} = 10 \log_{10} \left\{ \frac{1}{\Omega_u} \int_{\Omega_u} G(\Omega) d\Omega \right\}. \quad (16)$$

To this degree of approximation, the voice intelligibility index is seen to be a linear function of the threshold level, y, independent of the radiation pattern. Differences in pattern merely change the position of this function, with respect to the g coordinate, in the same manner as do changes in the power transfer efficiency. An analysis of a large number of radiation patterns shows that these approximations are essentially justified.

Let us now examine further the relationship between average articulation score and the voice intelligibility index. The variations with time of the signal-to-noise ratio may be thought of as variations of the threshold level, y. These values of y are distributed with a density, $p(y)$, that is approximately stationary if suitable time intervals are considered. The average articulation score, $\overline{A}$, is then given in terms of the voice intelligibility index by

$$A = \int_{-\infty}^{+\infty} p(y) I(y) dg. \quad (17)$$

Using the approximate expression of (15) for the voice intelligibility index, the average articulation score is found to be given by

$$\overline{A} = \frac{100}{d} (\bar{g} - \bar{y}) \quad (18)$$

where $\bar{y}$ is the expected value of the variations in threshold level. This level depends, of course, on the mean signal power as well as on the noise. The significance of (18) lies in the fact that $\bar{y}$ is a constant, practically independent of the particular aircraft antenna used for transmitting. In a rating of antennas on a relative basis, $\bar{y}$ will cancel out and an evaluation based on the voice intelligibility index can be compared directly with the results obtained in terms of actual articulation scores.

The Minimum Level Criterion or Radiation Pattern Distribution Function

The radiation pattern distribution function (or minimum level criterion) given by (13) has itself been used as a measure of antenna performance.[2] It has been found useful where the noise level is fixed, and its relationship to the power density of the signal at the receiver location is known. In that case, only a single value of the distribution function is obtained, which is given by the fraction of the useful solid angle over which the gain function exceeds some fixed minimum level. In our case, however, the entire distribution function is required, for which the minimum level may take on all values between $-\infty$ and $+\infty$. It is easily shown that (13) is identical to the following average over the unit-step function:

$$\Phi(g > y) = \frac{1}{\Omega_u} \int_{\Omega_u} u(g - y) d\Omega \quad (19)$$

which is a more convenient form for computation. Here again, changes in power-transfer efficiency can be accounted for by a simple translation in origin of the g coordinate.

The Antenna System Efficiency

The antenna system efficiency is defined as the fraction of the total power radiated in useful directions.[4] In terms of the gain function, $G(\Omega)$, the antenna system efficiency is given by the integral

$$\eta_s = \frac{1}{4\pi} \int_{\Omega_u} G(\Omega) d\Omega. \quad (20)$$

It should be remembered that the gain is defined here in terms of the total available power. If the usual gain function defined in terms of the total radiated power is used instead, the resulting expression is known as the radiation pattern efficiency, η_p. Letting η_{tr} be the ratio between total radiated power and total available power, the antenna system efficiency will be given by

$$\eta_s = \eta_{tr} \eta_p. \quad (21)$$

The approximate expression of (15) shows the following relationship between voice intelligibility index and antenna system efficiency:

$$I(y) = \frac{100}{d}\{K + 10\log_{10}\eta_s - y\} \tag{22}$$

where K is a constant. A similar expression is obtained from (18) for the average articulation score.

To the degree of this approximation, the voice intelligibility index and the logarithm of the antenna system efficiency are linearly related. The close relationship between articulation scores and voice intelligibility index makes it possible, then, to interpret differences in antenna system efficiency in terms of articulation scores —the parameter most significant to the system as a whole. This is more fully investigated in the next section.

Relative Performance of Antenna Systems

In general, useful antenna ratings must be relative, since the performance of the system as a whole depends on a large number of other factors. The quantity of interest is the relative standing of several proposed antennas that might be used for an application, the performance of one of the antennas being chosen as a reference.

Consider first a comparison of antennas based on the voice intelligibility index. It will be shown presently that the linear approximation of (22) is valid over a considerable range of values of y. Let the comparison be made at the same noise level, y_a. Denoting quantities for the two antennas under comparison by subscripts 1 and 2, one finds for the difference in voice intelligibility index:

$$I_2 - I_1 = \frac{100}{d}\left\{10\log_{10}\frac{\eta_{s_2}}{\eta_{s_1}}\right\}. \tag{23}$$

It should now be recalled that in deriving the voice intelligibility index all time variations in signal-to-noise ratio were neglected. When fading is taken into consideration, it will be found that the range in signal-to-noise ratio between 0 per cent articulation and 100 per cent articulation is, in general, considerably larger than the range, d, obtained for tests using white noise and a steady signal. The difference in voice intelligibility index as given by (23) therefore differs by some factor from a true difference of articulation scores, and this proportionate factor depends on the time variations of the ionosphere.

If, under otherwise identical conditions, two antenna systems are found to have equal voice intelligibility indexes, average articulation scores over the two systems will be observed as identical also. This is evident by inspection of (17). Consider, therefore, changes in the variable y as being due to changes in available transmitted power, and examine (22) for the conditions under which equal voice intelligibility indices are obtained. It is then found that

$$y_2 - y_1 = 10\log_{10}\frac{\eta_{s_2}}{\eta_{s_1}} \tag{24}$$

where $(y_2 - y_1)$ is the increase (in decibels) in available power required in the system using antenna no. 1, over that required in the system using antenna no. 2, so that the average articulation score is the same for both systems. This measure of the relative performance of the antennas is independent of ionospheric time variations. The power change required to obtain equal system performance can be visualized in terms of size, weight, and cost of the transmitting equipment, and, as just shown, it is simply related to the ratio of the antenna system efficiencies. Finally, the term "equal system performance" as used here is synonymous with "equal articulation score, on the average." A comparison of antennas on this basis, therefore, seems most useful for practical application.

It may be noted that the antennas can be rated in terms of power changes required for equal system performance, where system performance is measured by the radiation pattern distribution function. It can be seen however, that such comparisons depend rather critically on the parameter y. Furthermore, the radiation pattern distribution function lacks the direct operational significance of the average articulation score. This means of rating antennas is therefore not recommended here.

In order to demonstrate the validity of the various assumptions made in the analysis just presented, an examination was made of a large number of radiation patterns for different HF antennas on several aircraft. A complete report on the results of the computations performed on these patterns will be found in Moore.[1] Fig. 2 shows an example of the results obtained. This figure shows the relative performance as a function of frequency of several antennas mounted on a C-54 aircraft. The pattern data from which these curves were computed were obtained from model measurements at the Antenna Laboratory of The Ohio State University Research Foundation. The antennas consisted of an isolated section of the vertical stabilizer, isolated wing tips on each side of the aircraft, and a fixed-wire antenna. The two wing tips were either driven symmetrically with respect to the fuselage (out of phase) or antisymmetrically (in phase), or a single isolated wing tip was used. The fixed-wire antenna was taken as a basis of comparison for the other antennas.

The first set of curves shows the relative standing of the various antennas when the radiation pattern efficiency is used as the performance measure, while for the second set of curves the voice intelligibility index has been used. The similarity between the results obtained using these two methods justifies the assumptions made in the analysis.

A large-scale flight testing program was carried out using a C-54 aircraft with fixed-wire, wing-cap, and tail-

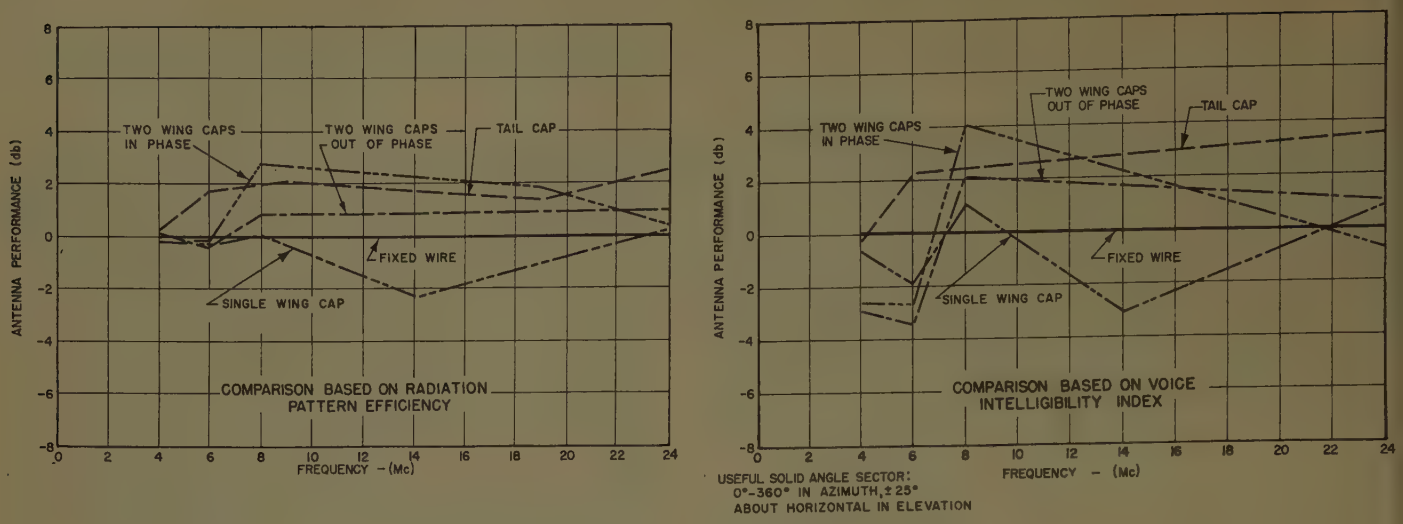

Fig. 2—Performance ratings of antennas on C-54 aircraft.

cap antennas to test further the validity of the concepts presented here. Results of the flight tests, which are described by Moore,[1] again showed the close relationship between average articulation scores and antenna ratings based on the radiation pattern efficiency.

ACKNOWLEDGMENT

The author gratefully acknowledges the help and guidance given during the course of this work by Drs. J. V. N. Granger and John Taylor, both formerly of Stanford Research Institute.

Effects of Satellite Spin on Ground-Received Signal*

J. T. BOLLJAHN†

Summary—**This report presents an analysis of those characteristics of the radio signal received on the ground from an artificial earth satellite which are caused by satellite spin. It is shown that if the spin axis of the satellite does not coincide with the axis of symmetry of the satellite antenna system, a CW transmitted signal will be split into three closely spaced spectral components in a manner similar to the Zeeman effect in atomic spectra.**

The relative amplitudes of the three spectral components are calculated for various combinations of satellite antenna type, ground antenna type, antenna observation angle, and angle between the spin axis and antenna symmetry axis of the satellite, and the significance of these results is discussed.

INTRODUCTION

THE antennas carried by the U. S. earth satellites[1] to be launched during the International Geophysical Year will consist of a pair of crossed dipoles driven in phase quadrature. The 20-inch conducting sphere will be sufficiently small relative to the wavelength for the 100-mc radiated signal so that the dipole patterns will be essentially unaffected by its presence. We are told that the final stage of the launching vehicle is to be spun at about 2 cps for stabilization purposes before the satellite is ejected. Although it is intended that the satellite spins about its axis of symmetry after ejection, the result of imperfect application of the ejection forces will be to cause the spin axis to depart from the symmetry axis. Since the satellite will presumably have different moments of inertia about its symmetry axis and about the other mutually perpendicular axes, imperfect ejection will lead to a precession of the spin axis. However, if the moments of inertia do not differ greatly, it can be shown that the precession frequency will be much smaller than the spin frequency. Assuming that this is to be the case, precession will be neglected for the purpose of this study.

This report is concerned with the effect of the satellite spin on the ground-received signal, assuming that the spin axis may be arbitrarily oriented with respect to the symmetry axis. Spin is not the only factor leading to dynamic signal variations in the ground-received signal,

* Manuscript received by the PGAP, October 21, 1957. This work was supported by the U. S. Army Ordnance Dept., Ballistic Res. Labs., under Contract DA 03-400-ORD-273. This paper was presented at the Spring URSI meeting, May, 1957.

† Stanford Res. Inst., Menlo Park, Calif.

[1] The satellite considered is the Vanguard.

since substantial Doppler frequency shifts will occur, as well as Faraday rotation of the polarization plane and atmospheric refraction; however, an analysis of the spin effect is necessary to complete understanding of the signal character.

The Satellite Antenna

Let us first review briefly the nature of the signal radiated by the satellite antenna. Fig. 1 shows an idealized satellite antenna in the form of simple-crossed dipole pair.

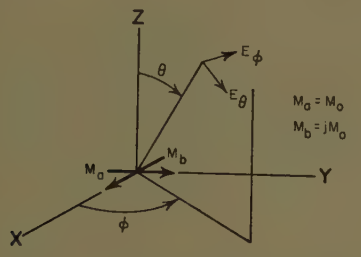

Fig. 1—Idealized satellite antenna.

Although the antenna elements on the satellite will be half-wave element, the small difference between the patterns of a half-wave element and an electrically short dipole will be neglected in this analysis, and it will be assumed that each element radiates as a short dipole having a moment M_0. It is readily shown that the θ and ϕ components of electric field from this antenna are given by the expression:

$$E_\theta = jKM_0 \cos\theta e^{j\phi}$$
$$E_\phi = KM_0 e^{j\phi} \qquad (1)$$

where

$$K = \frac{\omega\mu e^{-jkr}}{4\pi r},$$

$$k = \frac{2\pi}{\lambda}.$$

When the satellite is spun about an arbitrary axis, a fixed receiving antenna will see the satellite antenna from a succession of different aspects during the course of a spin cycle. As far as the geometry of the problem is concerned, spinning the satellite is equivalent to moving the receiving antenna about a circular path on a large sphere centered at the satellite antenna while the latter remains fixed. The circular path followed by the receiving antenna is centered on the satellite spin axis, θ_s, ϕ_s (Fig. 2), while the size of the circle depends upon the angle, θ_0, between the spin axis and the line joining the satellite and the receiving antenna.

We now wish to show, in order to simplify later calculations, that a given spin situation is completely specified by the angles θ_s and θ_0, so that we need not consider ϕ_s as a significant variable.

From the form of (1), it is seen that both field components have amplitudes that are independent of ϕ and phase angles that are linearly related to ϕ. Regardless of the polarization characteristics of the receiving antenna, therefore, moving this antenna along a line of constant θ will simply vary the phase of the received signal without affecting its amplitude. If we now compare the signal variations observed in two spin situations having the same values of θ_s and θ_0 but with different values of ϕ, we see that corresponding positions on the two circular paths traced out by the receiving antenna yield signals which are the same except for a difference in RF phase. Furthermore, the phase difference between the signals received on two antennas, which are simultaneously moved around these two paths, will remain constant for the entire circuit. It follows that the relative signal variations observed in the two cases will be the same, the only difference being a shift in the RF phase. Since no phase-locked reference will be available for use in demodulating the satellite signal, we are concerned only with relative signal variations, and hence we need not consider the angle ϕ_s as a separate variable.

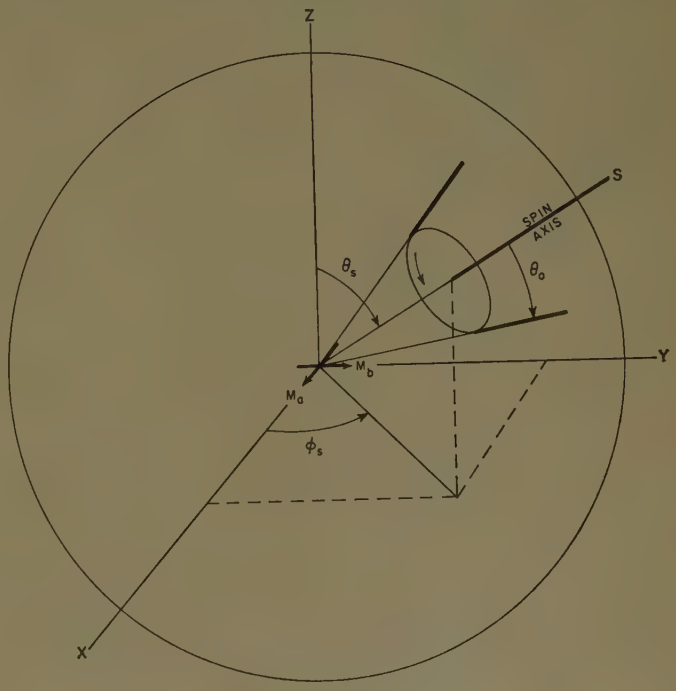

Fig. 2—Spin geometry.

Analysis of Spin Effect

Circularly Polarized Satellite Antenna and Circularly Polarized Observation Antenna

Consider the signal transmitted between the satellite antenna and an arbitrarily polarized antenna having polarization components M_1 and M_2, as shown in Fig. 3.[2] In accordance with the conclusions reached in the

[2] Note that the selection of positive directions for the various dipole moments has been completely arbitrary. Changes in these directions lead to various changes in the signs of expressions throughout the analysis, but not to any basic changes in the form of the results.

preceding section, the angle ϕ_s has been taken (without loss of generality) as 180 degrees, to minimize the complexity of the expressions involved in the analysis. We shall calculate the voltage induced in the satellite antenna due to a signal transmitted from the other antenna by means of the expression:

$$V = \frac{1}{2I_0}(\overline{E}\cdot\overline{M}_a + \overline{E}\cdot\overline{M}_b) \tag{2}$$

where

V = induced voltage,
$\overline{E}$ = electric field at origin due to excitation of M_1 and M_2,
I_0 = feed-point current in each satellite-antenna element corresponding to dipole moment M_0,
$\overline{M}_a$ and $\overline{M}_b$ are the vector dipole moments of the satellite-antenna elements (Fig. 3).

The computation of V is accomplished most readily by considering separately the two components of $\overline{E}$ produced by M_1 and M_2 and by resolving $\overline{M}_a$ into components that are parallel and perpendicular to the spin axis, as shown in Fig. 4. Assuming that the source antenna M_1M_2 is held fixed while the satellite antenna is turned through an arbitrary angle, ψ, about the spin axis (where the orientations for $\overline{M}_a$ and $\overline{M}_b$ in Fig. 4 correspond to the case $\psi=0$) we may calculate the following contributions to V:

1) due to the dipole moment $M_0 \sin\theta_s$

$$\frac{-KM_1M_0}{2I_0}\sin\theta_s\sin\theta_0$$

2) due to the dipole moment $M_0\cos\theta_s$

$$\frac{K}{2I_0}(M_1M_0\cos\theta_s\cos\theta_0\cos\psi - M_2M_0\cos\theta_s\sin\psi)$$

3) due to the dipole moment jM_0

$$\frac{-jK}{2I_0}(M_2M_0\cos\psi + M_1M_0\cos\theta_0\sin\psi).$$

The expression for induced voltage hence becomes

$$V = \frac{KM_1M_0}{2I_0}\left[-\sin\theta_s\sin\theta_0 + \cos\theta_s \cdot\left(\cos\theta_0\cos\psi - \frac{M_2}{M_1}\sin\psi\right) - j\left(\frac{M_2}{M_1}\cos\psi + \cos\theta_0\sin\psi\right)\right]. \tag{3}$$

Substituting $K'=KM_1M_0/2I_0$ and specializing to the case of a circularly polarized observation antenna by taking $M_2=jM_1$, we find

$$\frac{V}{K'} = \sin\theta_s\sin\theta_0 + \cos\psi(1+\cos\theta_s\cos\theta_0) - j\sin\psi(\cos\theta_s+\cos\theta_0). \tag{4}$$

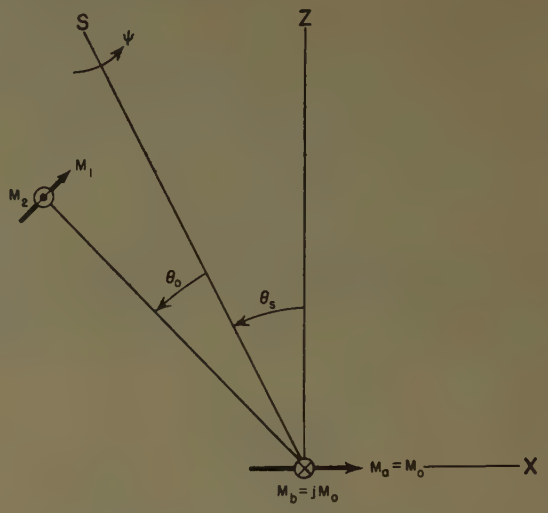

Fig. 3—Coordinates used in analysis.

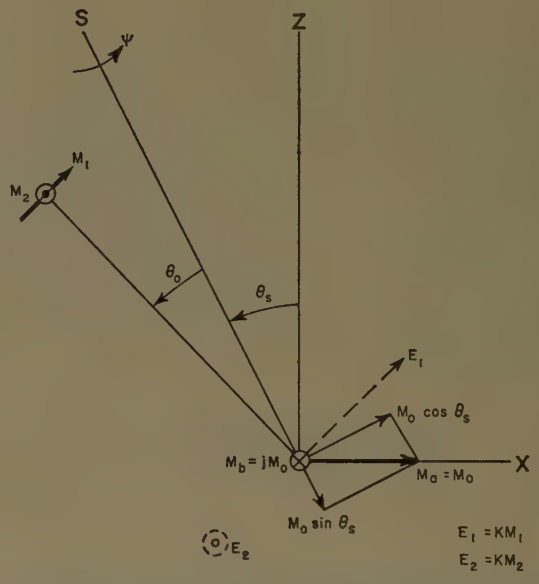

Fig. 4—Resolution of fields and dipole moments into components.

In the case of the spinning satellite, the angle $\psi=\omega_s t$, where ω_s is the radian frequency of mechanical rotation. It is seen from (4) that the first term is independent of ψ and hence will not vary with time as a result of spin, while the other two terms both undergo cyclical variations due to spin.

It may be seen with the aid of Fig. 5(a) that this signal can be resolved into three components, namely a carrier component at the frequency of the original transmission plus an upper and a lower sideband component separated from the carrier by the spin frequency. Noting that the expression for the composite signal shown in Fig. 5(a) may be written as:

$$\frac{V}{K'} = C + (U+L)\cos\psi - j(L-U)\sin\psi, \tag{5}$$

and equating (4) and (5), the three components may be solved for with the following results:

$$\left.\begin{aligned} C &= -\sin\theta_s \sin\theta_0 \\ U &= \tfrac{1}{2}(1-\cos\theta_0)(1-\cos\theta_s) \\ L &= \tfrac{1}{2}(1+\cos\theta_0)(1+\cos\theta_s) \end{aligned}\right\}. \qquad (6)$$

The relative phase of the sideband components are as shown in Fig. 5(a); *i.e.*, when they are in phase they either add to or subtract from the carrier component.

Since the upper and lower sidebands generally have different amplitudes, the resultant signal contains both amplitude and phase modulation. The terminus of the received voltage vector traces out an elliptical path as a function of time as shown in Fig. 5(b). It executes one complete circuit around this path for each rotation of the satellite. Of interest from this point of view is the possibility of spin errors in certain proposed experiments in which the Doppler shift of the satellite signal is measured by comparing the frequency of the satellite signal with that of a stable ground reference. The effect of spin on such an experiment is not easy to predict completely, but a reasonable assumption is that the satellite frequency will appear to be shifted upward or downward by a frequency equal to the spin frequency if the locus of the received signal encloses the origin. This effect will not be serious if it merely leads to an apparent frequency shift since the uncertainty in the frequency of the satellite transmitter will be considerably greater than the difference in frequencies between the spin sidebands. However, short-term stabilities (for the duration of a single satellite passage) of one part in 10^8, or about one cycle per second, are hoped for. If the sense of the spin error should be reversed during passage of the satellite, a frequency shift of twice the spin frequency, or about four cycles, would occur, thereby causing the effective short-term stability to be much poorer than anticipated.

Using the dimensions of the locus shown in Fig. 5(b) and the criterion that spin error will occur when this locus encloses the origin, it is seen that spin error is predicted for

$$1 + \cos\theta_s \cos > \sin\theta_s \sin\theta_0$$

or

$$1 > [-\cos(\theta_s + \theta_0)]. \qquad (7)$$

Eq. (7) may be derived alternatively by making use of the spectral component point of view. Referring to the composite signal in the form illustrated in Fig. 5(a), it is seen that the terminus of the composite signal vector will enclose the origin if $|U+L| > C$, which leads again to the condition expressed in (7).

From (7) one concludes that spin error will occur for all values of θ_s and θ_0, except possibly for $(\theta_s+\theta_0) = 180$ degrees. This condition is seen from (6) to be the same condition that leads to equal amplitudes for the two sidebands U and L, and from Fig. 3 it is seen to be also the condition common to all spin situations for which the observation point passes through the negative portion of the axis of symmetry of the satellite. A brief additional consideration of (4) and (6) shows that the spin error may be either positive or negative, depending upon the values of θ_s and θ_0, as in Fig. 6. Reversals of the sign of the spin error during a single passage of the satellite are seen to be possible in general since, as the satellite passes over an observer, θ_s will remain constant while θ_0 varies over a wide range. Fig. 6 expresses also the conditions that will cause only one of the three spectral components to appear, and the conditions for which $L = U$.

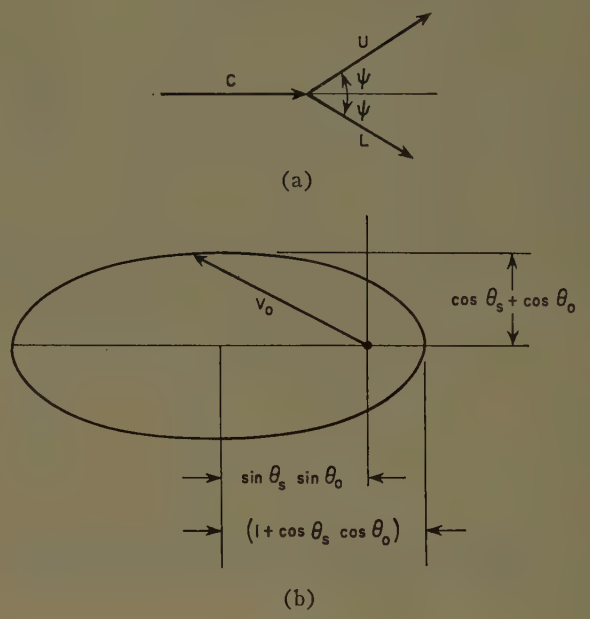

Fig. 5—Characteristics of received signal; circularly polarized satellite antenna, circularly polarized receiving antenna.

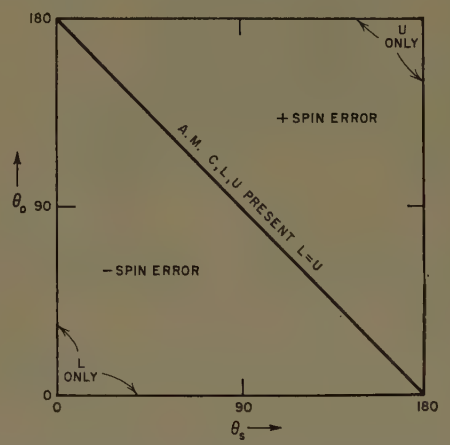

Fig. 6—Summary of signal characteristics; circularly polarized satellite antenna, circularly polarized receiving antenna.

Fig. 7 summarizes the results for a circularly polarized receiving antenna by showing radiation patterns for each of the three signal components measured about the spin axis for different values of θ_s. It is interesting to note that the significantly different radiation patterns shown would be measured by changing the receiving frequency only a few cycles at about 100 mc. The effect of errors in the relative amplitudes or phases of the

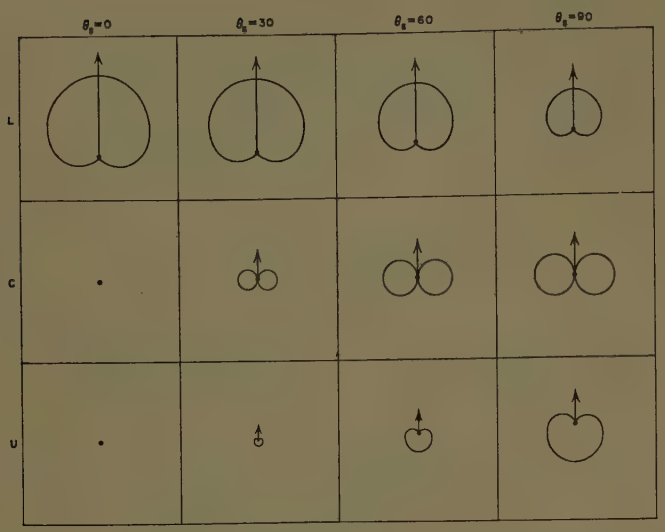

Fig. 7—Radiation patterns for spectral components; circularly polarized satellite antenna, circularly polarized receiving antenna.

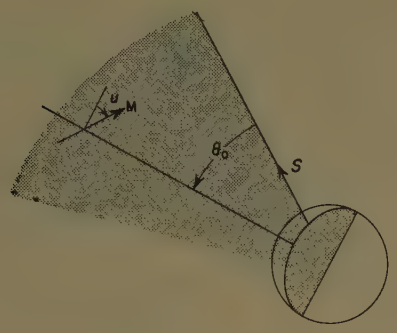

Fig. 8—Geometry for linearly polarized receiving antenna.

satellite antenna feeds can be inferred from these patterns. If the on-axis signal from the satellite is known to be elliptically polarized, we may regard the total radiation as the superposition of signals radiated in a right- and left-hand circularly polarized mode. In this case we would have to add another cardioid pattern to indicate an upper sideband component in the first column since the undesired mode of radiation would produce an upper sideband signal. Both modes would contribute to the other patterns proportionately as shown here for the proper mode, but the relative phases of these contributions and, hence, the resultant amplitudes would depend upon the orientation of the satellite antenna polarization ellipse relative to the spin axis.

Circularly Polarized Satellite Antenna and Linearly Polarized Observation Antenna

A similar analysis may be carried out for the case of a linearly polarized receiving antenna. In this case, it is necessary to introduce a new variable in order to specify the orientation of the receiving antenna polarization. This has been done, as in Fig. 8, by defining the angle, u, between the receiving antenna polarization axis and the plane defined by the spin axis and the line joining the observation point and the satellite. The calculation

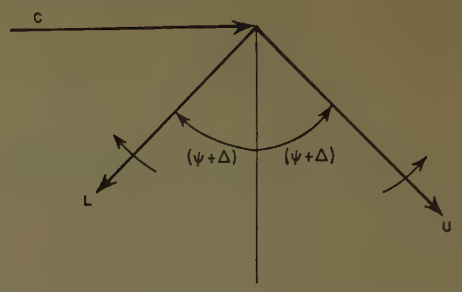

Fig. 9—Sideband phase relationship for u arbitrary.

of the signal characteristics may be carried out by resolving the dipole moment, M, of the receiving antenna into components M_1 and M_2 (Fig. 3), where $M_1=M\cos u$ and $M_2=M\sin u$.

Substituting these values into (3) and proceeding as before, we find the spectral components to be:

$$\left.\begin{aligned} C &= -\sin\theta_s \sin\theta_0 \cos u \\ U &= \frac{1-\cos\theta_s}{2}\sqrt{\sin^2 u+\cos^2\theta_0\cos^2 u} \\ L &= \frac{1+\cos\theta_s}{2}\sqrt{\sin^2 u+\cos^2\theta_0\cos^2 u} \\ \Delta &= \tan^{-1}(\cos\theta_0\cot u) \end{aligned}\right\}, \tag{8}$$

where the sideband phase relationship is as illustrated in Fig. 9.

It is of interest to note that, in addition to the basic difference in sideband phasing between this case and the case of a circularly polarized receiving antenna (*i.e.*, when the sidebands are in phase in this case, their common phase is in quadrature with the carrier) the modulation-envelope phase is also a function of the polarization angle u and the observation angle θ_0. It follows that if the receiving antenna is elliptically polarized, and therefore can be represented as the superposition of circularly polarized and linearly polarized components, no general rule can be stated for the phase relationships between the three spectral components received. This factor must be taken into account in any attempt to devise optimum methods of detection for the composite signal.

The analysis of the phase-error problem is somewhat more complicated in this case because of the addition of the polarization angle as a variable. Using the same definition as above for the condition leading to phase error and noting the sideband phase relationship as shown in Fig. 9, it is seen that phase errors are predicted when

$$|U-L| > |C|.$$

Substituting from (14) into this expression, one finds after some manipulation that phase errors occur for

$$\frac{\tan^2 u+\cos^2\theta_0}{\sin^2\theta_0} > \tan^2\theta_s. \tag{9}$$

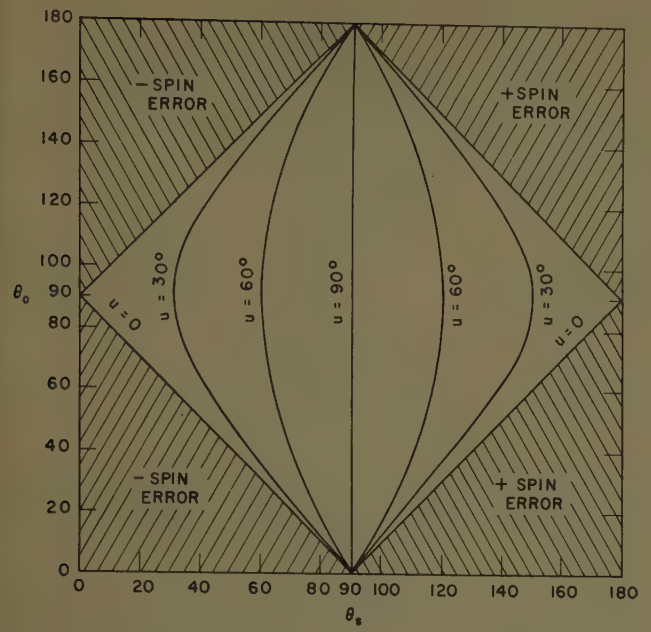

Fig. 10—Summary of signal characteristics; circularly polarized satellite antenna, linearly polarized receiving antenna.

making use of part of the solution already derived for two crossed dipoles, each of which is at right angles to the desired spin axis.

Consider a single dipole of moment M_0 oriented along the Z axis in Fig. 4 instead of the two dipoles M_a and M_b. Following the procedure used previously, the dipole element may be resolved into a component $M_0 \cos \theta_s$ along the spin axis and a component $M_0 \sin \theta_s$ perpendicular to the spin axis. Introducing a rotation of the dipole through an angle, ψ, about the spin axis, S, and calculating the induced voltage, V, from

$$V = \frac{1}{I_0} (\bar{E} \cdot \bar{M}_0)$$

one finds

$$V = \frac{KM_1M_0}{I_0} \left[\cos \theta_s \sin \theta_0 + \sin \theta_s \cos \theta_0 \cos \psi - \frac{M_2}{M_1} \sin \theta_s \sin \psi \right]. \quad (10)$$

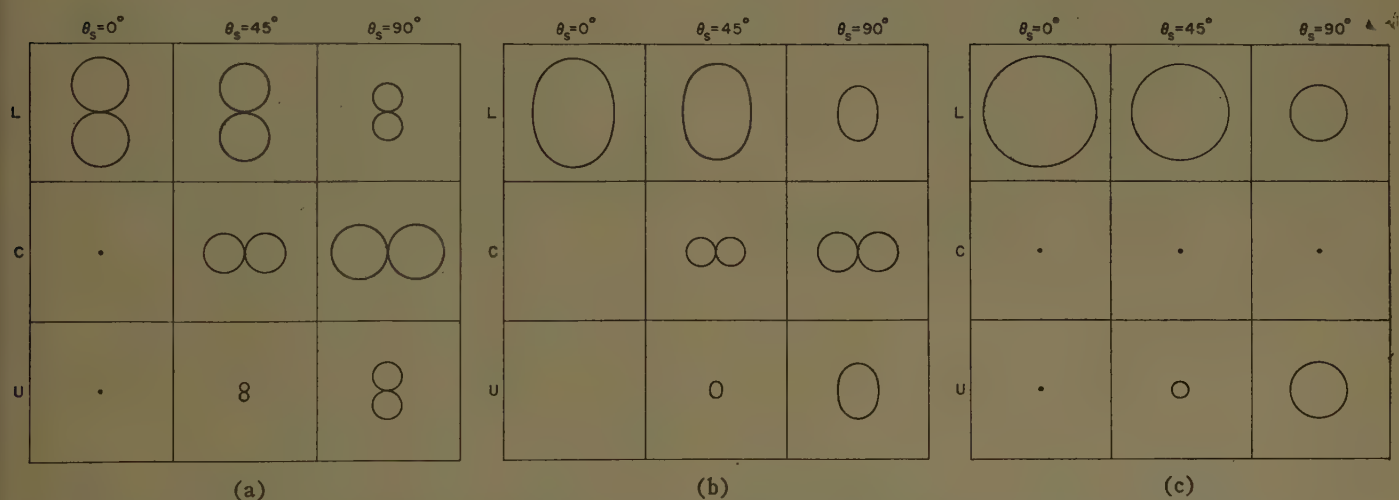

Fig. 11—Radiation patterns of spectral components; circularly polarized satellite antenna, linearly polarized receiving antenna. (a) $u=0$, (b) $u=45°$, (c) $u=90°$.

The regions of phase error predicted by (9) are presented for various values of u in Fig. 10.

The radiation patterns for the three spectral components have been calculated from (14) for $u=0$, 45, and 90 degrees. These are shown in Fig. 11.

C. Linearly Polarized Satellite Antenna and Circularly Polarized Observation Antenna

Since interest has been expressed in the possibility of employing a single antenna element on the satellite, rather than the crossed dipole pair, an analysis of this case has been included in this study. On the assumption that such an element would be oriented along the desired spin axis, the single element problem will be reformulated to fit this situation naturally, rather than simply

To consider the case of a circularly polarized observation antenna, again take $M_2=jM_1$. Setting

$$K'' = KM_1M_2/I_0,$$

we obtain

$$\frac{V}{K''} = \cos \theta_s \sin \theta_0 + \sin \theta_s (\cos \theta_0 \cos \psi - j \sin \psi).$$

Writing this in the form

$$\frac{V}{K''} = C + (U - L) \cos \psi - j(U + L) \sin \psi,$$

the spectral components may be immediately identified as follows:

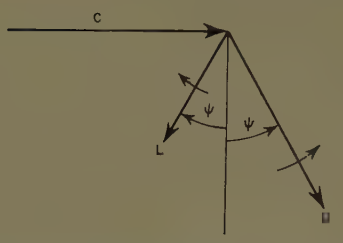

Fig. 12—Sideband phase relationships; linearly polarized satellite antenna, circularly polarized receiving antenna.

$$\left.\begin{aligned} C &= \cos\theta_s \sin\theta_0 \\ U &= \tfrac{1}{2}\sin\theta_s(1+\cos\theta_0) \\ L &= \tfrac{1}{2}\sin\theta_s(1-\cos\theta_0) \end{aligned}\right\} \qquad (11)$$

with phase relationships as in Fig. 12.

The condition for spin error is

$$|U-L| > |C|$$

which reduces in this case to

$$|\tan\theta_s| > |\tan\theta_0|. \qquad (12)$$

Fig. 13 shows the regions of spin error to which this condition leads in the θ_s-θ_0 plane. Also indicated in Fig. 13 are the lines along which certain conditions arise with respect to the three spectral components.

Linearly Polarized Satellite Antenna and Linearly Polarized Observation Antenna

Proceeding as in the case of the linearly polarized observation antenna with the circularly polarized satellite antenna, we find the following spectral components

$$C = \cos\theta_s \sin\theta_0 \cos u$$

$$U = L = \frac{\sin\theta_s}{2}\sqrt{\sin^2 u + \cos^2\theta_0 \cos^2 u}. \qquad (13)$$

The two sidebands, which in this case are equal, are so phased relative to the carrier that the resultant modulation on the signal is pure AM. The phase of the modulation envelope is dependent upon both the polarization angle, u, and the observation angle, θ_0, through the expression

$$x = \tan^{-1}\frac{(\tan u)}{(\cos\theta_0)}, \qquad (14)$$

where x is the phase angle between the carrier and each sideband when $\psi=0$. Because of the lack of phase modulation on the signal, there will be no spin error in the sense that spin error was defined above. However, it is noted that the modulation index will exceed 100 per cent (a condition which might well lead to phase errors with an AM signal) for

$$\tan^2\theta_s > \frac{\sin^2\theta_0}{\tan^2 u + \cos^2\theta_0}. \qquad (15)$$

Distribution of Radiated Power in Spectral Components

It would be of interest to evaluate the significance of these results by selecting representative ground station situations and examining the nature of the signal variations as the satellite passes through the coverage area of the ground station. A brief reflection on the degree of variation possible in the many geometrical parameters involved, however, shows that a wide range of results may be obtained, depending upon which of a great many equally plausible cases are chosen as representative. A much simpler method for summarizing these results, and one which is probably no less revealing, is to calculate what fraction of the total radiated power goes into the patterns of the three spectral components as a function of the spin angle θ_s. Assuming that each element of solid angle about the spinning satellite is equally likely to include a receiving site, then the relative power in the three complementary patterns will also give the mean relative values of the power received in the three spectral components at all receiving sites.

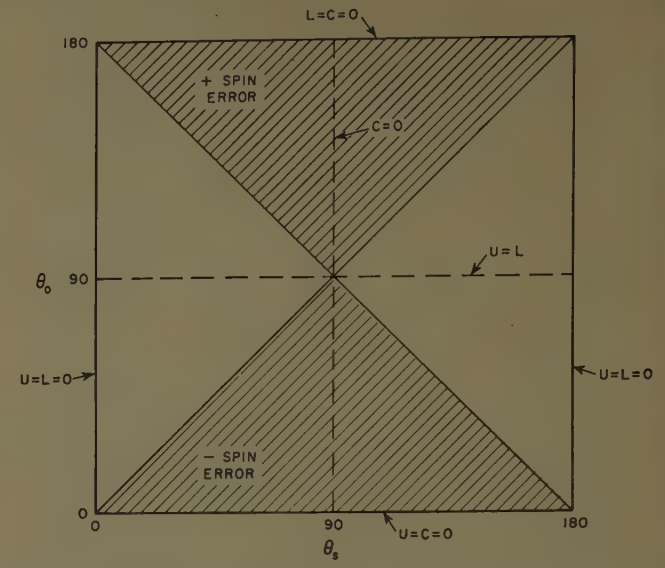

Fig. 13—Summary of signal characteristics; linearly polarized satellite antenna, circularly polarized receiving antenna.

To calculate these relative power levels, we note that the patterns calculated above apply equally well when transmissions emanate from the satellite. Choosing the case of the linearly polarized ground antenna, it is noted that setting $u=0$ and $u=90°$ yields the θ and ϕ polarization patterns, respectively (in the spherical coordinate system having the $\theta=0$ axis coincident with the satellite spin axis). Squaring and integrating these patterns for each spectral component, and normalizing the resultant values of radiated power to the total radiated power, gives the following expressions for the fraction of the total radiated power in each spectral component.

$$\left.\begin{aligned} p_C &= \tfrac{1}{2}\sin^2\theta_s \\ p_U &= \tfrac{1}{4}(1-\cos\theta_s)^2 \\ p_L &= \tfrac{1}{4}(1+\cos\theta_s)^2 \end{aligned}\right\} \qquad (16)$$

for the circularly polarized satellite antenna and

$$\left.\begin{aligned} p_C &= \cos^2\theta_s \\ p_L &= p_U = \tfrac{1}{2}\sin^2\theta_s \end{aligned}\right\} \qquad (17)$$

for the linearly polarized satellite antenna.

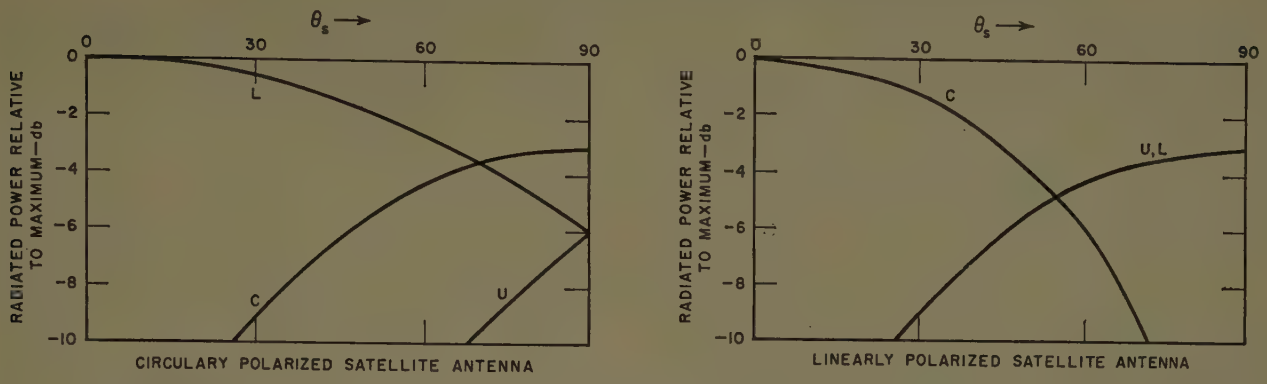

Fig. 14—Relative power radiated in various spectral components for circularly polarized and linearly polarized satellite antennas as functions of spin angle. Note: 0 db reference is same for both cases.

The results of (16) and (17) have been plotted in Fig. 14. It is noted that for relatively small spin angles the circularly polarized antenna retains a greater fraction of the total radiated power in a dominant spectral component and that the ratio of power in the dominant component to power in the next strongest component is higher than for the linearly polarized antenna.

Conclusions

The signal received from the spinning satellite normally consists of three components, all of which may have significant amplitudes unless the spin axis is maintained very close to the axis of symmetry of the satellite antenna. The phases of these signals, if received on a elliptically polarized antenna, will not be simply related so as to permit relatively easy extraction of the total received power from the noise. The total spectral spread of the received energy covers a band comparable to that used with tracking-filter techniques. Designers of tracking filters should recognize that they will have a relatively complicated signal to deal with rather than a single frequency signal whose frequency varies in accordance with the Doppler shift. Perhaps the most significant conclusion of this investigation is that every effort should be made to maintain the spin axis as nearly parallel as possible to the axis of symmetry of the antenna. If it is necessary to anticipate large deviations of the spin axis from the symmetry axis, a polarization diversity receiving system, employing both right- and left-hand circularly polarized receiving antennas, appears to give the best assurance that an adequate signal will always be received.

Applications of Operational Calculus to Ground-Wave Propagation, Particularly for Long Waves*

H. BREMMER†

Summary—**All results of the approximative diffraction theory dealing with the propagation of radio waves around a smooth spherical earth (surrounded by a homogeneous atmosphere) can be derived from a one-dimensional integral equation originally discussed by Hufford.**

This equation can be solved in terms of operational calculus which leads, first of all, to the well-known residue series. In this treatment the Sommerfeld theory for a flat earth appears at once as a limiting case; moreover, analytic expressions for correction terms accounting for the finite value of the earth's radius are easily determined. Finally, the equation in question can also be used for the extension to inhomogeneous soil conditions, without neglecting the earth's curvature.

* Manuscript received by the PGAP, September 18, 1957. Paper presented at the Symposium of VLF Propagation, Boulder, Colo., January 23–25, 1957.

† Philips Res. Labs., Eindhoven, The Netherlands.

I. Introduction

THE conventional diffraction theory of the propagation of the ground wave around a homogeneous spherical earth results in a final expansion which is most suitable for large distances $x=a\theta$ from the receiver R to the transmitter T. The inefficiency of this expansion at short distances is stressed by the difficulty of showing the transition to the flat-earth theory if the earth's radius a tends to infinity. However, the latter theory clearly emerges as a limiting case if the entire diffraction problem is treated with the aid of operational analysis. Such a treatment, introduced by Hufford,[1] is

[1] G. A. Hufford, "An integral equation approach to the problem of wave propagation over an irregular surface," *Quart. Appl. Math.*, vol. 9, pp. 391–404; January, 1952.

amply discussed in this paper. It leads not only to expansions, the coefficients of which very clearly represent the influence of the earth's curvature a^{-1} (see Sections VII and VIII), but it also shows the connection between Hufford's theory and an integral equation derived by Feinberg[2] for the propagation over two adjacent homogeneous sections (see Section III).

II. The Basic Integral Equation

The diffraction problem dealing with the propagation of electromagnetic waves around the spherical earth is considerably simplified by assuming Leontovich's approximative boundary condition. In terms of the amplitude Π of a radially directed Hertzian vector this condition reads $\partial\Pi/\partial r=\gamma\Pi$. In the two cases of vertical and horizontal polarization γ is given by

$$\gamma_v = \frac{k_0}{in^2}\sqrt{n^2-1} \quad \text{and} \quad \gamma_h = \frac{k_0}{i}\sqrt{n^2-1}$$

($k_0=2\pi/\lambda$) respectively, in which the refractive index $n=(\epsilon+i4\pi\sigma/k_0c)^{1/2}$ comprises the electrical constants ϵ and σ (gaussian units) of the earth.

The substitution of the mentioned boundary condition to a special application of Green's theorem leads to a two-dimensional integral equation for the distribution of Π over the earth's surface, which may be either smooth or irregular. The equation in question, to be applied here for a smooth curved earth, can further be reduced to a one-dimensional integral equation by using a saddlepoint approximation. The validity of the latter is associated with the oblong form of the Fresnel ellipse around TR. The resulting final integral equation is equivalent to (31) in Hufford's analysis [in which, however, $\xi^{-1/2}$ has to be replaced by $\xi^{1/2}$ in (31), whereas the last line of (30) should read $\gamma=i/(ka)^{1/3}\delta$]. It can be represented as follows in the case of zero heights of the transmitter and the receiver:

$$\psi(x) = \frac{e^{k_0x^3/24ia^2}}{\sqrt{x}} + \frac{i}{\sqrt{\pi}}\int_0^x \frac{\psi(\xi)\left\{\mu(\xi)+\sqrt{\frac{ik_0}{2}}\,\frac{(x-\xi)}{2a}\right\}}{\sqrt{x-\xi}} \cdot e^{k_0(x-\xi)^3/24ia^2}d\xi. \tag{1}$$

Quantity ψ constitutes a measure for the attenuation due to the presence of the earth since it is defined by

$$\Pi(x) = 2\Pi_{pr}(x)\sqrt{x}e^{ik_0x^3/24a^3}\psi(x), \tag{2}$$

in which Π_{pr} refers to free-space propagation. Further, $\mu(x)$ represents, for either type of polarization, the quantity

$$\mu(x) = -\frac{\gamma(x)}{\sqrt{2ik_0}}.$$

This parameter becomes real in the limiting case of vertical polarization at very low frequencies (negligible displacement current); it then reads

$$\mu(x) = k_0\sqrt{\frac{c}{2\sigma_{esu}}} = \frac{k_0}{\sqrt{2c\sigma_{emu}}}$$

for a conductivity measured in electrostatic or electromagnetic units, respectively. Though Hufford considered an electrically homogeneous earth, his derivation of (1) applies also to variable electrical constants provided that the angles between the transmission path and the boundaries separating individual homogeneous domains are not too small. The function $\mu(\xi)$ then refers to the local value of μ at the special point on the great-circle path TR, situated at a distance ξ from T. According to an investigation by Wait,[3] a proper value of μ may also account for the effect of stratifications in the ground.

III. The Operational Solution of the Basic Integral Equation; Derivation of Feinberg's Alternative Equation

The solution of (1) with respect to $\psi(x)$, $\mu(x)$ being given, amounts to elementary algebra if we replace (1) by its operational image. The latter can be obtained at once by starting from the equivalent equation:

$$\psi(x)U(x) = \frac{e^{k_0x^3/24ia^2}}{\sqrt{x}}U(x) + \frac{i}{\sqrt{\pi}}\left[\int_{-\infty}^{\infty}\psi(\xi)\mu(\xi)U(\xi)\times\frac{e^{k_0(x-\xi)^3/24ia^2}}{\sqrt{x-\xi}}U(x-\xi)d\xi + \sqrt{\frac{ik_0}{2}}\,\frac{1}{2a}\int_{-\infty}^{\infty}\psi(\xi)U(\xi)\times(x-\xi)\frac{e^{k_0(x-\xi)^3/24ia^2}}{\sqrt{x-\xi}}U(x-\xi)d\xi\right], \tag{3}$$

in which $U(x)$ represents the Heaviside unit function (which equals unity for $x>0$, and zero for $x<0$). In fact, (3) reduces to (1) for $x>0$, whereas we find $0=0$ for $x<0$. We next introduce operational images according to

$$\psi(x)U(x) \doteqdot f(p); \quad \psi(x)\mu(x)U(x) \doteqdot f\mu(p), \quad \frac{e^{k_0x^3/24ia^2}}{\sqrt{x}}U(x) = pv(p) \tag{4}$$

the general relation $h(x)\doteqdot f(p)$ being defined, for some values of α and β, by

$$f(p) = p\int_{-\infty}^{\infty}e^{-px}h(x)dx, \qquad \alpha<\operatorname{Re}p<\beta. \tag{5}$$

[2] E. Feinberg, "On the propagation of radio waves along an imperfect surface," *J. Phys. (Moscow)*, vol. 9, pp. 1–6; 1945.

[3] J. R. Wait, "Radiation from a vertical antenna over a curved stratified ground," *J. Res. Natl. Bur. Standards*, vol. 56, pp. 237–444; April, 1956.

An application of the general rules:

$$\left.\begin{aligned}\int_{-\infty}^{\infty} h_1(\xi) \times h_2(x-\xi)d\xi \doteq \frac{f_1(p)f_2(p)}{p},\\ xh(x) \doteq -p\frac{d}{dp}\{f(p)/p\},\end{aligned}\right\} \quad (6)$$

and of the special relation

$$x^\nu U(x) \doteq \frac{\Gamma(\nu+1)}{p^\nu} \quad (\mathrm{Re}\, p > 0;\ \mathrm{Re}\,\nu > -1) \quad (7)$$

leads to the following operational "translation" of (3):

$$f = pv + \frac{i}{\sqrt{\pi}}\left(f_\mu v - \sqrt{\frac{ik_0}{2}}\frac{fv'}{2a}\right) \qquad (\mathrm{Re}\, p > 0). \quad (8)$$

A homogeneous earth is characterized by a constant value μ_0 of $\mu(\xi)$ and by the resulting relation $f\mu = \mu_0 f$. The corresponding solution of (8) for the image f_0 of $\psi_0(x)\ U(x)$ becomes

$$f_0 = \frac{pv}{1 - \frac{i}{\sqrt{\pi}}\left(\mu_0 v - \sqrt{\frac{ik_0}{2}}\frac{v'}{2a}\right)}. \quad (9)$$

The final determination of the original $\psi(x)\,U(x)$ of f depends on the explicit form of v which is discussed in the next section. However, without knowing this explicit form, an interesting relation can be found by considering the following identity which results from (8) and (9) (for instance, by eliminating v'):

$$f = f_0 + \frac{i}{\sqrt{\pi}}\frac{f_0(f_\mu - \mu_0 f)}{p}.$$

The operational "original" of this new relation follows by once again applying the relations (6). The result for $x > 0$ reads

$$\psi(x) = \psi_0(x) + \frac{i}{\sqrt{\pi}}\int_0^x \psi_0(x-\xi)\{\mu(\xi) - \mu_0\}\psi(\xi)d\xi. \quad (10)$$

This identity connects the attenuation function $\psi(x)$ for an arbitrary distribution of the parameter $\mu(x)$ along the transmission path with the special attenuation function $\psi_0(x)$ that corresponds to a homogeneous earth characterized by the constant μ_0. The substitution of the flat-earth value of $\psi_0(x)$ [that is, of the first term of the expansion (24) discussed later on] shows the equivalency of (10) to an integral equation derived by Feinberg[4] in which the inhomogeneity of the earth refers to an imperfect surface instead of to its electrical properties.

IV. The Determination of the Image Function $v(p)$ in (4)

The definition of $v(p)$ by means of a Laplace transform involves the representation

$$v(p) = \left(\frac{24a^2}{ik_0}\right)^{1/6} g\left\{\left(\frac{24a^2}{ik_0}\right)^{1/3} p\right\},$$

in which

$$g(z) \equiv \int_0^\infty \frac{e^{-\tau^3 - z\tau}}{\sqrt{\tau}}\,d\tau. \quad (11)$$

The resulting differential equation

$$6g'''(z) + 2zg'(z) + g(z) = 0,$$

which also was considered by Hufford,[5] has the general solution[6]

$$g(z) = C_1 w_1^2(z) + C_2 w_1(z)w_2(z) + C_3 w_2^2(z), \quad (12)$$

in which the functions

$$w_{1,2}(z) = \sqrt{z}H_{1/3}^{(1),(2)}(z^{3/2}/3^{3/2})$$

are two particular solutions of the simpler equation $w'' + (1/12)zw = 0$. A comparison of the asymyptotic behavior of (11) and (12) for $|z| \to \infty$ while $|\arg z| < \frac{2}{3}\pi$ shows that C_1 and C_3 have to vanish, whereas $C_2 = (1/2)(\pi/3)^{3/2}$. The function g thus being fixed, we obtain the following explicit expression for v:

$$v(p) = \left(\frac{\pi}{3}\right)^{3/2}\left(\frac{24}{ik_0}\right)^{1/2}\frac{ap}{2}\cdot H_{1/3}^{(1)}\left\{a\left(\frac{24}{ik_0}\right)^{1/2}\left(\frac{p}{3}\right)^{3/2}\right\}$$
$$\cdot H_{1/3}^{(2)}\left\{a\left(\frac{24}{ik_0}\right)^{1/2}\left(\frac{p}{3}\right)^{3/2}\right\}. \quad (13)$$

V. The Operational Relation Determining the Diffraction Around the Spherical Earth

The substitution of (13) into (9) yields the Laplace transform $f_0(p)$ of the attenuation function $\psi(x)$ qua function of the distance x (measured along the great circle connecting the transmitter and the receiver, either of which is assumed to be on the earth's surface). The denominator of (9) can be simplified with the aid of the identity

$$\frac{1}{v} - \frac{1}{2a}\sqrt{\frac{k_0}{2\pi i}}\frac{v'}{v} = e^{-i\pi/6}\sqrt{\frac{p}{\pi}}\,\frac{H_{2/3}^{(2)}\left(\sqrt{\frac{8}{g_i k_0}}\,ap^{3/2}\right)}{H_{1/3}^{(2)}\left(\sqrt{\frac{8}{g_i k_0}}\,ap^{3/2}\right)},$$

which is a consequence of elementary properties of Bessel functions. Remembering the definition by (2) of $\psi(x)$, the final result can be put into the form:

[4] Feinberg, *op. cit.*, (8.9)

[5] Hufford, *op. cit.*, (45).

[6] See E. Kamke, "Differentialgleichungen I," Akademische Verlagsgesellschaft Becker & Erler Kom.-Ges., Leipzig, pp. 508–523, 1943. See (3.6, p. 509.

$$\frac{\Pi(\bar{x})}{2\Pi_{pr}(x)e^{ik_0x^3/24a^2}} \frac{U(x)}{\sqrt{x}} \doteq \frac{\sqrt{\pi}p}{-i\mu_0 + e^{-i\pi/6}\sqrt{p}\,\dfrac{H_{2/3}^{(2)}\left(\sqrt{\dfrac{8}{ik_0}}\,\dfrac{ap^{3/2}}{3}\right)}{H_{1/3}^{(2)}\left(\sqrt{\dfrac{8}{ik_0}}\,\dfrac{ap^{3/2}}{3}\right)}}, \quad (\mathrm{Re}\ p > 0). \quad (14)$$

We notice that the product $\Pi_{pr}(x)$ exp $(ik_0x^3/24a^2)$ is simply proportional to exp (ik_0TR), in view of the approximative relation

$$TR \sim x - x^3/(24a^2) = a\theta - a\theta^3/24. \quad (15)$$

Therefore, the exponential factor in the left-hand side of (14) merely constitutes an unimportant phase factor.

In the flat-earth theory it is customary to change over from the actual distance x to Sommerfeld's numerical distance $\rho = \mu_0^2 x$. The introduction of a new unit of distance is particularly useful for very long waves in which case ρ becomes real. The original functions $\Pi(x)$ and $\Pi_{pr}(x)$ then pass into new functions according to

$$\Pi(x) = \Pi_\rho(\mu_0^2 x); \qquad \Pi_{pr}(x) = \Pi_{\rho,pr}(\mu_0^2 x). \quad (16)$$

The Laplace transform associated with the new function $\Pi_\rho(x)$ follows from (14) by *dividing* x by μ_0^2; this division implies that p has to be *multiplied* by μ_0^2. In the operational relation thus obtained for $\Pi_\rho(x)$ we further substitute

$$\mu_0 = \frac{\sqrt{k_0}e^{i3\pi/4}}{\sqrt{2}(k_0a)^{1/3}\delta}, \quad (17)$$

and apply the identity

$$\frac{H_{2/3}^{(2)}(ze^{2\pi i})}{H_{1/3}^{(2)}(ze^{2\pi i})} = -e^{\pi i/3}\frac{H_{2/3}^{(1)}(z)}{H_{1/3}^{(1)}(z)}.$$

This leads to the following alternative operational relation in which the numerical distance ρ instead of the actual distance $x = a\theta$ constitutes the operational variable:

$$\frac{\Pi_\rho(x)}{2\Pi_{\rho,pr}(x)e^{\delta^6x^3/3}} \frac{U(x)}{\sqrt{x}} \doteq \frac{i\sqrt{\pi p}}{1 + e^{-i\pi/3}\sqrt{p}\,\dfrac{H_{2/3}^{(1)}\left(\dfrac{p^{3/2}}{3\delta^3}\right)}{H_{1/3}^{(1)}\left(\dfrac{p^{3/2}}{3\delta^3}\right)}}, \quad (\mathrm{Re}\ p > 0). \quad (18)$$

We observe that the p functions occurring in (14) and (18) are unique in spite of the multivaluedness of each individual Hankel function. Either relation completely determines the diffraction theory for a spherical earth (for zero heights of the transmitter and the receiver) in the approximation under consideration. We therefore expect that the conventional form of this theory should be derivable from each of these relations. This is verified in the next section.

VI. Derivation of the Residue Series for a Curved Earth from the Operational Relation (18)

The attenuation function $\Pi_\rho(x)/2\Pi_{\rho,pr}(x)$ itself follows from a substitution of the right-hand side $f(p)$ of (18) into the "inversion integral"

$$h(x) = \frac{1}{2\pi i}\int_{c-i\infty}^{c+i\infty} e^{px}\frac{f(p)}{p}\,dp \quad (\alpha < c < \beta),$$

that is associated with the Laplace integral (5). Substituting $p = 2\delta^2\tau e^{-i\pi}$, the evaluation of this integral yields,

$$\frac{\Pi_\rho(x)}{2\Pi_{\rho,pr}(x)e^{\delta^6x^3/3}} \frac{U(x)}{\sqrt{x}} = -\frac{\delta^2}{\sqrt{\pi}}\int_{-\infty-ic}^{\infty-ic} \frac{e^{-2\delta^2x\tau}}{1 + e^{-i\pi/3}\delta\sqrt{-2\tau}\,\dfrac{H_{2/3}^{(1)}\{(-2\tau)^{3/2}/3\}}{H_{1/3}^{(1)}\{(-2\tau)^{3/2}/3\}}}\,d\tau \quad (c > 0).$$

The asymptotic behavior of the Hankel functions involves a nonexponential character of the denominator of the integrand for $|\tau| \to \infty$. In view of the exponential in the numerator, the integration path can, therefore, be closed for $x > 0$ along the semi-infinite circle of the half plane $Im\ \tau > 0$. The resulting contour integral reduces to the sum of the residues at the poles τ_s; the latter are the zeros of the denominator. The sum in question amounts to

$$\frac{\Pi_\rho(x)}{2\Pi_{\rho,pr}(x)e^{\delta^6x^3/3}\sqrt{x}} = 2\sqrt{\pi}e^{-i\pi/6}\delta\sum \frac{e^{-2\delta^2\tau_sx}}{\dfrac{\partial}{\partial\tau}\left[\sqrt{-2\tau}\,\dfrac{H_{2/3}^{(1)}\{(-2\tau)^{3/2}/3\}}{H_{1/3}^{(1)}\{(-2\tau)^{3/2}/3\}}\right]_{\tau=\tau_s}}.$$

The Hankel functions can be eliminated by applying both the equation for the zeros τ_s and elementary properties of the Hankel functions. The result reads

$$\frac{\Pi_\rho(x)}{2\Pi_{\rho,pr}(x)e^{\delta^6x^3/3}} = -2i\delta\sqrt{\pi x}\sum \frac{e^{-2\delta^2\tau_sx}}{2\tau_s - 1/\delta^2}. \quad (19)$$

We next replace x by μ_0^2x, in order to pass from Π_ρ to the original function Π [compare (16)]. A final substitution of $a\theta$ for x, using (17) and (15), leads to

$$\frac{\Pi}{2e^{ik_0a\theta}} = (k_0a)^{1/6}(2\pi i\theta)^{1/2}\sum \frac{e^{i(k_0a)^{1/3}\tau_s\theta}}{2\tau_s - 1/\delta^2},$$

provided that the primary field is normalized according

to $\Pi_{pr}=\exp(ik_0TR)/TR$. The latter expansion amounts to the residue series (for zero heights of transmitter and receiver) for the so-called "Hankel approximation" of the curved-earth theory.[7] The approximations introduced above (Leontovich's boundary condition, saddle-point approximation) thus prove to be equivalent to those underlying the Hankel approximation.

VII. Expansion of the Field in Powers of the Numerical Distance

We return to the operational relation (18) which determines the field $\Pi_\rho(x)$ in terms of the numerical distance x and the parameter δ. Suitable expansions can be derived by applying the well-known asymptotic expansions for $H_{2/3}^{(1)}(z)$ and $H_{1/3}^{(1)}(z)$ which are valid simultaneously if $-\pi<\arg z<2\pi$. However, in view of $\mathrm{Re}\,p>0$ and the phase $3\pi/4$ of δ in the case of very long waves, the arguments z of the Hankel functions occurring in (18) are situated between -3π and $-(3/2)\pi$. We therefore substitute $z=z'e^{3\pi i}$ to obtain new asymptotic expansions for $H_{2/3}^{(1)}(z')$ and $H_{1/3}^{(1)}(z')$ which are valid for $-4\pi<\arg z'<-\pi$, that is, in an interval including the one we are interested in. A division of these new expansions yields the further development

$$\frac{H_{2/3}^{(1)}(z)}{H_{1/3}^{(1)}(z)}\sim -e^{-i\pi/6}\left(1-\frac{i}{6z}+\frac{5}{72z^2}+i\frac{5}{72z^3}+\cdots\right)$$
$$-4\pi<\arg z<-\pi;\ |z|\to\infty,$$

which can be substituted at once in (18) while taking $z=p^{3/2}/(3\delta^3)$. We find

$$\frac{\Pi_\rho(x)}{2\Pi_{\rho,pr}(x)e^{\delta^6x^3/3}}\frac{U(x)}{\sqrt{x}}\doteq\frac{i\sqrt{\pi}p}{1+i\sqrt{p}\left(1-i\dfrac{\delta^3}{2p^{3/2}}+\dfrac{5}{8}\dfrac{\delta^6}{p^3}+i\dfrac{15}{8}\dfrac{\delta^9}{p^{9/2}}+\cdots\right)}$$
$$(\mathrm{Re}\,p>0).\quad(20)$$

We now are able to derive two different expansions from this operational relation, namely a power series with respect to the numerical distance and another power series referring to the earth's curvature. The latter series is discussed in the next section. In order to obtain the former, we simply have to develop the right-hand side of (20) into powers of p^{-1} and to return to the operational originals of the individual terms with the aid of (7). The first terms of the resulting expansion read as follows if the operational variable x is ultimately replaced by the physical parameter ρ:

$$\frac{\Pi}{2\Pi_{pr}e^{\delta^6\rho^3/3}}=1+i\sqrt{\pi}\rho^{1/2}-2\rho-i\sqrt{\pi}\left(1-\frac{\delta^3}{2}\right)\rho^{3/2}$$
$$+\frac{4}{3}(1-\delta^3)\rho^2+\frac{i\sqrt{\pi}}{2}\left(1-\frac{3}{2}\delta^3\right)\rho^{5/2}$$
$$-\frac{8}{15}\left(1-2\delta^3+\frac{7}{8}\delta^6\right)\rho^3-\frac{i\sqrt{\pi}}{6}\left(1-\frac{5}{2}\delta^3+2\delta^6\right)\rho^{7/2}$$
$$+\frac{16}{105}\left(1-3\delta^3+\frac{27}{8}\delta^6\right)\rho^4$$
$$+\frac{i\sqrt{\pi}}{24}\left(1-\frac{7}{2}\delta^3+5\delta^6-\frac{21}{8}\delta^9\right)\rho^{9/2}$$
$$-\left(\frac{32}{945}-\frac{128}{945}\delta^3+\frac{44}{189}\delta^6-\frac{28}{135}\delta^9\right)\rho^5+\cdots.\quad(21)$$

The exponential in the left-hand side is the former phase factor $\exp(ik_0a\theta^3/24)$ which is connected with the difference in path length of the distance $a\theta$ along the great circle and the length of the corresponding chord.

Each coefficient of (21) has a limiting value for $\delta\to0$ which is characteristic for the situation in the flat-earth approximation since the parameter

$$\delta^3=\frac{\sqrt{ik_0/2}}{2\mu_0{}^3}\frac{1}{a}$$

then vanishes in proportion to the earth's curvature a^{-1}. Obviously, the influence of this curvature only becomes appreciable at actual distances that correspond to numerical distances ρ exceeding unity. Moreover, the long-wave approximation

$$\delta^3\sim\frac{\sqrt{i}}{c^{3/2}}\frac{\sigma_{\mathrm{esu}}{}^{3/2}}{ak_0{}^{5/2}}$$

shows how this influence increases in proportion to $\lambda^{5/2}$ for a fixed value of ρ.

VIII. Expansion of the Field in Powers of the Earth's Curvature

Another representation of the field results from an expansion of the right-hand side of (20) with respect to δ^3, the parameter proportional to the earth's curvature. The first few terms of the series then obtained read as follows:

$$\frac{\Pi_\rho(x)}{2\Pi_{\rho,pr}(x)e^{\delta^6x^3/3}}\frac{U(x)}{\sqrt{x}}\doteq\frac{i\sqrt{\pi}p}{1+i\sqrt{p}}-\frac{i\sqrt{\pi}}{2(1+i\sqrt{p})^2}\delta^3$$
$$+\sqrt{\pi}\left\{\frac{i}{4p(1+i\sqrt{p})^3}+\frac{5}{8}\frac{1}{p^{3/2}(1+i\sqrt{p})^2}\right\}\delta^6$$
$$-\frac{\sqrt{\pi}}{8}\left\{\frac{i}{p^2(1+i\sqrt{p})^4}+\frac{5}{p^{5/2}(1+i\sqrt{p})^3}\right.$$
$$\left.-\frac{15i}{p^3(1+i\sqrt{p})^2}\right\}\delta^9+\cdots\quad(22)$$

[7] Compare, B. Van der Pol and H. Bremmer, "The propagation of radio waves over a finitely conducting spherical earth," *Phil. Mag.*, vol. 25, p. 817–834; Suppl. June, 1938. See (20b), p. 829.
H. Bremmer, "Terrestrial Radio Waves," Elsevier Publishing Co., New York, N. Y., pp. 46–50; 1949. See, (33), p. 50.

We have to determine the operational "originals" of the various terms. Obviously, that of the first term yields the flat-earth approximation ($\delta \to 0$). The latter proves to be determined by the relation

$$\frac{i\sqrt{\pi}p}{1+i\sqrt{p}} \doteq \frac{y(x)}{\sqrt{x}}\,U(x), \qquad (\mathrm{Re}\,p>0) \qquad (23)$$

in which

$$y(x) \equiv 1 + 2\sqrt{x}e^{-x}\int_{\sqrt{x}}^{\infty} e^{s^2}ds$$

represents the well-known Sommerfeld function of the flat-earth theory. The assumptions introduced so far are thus shown to be equivalent to those underlying the approximative Sommerfeld theory for the flat-earth case. The derivation of the latter from a Laplace transform has also been considered by Hufford.[8]

The originals of the subsequent terms in (22) determine corrections due to the earth's curvature. All these terms depend on contributions of the following standard form which can be split into partial fractions of types indicated below:

$$\frac{1}{p^{m/2}(1+i\sqrt{p})^n} = \sum_{r=1}^{m}\frac{a_r}{p^{r/2}} + \sum_{r=1}^{n}\frac{b_r}{(1+i\sqrt{p})^r}.$$

The originals of the fractions of the first type follow from (7); those of the second type can be derived in a convenient way from the generating function

$$\sum_{r=0}^{\infty}\frac{\alpha^r}{(1+i\sqrt{p})^r} = 1 + \frac{\alpha}{(1-\alpha)+i\sqrt{p}},$$

the original of which is easily derived with the aid of the following relation obtained by integrating (23):

$$\frac{i\sqrt{\pi}}{1+i\sqrt{p}} \doteq \left\{i\sqrt{\pi} + \frac{1-y(x)}{\sqrt{x}}\right\}U(x) \qquad (\mathrm{Re}\,p>0).$$

The outlined procedure results into the further relation

$$\frac{i\sqrt{\pi}}{(1+i\sqrt{p})^r} \doteq \left\{i\sqrt{\pi} - 2\sum_{s=0}^{r-1}\epsilon_s(x)\right\}U(x) \qquad (\mathrm{Re}\,p>0),$$

in which

$$\epsilon_0(x) = \frac{y(x)-1}{2\sqrt{x}}, \qquad \epsilon_1(x) = \sqrt{x}y(x),$$

whereas the higher order functions ϵ_n can be obtained in succession with the aid of the recurrence relation

$$n\epsilon_n = 2x(\epsilon_{n-1} - \epsilon_{n-2}) \qquad (n>1).$$

The evaluation of the originals of the terms written out in (22) yields the following expansion if x is ultimately replaced by the numerical distance ρ:

$$\frac{\Pi}{2\Pi_{pr}e^{\delta^6\rho^3/3}} = y(\rho) + \frac{1}{2}\left\{(1+2\rho)y(\rho) - 1 - i\sqrt{\pi\rho}\right\}\delta^3$$

$$+\left\{\left(\frac{\rho^2}{2}-1\right)y(\rho) + i\sqrt{\pi\rho}(1-\rho) + 1 - 2\rho + \frac{5}{6}\rho^2\right\}\delta^6$$

$$+\left\{\left(\frac{35}{8} - \frac{\rho^2}{4} + \frac{\rho^2}{6}\right)y(\rho)\right.$$

$$-i\sqrt{\pi\rho}\left(\frac{35}{8} - \frac{35}{8}\rho + \frac{31}{16}\rho^2 - \frac{5}{16}\rho^3\right)$$

$$\left.-\frac{35}{4} + \frac{35}{4}\rho - \frac{67}{12}\rho^2 + \frac{5}{3}\rho^3\right\}\delta^9 + \cdots. \qquad (24)$$

Therefore, the Sommerfeld function $y(\rho)$ does determine not only the flat-earth approximation itself, but also the corrections due to the finite curvature of the earth. If we substitute the power series (with respect to $\rho^{1/2}$) for $y(\rho)$ in all the terms of (24), we should arrive once again at (21). The expansion (24) has been applied by Wait[9] for the computation of transient fields.

IX. The Influence of the Heights of the Antennas above the Ground

So far we have assumed both transmitter and receiver to be on the ground. The extension to the case of elevated transmitter and receiver (at heights h_1 and h_2) is simple since each term of the residue series (19) then merely has to be multiplied by the corresponding "height-gain factors" $f_s(h_1)$ and $f_s(h_2)$. According to the Hankel approximation, the latter quantities constitute the values at $\tau=\tau_s$ and $h=h_1$ or h_2 of the function[10]

$$f(h) \sim \left(1-\frac{\chi^2}{2\tau}\right)^{1/2}\frac{H_{1/3}^{(1)}\{(\chi^2-2\tau)^{3/2}/3\}}{H_{1/3}^{(1)}\{(-2\tau)^{3/2}/3\}},$$

in which $\chi^2 = 2hk_0^{2/3}/a^{1/3}$. It is verified at once that the multiplication of each term of (19) by $f(h_1)f(h_2)$ for $\tau=\tau_s$ does correspond to a multiplication of the right-hand side of (18) by the same factor, provided that we return from the variable τ to the original variable p (remembering that $p=-2\delta^2\tau$). The elevation of the transmitter and the receiver thus proves to be accounted for by completing the p function in (18) by the factor

$$\left(1+\frac{\delta^2\chi_1^2}{p}\right)^{1/2}\frac{H_{1/3}^{(1)}\left\{\frac{1}{3}\left(\chi_1^2+\frac{p}{\delta^2}\right)^{3/2}\right\}}{H_{1/3}^{(1)}\left(\frac{p^{3/2}}{3\delta^3}\right)}$$

$$\times\left(1+\frac{\delta^2\chi_2^2}{p}\right)^{1/2}\frac{H_{1/3}^{(1)}\left\{\frac{1}{3}\left(\chi_2^2+\frac{p}{\delta^2}\right)^{3/2}\right\}}{H_{1/3}^{(1)}\left(\frac{p^{3/2}}{3\delta^3}\right)}.$$

This extension of operational method was applied by Wait[11] for computation of fields at short distances.

[8] See, Hufford, *op. cit.*, (20) and (21).

[9] J. R. Wait, "Transient fields of a vertical dipole over a homogeneous curved ground," *Can. J. Phys.*, vol. 34, pp. 27–35; January, 1956.

[10] See, B. Van der Pol and H. Bremmer, "The diffraction of electromagnetic waves from an electrical point source round a finitely conducting sphere, with applications to radiotelegraphy and the theory of the rainbow," *Phil. Mag.*, vol. 24, pp. 825–864; Suppl. November, 1937. See (97).
H. Bremmer, "Terrestrial Radio Waves," *op. cit.* (8), p. 68.

[11] See reference 3, Section III.

On the Measurement of Ground Conductivity at VLF*

J. R. WAIT† AND A. M. CONDA†

Summary—The applicability of the four electrode methods of measuring ground conductivity at very low radio frequencies is discussed. The general theory is extended to include anisotropy in the substrata. In view of the spurious coupling between the current and potential line in conventional configurations, an alternative array is proposed which is arranged so that the inductive coupling is zero. A number of charts are computed which facilitate the interpretation of the measured or apparent conductivity in terms of a two-layer earth.

Introduction

THERE are many instances in the design of communication systems for VLF where a knowledge of the electrical characteristics of the ground is required. For example, the input resistance, and consequently the efficiency of a VLF transmitting antenna is a function of the conductivity of the neighboring land.[1] Correspondingly, for a given antenna current, the field of the transmitter at some distant receiving station depends on the effective ground conductivity of the intervening path.[2]

At broadcast frequencies and higher, it is customary to use the so-called "wave tilt" method.[3] Essentially, the ratio of the horizontal and vertical component of the electric field of the vertically polarized ground wave is measured. Unfortunately, the magnitude of the wave tilt is extremely small at VLF, being of the order of 10^{-2} at 15 kc for typically conducting ground. Consequently, misorientation and unbalance of the horizontal receiving antenna can produce excessive errors. To obtain the average conductivity for a path, at broadcast frequencies, the attenuation method has been employed with some success. The scheme here is to match the measured field-strength-vs-distance curve with the theoretical ground wave curves of Norton.[2] At VLF, however, the attenuation rate of the ground wave is so small that any departures from the inverse distance law would be negligible except at large distances.

In view of the aforementioned drawbacks of conventional radio frequency techniques for measuring ground conductivity, it is desirable to consider the applicability of the "four-electrode Wenner" method. This method was developed many years ago for measurements of soil resistivity using dc.[4–6] At radio frequencies, however, it is necessary to consider other arrangements of the electrodes which minimize inductive coupling effects between the lead wires. The present paper contains a discussion of the general problem and numerical results for specific cases.

* Manuscript received by the PGAP, December 17, 1957.

† Radio Propagation Eng. Div., Natl. Bur. of Standards, Boulder, Colo.

[1] J. R. Wait and W. A. Pope, "Input resistance of l.f. unipole aerials," *Wireless Eng.*, vol. 32, pp. 131–138; May, 1955.

[2] K. A. Norton, "Calculation of the ground wave field intensity," PROC. IRE, vol. 29, pp. 623–643; December, 1941.

[3] R. H. Barfield, "Some measurements of the electrical constants of the ground by the wave-tilt method," *J. IEE*, vol. 75, p. 214; 1934.

[4] S. Stefanescu and R. M. Schlumberger, "Electric potential distribution around a point in the earth," *J. Phys. Rad.*, vol. 1, pp. 10–20; January, 1930.

[5] M. Muskat, "Potential distribution about an electrode on the surface of the earth," *Physics*, vol. 4, pp. 129–147; April, 1933.

[6] L. B. Slichter, "The interpretation of the resistivity method for horizontal structures," *Physics*, vol. 4, pp. 307–332 and 407; September, 1933.

Basic Theory

In the interpretation of electrical-resistivity measurements of the ground, it is usually assumed that the earth media are made up of isotropic conductors. In many cases this is not justified in a macroscopic sense when the soil or geological structure is horizontally stratified. For example, consider a medium made up of thin horizontal layers consisting of parallel sheets of thickness T with a conductivity σ_1, and the thin intervening layers having a thickness W and a conductivity σ_2. The macroscopic conductivity σ_h in the horizontal direction is given by

$$\sigma_h = \frac{\sigma_1 T + \sigma_2 W}{T + W} \tag{1}$$

and the macroscopic conductivity in the vertical direction is given by

$$\sigma_v = \frac{\sigma_1 \sigma_2 (T + W)}{\sigma_2 T + \sigma_1 W} . \tag{2}$$

It is thus apparent that such media, in a macroscopic sense, are anisotropic.

The solution is now given for the problem of the current flow, I, from a point electrode on the surface of a two-layer earth that has simple anisotropic electrical characteristics. The upper layer of thickness d has conductivities σ_h and σ_v in the horizontal and vertical directions, respectively. The lower region, for depths greater than d, has conductivities σ_h' and σ_v'. The medium above the earth is assigned an isotropic conductivity σ_0 which is later allowed to vanish. A cylindrical coordinate system (ρ, ϕ, z) is introduced with the earth plane specified by $z=0$; the interface between the earth media is at $z=-d$. Current is introduced into the region from a point $z=h$ on the z axis. The value of h, which is always positive, is later allowed to become vanishingly small.

The fundamental equations of dc flow are

$$\text{curl } \boldsymbol{E} = \frac{\partial E_\rho}{\partial z} - \frac{\partial E_z}{\partial \rho} = 0 \tag{3}$$

and

$$\text{div } \boldsymbol{J} = \frac{1}{\rho} \frac{\partial}{\partial \rho} (\rho J_\rho) + \frac{\partial J_z}{\partial z} = 0 \tag{4}$$

where $\boldsymbol{E}$ and $\boldsymbol{J}$ are the vector electric field intensity and the vector current density, respectively. They are re-

lated by a tensor form of Ohm's Law which for the simple anisotropic medium is given by

$$J_\rho = \sigma_h E_\rho = -\sigma_h \frac{\partial \Phi}{\partial \rho} \tag{5}$$

and

$$J_z = \sigma_v E_z = -\sigma_v \frac{\partial \Phi}{\partial z} \tag{6}$$

where Φ is the electric potential. These equations can be readily combined to give the differential equation for Φ:

$$\sigma_h \frac{1}{\rho}\frac{\partial}{\partial \rho}\rho\frac{\partial \Phi}{\partial \rho} + \sigma_v \frac{\partial^2 \Phi}{\partial z^2} = 0. \tag{7}$$

Solutions of this equation that are finite at $\rho = 0$ are of the form

$$\exp\left[\pm(\sigma_h/\sigma_v)^{1/2}\lambda z\right]J_0(\lambda\rho)$$

where J_0 is the Bessel function of the first type of order zero. The potential Φ_0, Φ, and Φ' corresponding to the air, the upper layer, and the lower region, respectively, are then of the following form

$$\Phi_0 + \frac{I}{4\pi\sigma_0 R} + \int_0^\infty D_0(\lambda)\exp(-\lambda z)J_0(\lambda\rho)d\lambda \tag{8}$$

$$\Phi = \int^\infty \{C(\lambda)\exp\left[+(\sigma_h/\sigma_v)^{1/2}\lambda z\right] + D(\lambda)\exp\left[-(\sigma_h/\sigma_v)^{1/2}\lambda z\right]\}J_0(\lambda\rho)d\lambda \tag{9}$$

$$\Phi_1 = \int_0^\infty C'(\lambda)\exp\left[+(\sigma_h'/\sigma_v')^{1/2}\lambda z\right]J_0(\lambda\rho)d\lambda \tag{10}$$

where $R^2 = (z-h)^2 + \rho^2$.

The functions D_0, C, D and C' are determined from the boundary conditions which require that the potentials and the normal current density are continuous across the interfaces $z = 0$ and $z = -d$. The solution is easily carried out to give the following expression for the potential Φ_s on the surface of the ground

$$\Phi_s = \frac{I}{2\pi}\int_0^\infty \frac{e^{-\lambda h}(1+x)J_0(\lambda\rho)d\lambda}{\sigma(1+x) + \bar{\sigma}(1-x)} \tag{11}$$

where

$$x = \frac{\bar{\sigma} - \bar{\sigma}'}{\bar{\sigma} + \bar{\sigma}'}e^{-2\alpha\lambda d}$$

with $\bar{\sigma} = (\sigma_h\sigma_v)^{1/2}$, $\bar{\sigma}' = (\sigma_h'\sigma_v')^{1/2}$, and $\alpha = (\sigma_h/\sigma_v)^{1/2}$. In deriving (11), the identity[7]

$$\int_0^\infty J_0(\lambda\rho)e^{-\lambda(b)}d\lambda = (\rho^2 + b^2)^{-1/2} \quad \text{for } b > 0, \tag{12}$$

has been used. Now letting $h = 0$ and $\sigma_0 = 0$ the expression for the potential is

$$\Phi_s = \frac{I}{2\pi\bar{\sigma}}\int_0^\infty \left[1 + \frac{2x}{1-x}\right]J_0(\lambda)d\lambda \tag{13}$$

and by using a binominal expansion for $(1-x)^{-1}$ this is given by

$$\Phi_0 = \frac{I}{2\pi\bar{\sigma}}\int_0^\infty \left[1 + 2\sum_1^\infty \left(\frac{\bar{\sigma} - \bar{\sigma}'}{\bar{\sigma} + \bar{\sigma}'}\right)^n e^{-2n\alpha\lambda d}\right]J_0(\lambda\rho)d\lambda. \tag{14}$$

Again it is seen that these are integrals of the type given by (12). The potential on the surface is then

$$\Phi_s = \frac{IG(\rho)}{2\pi\bar{\sigma}} \tag{15}$$

where

$$G(\rho) = \left[\rho^{-1} + 2\sum_1^\infty k^n[\rho^2 + (2n\alpha d)^2]^{-1/2}\right]$$

where

$$k = \frac{\bar{\sigma} - \bar{\sigma}'}{\bar{\sigma} + \bar{\sigma}'}.$$

The mutual or transfer resistance for a general four-electrode system consisting of two current electrodes P and Q and two potential electrodes p and q all located on the surface of the ground is then given by

$$2\pi\bar{\sigma}R = G(PQ) + G(pq) - G(Pp) - G(Qq) \tag{16}$$

where PQ is the linear distance measured along the ground surface between the points P and Q.[8] If the ground were homogeneous, (16) would take the form

$$2\pi\bar{\sigma}R]_{d\to\infty} = \frac{1}{PQ} + \frac{1}{pq} - \frac{1}{Pp} - \frac{1}{Qq} = 2\pi\bar{\sigma}R. \tag{17}$$

where $\bar{\sigma}$ is the geometric mean conductivity of the half-space. In view of the form of (17), it is desirable to define an apparent conductivity σ_a of the stratified two-layer half-space, by

$$\sigma_a = \frac{1}{2\pi R}\left[\frac{1}{PQ} + \frac{1}{pq} - \frac{1}{Pp} - \frac{1}{Qq}\right] \tag{18}$$

where R is the actual transfer resistance for the four-electrode array. It then follows that

$$\frac{\sigma_a}{\bar{\sigma}} = \frac{\frac{1}{PQ} + \frac{1}{pq} - \frac{1}{Pp} - \frac{1}{Qq}}{G(PQ) + G(pq) - G(Pp) - G(Qq)}. \tag{19}$$

Applications

The preceding formulas are now applied to various configurations of the electrodes, each of which have certain advantages.

[7] G. N. Watson, "Theory of Bessel Functions," Cambridge University Press, Cambridge, Eng., 1945.

[8] $R = \frac{\text{potential difference between } p \text{ and } q}{\text{current } I \text{ to } P \text{ and } Q}$.

In the so-called "Wenner array" which has been used for 40 years in dc resistivity measurements, the electrodes are arranged in a straight line and are equispaced. The current electrodes, PQ, are located at the ends of the array, and the potential electrodes, pq, are centrally located. The "spacing" between the electrodes is a and is identically equal to Pp, pq, and qQ. The formulas for the apparent conductivity are then given by

$$\sigma_a = \frac{1}{2\pi aR} \text{ (for Wenner array)}$$

and

$$\frac{\bar{\sigma}}{\sigma_a} = 2\sum_{n=0}^{\infty} \epsilon_n k^n \{[1 + (2n\alpha d/a)^2]^{-1/2} - [4 + (2n\alpha d/a)^2]^{-1/2}\} \quad (20)$$

where $\epsilon_0 = 1$ and $\epsilon_n = 2 (n \neq 0)$.

Another arrangement of the electrodes is the "Eltran array" in which the electrodes are also in line and equispaced but now the current electrodes, PQ, are at one end of the array and the potential electrodes, pq, are at the other. The "spacing" is again denoted by a and is now identically equal to PQ, Qp, pq. The formulas for the apparent conductivity are:

$$\sigma_a = \frac{1}{6\pi aR} \text{ (for Eltran array)}$$

and

$$\frac{\bar{\sigma}}{\sigma_a} = 3\sum_{n=0}^{\infty} \epsilon_n k^n \{[1 + (2n\alpha d/a)^2]^{-1/2} + [9 + (2n\alpha d/a)^2]^{-1/2} - 2[4 + (2nd/a)^2]^{-1/2}\}. \quad (21)$$

A novel and a very desirable arrangement is what may be called a "right angle array." In this instance, the current electrodes PQ are joined by a line which is at right angles to the line joining the potential electrodes. The "spacing," a, is equal here to the linear distances PQ, Qp, and pq. This array may be visualized as a contortion of the Eltran array by a 45° displacement of the end electrodes P and q along an arc of a circle of radius a and centers at Q and p, respectively.

The formulas for the apparent conductivity now read

$$\sigma_a = \frac{0.05605}{aR} \text{ (for "right-angle" array)}$$

and

$$\frac{\bar{\sigma}}{\sigma_a} = 2.84\sum_{n=0}^{\infty} \epsilon_n k^n \{[1 + (2n\alpha d/a)^2]^{-1/2} + [(2.414)^2 + (2n\alpha d/a)^2]^{-1/2} - 2[(1.849)^2 + (2n\alpha d/a)^2]^{-1/2}\}. \quad (22)$$

Using (20)–(22), the apparent conductivity ratio is plotted as a function of the spacing parameter $a/\alpha d$ in the figures. The curves for the Wenner array are shown in Fig. 1(a) and 1(b), next page, for k positive and k negative, respectively. The corresponding curves for the Eltran array are shown in Fig. 2(a) and 2(b) and those for the "right angle" array are shown in Fig. 3(a) and 3(b). The results for the Wenner array agree with previously published results.[4–6] The Eltran curves are quite similar although there is a pronounced "bump" for small values of the spacing. This implies that the Eltran array "sees" much deeper layers than the Wenner array. For larger spacings, however, the departure of $\sigma_a/\bar{\sigma}$ from unity is more pronounced for the Wenner array. The right angle array seems to have a behavior somewhat between that for the Wenner and Eltran arrays.

To retain the maximum generality, the two-layer model employed in the preceding discussion consists of anisotropic material. In the isotropic case, $\bar{\sigma}$ becomes σ and α is unity. In an interpretation of experimental results, however, it seems desirable to regard αd as the effective thickness of the upper stratum, and k as an effective reflection factor for the lower interface of the upper stratum. In the present scheme of things, there is no way to estimate the degree of anisotropy unless the actual thickness for the upper stratum is known.

Appendix

The foregoing analysis and computed results are strictly valid only for dc. It can be expected that the results are valid, however, for ac if the frequency is sufficiently low. Following the work of Wait[9] it can be shown, for a homogeneous half-space of conductivity, σ, that the mutual impedance between the circuits P, Q and p, q can be written

$$Z = \int_p^q \int_P^Q F(r) \cos \epsilon \, dS \, ds + G(PQ) + G(pq) - G(Pp) - G(Qq)$$

where dS and ds are elemental lengths of the insulated wires connecting P and Q, and p and q, respectively; $\cos \epsilon$ is the angle subtended by the elements dS and ds and r is the distance between the elements. In the above

$$F(r) = \frac{i\mu\omega}{2\pi r} \frac{1 - (1 + \gamma r)e^{-\gamma r}}{(\gamma r)^2} = \frac{i\mu\omega}{4\pi r}\left[1 - \frac{2}{3}(\gamma r) + \frac{1}{4}(\gamma r)^2 \pm \cdots\right]$$

and

$$Q(r) = \frac{1}{2\pi\sigma r}$$

where $\gamma = (i\sigma\mu\omega)^{1/2}$ and $\mu = 4\pi \times 10^{-7}$. The preceding formula for Z has been derived on the basis that displacement currents can be neglected compared to the

[9] J. R. Wait, "Mutual electromagnetic coupling of loops over a homogeneous ground," *Geophysics*, vol. 20, pp. 630–637; July, 1955. (Reference to earlier papers by J. R. Wait and others on the subject are given here.)

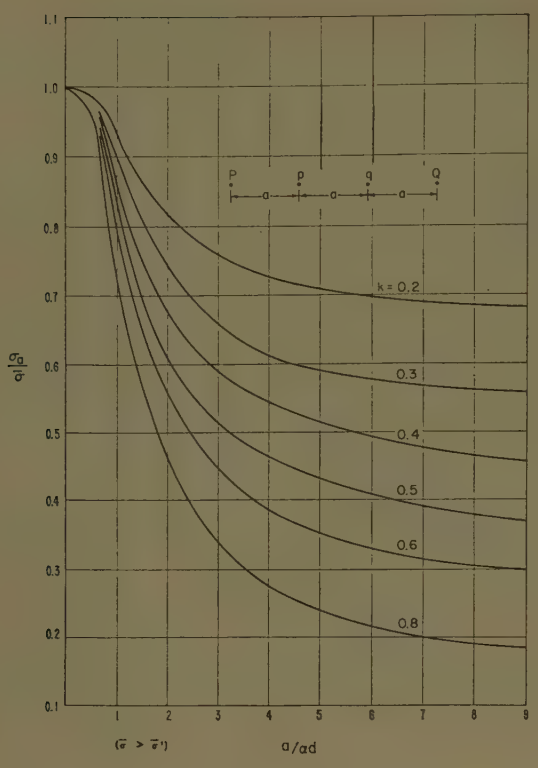

(a)

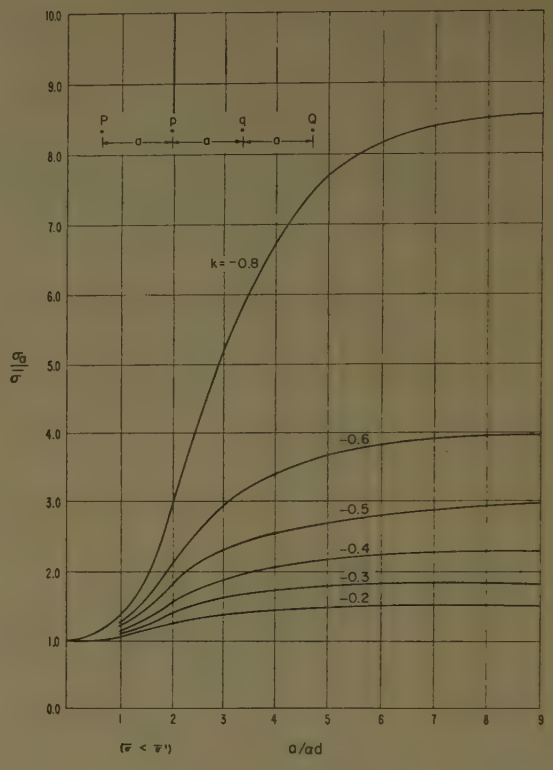

(b)

Fig. 1—Wenner array. The abcissa is $a/\alpha d$.

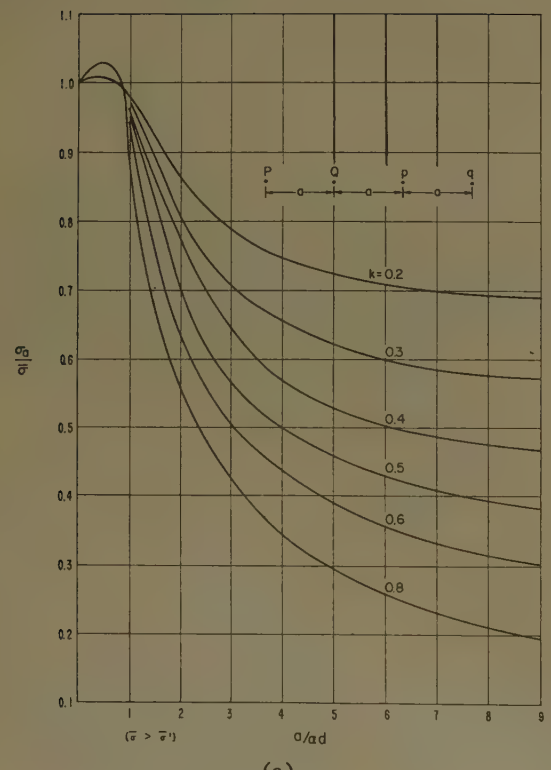

(a)

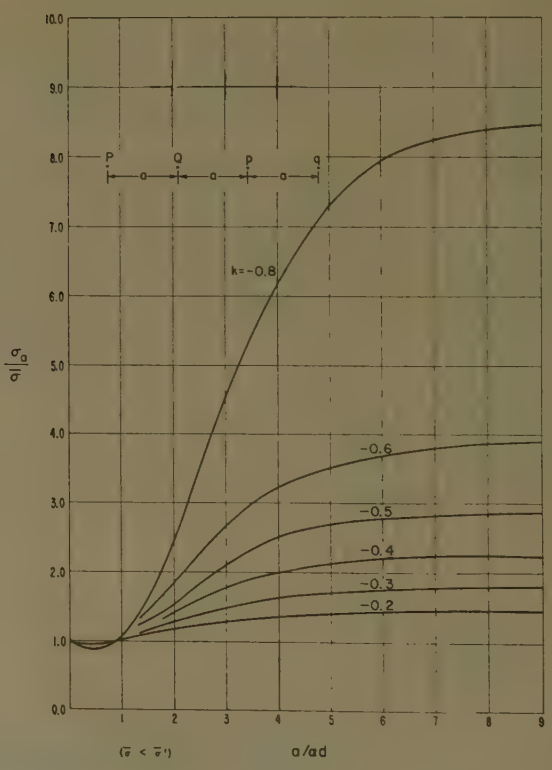

(b)

Fig. 2—Eltran array.

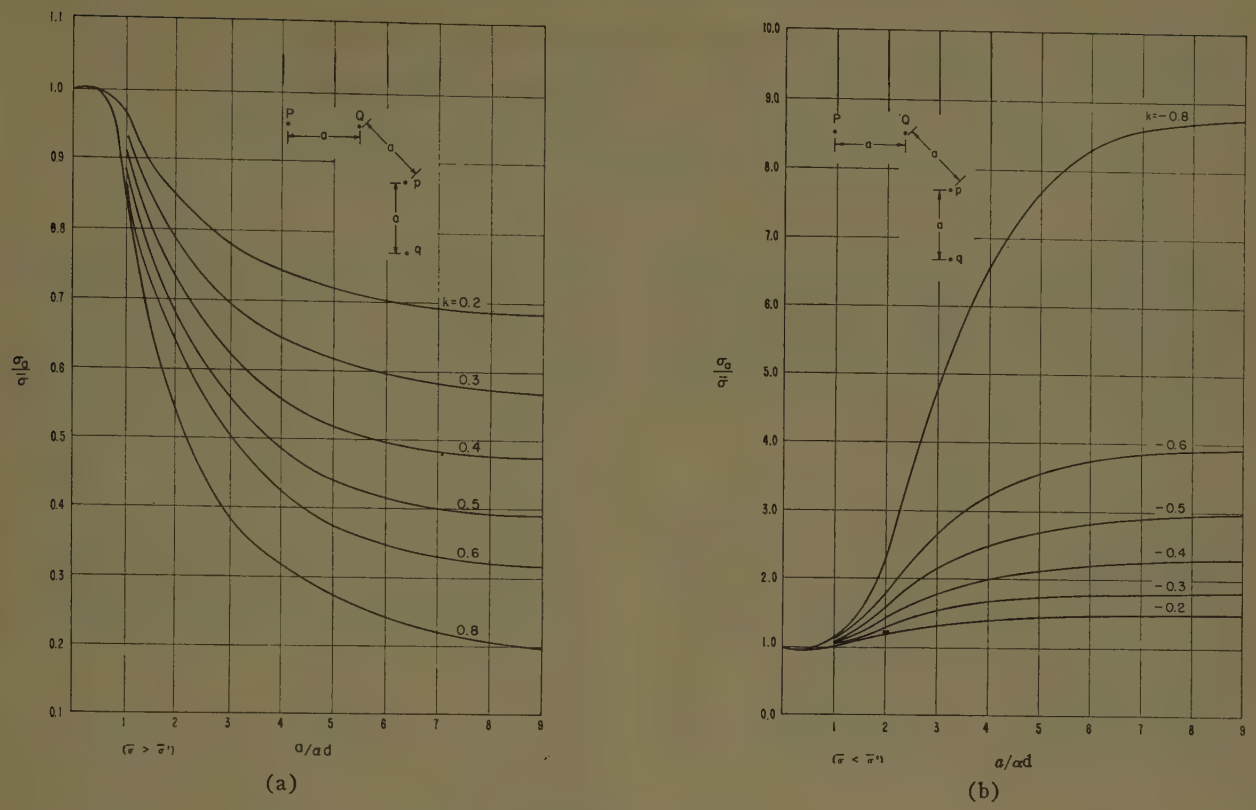

(a) (b)

Fig. 3—Right angle array.

earth conduction currents. Furthermore, if significant distances are small compared to the "electrical skin depth," $|2/\gamma|$, in the ground, $|\gamma r| \ll 1$, and consequently

$$F(r) \cong i\mu\omega/4\pi r.$$

The mutual impedance Z is now of the form

$$Z = R + i\omega L$$

where R is a transfer resistance and L is the "Neumann" mutual inductance given by

$$L = \frac{\mu}{4\pi r}\int_p^q \int_P^Q \frac{\cos\epsilon}{r}\, dSds.$$

It is not difficult to show that the $[|Z/R| - 1]$ is of order of bL/δ^2 where δ is the skin depth, L is the length of the current and potential lines that are essentially coupled, and b is their average separation. In other words, if the magnitude of Z is measured, inductive coupling between the circuits is negligible if the circuits are separated such that $\delta \gg (bL)^{1/2}$.

If the wires are always at right angles to one another so that $\cos\epsilon = 0$, the mutual inductance is identically zero. Such is the case in the "right angle" array.

List of Symbols Used in Diagrams

σ_a = the apparent conductivity of the two-layer model of the ground.

$\bar{\sigma}$ = the geometric mean conductivity of the upper stratum.

$\bar{\sigma}'$ = the geometric mean conductivity of the lower (semi-infinite) stratum.

$$k = \frac{\bar{\sigma} - \bar{\sigma}'}{\bar{\sigma} + \bar{\sigma}'}.$$

a = distance of separation between two neighboring electrodes in the Wenner, Eltran and "right angle" arrays.

d = thickness of the upper stratum.

$$\alpha = \left[\frac{\text{conductivity in horizontal direction}}{\text{conductivity in vertical direction}}\right]^{1/2}$$

for upper stratum.

P and Q are current electrodes, and p and q are potential electrodes. The following is a schematic representation of the two-layer anisotropic ground.

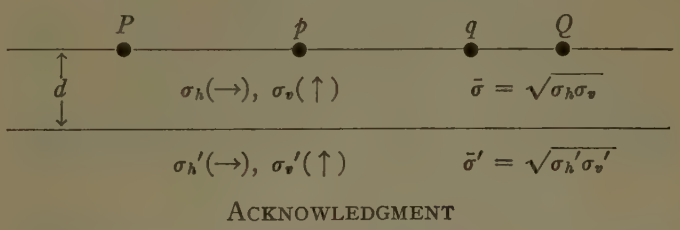

Acknowledgment

The authors would like to thank Dr. Norman Ricker for supplying some of the earlier references and A. D. Watt, our colleague, for many helpful comments.

Altitude Variation of Field Strength for Vertically Polarized Low and Broadcast Frequency Radiation*

J. R. McGONEGAL†, J. W. SAVAGE†, AND C. A. ZIELINSKI‡

Summary—**Height-gain calculations have been made using Norton's formulas at low and broadcast frequencies in cases where the values of numerical distance and numerical height do not permit the use of simplified graphical methods. Field strength measurements at various altitudes showed good agreement with the calculated values. The airborne field strength measuring installation and the manner of its use are described.**

Introduction

During recent investigations of propagation phenomena in the LF and broadcast regions of the RF spectrum, the field strength of vertically polarized transmissions from antennas close to the ground was measured at various altitudes, and the results were compared with computed values. In view of the small amount of published data available on height-gain effects at these frequencies, the somewhat limited results of this study are presented to extend the information on record.

Equipment and Procedure for Airborne Measurements

Measurements were carried out on frequencies of 181 and 524 kc, using an experimental transmitter located at Wright-Patterson Air Force Base, and on 700 and 1290 kc, using two Ohio broadcast stations, WLW and WHIO.

For the measurement of field strengths at altitude, a Stoddart type NM-20A field strength meter was installed in an Air Force C-47 aircraft, with a Bendix MN-24B loop antenna mounted atop the midsection of the fuselage. An Esterline-Angus RD-59/U recording milliammeter was arranged to chart the output of the Stoddart.

Prior to installation in the aircraft, the field strength meter and recorder were calibrated in the laboratory at 181, 524, 700, and 1290 kc, using an RF generator coupled to the antenna input terminals of the NM-20A through an attenuator.

After the loop and instruments were mounted in the C-47, calibration of the entire installation was undertaken. The aircraft was towed to a location on the ground satisfactorily clear of large structures and overhead wires, and field strength readings were taken with the transmitter forward, aft, and abeam of the ship. This process was repeated at each of the four frequencies of interest. In each case, the ratio of meter indication to true field strength when the transmitter was abeam was found to be about two-thirds of the value when the transmitter was on the flight path of the aircraft.

Using this measuring installation, the data required for determination of height-gain factors were secured either by flying the aircraft at a fixed altitude over a radial on which surface measurements had been made previously, with the Stoddart and recorder in continuous operation, or by making repeated passes at various altitudes over a readily identified landmark. Measurements were confined to altitudes of 10,000 feet or less to avoid the use of oxygen equipment.

Calculation of Field Strength at Altitude

Techniques for the calculation of surface field strength variations on paths radial to a transmitter are well known, and described in the work of Norton.[1] Methods of measuring these field strength variations are similarly well known and have been practiced extensively in this frequency range.

Surface field strength measurements were made on the Wright-Patterson transmitter at frequencies of 181 and 524 kc, and on WLW and WHIO. Comparison of the measured values with theoretical surface-wave attenuation curves indicated a ground conductivity of 9.5×10^{-14} emu and a dielectric constant of 15 for the region in which the tests were carried out. The measured points and theoretical curves are shown in Fig. 1.

To calculate the variation of field strength with altitude above any point on the ground, the methods of Norton[1] may be utilized. Eq. (1) gives the value of the ground wave E at any altitude for distances at which a plane earth may be assumed.

$$E = \frac{E_0}{d}\left[\cos^3\psi_1 e^{2\pi i r_1/\lambda} + R\cos^3\psi_2 e^{2\pi i r_2/\lambda} + (1-R)\cos^2\psi_2 F(P, B) e^{i\phi} e^{2\pi i r_2/\lambda}\right]. \quad (1)$$

Three terms appear in this expression: the first represents the direct wave from the transmitting antenna to the receiver. A second component is propagated by regular reflection from the ground, while the third term represents the "surface wave" which is guided by the earth-air interface. Although the equation assumes short doublet antennas at transmitter and receiver, it

* Manuscript received by the PGAP, August 23, 1957. This work was supported by the Air Force under Contract AF 33(616)-2908, and under the technical supervision of the Commun. and Navig. Lab., Wright Air Dev. Center, Wright-Patterson AFB, Ohio.

† Jansky and Bailey, Inc., Washington, D. C.

‡ Light Military Electronic Equip. Dept., General Electric Co., Utica, N. Y.; formerly with Jansky and Bailey, Inc., Washington, D. C.

[1] K. A. Norton, "The calculation of ground-wave field intensity over a finitely conducting spherical earth," Proc. IRE, vol. 29, pp. 623–639; December, 1941.

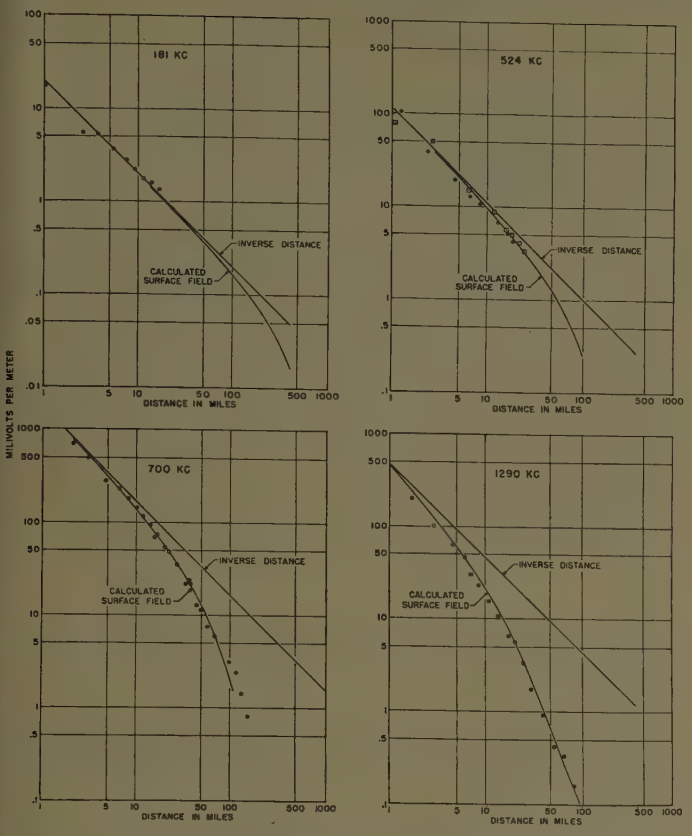

Fig. 1—Field strength on surface—measured values and curves computed for $\sigma = 9.5 \times 10^{-14}$ emu, $\epsilon = 15$.

can be used with negligible error where neither antenna is highly directive in the vertical plane.

Fig. 2 illustrates the geometry involved. When both antennas are sufficiently close to the ground, ψ_1 and ψ_2 become small, the reflection coefficient R for imperfect earth becomes equal to -1, and r_1 equal to r_2, so that the received field consists only of the surface wave. For perfectly conducting earth, the reflection coefficient becomes $+1$; thus in this case the field at unit distance from the transmitting antenna is seen to be equal to $2E_0$.

For vertically polarized radiation, the terms of the equation are defined in terms of the distance d, antenna heights h, frequency and ground constants as follows:

E_0 = unattenuated free-space field strength at unit distance in the equatorial plane of the transmitting doublet.

$$\tan \psi_1 = \frac{h_1 - h_2}{d} \qquad \tan \psi_2 = \frac{h_1 + h_2}{d}.$$

h_1 and h_2 are measured from the terrain level to the center of radiation of the antenna.

$$r_1 = \frac{d}{\cos \psi_1} \qquad r_2 = \frac{d}{\cos \psi_2}$$

σ = ground conductivity, in emu.

ϵ = ground dielectric constant, relative to air.

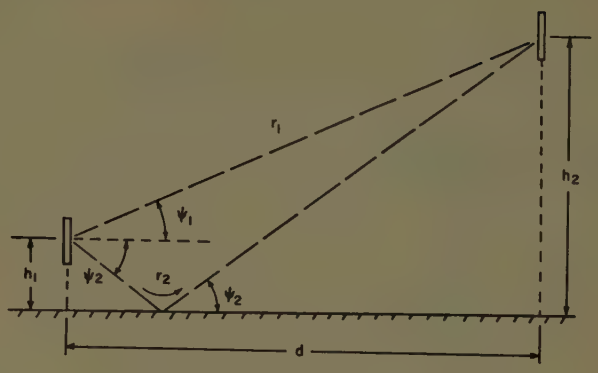

Fig. 2—Geometric parameters for field-strength computations.

$$x = \frac{1.797(10^{15})\sigma}{f_{MC}}$$

$$\tan b' = \frac{\epsilon - \cos^2 \psi_2}{x} \qquad \tan b'' = \frac{\epsilon}{x}$$

$$b = 2b'' - b'$$

$$p = \pi \frac{r_2}{\lambda} \left[\frac{\cos^2 b''}{x \cos b'} \right]^{1/2} \qquad q_{1.2} = \frac{2\pi h_{1.2}}{\lambda} \left[\frac{\cos^2 b''}{x \cos b'} \right]^{1/2}$$

$$R = \frac{\left(\frac{q_1 - q_2}{2p} \right) \exp i\left(\frac{\pi}{4} - \frac{b}{2} \right) - 1}{\left(\frac{q_1 + q_2}{2p} \right) \exp i\left(\frac{\pi}{4} - \frac{b}{2} \right) + 1}$$

$$Pe^{iB} = 4pe^{ib}/(1 - R)^2.$$

$F(P, B)e^{\phi(P, B)}$ is a surface-wave propagation function, the value of which is most conveniently determined from charts given by Norton.[1]

An inspection of these equations will reveal the tediousness of the computations required to solve them for a variety of distance and altitude combinations at several frequencies. To simplify this process, graphical solutions have been devised,[1] but these methods may be used only when certain values of p and q simultaneously obtain. The antenna heights and the frequencies involved in this study do not yield values of p and q in the proper ranges. Under these conditions, there is no recourse other than to perform the computations directly.

Values of Height-Gain Factors

Tables I through IV list the values of height-gain factors at distances up to 100 miles. Calculated values are given for altitudes up to 40,000 feet, although as previously mentioned, measurements were restricted to altitudes below 10,000 feet. The tabulated quantities are ratios (in db) of the field at altitude to the field on the surface at the same distance. Fig. 3 presents the same data in graphical form.

It should be noted that in the calculations, the height of the transmitting antenna was fixed for each frequency at a value corresponding to the height of the center of

TABLE I*

Freq. = 181 kc; $\sigma = 9.5 \times 10^{-14}$ emu, $\epsilon = 15$, $h_1 = 35$ feet

Distance (Stat. Mi.)		Altitude (feet) 2500	4500	9200	15,000	40,000
10	meas.			−1.5		
	calc.	−0.5	−0.7	−0.8	−0.6	−0.3
20	meas.			−1.8		
	calc.	1.2	−0.1	−0.1	−0.8	−0.3
40	meas.			−2.5		
	calc.	−0.4	1.8	−1.2	−1.1	2.1
60	meas.			−3.5		
	calc.	−0.3	−0.6	−0.9	−1.1	−0.6
100	meas.			−2.0		
	calc.		−0.5	−1.7	−1.4	−0.8

* All values in db above surface field.

TABLE II*

Freq. = 524 kc; $\sigma = 9.5 \times 10^{-14}$ emu, $\epsilon = 15$, $h_1 = 35$ feet

Distance (Stat. Mi.)		Altitude (feet) 2500	4500	9200	15,000	40,000
10	meas.	−2.8	−0.3	−1.3		
	calc.	−4.1	−1.6	−1.1	−1.2	−5.4
20	meas.	−1.7	−2.2	−1.2		
	calc.	−1.8	−3.0	−1.4	−0.5	−0.8
40	meas.	−2.1	−1.2	−1.2		
	calc.	−2.2	−2.2	−1.2	−0.1	1.9
60	meas.	−1.6	−1.1	−2.6		
	calc.	−2.7	−0.7	−2.3	−0.6	2.8
100	meas.	−0.9		−2.9		
	calc.		−0.6	−0.7	2.2	6.7

* All values in db above surface field.

TABLE III*

Freq. = 700 kc; $\sigma = 9.5 \times 10^{-14}$ emu, $\epsilon = 15$, $h_1 = 350$ feet

Distance (Stat. Mi.)		Altitude (feet) 2500	4500	9200	15,000	40,000
10	meas.					
	calc.	−2.8	−2.1	−1.4	−0.7	−4.4
20	meas.	−3.0	−2.1	−0.8		
	calc.	−3.1	−2.3	−0.8	0.3	0.3
40	meas.	−6.1	−4.1	−1.8		
	calc.	−3.2	−3.6	−0.8	1.2	3.6
60	meas.	−2.9	−2.3	−0.6		
	calc.	−2.5	−3.7	−0.1	0.8	7.5
100	meas.	−1.1	−1.4	1.7		
	calc.		−4.4	−0.4	1.7	12.1

* All values in db above surface field.

TABLE IV*

Freq. = 1290 kc; $\sigma = 9.5 \times 10^{-14}$ emu, $\epsilon = 15$, $h_1 = 150$ feet

Distance (Stat. Mi.)		Altitude (feet) 2500	4500	9200	15,000	40,000
10	meas.					
	calc.	2.1	0.5	2.3	3.4	2.2
20	meas.	−1.7	2.3	5.1		
	calc.	−1.6	2.2	6.3	10.6	7.1
40	meas.	1.3	4.0	9.6		
	calc.	0.3	4.8	8.2	13.2	14.9
60	meas.	−5.7	−1.5	7.3		
	calc.	2.7	6.5	11.1	15.8	19.1
100	meas.	0.6	4.6	10.9		
	calc.		8.0	12.5	19.4	24.8

* All values in db above surface field.

radiation of the antenna used at the frequency in question during the experimental portion of the study. At 181 and 524 kc, the transmitting antenna used had an over-all height of 70 feet, and was heavily top-loaded. For the application of (1) it was assumed that the height of the center of radiation was 35 feet. Broadcast stations WLW and WHIO are equipped with antennas 695 and 292 feet in height, respectively; thus the radiation-center heights were taken as 350 feet at 700 kc, and 150 feet at 1290 kc.

The maximum distance for strict validity of a plane-earth assumption ranges from 88 miles at 181 kc to 46 miles at 1290 kc. Many of the distances for which height-gain values are tabulated are beyond these limits. However, (1) is considered valid for use at distances beyond the plane-earth limits for cases in which the receiving antenna is above the radio horizon of the transmitting antenna. This use is based on the assumption that the divergence of the reflected wave from a spherical earth offsets the effect of the decrease in the effective height of the receiving antenna compared to its actual height above the surface of the earth.[2] It will be noted that no calculated values are tabulated for a distance of 100 miles and an altitude of 2500 feet, since this point is not within sight of the ground antenna.

Fig. 3 and the Tables show that the plane-earth equation yields a prediction of the measured field strengths which is accurate within about 1.5 db at points above the radio horizon. The greatest discrepancies are found at large distances; at 100 miles the radio horizon (assuming an earth radius of 4/3 of the true value) is about 6000 feet from the ground. Hence, since the measurement points have altitudes no greater than 10,000 feet, some loss of accuracy here is not unexpected. It should also be remembered that the calculations assume a homogeneous spherical earth, and that the measured field strengths may be affected by local irregularities in the terrain or variations in earth conductivity.

[2] F. E. Terman, "Radio Engineer's Handbook," McGraw-Hill Book Co., Inc., New York, N. Y., p. 692; 1943.

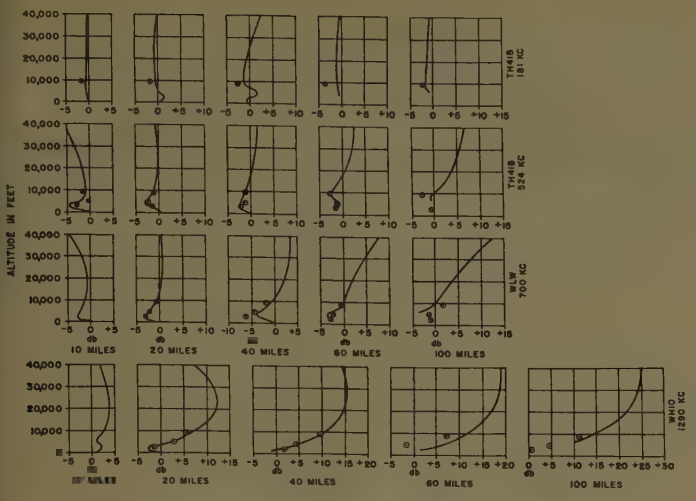

Fig. 3—Measured and calculated height-gain factors, in db above surface field.

Surface field strength values must be used in conjunction with the height-gain factors to obtain the field strength at altitude. Large positive values for height gain observed at 700 and 1290 kc do not imply that the field at altitude for a given radiated power is greater than it would be at 181 kc, since the lower frequencies are attenuated much less rapidly on the surface. As shown by Fig. 4, which presents contours of constant field strength (relative to the surface field at 1 mile), the increased values of height gain at higher frequencies should be considered as representing an attenuation of the field close to the ground which increases with frequency in this range.

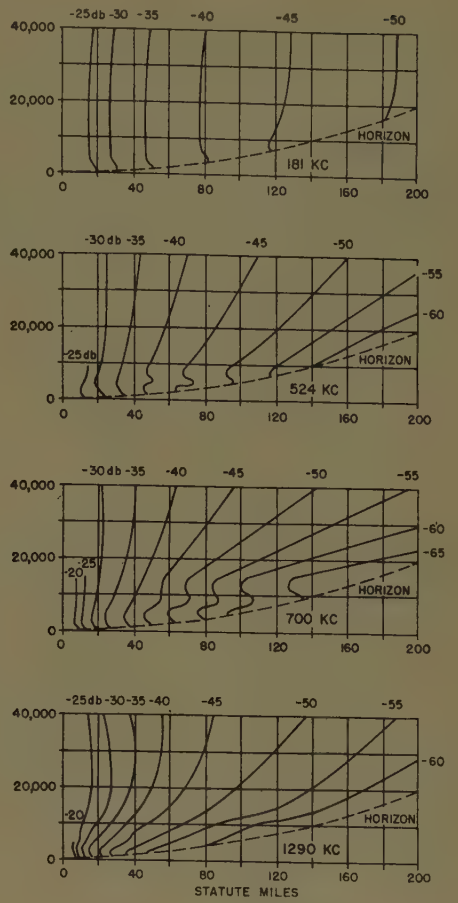

Fig. 4—Contours of constant field strength for transmitting antennas close to ground. Curves labelled in db relative to unattenuated surface field at 1 mile from transmitter. Computed with $\sigma = 9.5 \times 10^{-4}$ emu, $\epsilon = 15$.

Simplified Method for Computing Knife Edge Diffraction in the Shadow Region*

L. J. ANDERSON† AND L. G. TROLESE†

Summary—**A simplified method of computing knife edge diffraction in the shadow region is presented which is applicable to most obstacle gain paths, that is, paths with a dominant mountain obstacle. The method has been worked out for 1) the four-ray model—specular reflection on each side of the obstacle, 2) the two-ray model—reflection on one side only, and 3) the single-ray model—no reflection on either side. The obstacle can be at any location along the path. The accuracy is within 2 db for path geometries such that the usual diffraction parameter v is greater than 1 and the two terminal heights are less than the obstacle height. Curves which further simplify the computation procedure are presented.**

* Manuscript received by the PGAP, November 29, 1957. This work was partially supported by the Signal Communications Dept., Army Electronic Proving Ground, Fort Huachuca, Ariz.

Introduction

According to classical electromagnetic theory, the field strength behind a knife edge can be represented as:

$$\frac{E}{E_0} = F \exp(i\beta), \tag{1}$$

where E_0 is the free space field (no knife edge present), F is the amplitude, and β is the phase angle with respect to the direct path. Both F and β may be expressed in terms of the Fresnel Integrals

† Smyth Research Associates, San Diego, Calif.

$$C = \int_0^v \cos\frac{\pi}{2} v^2 dv$$

$$S = \int_0^v \sin\frac{\pi}{2} v^2 dv,$$

where v is a dimensionless parameter which will be defined later. Using these integrals,[1] which are tabulated over a limited range of v, one can write

$$F = \frac{S + 0.5}{\sqrt{2}\sin\left(\beta + \frac{\pi}{4}\right)} \tag{2}$$

and

$$\beta = \tan^{-1}\left(\frac{S + 0.5}{C + 0.5}\right) - \frac{\pi}{4}. \tag{3}$$

In most cases of practical interest in radio propagation, one must consider not only the direct ray from transmitter to receiver via the knife edge, but also the rays which are reflected from the ground on either or both sides of the knife edge. In Fig. 1, ray 0 is the direct ray, ray 1 is reflected only on the receiver side, ray 2 is reflected only on the transmitter side, and ray 3 is reflected on both sides of the knife edge. In cases where such reflections occur, all rays must be added in their proper phase and amplitude in order to determine the resultant field:

$$\frac{E}{E_0} = \sum_{j=1}^{j=n} F_j \exp(i\beta_j), \tag{4}$$

where F_j refers to the amplitude and β_j to the phase of the jth ray. This expression may be rewritten:

$$\left|\frac{E}{E_0}\right|^2 = (\sum F_j \cos\beta_j)^2 + (\sum F_j \sin\beta_j)^2. \tag{5}$$

In Fresnel diffraction problems, the path geometry is expressed by a dimensionless parameter v:

$$v = h\sqrt{\frac{2}{\lambda}\left(\frac{1}{d_1} + \frac{1}{d_2}\right)}, \tag{6}$$

where λ is the wavelength and other quantities are shown in Fig. 1. F and β for each ray are then determined using (2) and (3), and substitution in (5) yields the resultant field. This procedure is such a tedious one that knife edge diffraction patterns are computed as seldom as possible. Various attempts have been made to simplify the computations,[2,3] but these have been done at the expense of restricting the area of applicability.

[1] J. C. Schelleng, C. R. Burrows, and E. B. Ferrell, "Ultra short wave propagation," Proc. IRE, vol. 21, pp. 427–463; March, 1933.
[2] F. H. Dickson, J. J. Egli, J. W. Herbstreit, and G. S. Wickizer, "Large reductions of vhf transmission loss and fading by the presence of a mountain obstacle in beyond line of sight paths," Proc. IRE, vol. 41, pp. 967–969; August, 1953.
[3] C. E. Sharp, "Experimental Investigation of Mountain Obstacle Path Transmission," Res. Lab., Motorola, Inc., Riverside, Calif., Final Report Contract DA 36-039-SC-64556; November, 1955.

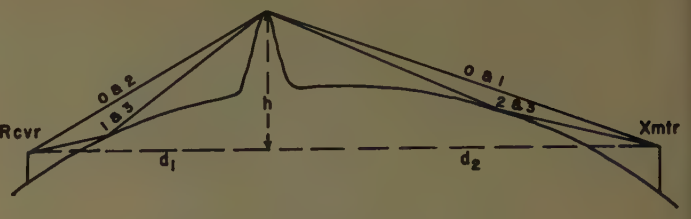

Fig. 1—Four-ray obstacle gain geometry.

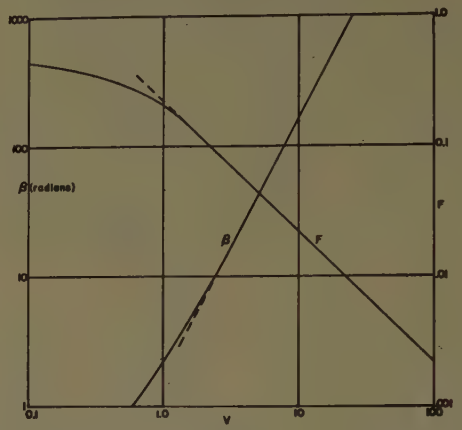

Fig. 2—Amplitude and phase vs v in the shadow region.

Development of Simplified Method

The method presented below greatly reduces the labor of knife edge diffraction computations in the shadow region. It is sufficiently accurate for most purposes and is applicable over a wide range of path geometry conditions.

Fig. 2 is a plot of F and β in the shadow region. The straight line asymptotes are given by:

$$F_j = \frac{1}{\sqrt{2}\pi v_j} \text{ and } \beta_j = \frac{\pi}{4} + \frac{\pi}{2} v_j^2, \text{ when } v \gg 1.$$

Thus (5) can be written

$$\left|\frac{E}{E_0}\right|^2 = \frac{1}{2\pi^2}\left[\sum \frac{\cos\left(\frac{\pi}{4} + \frac{\pi}{2} v_j^2\right)}{v_j}\right]^2 + \left[\sum \frac{\sin\left(\frac{\pi}{4} + \frac{\pi}{2} v_j^2\right)}{v_j}\right]^2. \tag{7}$$

A reflection coefficient of unity and a change of phase on reflection of π have been assumed. Divergence has been ignored since overland paths are seldom truly spherical.

If we now define

$$v_0 = h_0\sqrt{\frac{2}{\lambda}\left(\frac{1}{d_1} + \frac{1}{d_2}\right)} \tag{8}$$

and

$$v_1 = v_0 + \Delta v_1$$

$$v_2 = v_0 + \Delta v_2$$

$$v_3 = v_0 + \Delta v_1 + \Delta v_2$$

then

$$\beta_1 - \beta_0 = \pi(1 + \Delta v_1(v_0 + \Delta v_1/2))$$
$$\beta_2 - \beta_0 = \pi(1 + \Delta v_2(v_0 + \Delta v_2/2))$$
$$\beta_3 - \beta_0 = \pi(\Delta v_1(v_0 + \Delta v_1/2) + \Delta v_2(v_0 + \Delta v_2/2)).$$

Substituting these parameters in (7), subtracting β_0 from all phase angles, and performing the operations indicated, gives for the 4-ray case (reflection on both sides):

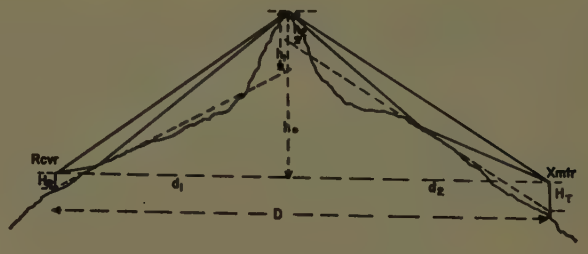

Fig. 3—Typical profile of a path with a prominent obstacle.

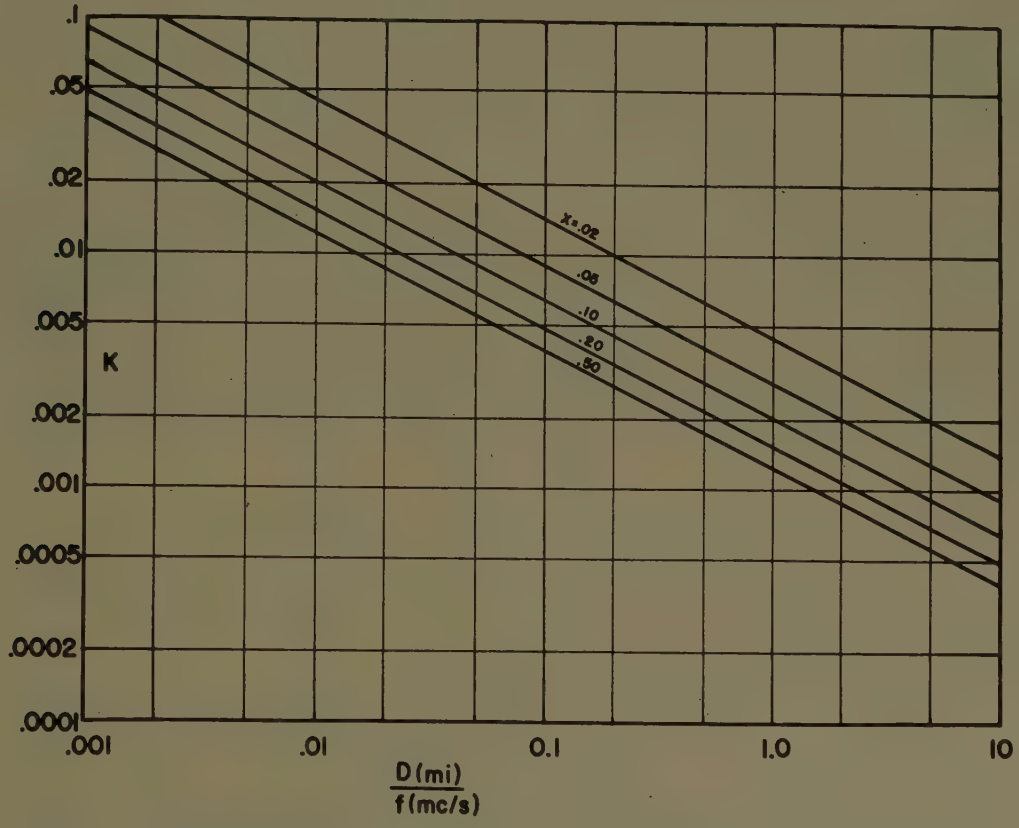

Fig. 4—K vs D/f for various obstacle positions.

$$\left|\frac{E}{E_0}\right|^2 = \frac{2}{\pi^2 v_0^2}(1 - \cos \pi\Delta v_1(v_0 + \Delta v_1/2)) \cdot (1 - \cos \pi\Delta v_2(v_0 + \Delta v_2/2)). \quad (9)$$

In the 2-ray case (reflection on one side only) the expression reduces to:

$$\left|\frac{E}{E_0}\right|^2 = \frac{1}{\pi^2 v_0^2}(1 - \cos \pi\Delta v(v_0 + \Delta v/2)). \quad (10)$$

Finally, for the 1-ray case (no reflections):

$$\left|\frac{E}{E_0}\right|^2 = \frac{1}{2\pi^2 v_0^2}.$$

The only restrictions imposed in the derivation are that the receiver be well in the shadow region ($v_0 \geq 1$) and that the Δv's be small compared to v_0.

In using the above expressions, one must first determine v_0 and the Δv's corresponding to the particular path of interest. Fig. 3 shows a typical path profile, with the various parameters used in determining these quantities. In order to eliminate ray bending resulting from atmospheric refraction, the profile is plotted on a 4/3 earth basis.

To compute v_0, we rewrite (8) as

$$v_0 = \frac{h_0}{2280\sqrt{D/f}}\sqrt{\frac{2}{X(1-X)}} = Kh_0, \quad (11)$$

where $X = d_1/D$. Fig. 4 is a plot of K vs D/f for various values of X. In the figure, D is expressed in statute miles, f in megacycles per second, and X is the ratio of the distance from the obstacle to the nearest terminal, divided by the total path length D. Since K is a constant for a given path and frequency, it needs to be determined only once. When height-gain computations are made, the v_0 corresponding to each of the assumed terminal heights is simply the K factor multiplied by

the h_0 (in feet) appropriate to the terminal heights.

The Δv's are determined in the following way. First we can write

$$\beta_1 - \beta_0 \approx \pi + \pi v_0 \Delta v_1.$$

This incremental phase difference can also be equated to the path difference

$$\beta_1 - \beta_0 = \pi + \frac{2\pi\delta_1}{\lambda}.$$

Thus

$$\Delta v_1 = \frac{2\delta_1}{\lambda v_0}. \tag{12}$$

Similarly,

$$\Delta v_2 = \frac{2\delta_2}{\lambda v_0}$$

and

$$\Delta v_3 = \frac{2(\delta_1 + \delta_2)}{\lambda v_0}.$$

The path differences are computed by the usual expression:

$$\delta_1 = \frac{2H_R h_1}{d_1}; \qquad \delta_2 = \frac{2H_T h_2}{d_2}. \tag{13}$$

By combining (12) and (13) one can eliminate the δ's and write:

$$\Delta v_1 = \frac{2H_R h_1}{h_0} KX \tag{14}$$

and

$$\Delta v_2 = \frac{2H_T h_2}{h_0} K(1 - X).$$

When written in this form, X is d_1/D (Fig. 3), and of course $(1-X)$ is d_2/D. K is the constant appearing in (11), and is obtained from Fig. 4. In measuring the H's and h's from the profile, one must lay a straight edge on the reflecting surface and project this surface to the knife edge plane and to the terminal plane. Both H_R and h_1 are measured from this extension of the reflecting plane on the receiver side, and H_T and h_2 from the reflecting plane on the transmitter side, as shown in Fig. 3. In making the v_0 and Δv computations then, one uses (11) and (14) and Fig. 4, combined with the required profile measurements.

After the Δv's have been computed, the values of each of the factors in (9) can be readily determined. Fig. 5 (opposite) is a plot in db of each of the last two terms vs $\Delta v(v_0+\Delta v/2)$. The dashed curves in Fig. 5 are on an expanded scale (top and right) for use with abscissa values very close to 0 or 2. For $\Delta v(v_0+\Delta v/2)$ greater than 2, one subtracts 2, 4, 6, etc., until the value is between 0 and 2.

Finally the db corresponding to $2/\pi^2 v_0^2$ (4-ray line) are read from Fig. 6. Adding these three db factors gives the resultant field in db below the free space field.

In the case where reflection takes place only on one side of the knife edge, (10) is used, and the db factors are obtained from Figs. 5 and 6, as before, using the 2-ray line in Fig. 6.

Sample Computation

In order to illustrate the procedure for working out a height-gain curve using the method described above, let us consider a hypothetical link with the following parameters:

$d_1 = 30$ miles $\quad h_1 = 1200' \quad H_T = 50'$

$d_2 = 50$ miles $\quad h_2 = 800' \quad f = 1000$ mc

$H_R = 10', 25', 50', 75',$ and $100'$

h_0 (receiver at $100'$) $= 2500'$.

Since h_0 will be different for each receiver height, we first compute the h_0's for each assumed H_R

$$(h_0 \text{ at } H_R) = (h_0 \text{ at } 100') + 5/8(100 - H_R)$$

These values are tabulated in column 2 of Table I (p. 286). Next, one finds

$$\left(\text{for } X = \frac{30 \text{ mi}}{80 \text{ mi}} = 0.375 \text{ and } \frac{D}{f} = \frac{80 \text{ mi}}{1000 \text{ mc}} = 0.08\right)$$

that $K=0.0046$ (Fig. 4). Column 3 is thus $0.0046\ h_0$. Since the transmitter remains at fixed height, Δv_2 (14) is

$$\frac{2 \times 50 \times 800 \times 0.0046 \times 0.625}{h_0} = \frac{230}{h_0}.$$

Similarly

$$\Delta v_1 = \frac{H_R}{h_0}(2 \times 1200 \times 0.0046 \times 0.375) = 4.14\frac{H_R}{h_0}.$$

These values are tabulated in columns 4 and 5. One next computes $\Delta v_2(v_0+\Delta v_2/2)$ and $\Delta v_1(v_0+\Delta v_1/2)$ using columns 3, 4, and 5. These values are tabulated in columns 6 and 7.

Finally the three factors of (9) are obtained, using Figs. 5 and 6, together with the tabulations in columns 3, 6, and 7. The resultant field at each receiver height is the sum of the values in columns 8, 9, and 10.

Accuracy of the Method

In order to test the accuracy of the above method, calculations were made of the 4-ray resultant fields over a range of $v_0 \geq 1$ and $\Delta v/v_0 \leq 1$. These were compared with rigorous calculations using (2), (3), and (5). Fig. 7 shows the errors in the simplified method vs $\Delta v/v_0$ for various v_0's. Both Δv's were assumed equal in these comparisons; thus the errors in Fig. 7 are maximum errors to be expected.

If ± 2 db is regarded as a satisfactory limit of error, then the present method is applicable for $\Delta v/v_0 \leq 0.3$ and $v_0 \geq 1$. If one wishes to limit the error to ± 1 db, then $\Delta v/v_0$ must be less than 0.15. With either of these

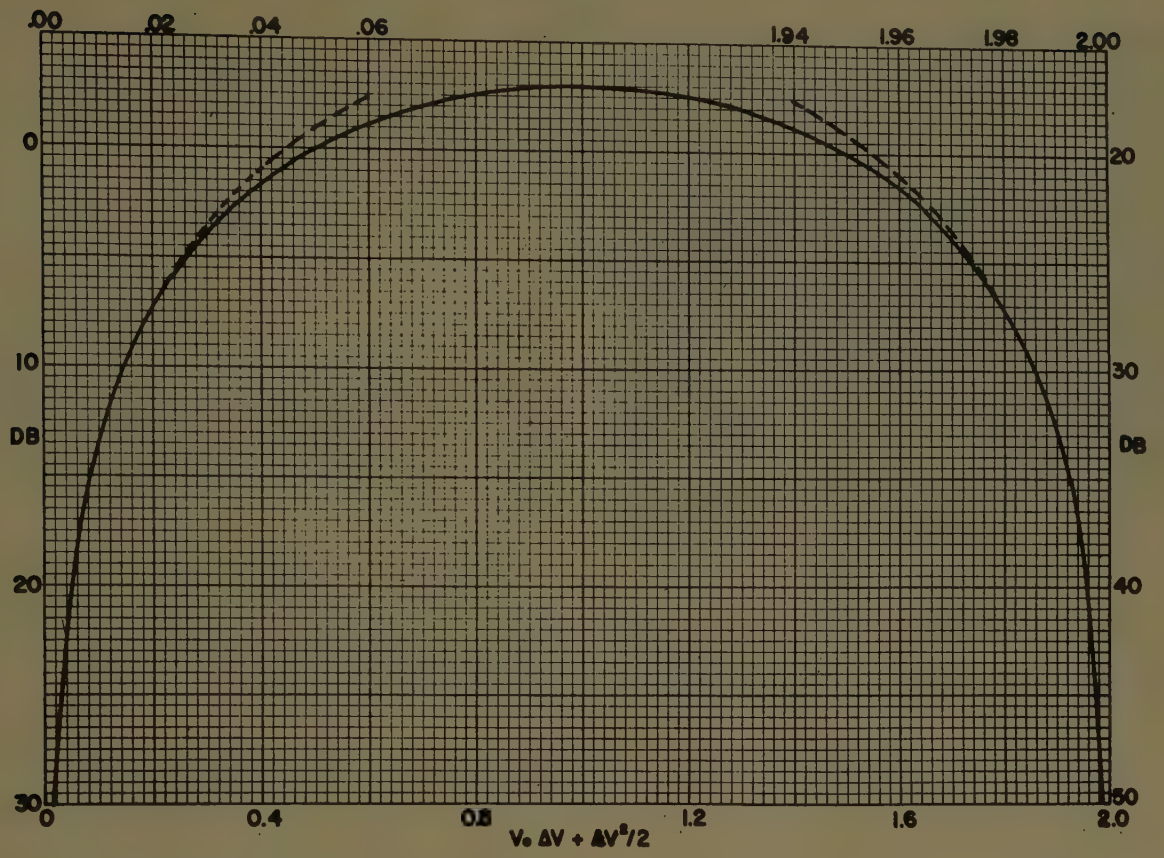

Fig. 5—$1-\cos \pi\Delta v(v_0+\Delta v/2)$ in db below unity. Dashed curves plotted against scales at top and right.

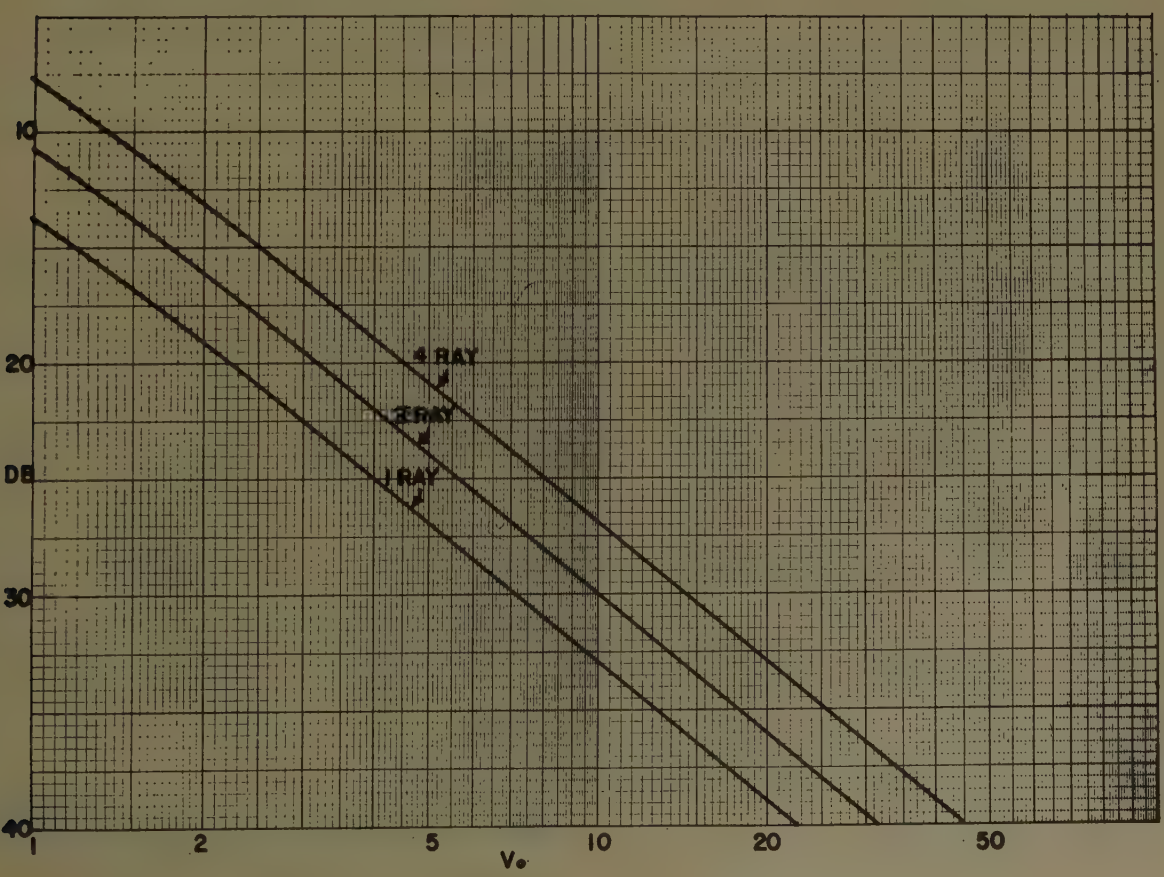

Fig. 6—Amplitude factors of resultant field vs v_0 for 4-ray, 2-ray, and 1-ray cases.

TABLE I

1	2	3	4	5	6	7	8	9	10	11
H_R ft	h_0 ft	v_0	Δv_2	Δv_1	$v_0\Delta v_2+\Delta v_2^2/2$	$v_0\Delta v_1+\Delta v_1^2/2$	db (v_0)	db (Δv_2)	db (Δv_1)	$\lvert E/E_0\rvert^2$
10	2556	11.8	0.090	0.016	1.07	0.19	28.4	−3.0	7.6	33.0
25	2547	11.7	0.090	0.041	1.06	0.48	28.4	−3.0	0.3	25.7
50	2531	11.7	0.091	0.082	1.06	0.96	28.3	−3.0	−3.0	22.3
75	2516	11.6	0.091	0.123	1.06	1.44	28.2	−3.0	−0.7	24.5
100	2500	11.5	0.092	0.166	1.05	1.96	28.1	−3.0	15.0	40.1

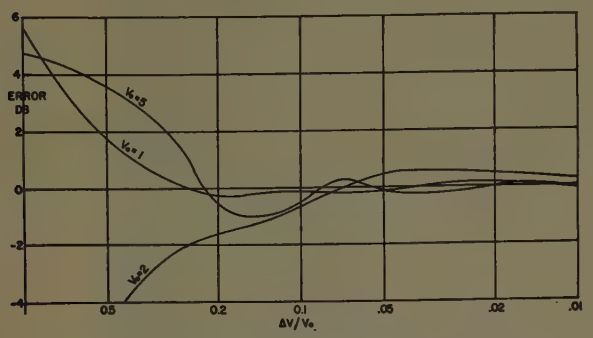

Fig. 7—Errors of simplified method vs $\Delta v/v_0$ for various v_0's.

limits most of the paths of practical interest are within the range of applicability. Inasmuch as accuracies of 1 or 2 db are normally adequate for obstacle gain computations, it appears that the reduction in time and effort, which the method affords, will make it very useful for such purposes.

Acknowledgment

The authors are grateful to Dr. G. E. Hudson for his helpful suggestions, and in particular for the asymptotic expressions for F and β.

Electromagnetic Noise and Propagation Observations in the Vicinity of a Nuclear Reactor*

W. W. FAIN†, C. M. CRAIN‡, AND W. C. DUESTERHOEFT§

Summary—**Electromagnetic noise and propagation measurements have been made in the vicinity of a nuclear reactor to determine whether reactor radiation would affect *X*-band and VHF signals. No radiation effects were observed. A 15-foot *X*-band propagation path was instrumented for observation of attenuation and phase changes. The over-all sensitivity was one part in 10^5 or 10 *N* units average over the path. Reactor radiation over the path was greater than 10^4 roentgen per hour. No significant phase or attenuation change was observed as reactor power level varied. A 12-db noise figure, 8-mc bandwidth, 18-inch dish antenna, X-band receiving system, and a 12-db noise figure, 4-mc bandwidth, tuned dipole antenna, 94-mc receiving system were pointed at the reactor from approximately 18 feet. No significant electromagnetic noise generated by reactor radiation was observed with these receiving systems.**

* Manuscript received by the PGAP, July 5, 1957; revised manuscript received, January 7, 1958. This research was performed under Wright Air Dev. Center, Contract AF 18(600)-113 and was presented at the First 125A ANP Radiation Effects Symposium, Convair, Fort Worth, Texas, May 22–23, 1957.

† Chance Vought Aircraft, Dallas, Texas; formerly with Elec. Eng. Res. Lab., University of Texas, Austin, Texas.

‡ Rand Corp., Santa Monica, Calif.; formerly with Elec. Eng. Res. Lab., Univ. of Texas, Austin, Texas.

§ Elec. Eng. Res. Lab., Univ. of Texas, Austin, Texas.

Introduction

AMONG the many problems created by the development of fission piles as energy sources for aircraft motive power is the possible change in dielectric constant of the atmosphere around the pile caused by pile radiation. A change in dielectric constant caused by the presence of large free electron densities could have significant effects on electromagnetic propagation in the vicinity of the reactor.

The presence of ions and electrons affects both the dielectric constant and conductivity of an ionized region. Since the mobility of the electron is much larger than that of an ion, the effect is primarily due to the free electron population. Where the conductivity is largely electronic, the dielectric constant and conductivity are given by[1]

[1] E. Everhart and S. C. Brown, "The admittance of high frequency gas discharges," *Phys. Rev.*, vol. 76, pp. 839–842; September, 1949.

$$\epsilon_r = 1 - \frac{Ne^2}{\epsilon_v m(\nu^2 + \omega^2)} \quad (1)$$

$$\sigma = \frac{Ne^2\nu}{m(\nu^2 + \omega^2)} \quad (2)$$

where

N = electron density
e = electron charge
m = electron mass
ϵ_v = permittivity of vacuum
ν = electron molecule collision frequency
ω = radian frequency of electromagnetic propagation.

The equilibrium free electron density in the vicinity of a reactor depends upon the rate at which ionization occurs in the atmosphere due to reactor radiation and the mechanisms by which the electrons are removed from the region; namely, attachment to oxygen molecules, recombination, and diffusion. Accurate prediction of the free electron density based on present knowledge and data of these mechanisms in a complex gas such as air is difficult.

Although general opinion held that the necessary shielding of the pile would reduce the dielectric constant change to an insignificant effect, the observations reported in this paper were made for verification. A concurrent series of direct microwave index of refraction measurements demonstrated no observable refractive index change for air that could be attributed to ionization effects.[2] These direct refractive index measurements were made in a closed cavity and were more sensitive by a factor of 10^3.

Description of Test Site

VHF and X-band noise and X-band phase and amplitude propagation measurements were made in the vicinity of the Convair reactor at Fort Worth in May, 1956. The reactor is located in the bottom of a 20- by 30-foot cross-section pit. Fig. 1 is a photograph of the pit showing the antennas as installed for the tests. Fig. 2 is a plan view showing the location of the antennas as well as reactor radiation level contours.

A series of phosphate glass totalizing dosimeters were located in a detailed grid surrounding the reactor at a height of 54 inches above the floor of the pit. Fig. 2 summarizes the results of the readings of these dosimeters by showing contours of the total gamma dose in roentgens for one hour of reactor operation at 100 kw. A continuously recording gamma-flux meter was used for correlation with the radio measurements.

[2] C. M. Crain, "Some Observations of the Effect of Radiation on Refractive Indices of Certain Gases," presented at the First 125A ANP Radiation Effects Symposium, Convair, Fort Worth, May 22–23, 1957. *J. Appl. Phys.*, to be published.

Fig. 1—Photograph showing the propagation and noise measuring antennas located around the Convair reactor. The small white elements are chemical dosimeters.

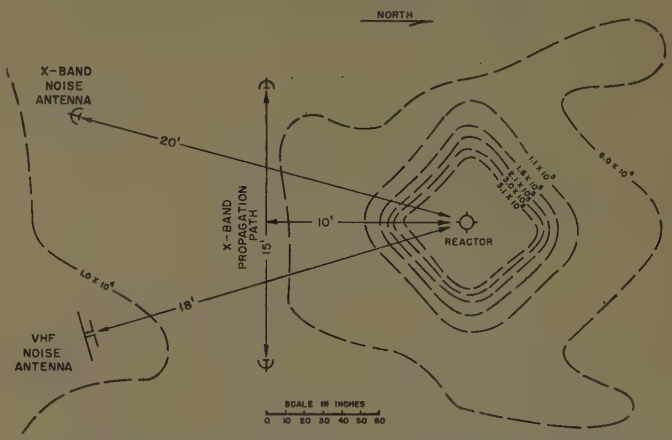

Fig. 2—Gamma integrated dose map for Convair reactor operating for one hour at 100 kw. Data expressed in roentgens contour interval 5×10^4 R.

X-Band Propagation Measurements

The X-band propagation measurements were made utilizing an interferometer technique. A signal sent along an air path adjacent to the reactor was compared with a signal transmitted along an equally long waveguide path removed from the ionizing atmosphere. The propagation path was between two dish antennas placed some 15 feet apart on a line 10 feet from the reactor center. Fig. 3 is a block diagram indicating the equipment used.

The magic tee divides the 9300-mc signal from the TS 120 signal generator into two equal components. Half of the energy is sent across the propagation path to the slotted line while the other half is supplied through an attenuator to the slotted line where a standing wave is produced. The attenuator was adjusted so that both signals had the same magnitude in the slotted line. The resulting standing wave is detected in the slotted line and sent to a pulse amplifier and recorder. Movement of the probe along the slotted line would result in a voltage at the recorder which varies as shown in Fig. 4.

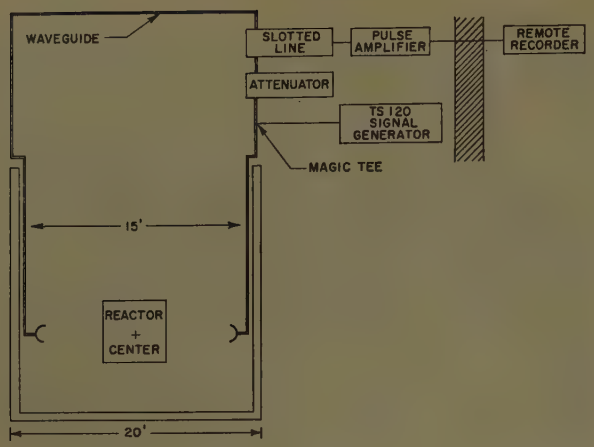

Fig. 3—Diagram of air path propagation measuring equipment.

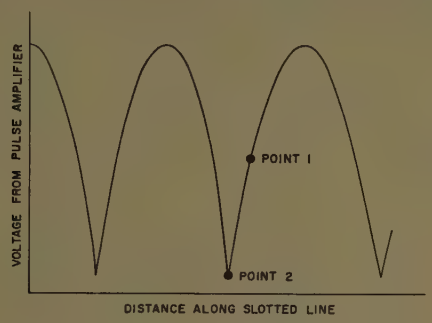

Fig. 4—Voltage variation along slotted line.

With the probe adjusted to read the voltage at point 1 on the curve of Fig. 4, a change in the propagation path would result in a phase shift which would produce a change in voltage. Similarly, attenuation changes would produce an increase in null amplitude at point 2. The sensitivity of the over-all system has been computed to be approximately one part in 10^5; that is, an index of refraction change along the entire propagation path of 10 N units would result in a one-division change at the recorder. Fig. 5 illustrates the slotted line output during the reactor-scramming operation. Curves for both positions of the probe are shown. No significant propagation changes were noted during scramming operation from 160-kw power level.

VHF and X-Band Noise Measurements

Passive antennas (see Fig. 1) feeding sensitive receivers were aimed at the reactor to determine if any significant microwave noise is generated by radiation from the reactor. The X-band receiver was connected to a dipole antenna with an 18-inch dish reflector. The receiver tuned to 9300 mc had a bandwidth of 8 mc and noise figure of approximately 12 db. Attenuation inserted between the antenna and receiver could be removed by remote control. A tuned dipole with a reflector was used as an antenna for the 94-mc test. The antenna was connected through a Wallman amplifier to an AN/APR-4 radar receiver having a bandwidth of 4 mc. The over-all noise figure of the amplifier and receiver was less than 12 db.

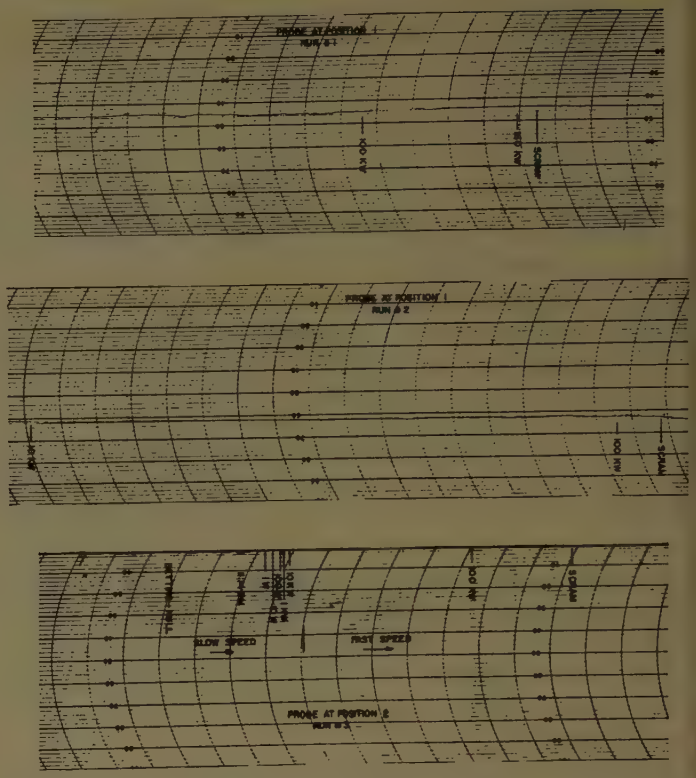

Fig. 5—Esterline-Angus recordings of X-band-air propagation test

The reactor was operated at several power levels up to 160 kw. No significant change in receiver noise level could be observed due to change in reactor power. No change was observed during reactor operations where the gamma dose rate decreased by a factor of nine in approximately one second.

Acknowledgment

The measurements reported here were carried out at the Convair Fort Worth Reactor Facility. The cooperation and assistance of Convair personnel in making their facility available and performing the radiation measurements is gratefully acknowledged.

The Correlation Between the Electric Field at a Great Distance and a New Radio-Meteorological Parameter*

PIERRE MISME†

Summary—**The daily variations of hourly median 1046-mc transmission loss, recorded over a 370-km propagation path, are found to be correlated with a new meteorological parameter that combines the thermodynamic stability of the atmosphere and the "useful gradient" of the radio refractive index. The thermodynamic stability is evaluated from the area contained between the observed temperature distribution with height and the pseudo-adiabatic temperature lapse, while the useful gradient of the refractive index is derived from ray tracing considerations, and is weighted towards the initial gradient.**

Introduction

FOR several years, numerous works have attempted to correlate the electric field beyond the horizon of the transmitter and the refractive index gradient[1–3] which are calculated from meteorological radiosoundings. These results can be summarized in the following fashion: The correlations between the monthly median values of the field and the refractive index gradient are in the neighborhood of unity, whereas the correlations between the instantaneous values of the field and the gradient are very small.

In the following work, we shall see whether it is possible to define a new radio-meteorological parameter which permits correlation, with an acceptable value, of the electric field beyond the horizon and this new parameter.

We should notice that the thermodynamic knowledge of the atmosphere during the duration of the radiosounding should explain the value of the measured electric field during the same period. Since the refractive index gradient does not allow us to obtain an acceptable correlation, we must admit that either the inertia of the measuring instrument is very great, or that the idea of gradient of index is insufficient. We shall study the results furnished by the experimental link of NBS which has the following characteristics:

Distance: 370 km[4]

Transmitter: 1046 mc—4 kw

Altitude of the transmitter: 697 m above the local terrain

Altitude of the receiver: 6 m above the local terrain

Station of radiosounding: Dodge City. Because of the proximity of this station, we can assume it represents the meteorological conditions prevailing over the path.

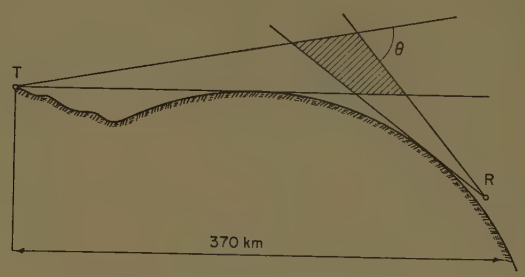

Fig. 1—Diagram of the experimental path.

The arrangement of this link is given in Fig. 1.

Whatever the mechanism of propagation that is accepted to explain the field strength at the receiver, R, a volume defined approximately by that part of the atmosphere common to the lobes of the two antennas should be particularly considered. In effect, the theories of scattering or those of partial reflections have shown the role played by this part of the atmosphere. For the same reasons, the variations of the angle θ should be considered. In the theories of scattering, the field received at R decreases rapidly when θ increases; in the theories of partial reflections, the coefficient of reflection follows a similar law. We notice, in general, that when θ is zero we have line-of-sight propagation in the radioelectrical sense of the word; that is, the field at R is maximum. (The accompanying phenomena of focusing[5] is neglected.) When θ increases, the receiver is farther into the zone of geometric shadow, and the field at R is weaker. But this angle θ for a given path is uniquely a function of the refractive index gradient.

* Manuscript received by the PGAP, January 2, 1958. The research contained in this report was done at the Natl. Bur. Stand., Boulder, Colo., under Purchase Requisition No. 83-0190. Translation by M. C. Thompson, Jr. and Ann Fails.

Author's Note: In this article the heights and the thicknesses have been measured either in millibars or in kilometers. The author, having stayed but a short time in the United States, had to use the data as rapidly as possible, which explains why levels in millibars were not converted to altitudes in kilometers. The author excuses himself to the reader.

† Engineer, French Meteorological Office, collaborating with the Centre National d'Etudes des Telecommunications, Paris, France.

[1] B. Bean and F. M. Meaney, "Some applications of the monthly median refractivity gradient in the tropospheric propagation," PROC. IRE, vol., 43, pp. 1419–1429; October, 1955.

[2] K. Tao, "Meteorological influences on the hourly median field strength of U. S. W. in the diffraction region," *J. Radio Res. Labs., Tokyo*, vol. 16, pp. 155–254; April, 1957.

[3] R. F. Dreyfus, P. J. Augier, L. J. Boithias, F. E. DuCastel, Mercier, and P. Misme, "Essais de propagation radioélectrique en ondes ultracourtes au Cameroun," *B. C. E. O. M. Paris*, February, 1957.

[4] *Translator's Note:* This is the Cheyenne Mountain-Garden City path of the Cheyenne Mountain Field Station.

[5] P. Rivet, "Etude de l'effet de focalisation sur des liaisons longues en visibilité," *Ondé Elect.*, vol. 346, pp. 23–31; January, 1956.

Idea of Useful Gradient

If the variation of the refractive index with the altitude is nonlinear, the gradient is not constant. Thus, it is useful to define the number that represents the refraction over the given path. Consider first a ray emitted from the transmitter and arriving at a certain point in the atmosphere, and second, a ray following a circular path, emitted from the same transmitter, in the same direction, and arriving at the same point. The effects due to the refraction will be the same for these two rays. The second ray follows a circular path completely defined by three conditions: position of the transmitter, angle of emission, and position of the receiver. This unique circular path defines a constant refractive index gradient. We will call this constant number "useful gradient."

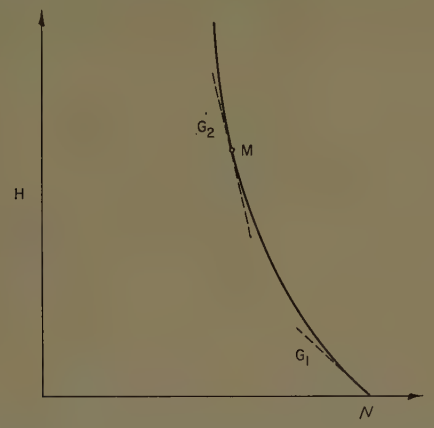

Fig. 2—Distribution of refractive index with altitude.

It can be shown[6] that if the variation of refractive index with altitude follows a law approximately parabolic (Fig. 2), and if M represents the index at the altitude at which we want to study a ray emitted from the ground level at a very small angle, the useful gradient G is given by

$$G = \frac{2G_1 + G_2}{3}$$

in which G_1 = gradient at the ground (that is, mean gradient in the lower layers), and G_2 = gradient at M.

To evaluate the effect of the refraction on the angle θ in the case of the link considered above, we will adopt the following conventions:

G_1 = difference of the value of the index between the 700-mb level and the surface. The 700-mb level is situated in the lower part of the common volume of the two antennas, and its altitude is of the order of 2000 m above the surface.

G_2 = gradient at 8000 m. This altitude corresponds to the upper part of the same volume.

Since the difference of altitude between the radiosonde station and 700 mb is approximately 2000 m, it will be sufficient to add G_1+G_2 to obtain three times the useful gradient.

Parameter of Stability

It appears that the idea of thermodynamic stability of the atmosphere plays an important part which is not given by the variations of the refractive index which are calculated from measurements made by the radiosoundings. We see this idea of stability on the line-of-sight links and know, in particular, that the afternoon fluctuations of the field are much more irregular than the night fluctuations. Since the instantaneous maxima depart little from the free-space attenuation, the irregular fields correspond less to the average hours than to the stable fields.

We may attempt to evaluate the stability of the atmosphere by the work which must be furnished to an elementary volume of air situated at the surface, to raise it to the 700-mb level. The stability at the interior of the common volume to the two antennas cannot be studied alone, for this stability is a function of the atmospheric conditions between the surface and the 700-mb level.

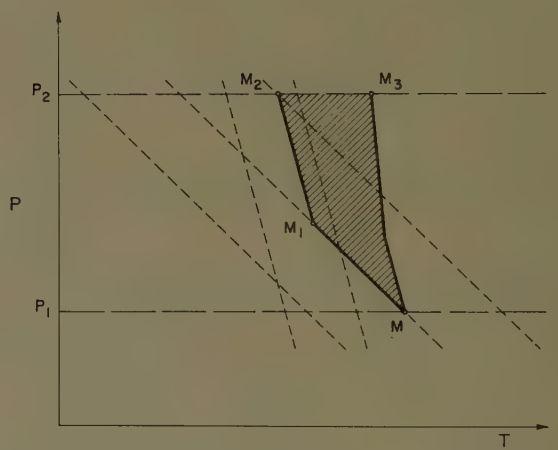

Fig. 3—MM_3 = measured pressure-temperature curve. MM_1M_2 = the adiabatic transformation raising an elementary volume from the level P_1 to the level P_2. The dotted curves correspond to the adiabatic and pseudoadiabatic curves. The same representation is used for following figures.

Let us consider a pressure-temperature diagram on which a network of adiabatic curves and a network of pseudoadiabatic curves have been traced (Fig. 3). Let MM_3 be the pressure-temperature curve measured. Let us raise an elementary volume situated at M to bring it to the level P_2. It undergoes an adiabatic expansion up to the level where, following the condensation of the water vapor contained in this volume, it becomes saturated. M_1 will be this point. To leave this level after

P. Misme and A. Perlat, "Erreurs d'altitudes dans la radiodétection des sondes, météorologiques," Communication to the Commission Internationale of Méthodes d'Observation, W. M. O., Paris, June, 1957.

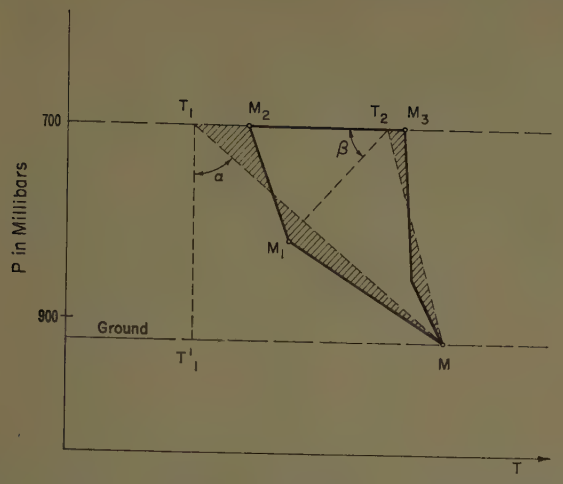

Fig. 4—Evaluation of the work necessary to raise an elementary volume from the surface to the 700-mb level.

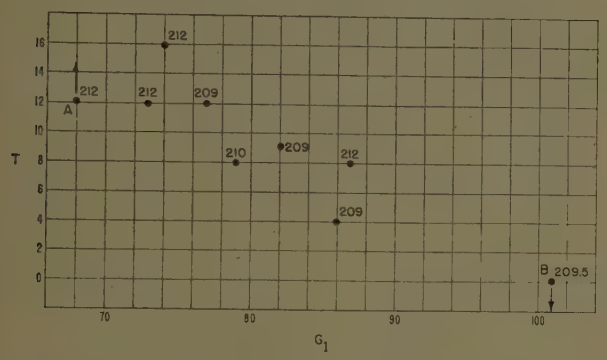

Fig. 5—Refractive index gradient as a function of the work of instability for nearly constant electric field intensities. Values of basic transmission loss are indicated beside the points. The arrows indicate the probable direction of the points A and B for slightly different values for the work of instability.

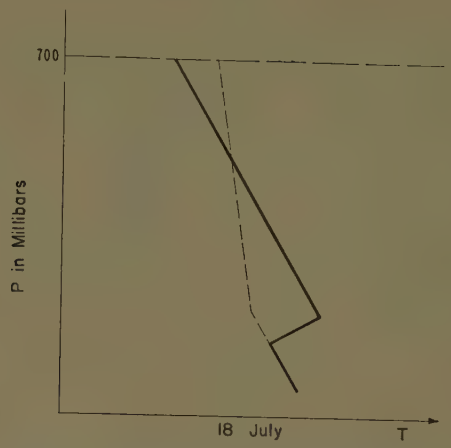

Fig. 6—Sounding of July 18 (point B).

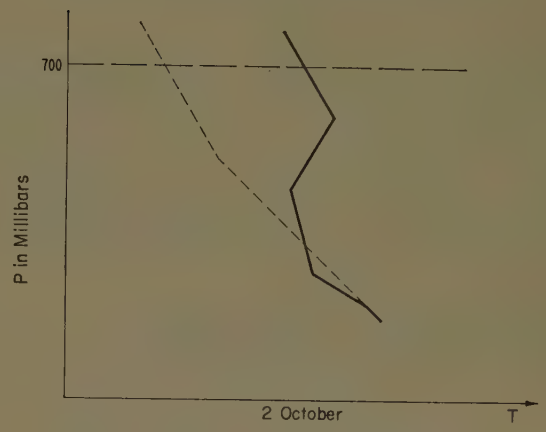

Fig. 7—Sounding of October 2 (point A).

the saturation, it follows the curve M_1M_2 which is called psuedo-adiabatic. The area $MM_1M_2M_3$ is proportional to the work which must be supplied to the volume to displace it from M to M_2. If the area is situated in the region of the diagram corresponding to temperatures lower than those of the curve MM_3, this work is positive; in the opposite case the work is negative. That is, the atmosphere is particularly unstable.

The area considered can be evaluated. Let MT_1 be a straight line dividing the parts of the curve MM_1M_2 into equal areas, and let MT_2 be the corresponding straight line for the curve MM_3 (Fig. 4). To achieve the required precision we can assume that on the pseudo-adiabatic diagram of the weather bureau the angles α and β are constants as well as the distance and surface—700 mb. Consequently the area will be proportional to the length T_1T_2 which can be evaluated in degrees. We shall call it T.

Let us now view some different meteorological conditions which resulted in essentially equal values of transmission loss: for example, 209 to 212 db. These values correspond to the median values for the link studied. In the plot of Fig. 5 a noticeable correlation between T and G_1 is perceived. This correlation suggests that for equal attenuations the parameter which best describes the atmosphere will not be G. Instead, it will be a function of the form $G+aT$ in which a is a coefficient which will be determined experimentally; its dimensions will be $M^{-1}L^{-3}T^2$. On Fig. 5, we notice that the points A and B correspond to the soundings of October 2 and July 18 (Figs. 6 and 7). Note that on the figures if a level slightly higher than 700 mb had been arbitrarily chosen, the values of T would have been very different, and the points A and B would have a position which could be estimated in the direction of the arrows.

Using the same representation for the strong fields (198 to 202 db), we find a similar correlation. On the other hand, for very weak fields (220 to 225 db), this correlation is much lower. It should be remembered that we admitted the instability of the lower layers could influence the instability in the common volume of the two antennas. Let us postulate that the stability is particularly great in the lower layers, resulting, for example, from a temperature inversion. The parameter chosen will not give a good evaluation of the instability (Fig. 8) since the low atmosphere has no influence at all at the higher altitudes. Then we are not led to consider the very low layers, and it seems logical to eliminate the

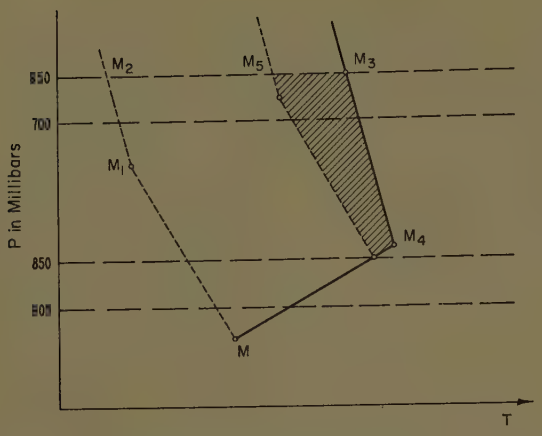

Fig. 8—Evaluation of the work of instability in the case of a temperature inversion at the surface.

first 500 meters, that is, to study the slab from 850 to 650 mb. Evidently, the other part of the mean gradient, surface—700 mb—can be preserved. A correlation as good as in the preceding cases is found. Consequently to represent the state of the atmosphere from the point of view of propagation beyond the horizon, the sum of the useful gradient and of a parameter of instability as defined above must be examined.

We have chosen experimentally the function G_M which we will call the modified gradient.[7]

$$G_M = G + T/2 \qquad (1)$$

where G=useful gradient and T=work of instability measured as indicated above. Fig. 9 represents the transmission loss as a function of the modified gradient.

Let us recall that the transmission losses are the mean values measured during the execution of the radiosoundings. That is, we have noted the mean over a period of two hours. The days during which the attenuation varied substantially near the hours when radiosoundings were taken have been avoided. On these days, it is possible that a front of discontinuity intersected the path, and the radiosounding was not considered representative of the mass of air situated on the transmitter-receiver path.

Thus it is perceived from Fig. 9 that the correlation between the modified gradient and the transmission loss is much higher than the gradient-attenuation correlation previously obtained. It seems then that it might be useful to consider a parameter of atmospheric instability and not just the mean gradient. Naturally, other parameters of instability can be studied. The present study represents only the first attempt.

Interpretation of the Results

1) If we admit that the correlation between the transmission loss and the modified gradient is good

[7] *Translator's Note:* This should not be confused with the parameter $M=[n+(h/a)-1]\times 10^6$ often called "refractive modulus."

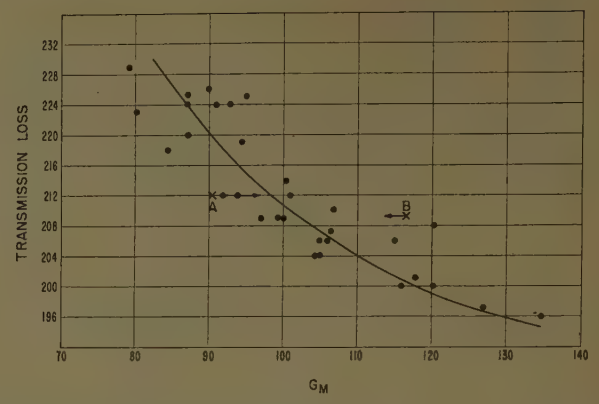

Fig. 9—Distribution of basic transmission loss as a function of the modified gradient (applicable to hourly values of transmission loss and to values of the modified gradient corresponding to the radiosounding made at the same time). Points *A* and *B* correspond to the same values as on Fig. 5. The values indicated in the abcissa correspond to three times the value of the gradient per kilometer.

enough for these two quantities to be functionally related, we are led to the following conclusion:

For equal refractive index gradients, the atmosphere which is characterized by the greatest stability permits the highest fields to be received from a great distance.

It would seem then that if thermodynamic stability resulted in a good atmospheric stratification, the contribution of the layers is particularly important in the mechanism of propagation at a great distance.

2) It is known that the mean values of the temperature-pressure curve deviate little from the adiabatic equilibrium of the atmosphere. From this fact the mean values of the work which we have considered in order to define stability are small and sensibly constant from one month to another. It is then normal that the monthly means of the attenuation and of the gradient of index would be well correlated.

Remarks

1) In (1), defining the modified gradient, the coefficient $\frac{1}{2}$ has been used for the work. It would appear from the curve T, G (Fig. 5) that this coefficient would vary with T. But we have not analyzed enough results to be able to affirm this. Consequently, it is probable that we will be guided to adopt a formula slightly different for the modified gradient.

2) In the above work, we have only taken into consideration the radiosoundings at 1500 hours, Universal Time (0800 hours MST). We know that the phenomena of radiation influence the measurement of temperature by radiosoundings. For this reason, we have preferred not to compare the results of daytime and nighttime measurements.

Acknowledgement

The author wishes to thank the National Bureau of Standards for kindly furnishing the information which permitted this study. In particular, he thanks his friend, B. Bean, whose advice has been most useful.

communications

Comparison of Some Experimental Terrain Diffraction Losses with Predictions Based on Rice's Theory for Diffraction by a Parabolic Cylinder*

J. H. CRYSDALE†

IN a recent paper which presented the results of an experimental investigation of the diffraction of electromagnetic waves by a dominating ridge to the north of Ottawa,[1] it was mentioned that consideration was given to the possibility of applying to these measurements Rice's theory of diffraction by a parabolic cylinder.[2] It was concluded that the approximate theory was not applicable because of the relatively large radius of curvature associated with the top of the ridge.[3] In addition, there was some doubt as to boundary conditions. Nevertheless, Rice has found that there is surprisingly good agreement between the experimental diffraction losses for both horizontal and vertical polarization, and the theoretical losses predicted by his approximate theory for horizontal polarization.[4] In this note, some of Rice's theoretical results are presented in modified form, the vertical profiles through the ridge are set forth in greater detail, and the experimental results are compared with predictions based on the approximate Rice theory.

As in Crysdale, *et al.*,[1] let L_D denote diffraction loss expressed in db. Then define L_K as the diffraction loss predicted by knife edge theory, and L_A as the loss in excess of L_K, *i.e.*:

$$L_A = L_D - L_K. \tag{1}$$

On the assumption that the angle of diffraction is sufficiently large for the asymptotic formula for the Fresnel integral to be valid, and also that this angle is suffi-

* Manuscript received by the PGAP, September 27, 1957.

† Defence Res. Telecommun. Establishment, Shirley Bay, Ottawa, Can.

[1] J. H. Crysdale, J. W. B. Day, W. S. Cook, M. E. Psutka and P. E. Robillard, "An experimental investigation of the diffraction of electromagnetic waves by a dominating ridge," IRE TRANS. ON ANTENNAS AND PROPAGATION, vol. AP-5, pp. 203–210; April, 1957.

[2] S. O. Rice, "Diffraction of plane radio waves by a parabolic cylinder," *Bell Sys. Tech. J.*, vol. 33, pp. 417–504; March, 1954.

[3] The assumption $rh^{-2} \gg 1$ associated with (2.10) of Rice, *ibid.*, (see pp. 424–425) is not satisfied. Assuming an effective radius of curvature of 10 miles at the apex of the ridge, approximate values of rh^{-2} are as follows:

	RPL-Farm Point	*RPL-Farrellton*
173 mc	0.000027	0.000046
493	0.0000093	0.000016
1785	0.0000026	0.0000044

(It can be verified that the other two assumptions given on p. 425 are satisfied by the parameters of the experimental circuits.)

[4] S. O. Rice, Bell Telephone Labs., Inc., 463 West St., New York 14, N. Y., personal communication, April 15, 1957. (In the exchange of correspondence which followed, it was agreed that the material would be published as presented in this note.)

ciently small for the approximation $\sin\psi \approx \psi$ to hold, it can be verified that Rice's (2.10) predicts that:[5]

$$L_A \approx -20\log_{10}\left|1+\tau\Psi(\tau)\right|, \qquad (2)$$

where τ and $\Psi(\tau)$ are as defined by Rice. Fig. 1 is a graph of L_A for horizontal polarization, assuming (2) for a range of the parameter τ.[6] For purposes of calculation, it is convenient to express τ in the approximate form:

$$\tau \approx -4.86\times 10^{-4}H\left(\frac{1}{d_1}+\frac{1}{d_2}\right)(\eta f)^{1/3}, \qquad (3)$$

where H is the effective height of the obstruction in feet,[7] d_1 and d_2 are the distances from the terminals to the obstruction in miles, η is the radius of curvature at the apex expressed in miles, and f is the frequency in mc.

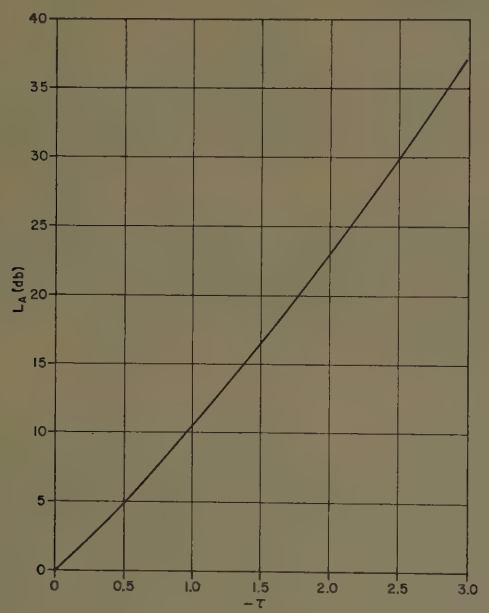

Fig. 1—Loss in excess of knife edge loss predicted by Rice's approximate theory for horizontal polarization.

Detailed vertical profiles through the ridge, based on 1:50,000 topographical sheets, are presented in Figs. 2 and 3.[8] For each circuit, profiles are shown for the vertical planes which contain the terminals and also for vertical planes 600 feet to the east and 600 feet to the west. (The lengths of the first Fresnel zones on the top of the ridge are given in Table I of Crysdale, *et al.*[1]) The solid circles, open circles, and triangles represent the points at which the contour lines are crossed. As the contouring is at intervals of 50 feet, it is evident that the profiles are somewhat arbitrary, particularly in the vicinity of the top of the ridge. Parabolas with radii of curvature at their apices of 10 and 20 miles are superimposed on the profiles. Fig. 2 suggests that the radius of curvature for the RPL-Farm Point circuit is probably of this order. Whether or not an effective radius of curvature can be defined in the case of the RPL-Farrellton circuit is conjectural.

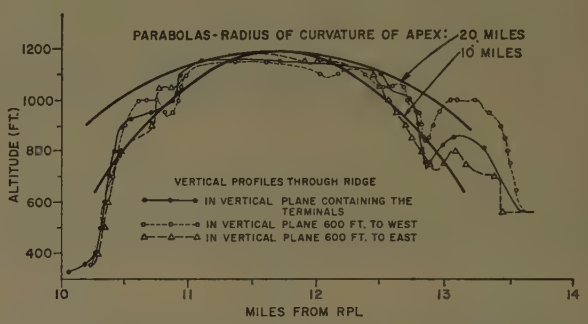

Fig. 2—Detailed vertical profile of ridge for the RPL-Farm Point circuit.

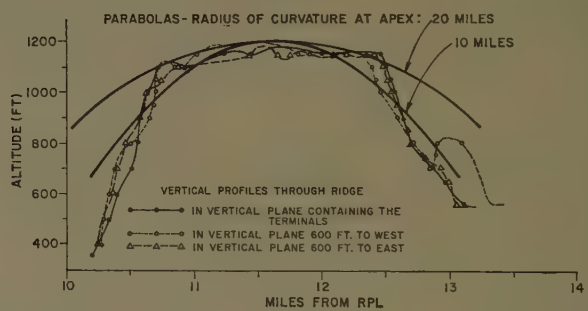

Fig. 3—Detailed vertical profile of ridge for the RPL-Farrellton circuit.

The experimental results and theoretical predictions based on Rice's approximate theory are compared in Figs. 4 and 5. The experimental results are taken from Table II of Crysdale *et al.*[1] The theoretical curves are based on Fig. 1 of this paper.

From an examination of Figs. 4 and 5, it is clear that Rice's approximate theory for horizontal polarization provides a more accurate prediction of the diffraction loss than does the simple knife edge theory.[9] However,

[5] This result is contained in (2.22) of Rice, reference 2, ($\psi<0$). Division of the first factor by τ, and multiplication of the second factor by τ (noting that $\tau=h^{1/3}\psi$) yields:

$$\left|E\right| \approx \left|\frac{c(\rho)}{\psi}\right|\left|1+\tau\Psi(\tau)\right|.$$

The first factor in this expression is the asymptotic value of $|E|$ predicted by knife edge theory. (It can be verified that the parameters of the experimental circuits are such that the restrictions with respect to angle of diffraction are satisfied.)

[6] This graph is based on Fig. (2.5) of Rice, reference 2, and some additional data kindly supplied by Rice.

[7] Crysdale, *et al.*, *op. cit.*, see Figs. 2 and 3.

[8] The profiles are based on the 31 G/5 West Half and the 32 G/12 West Half 1:50,000 sheets published by the Army Survey Establishment, Dept. of Natl. Defence, Ottawa, Can.

[9] For the parameters assumed, the values of τ are such that, except for the RPL-Farm Point circuit at 1785 mc and $\eta=20$ miles. Rice's approximate theory for vertical polarization actually predicts diffraction losses less than the values predicted by knife edge theory. (See Fig. 2.5 of reference 2.) (It seems more logical to use the horizontal polarization case since this corresponds to a reflection coefficient of -1, the value approached by the reflection coefficients of physical materials at grazing incidence.)

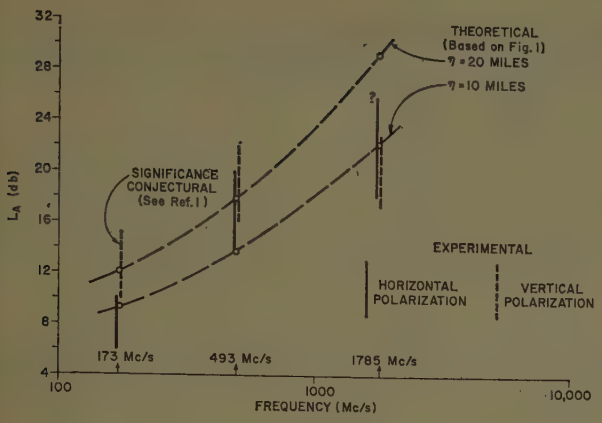

Fig. 4—Comparison of theory and experiment for the RPL-Farm Point circuit.

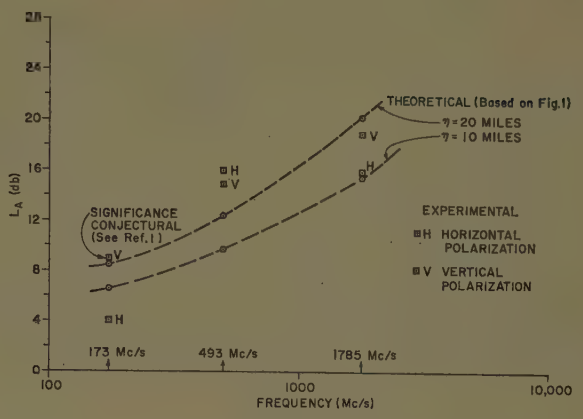

Fig. 5—Comparison of theory and experiment for the RPL-Farrellton circuit.

it is possible that this phenomenon is purely fortuitous. Nevertheless, it would appear that a theoretical investigation into the possibility of relaxation of the $rh^{-2} \gg 1$ condition would be worthwhile. In addition, experimental results for similar obstructed circuits should be compared with the predictions of the approximate theory.

The writer wishes to acknowledge a stimulating exchange of correspondence with S. O. Rice.

The Equivalence of Electric and Magnetic Sources*

PAUL E. MAYES†

THE convenience of introducing nonphysical magnetic current sources into electromagnetic analysis has long been recognized. The distributions of electric currents which yield the same fields are well-known for some elementary magnetic current sources, *e.g.*, a small current loop is equivalent to a magnetic dipole. The derivation of a general equivalence relation is quite simple and the application to various problems of propagation in waveguides is quite useful.

The Equivalence Equations

Consider electric and magnetic vectors $\overline{E}_1$ and $\overline{H}_1$ to be generated by an electric current described by the current density vector $\overline{J}$. $\overline{E}_1$ and $\overline{H}_1$ are then the particular solutions of

$$\text{curl } \overline{H}_1 = Y\overline{E}_1 + \overline{J} \tag{1}$$

$$\text{curl } \overline{E}_1 = -Z\overline{H}_1 \tag{2}$$

where $Y = \sigma + j\omega\epsilon$, $Z = j\omega\mu$ for steady-state sinusoidal conditions (σ = conductivity, ϵ = permittivity, μ = permeability, $\omega = 2\pi \times$ frequency, $e^{j\omega t}$ time dependence). Similarly, $\overline{E}_2$ and $\overline{H}_2$ are generated by a magnetic current described by the current density vector $\overline{K}$.

$$\text{curl } \overline{H}_2 = Y\overline{E}_2, \tag{3}$$

$$\text{curl } \overline{E}_2 = -Z\overline{H}_2 - \overline{K}. \tag{4}$$

Subtracting (3) from (1), and (4) from (2) yields

$$\text{curl } (\overline{H}_1 - \overline{H}_2) = Y(\overline{E}_1 - \overline{E}_2) + \overline{J}, \tag{5}$$

$$\text{curl } (\overline{E}_1 - \overline{E}_2) = -Z(\overline{H}_1 - \overline{H}_2) + \overline{K}. \tag{6}$$

Taking the curl of (5) and substituting from (6)

$$\text{curl curl } (\overline{H}_1 - \overline{H}_2) + \gamma^2(\overline{H}_1 - \overline{H}_2) = Y\overline{K} + \text{curl } \overline{J} \tag{7}$$

where $\gamma^2 = ZY$. Eq. (7) is now a second-order nonhomogeneous differential equation for the difference field, $\overline{H}_1 - \overline{H}_2$. Hence, if the source term on the right vanishes, the field likewise vanishes. That is not to say that the homogeneous equation corresponding to (7) has only a zero solution, but rather that the particular solution of (7), which represents the fields generated by the *given* source, must vanish when there is no source. Therefore, $\overline{H}_1 = \overline{H}_2$ everywhere when $Y\overline{K} + \text{curl } \overline{J} = 0$. Then, from (5)

$$0 = Y(\overline{E}_1 - \overline{E}_2) + \overline{J}, \tag{8}$$

so that the electric vectors $\overline{E}_1$ and $\overline{E}_2$ are likewise identical everywhere *outside* the region of the source $\overline{J}$ providing

* Manuscript received by the PGAP, November 18, 1957.
† University of Illinois, Urbana, Ill.

$$\overline{K} = -\frac{1}{Y}\operatorname{curl}\overline{J}. \tag{9}$$

In the same way, proceeding from (6)

$$\operatorname{curl}\operatorname{curl}(\overline{E}_1 - \overline{E}_2) + \gamma^2(\overline{E}_1 - \overline{E}_2) = -Z\overline{J} + \operatorname{curl}\overline{K} \tag{10}$$

and $\overline{E}_1 = \overline{E}_2$ in (6) yields

$$0 = -Z(\overline{H}_1 - \overline{H}_2) + \overline{K}, \tag{11}$$

so that the fields outside a magnetic current source distribution can be determined from an equivalent electric current distribution given by

$$\overline{J} = \frac{1}{Z}\operatorname{curl}\overline{K}. \tag{12}$$

Simple Examples

Suppose the magnetic current is distributed uniformly over an infinite plane

$$\overline{K} = \hat{z}K_{zs}\delta(x) \tag{13}$$

where $\hat{z}$ is a unit vector in the z direction, K_{zs} is the linear density of the magnetic surface current and $\delta(x)$ is the Dirac delta. Applying (12) to this magnetic current distribution yields

$$\overline{J} = -\hat{y}\frac{K_{zs}}{Z}\delta'(x), \tag{14}$$

so the magnetic current sheet is equivalent to a double electric current sheet of equal but opposite currents.

If the magnetic current is distributed uniformly along a line (the z axis)

$$\overline{K} = \hat{z}M\delta(x)\delta(y) \tag{15}$$

where M is the magnetic current. Again applying (12)

$$\overline{J} = \frac{M}{Z}[\hat{x}\delta(x)\delta'(y) - \hat{y}\delta'(x)\delta(y)] \tag{16}$$

which is a solenoid of electric current of small cross section along the z axis.

A point source of the magnetic current type (magnetic dipole) has the form

$$\overline{K} = \hat{z}Ml\delta(x)\delta(y)\delta(z) \tag{17}$$

where Ml is the magnetic dipole moment.

From (12) the equivalent electric current is

$$\overline{J} = \frac{Ml}{Z}\delta(z)[\hat{x}\delta(x)\delta'(y) - \hat{y}\delta'(x)\delta(y)] \tag{18}$$

which is a small loop of electric current.

Changing Normal Currents to Tangential Currents

Usually the problem of determining the fields generated by an arbitrary volume-source distribution can be obtained by superposing the results for surface distributions. The fields of surface distributions are more easily obtained for currents which are tangential to the surface. If the given source-vector field has normal components, then it is desirable to convert these to equivalent tangential sources.

Converting normal source currents to tangential ones may be accomplished easily by applying (9) and (12). For example, suppose an electric current is arbitrarily distributed over the xy plane but is normal to it.

$$\overline{J} = \hat{z}J_{zs}(x, y)\delta(z) \tag{19}$$

where J_{zs} is the surface-current density. Then, by (9), the equivalent magnetic current is

$$\overline{K} = -\frac{1}{Y}[\hat{z} \times \operatorname{grad} J_{zs}(x, y)]\delta(z) \tag{20}$$

which is tangent to the plane. Similarly, for an electric current on, and normal to, the sphere $r = a$

$$\overline{J} = \hat{r}J_{rs}(\theta, \phi)\delta(r - a) \tag{21}$$

and the equivalent magnetic current is

$$\overline{K} = \frac{1}{Y}[\hat{r} \times \operatorname{grad} J_{rs}(\theta, \phi)]\delta(r - a). \tag{22}$$

For the coordinate surface $u_1 = u_1^0$ of the orthogonal system u_1, u_2, u_3, if

$$\overline{J} = \hat{u}_1 J_{1s}(u_2, u_3)\delta(u_1 - u_1^0), \tag{23}$$

then

$$\overline{K} = \frac{1}{Y}[\hat{u}_1 \times \operatorname{grad} J_{1s}(u_2, u_3)]\delta(u_1 - u_1^0). \tag{24}$$

Even though the derivation of equivalence was made in an infinite, homogeneous medium, application of the equivalence is still valid for inhomogeneities in the medium outside of the source distribution. Equivalence of the incident fields (no inhomogeneity) guarantees equivalence of the total field (incident plus scattered) outside of the source. Hence application can be made of (9) and (12) to sources in the presence of any exterior scatterer and to sources interior to waveguides.

In cylindrical waveguides, for example, a distribution of transverse electric currents on a cross-sectional plane is analogous to constant current generators at the same point on equivalent transmission lines. The longitudinal behavior of the voltage and current on each line is the same as for the transverse components of electric and magnetic fields of the corresponding propagating mode in the waveguide. Similarly, a distribution of transverse magnetic currents on a cross-sectional plane is represented by constant voltage generators in the equivalent lines. Hence, a longitudinal electric current, transformable by (24) into a transverse magnetic current, is represented by constant voltage generators; and a longitudinal magnetic current, by constant current generators. Similar arguments apply in spherical coordinates for the propagation of waves between coaxial cones.

The Effect of the Size of a Two-Dimensional Array on Second-Order Beams*

G. C. McCORMICK†

TWO-DIMENSIONAL arrays in which the elements have a separation approximately $\lambda_0/2$ naturally generate second-order beams. The first comprehensive analysis of this problem was published by Kurtz and Yee.[1] Recently another treatment of the effect, from a somewhat different point of view, has appeared.[2] Two of the points raised by Kurtz and Yee are as follows:

1) that parallel-element arrays of shunt slots have no second-order beams provided the beamwidths are sufficiently narrow and that there is no lateral scan;
2) that in mirror-image element arrays second-order beams can be suppressed by reducing the array spacing.

In each case the size of the array is clearly involved. It is the purpose of the present note to express this dependence quantitatively.

It will be useful to have some arbitrary level in mind at which second-order beams can be considered "suppressed." It is suggested that at 30 db down with respect to the main beam the suppression must be regarded as incomplete, while from the point of view of manufacturing tolerances anything better than 40 db may be impractical. That is, second-order beams will require consideration if their amplitude exceeds 3 per cent, and they may require suppression to the 1 per cent level.

The formulas used here were previously derived by the author.[2,3] Since they refer specifically only to nonscanning arrays of mirror-image elements, the necessary modification to a scanning array and to parallel elements will be made. For a lateral scan produced by a phase shift of γ radians between rows of longitudinal slots, V_2 is given by

$$V_2(x, y) = V_1(x, y)\delta(x, y) \sec\left(\frac{\gamma\delta}{d}\right). \tag{1}$$

For parallel element arrays f_2 should be replaced by f_3 where

$$f_3 = \sum_i (-1)^q V_2(x_i, y_i) \cdot \exp\left[-ik(x_i \sin\theta \sin\phi + y_i \cos\theta)\right] \tag{2}$$

and $(-1)^q$ changes sign when the offset or inclination angle changes sign; that is, in going from one element to an adjacent element longitudinally, but not laterally. f_2 may be visualized typically as a four-pronged pattern, the lobes lying near the plane of the array. f_3 is a two-pronged pattern, the lobes lying in the plane of the main beam.

With the modifications noted, (2-21)[3] and (2-22)[2] are applicable. Thus for parallel-element longitudinal slots the amplitude of the second-order beams is given by

$$s(\theta, \phi) = \frac{2\pi}{\lambda} \frac{\sin\phi \cos u f_3}{\sum_i V_i}. \tag{3}$$

For an array without lateral taper,

$$s(\theta', \phi) = s_0 \frac{\sin\phi \sin\left(\frac{\pi\sigma M}{\lambda} \sin\theta' \sin\phi\right)}{M \sin\left(\frac{\pi\sigma}{\lambda} \sin\theta' \sin\phi\right)} \tag{4}$$

where

$$s_0 = \frac{2\pi}{\lambda} \cos u \frac{\sum V_2(x_i, y_i)}{\sum V_1(x_i, y_i)}.$$

s has its maximum value, obtained by differentiating (4), near

$$\sin\phi = \frac{\lambda}{2M\sigma \sin\theta'}. \tag{5}$$

This gives a maximum value of the second-order beams,

$$s_{\max} = \frac{\lambda}{\pi M\sigma \sin\theta'} s_0. \tag{6}$$

A lateral taper leads to a beam broadening which can be specified by the factor K where normally $1 < K < 1.5$. The taper to be used is that of the aperture function V_2, not V_1. Then,

$$s_{\max} = \frac{\lambda K}{\pi M\sigma \sin\theta'} s_0. \tag{7}$$

Substitution of numerical values gives as a typical result,

$$s_{\max} \approx \frac{0.1K}{M}. \tag{8}$$

It can be concluded that second-order beams will be reduced to the 30-db level for an array four elements wide.

* Manuscript received by the PGAP, December 12, 1957.
† Radio and Elec. Eng. Div., Natl. Res. Council, Ottawa, Can.
[1] L. A. Kurtz and J. S. Yee, "Second-order beams of two-dimensional slot arrays," IRE TRANS. ON ANTENNAS AND PROPAGATION, vol. AP-5, pp. 356–362; October, 1957.
[2] G. C. McCormick, "A two-dimensional slotted array," IRE TRANS. ON ANTENNAS AND PROPAGATION, vol. AP-6, pp. 26–35; January, 1958.
[3] In quoting equations of reference 2, the prefix "2" will be used; thus, (2-21).

Of somewhat greater interest is point 2) above, which will be treated differently. In this case the maxima of the second-order beams can be expected to occur near the plane of the array. The minimum adjacent to these maxima will occur at some angle above the plane of the array determined by the beamwidth of the second-order beams, which in turn depends on the size of the array. Such a minimum, in the notation of McCormick,[2] should occur at

$$\frac{\pi M\sigma}{R\lambda}(X - X_0') = -K\pi \tag{9}$$

where

$$\frac{X}{R} = \sin\theta\sin\phi, \qquad \frac{X_0'}{R} = \pm\frac{\gamma\lambda}{2\pi\sigma} \pm \frac{\lambda}{2\sigma}$$

and K is the factor which takes account of beam widening due to the X-direction taper of f_2. Then

$$\frac{\sigma}{\lambda}\sin\theta'\sin\phi \mp \frac{\gamma}{2\pi} \mp \frac{1}{2} = -\frac{K}{M}.$$

For suppression it will be supposed that the minimum lies in or beyond the plane of the array; that is, $\sin\phi \geq 1$. Therefore,

$$\frac{\sigma}{\lambda}\sin\theta' \leq \frac{1}{2} - \frac{\gamma}{2\pi} - \frac{K}{M} \tag{10}$$

or,

$$\cos\theta' \geq \sqrt{1 - \left(\frac{\lambda}{2\sigma}\right)^2\left(1 - \frac{\gamma}{\pi} - \frac{2K}{M}\right)^2}.$$

It will be assumed that the array region is loaded to reduce the guide wavelength, the extent of the loading being specified by an effective dielectric constant ϵ_{eff}. Then,

$$\left(\frac{\lambda}{\lambda_g}\right)^2 = \epsilon_{eff} - \frac{\lambda^2}{4a^2}$$

and using (2-24),[2] for forward second-order beams,

$$\epsilon_{eff} \geq \frac{\lambda^2}{4a^2} + 1 - \left(\frac{\lambda}{2\sigma}\right)^2\left(1 - \frac{\gamma}{\pi} - \frac{2K}{M}\right)^2. \tag{11}$$

For backward second-order beams,

$$\epsilon_{eff} \geq \frac{\lambda^2}{4a^2} + \left(\frac{d}{\lambda_g - d}\right)^2 \cdot\left[1 - \left(\frac{\lambda}{2\sigma}\right)^2\left(1 - \frac{\gamma}{\pi} - \frac{2K}{M}\right)^2\right]. \tag{12}$$

If $d < \lambda_g/2$, (11) suffices for all beams. It will be noted that for the array of the other paper of the author[2] where $a = \sigma$ and $\gamma = 0$, to sufficient accuracy,

$$\epsilon_{eff} \geq 1 + \frac{K}{M}\frac{\lambda^2}{\sigma^2}. \tag{13}$$

It is clearly necessary from (11) that $\epsilon_{eff} > 1$. Nevertheless, if M is reasonably large, a practicable degree of loading should permit the realization of a modest scan angle.

Some Observations on Scattering by Turbulent Inhomogeneities*

S. STEIN†

THE above paper[1] by Balser describes the great utility of the dyadic Green's Function for formally setting up integral equations for the electromagnetic field, especially where, as in the scatter hypothesis, useful first-approximation solutions can be directly obtained and the nature of the approximations put in evidence. It is unfortunate that this otherwise excellent presentation is marred by some incorrect mathematical statements, in particular, statements that the electric field, E, in an inhomogeneous space cannot be directly represented in terms of the dyadic Green's Function. Certain consequent discussions found necessary by the author overcomplicate the presentation unnecessarily.

In point of fact, however, it must be pointed out that the free-space dyadic Green's Function (using Balser's notation) is indeed

$$\Gamma(r, r') = \left(\varepsilon - \frac{1}{k_0^2}\nabla\nabla'\right)\frac{e^{ik_0|r-r|}}{4\pi|r-r|},$$

but that this is a solution to the vector wave equation[2]

$$\nabla \times \nabla \times \Gamma - k_0^2\Gamma = \varepsilon\delta(r - r')$$

rather than to the $(\nabla^2+k_0^2)$ form appearing as (6) of the paper.

It is then immediately obvious that

$$\nabla\cdot\Gamma(r, r') = -\frac{1}{k_0^2}\nabla\cdot[\varepsilon\delta(r - r')]$$

and hence is not identically zero, as claimed in the paper. It is, in fact, physically obvious that $\nabla\cdot\Gamma$ should not vanish identically, since Γ is after all just the electric field due to a point source of current and hence is without divergence only at all points *other than* the source point.

Further, the wave equation for E in an inhomogeneous current-free space can be written, as in Balser's (4), as

$$\nabla \times \nabla \times E - k_0^2 E = k_0^2\frac{\Delta\epsilon}{\epsilon_0}E,$$

in which the right-hand side is mathematically completely equivalent to a distribution of currents in otherwise homogeneous empty space. Thus the principle of superposition can be expected to hold. Indeed, upon application of the "vector Green's theorem,"[2] and the use of appropriate limitations upon field behavior at infinity, it is possible to arrive rather directly at the correct result [contrast to Balser's equation following his (7)]:

$$E_{sc}(r) = E(r) - E_{inc}(r) = \int \Gamma(r, r')\cdot\left[k_0^2\frac{\Delta\epsilon(r')}{\epsilon_0}E(r')\right]dr'.$$

The second term of Balser's expression, it may be noted, is completely absent here. It may be shown also, using the correct relation given earlier for $\nabla\cdot\Gamma$, that the above equation gives correctly

$$\nabla\cdot E_{sc} = -\nabla\cdot\left[\frac{\Delta\epsilon}{\epsilon_0}E\right]$$

as required, and contrary of course to the statement in the paper. It may also be noted that the correct form of the function $F(r)$ introduced in (8) of the paper is therefore exactly

$$F(r) = -\epsilon\left[k_0^2\frac{\Delta\epsilon}{\epsilon_0}E\right].$$

The author goes to much pains, following his (17) and the Appendix, to prove this last statement, but obtains it in such a way that it appears to be limited to the Fraunhofer approximation. This is patently not so, of course.

Because of these mathematical oversights the implication is given in the paper that some artfulness is necessary to correctly apply the dyadic Green's Function. This implication detracts considerably in the present case from the real utility of the dyadic Green's Function. Based on previous work in this direction, it seems likely to us that the "jungle" which presently exists in tropospheric propagation theory (scatter, normal mode theory, rough earth effects, diffraction by obstacles, etc.) is likely to be resolved systematically only through the use of a comprehensive formalism such as the dyadic Green's Function introduces. For example, there is no need to rely on the free-space Green's Function, and ignore completely the presence of the earth, as Balser does. One might very well introduce the effects of the earth sphere by constructing a dyadic Green's Function from the results of the well-known airless-earth diffraction theory. Perhaps one could even use these modifications to account for the standard atmosphere.

By introducing successive perturbations into such a basic model, it seems hopeful that the dyadic Green's Function formalism can yield new understanding of many of the "nonstandard" effects and their interrelation.

* Manuscript received by the PGAP, January 24, 1958.
† Hycon Eastern, Inc., Cambridge, Mass.
[1] M. Balser, IRE TRANSACTIONS ON ANTENNAS AND PROPAGATION, vol. AP-5, pp. 383–390; October, 1957.
[2] H. Levine and J. Schwinger, "On the theory of electromagnetic wave diffraction by an aperture, etc." in "Theory of Electromagnetic Waves" (Symposium), Interscience Publishers, New York, N. Y.; 1951.

Scalar-Vector Analog of Green's Theorem*

H. UNZ†

IN ADDITION to the Green's theorem and the vector analog of Green's theorem,[1] there exists a scalar-vector analog of Green's theorem, which gives similar relation between a vector function and a scalar function and is especially suitable for solving vector boundary value problems in terms of scalar Green's Functions.

The scalar-vector analog of Green's theorem may be stated as follows: Let V be a closed region of space bounded by a regular closed surface S and let $\overline{F}$ be a vector function of position and ψ a scalar function of position, which together with their first and second derivatives are continuous throughout V and on the surface S. Then the theorem is stated by

$$\int_V [\psi\overline{\nabla}\times\overline{\nabla}\times\overline{F}+\overline{F}\overline{\nabla}^2\psi-(\overline{F}\cdot\overline{\nabla})\overline{\nabla}\psi]dV = \oiint_S [\bar{n}\times(\overline{\nabla}\times\overline{F})\psi+(\bar{n}\times\overline{F})\times\overline{\nabla}\psi]dS, \quad (1)$$

where n is the outward directed normal unit vector. Eq. (1) may be written in a symbolic form, which is closer to the form of the original Green's theorem:

$$\int_V [\psi\cdot\overline{\nabla}\times\overline{\nabla}\times\overline{F}-\overline{F}\cdot\overline{\nabla}\times\overline{\nabla}\times\psi]dV = \oiint_S \bar{n}\times[\psi\overline{\nabla}\times\overline{F}+\overline{F}\times\overline{\nabla}\psi]dS, \quad (2)$$

where we take the symbolic notation

$$\overline{\nabla}\times\overline{\nabla} = \overline{\nabla\nabla}\cdot - \overline{\nabla}^2, \quad (3)$$

and where a dot product with a scalar is defined as a simple multiplication.

To prove (1) let us use the following vector identities:

$$\overline{\nabla}\times(\psi\overline{\nabla}\times\overline{F}) = \overline{\nabla\psi}\times(\overline{\nabla}\times\overline{F})+\psi\overline{\nabla}\times\overline{\nabla}\times\overline{F}, \quad (4)$$

$$\overline{\nabla}(\overline{\nabla\psi}\cdot\overline{F}) = (\overline{\nabla\psi}\cdot\overline{\nabla})\overline{F}+(\overline{F}\cdot\overline{\nabla})\overline{\nabla\psi}+\overline{\nabla\psi}\times(\overline{\nabla}\times\overline{F}). \quad (5)$$

From (4) and (5) we obtain

$$\psi\overline{\nabla}\times\overline{\nabla}\times\overline{F}-(\overline{F}\cdot\overline{\nabla})\overline{\nabla\psi} = \overline{\nabla}\times(\psi\overline{\nabla}\times\overline{F})-\overline{\nabla}(\overline{\nabla\psi}\cdot\overline{F})+(\overline{\nabla\psi}\cdot\overline{\nabla})\overline{F}. \quad (6)$$

From (6) we obtain

$$\int_V [\psi\overline{\nabla}\times\overline{\nabla}\times\overline{F}-(\overline{F}\cdot\overline{\nabla})\overline{\nabla\psi}+\overline{F}\overline{\nabla}^2\psi]dV = \int_V \overline{\nabla}\times(\psi\overline{\nabla}\times\overline{F})dV-\int_V \overline{\nabla}(\overline{\nabla\psi}\cdot\overline{F})dV+\int_V [(\overline{\nabla\psi}\cdot\overline{\nabla})\overline{F}+(\overline{\nabla}\cdot\overline{\nabla\psi})\overline{F}]dV. \quad (7)$$

Giving the vector identities:

$$\int_V \overline{\nabla}\times\overline{A}dV = \iint_S \bar{n}\times\overline{A}dS, \quad (8)$$

$$\int_V \overline{\nabla}\phi dV = \oiint_S \phi\bar{n}dS, \quad (9)$$

$$\int_V [(\overline{\nabla}\cdot\overline{A})\overline{B}+(\overline{A}\cdot\overline{\nabla})\overline{B}]dV = \oiint_S (\bar{n}\cdot\overline{A})\overline{B}dS, \quad (10)$$

identity (10), which usually is not found in vector analysis texts, may be proved by equating components.

Using (8)–(10) we can transform (7) into

$$\int_V [\psi\overline{\nabla}\times\overline{\nabla}\times\overline{F})-(\overline{F}\cdot\overline{\nabla})\overline{\nabla\psi}+\overline{F}\overline{\nabla}^2\psi]dV = \oiint_S \bar{n}\times(\psi\overline{\nabla}\times\overline{F})dS-\oiint_S (\overline{\nabla\psi}\cdot\overline{F})\bar{n}dS+\oiint_S (\bar{n}\cdot\overline{\nabla\psi})\overline{F}dS. \quad (11)$$

By vector identity

$$(\bar{n}\times\overline{F})\times\overline{\nabla\psi} = (\overline{\nabla\psi}\cdot\bar{n})\overline{F}-(\overline{\nabla\psi}\cdot\overline{F})\bar{n}. \quad (12)$$

Therefore we see that (11) may be transformed directly into (1).

The scalar-vector analog of Green's theorem in (1) may be modified, by using (10), into the form:

$$\int_V [\psi\overline{\nabla}\times\overline{\nabla}\times\overline{F}+\overline{F}\overline{\nabla}^2\psi+(\overline{\nabla}\cdot\overline{F})\overline{\nabla\psi}]dV = \iint_S [\psi\bar{n}\times(\nabla\times\overline{F})+(\bar{n}\times\overline{F})\times\overline{\nabla\psi}+(\bar{n}\cdot\overline{F})\overline{\nabla\psi}]dS. \quad (13)$$

Once we have proved the scalar-vector analog of Green's theorem, any solution of vector-boundary value problem in terms of scalar Green's Function (ψ) may be simplified. For example, it may be applied to vector potential,[2] electromagnetic fields[3] and similar vector boundary value problems.

* Manuscript received by the PGAP, September 30, 1957. This paper originally appeared in a Ph.D. Dissertation at the University of California, Berkeley, Calif.; November, 1956.

† Dept. Elec. Eng., University of Kansas, Lawrence, Kan.

[1] J. A. Stratton, "Electromagnetic Theory," McGraw-Hill Book Co., Inc., New York, N. Y., p. 250; 1941.

[2] *Ibid.*, pp. 250–252.

[3] S. Silver, "Microwave Antenna, Theory and Design," M.I.T. Rad. Lab. Ser., McGraw-Hill Book Co., Inc., New York, N. Y., no. 12, pp. 80–83; 1949.

Radiation Patterns of a Spherical Luneberg Lens with Simple Feeds*

ROBERT E. WEBSTER†

THE theory and practical design of spherical Luneberg lenses with index of refraction varying as $[2-(r/a)^2]^{1/2}$, where r is the radial distance and a is the radius of the sphere, have been based on the assumption of an idealized "point-source" feed on the focal surface.[1,2] Such a feed is, of course, unattainable in the strict sense, but fields sufficiently close to the ideal to yield satisfactory radiation patterns and gains have been obtained with practical feeds. The experimental results presented here show quantitatively the correlation between theoretical performance and feed conditions for four simple feed types:

1) Open-end waveguide,
2) Resonant slot in narrow waveguide wall,
3) Exponentially tapered horn,
4) Horn-lens combination.

In agreement with the optical approach, the condition most important to the Luneberg lens performance is found to be the feed phase-center location with respect to the focal surface.

Measurements

Measurements were made with an 18-inch diameter, ten-step styrofoam lens at 16.65 kmc; the projected aperture was thus a 25.4λ diameter circle. With uniform illumination, this aperture would yield 2.3 degrees HPBW and a 38 db gain (relative to an isotropic radiator). Gain measurements were made with feed no. 1 to check the over-all system performance. A 32-db gain and a 2.5-degree HPBW were obtained, the differences being explained by the tapered illumination and imperfect focusing of the limited-step lens. Measurements of the near fields for this feed (open-end K_u-band waveguide) alone showed that its effective phase centers were nearly coincident with the lens' focal surface ($\frac{1}{4}$ inch outside the physical surface) when the waveguide aperture was in contact with the lens.

Radiation patterns (linear plots of electric field intensity) are shown in Fig. 1 for the open-end waveguide alone and in combination with the Luneberg lens. E-plane patterns are given as functions of the radial position of the feed aperture. Gain and pattern degradations are observed when the feed phase centers are appreciably displaced from the focal surface.

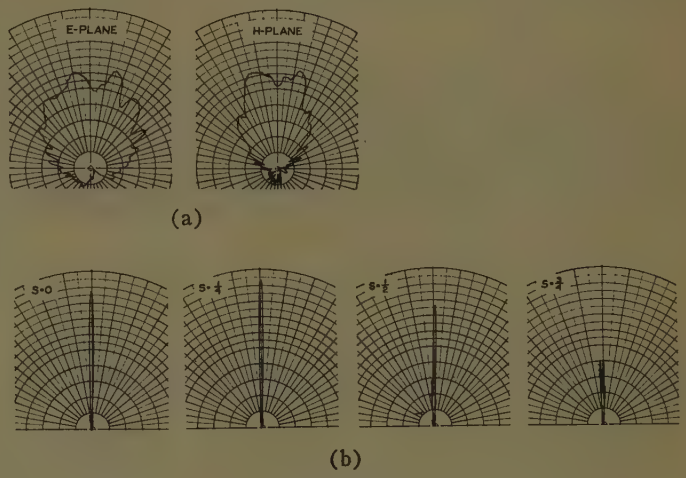

Fig. 1—Radiation patterns (electric field intensities) of an 18-inch-diameter spherical Luneberg lens and open-end K_u-band waveguide feed. Frequency = 16.65 kmc, s = spacing (inches) from lens to feed aperture. (a) Feed patterns, (b) lens E-plane patterns.

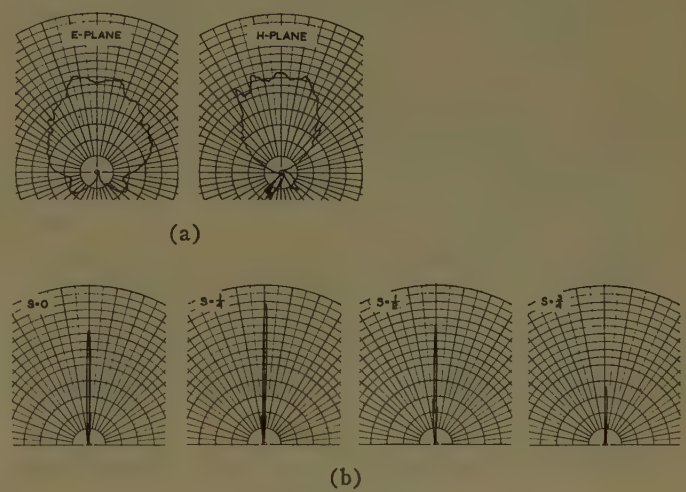

Fig. 2—Radiation patterns of an 18-inch-diameter spherical Luneberg lens fed by a resonant slot in the narrow wall of K_u-band waveguide. Frequency = 16.65 kmc, s = spacing (inches) from lens to feed aperture. (a) Feed patterns, (b) lens E-plane patterns.

Similar results with feed no. 2 (half-wave slot in the narrow wall of K_u-band waveguide) are shown in Fig. 2. Near-field measurements of this feed also established the location of its effective phase centers 0.1 to 0.5 inch inside the slotted waveguide.

Feed no. 3 was an exponentially tapered horn 5.0λ long with an aperture 2.8λ by 2.1λ. Measured effective phase centers for this feed occurred inside the horn approximately 2.1 inches (E plane) and 1.3 inches (H plane) from the aperture. Both amplitude and phase distributions of this field deviate considerably from the ideal, and large degradations in gain and beamwidth

* Manuscript received by the PGAP, February 21, 1958.
† Eng. Specialist, Electronic Dev. Group, North American Aviation Inc., Columbus, Ohio.
[1] R. K. Luneberg, "Mathematical Theory of Optics," Brown University Press, Providence, R. I., pp. 189–212; 1944.
[2] G. D. M. Peeler and H. P. Coleman, "Microwave Stepped-Index Luneberg Lenses," IRE Transactions on Antennas and Propagation, vol. AP-6, pp. 202–207; April, 1958.

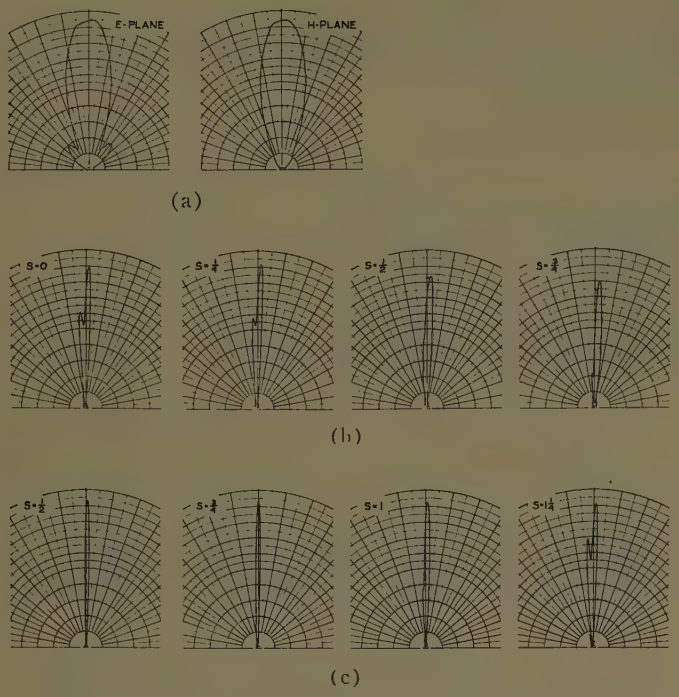

Fig. 3—Radiation patterns of an 18-inch-diameter spherical Luneberg lens fed by horn and horn-lens feeds. Frequency = 16.65 kmc, s = spacing (inches) from Luneberg lens to feed aperture. (a) Horn feed patterns, (b) lens E-plane patterns with feed horn, (c) lens E-plane patterns with horn-lens feed. Normalized gains.

result. The measured gain of the lens excited in this manner (horn aperture in contact with lens) was 26 db. Patterns are shown in Fig. 3.

A small dielectric lens was then designed to correct the horn's aperture-field distribution. The resulting horn-lens combination exhibited effective phase centers 0.1 to 0.4 inch in front of its aperture. The resulting patterns of the Luneberg lens with this feed are shown in Fig. 3(c). Performance comparable with that of feeds no. 1 and no. 2 is noted when the phase centers are near the focal surface.

Calculations

The experimental data were corroborated by calculations based on a geometrical optics formulation. Radiation patterns were evaluated on a digital computer for the 25.4λ diameter Luneberg lens fed by idealized point sources. Patterns and gains as functions of feed-point displacement radially from the focal surface were obtained. Fig. 4 shows the calculated main beams, first sidelobes, and a plot of gain degradation.

The large differences between results for displacements inside and outside the focal surface arise from different assumptions of feed-amplitude distributions. The point sources were considered as a fixed number of rays corresponding to the number of square wavelengths contained in a circle with a diameter 20 per cent greater than that of the lens. These rays were assumed to be of equal amplitude and were distributed at each displacement to intersect equal areas on a conical sector. This

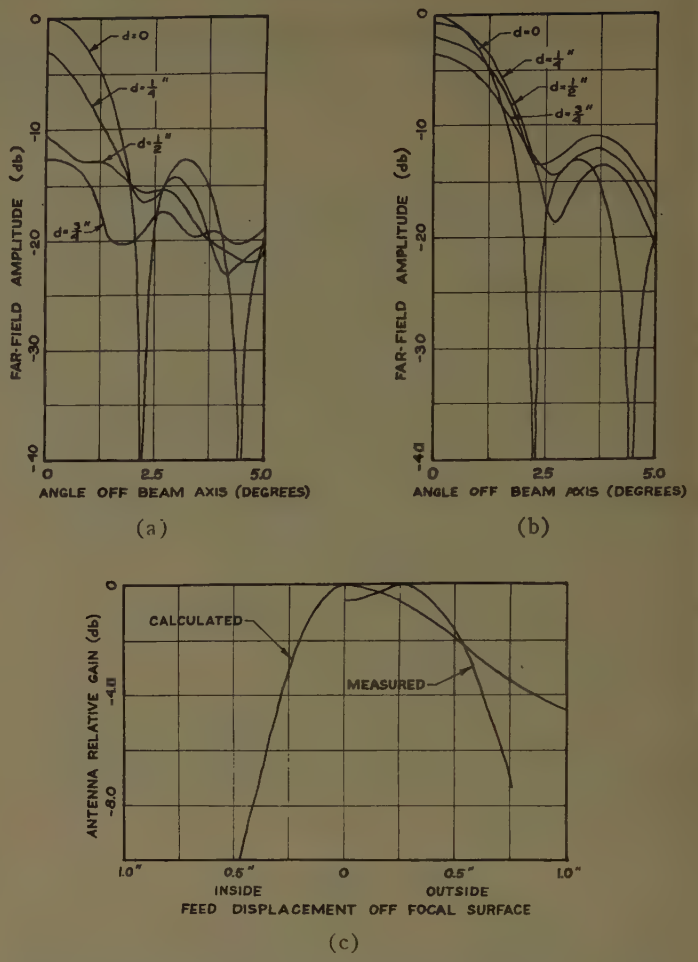

Fig. 4—Calculated radiation patterns and gains of an 18-inch-diameter spherical Luneberg lens fed by idealized point sources. Frequency = 16.65 kmc, d = displacement of sources from the focal surface. (a) Source inside focal surface, (b) source outside focal surface, (c) calculated and measured gains.

cone was established by tangents to the lens from the feed point for feed displacements outside the sphere, but was fixed as a hemisphere for displacements inside the focal surface.

The differences between these idealized feeds and the more tapered measured feed patterns, which were fixed as their spacings were varied, limited the correlation of measurements and calculations. The beamwidth and rates of sidelobe deterioration are nevertheless comparable, as are the calculated and measured gains (for the open-end waveguide feed) shown in Fig. 4(c). The calculated data for sources outside the lens indicate that gain degradation could be minimized at the larger feed displacements by simply sharpening the feed beam. Note, however, that increased sidelobes and filled-in nulls occur for all feed excursions from the focal surface.

Acknowledgment

The author is indebted to R. V. DeVore, R. E. Blake, L. W. Strobel, L. G. DeConnick, E. C. Clutter, R. J. Bailey, and C. Drinkle for their assistance in obtaining and processing these data.

Abstracts of Papers from the IRE-URSI Symposium Held April 23-26, 1958—Washington, D.C.

Lyman-Alpha Radiation as a Source of Nighttime *E*-Region Ionization—H. Friedman, J. E. Kupperian, Jr., and T. A. Chubb, *U. S. Naval Research Laboratory*—A directional survey of night sky ultraviolet radiation was made from an Aerobee rocket (NRL-31, March 28, 1957, at 2200 M.S.T.) using photon clunters and ionization chambers sensitive in the 1050-A to 1350-A spectral range. Most of the observed flux could be attributed to solar Lyman-Alpha radiation resonantly scattered from neutral hydrogen outside the earth's shadow. The flux from above the rocket at a height of 120 km was almost uniformly distributed over the entire hemisphere and amounted to 3.2×10^{-3} erg/cm²/sec/steradian. In addition, 1.4×10^{-3} erg/cm²/sec/steradian was observed in radiation backscattered from the atmosphere below the rocket.

Lyman Alpha may contribute to the nighttime *E* region by ionizing molecules of nitric oxide and atoms of Na, Cl, Ca, Mg, Fe, and Si of meteoritic origin. Using estimates of the nitric oxide concentrations which are based on the theory of formation of daytime *D* region and a recombination coefficient between 10^{-7} and 10^{-8} cm²/sec, it appears that ionization of nitric oxide by Lyman Alpha makes a minor contribution to nighttime *E* region. The action of Lyman Alpha on meteor atoms, however, may produce an ionization rate comparable to that attributed to meteor trails.

A Meteorological Interpretation of Wavelength Dependence in Transhorizon Propagation—R. Bolgiano, Jr., *Cornell University*—Contrary to available theories, each of which predicts a unique wavelength dependence for transhorizon propagation, recent radio data show rather definitely that this dependence varies widely in time, ranging from a first to a third power relation for the interval 400–2000 mc on a particular circuit. Meteorological conditions along the path have been analyzed for a number of cases in an attempt to discern the cause of these variations. In addition, a theoretical explanation has been sought, taking account of the stable density stratification which normally characterizes the atmosphere and which is the underlying cause of the typically pancake-like, anisotropic refractive index deviations noted lately by several investigators. A theory of the structure of homogeneous turbulence in stratified media has been deduced and incorporated in a model describing the turbulent mixing of an index gradient. This leads to predictions of the variation in wavelength dependence with meteorological conditions that appear to be borne out.

Instrumentation for High-Altitude Geomagnetic Measurements—J. P. Heppner and L. H. Meredith, *U. S. Naval Research, Laboratory*—The earth's magnetic field above White Sands Proving Grounds, N. M. and Fort Churchill, Can. has been measured with Varian proton precessional magnetometers carried in Aerobee-Hi rockets for the purpose of studying ionospheric currents. A Project Vanguard Satellite has been instrumented with a transistorized proton magnetometer to be flown primarily for determining the existence of a ring current during magnetic storms and for main field description. Magnetic stations have been established at nine of the Minitrack stations. The station magnetometers are proton instruments which have been adapted to measure the vector field as well as the absolute scalar field. The instrumental techniques employed in the above will be described. Results of a WSPG firing will be given. Results of at least one flight through an aurora at Fort Churchill will be shown if analysis is sufficiently complete by the time of presentation.

Earth to moon vehicles will, in the future, present opportunities for measurements of the earth's field at great distances, permanent ring currents, interplanetary fields, and the moon's magnetic field. Magnetometers of the alkali-vapor type now being developed by Varian Associates should permit absolute measurements of these weak fields. These possibilities will be briefly reviewed.

The Role of Radar in Space Research—B. S. Yaplee, *U. S. Naval Research Laboratory*—Radar echoes have been used to study the moon, the ionosphere, meteors, and the aurora. With the advent of high-power radars, large antennas, masers, and paramagnetic amplifiers, it is now becoming feasible to radar the planets, Venus and Mars, and the sun. The radar method will permit precise distance measurements to the moon, the planets and the sun; and thus, a more accurate value for the astronomical unit of distance can be determined. Radar studies of the sun's corona should yield information about ionized gases in the solar atmosphere. Using various radar frequencies, the reflection spectrum of the moon and planets; and the ionization gradient of the sun can be studied.

The Interpretation of High-Frequency Signal Strength Records from a Missile*—S. A. Bowhill, *Ionosphere Research Laboratory, Pennsylvania State University*—Some time ago, a long-range Jupiter C missile was launched by the Army Ballistic Missile Agency from the Air Force Missile Test Center at Cape Canaveral, Fla. It travelled over a range of more than 4000 km, and attained a height of more than 1000 km. A 108-mc transmitter was carried, developed by the Jet Propulsion Laboratories of the California Institute of Technology.

Records of signal strength at the launching site show distinctive sinusoidal fluctuations in amplitude, with varying period. It is suggested that these are due to the Faraday rotation effect. A method of reduction of these records to an electron-density-height profile is indicated, and preliminary results are given.

Radar Echoes Obtained from Earth Satellites 1957 Alpha and 1957 Beta*—A. M. Peterson, R. L. Leadabrand, R. B. Dyce, L. T. Dolphin, and R. I. Presnell, *Stanford Research Institute*—Radar echoes from Russian earth satellites, 1957 Alpha and 1957 Beta, have been obtained on radars located at Stanford, Calif., and College, Alaska. The fading rates of the radar signals and their polarization changes have been obtained. These data are interpreted in terms of satellite spin and Faraday rotation by the ionosphere.

Ionospheric Measurements Using Spaced-Receiver Doppler Observations of Earth Satellite Radio Transmission†—W. J. Ross, *Ionosphere Research Laboratory, The Pennsylvania State University*—An experiment is described whereby the radio transmissions from earth satellites may be used to measure integrated electron density along the slant path from the receiver to the satellite. Spaced stations recording received frequency and relaying this information to a master recording station make a precise knowledge of true transmitted frequency unnecessary and if two transmitted frequencies can be observed then the orbit need not be known to a high degree of accuracy. With transmissions at about 20 mc and 40 mc (not necessarily harmonic or very stable in frequency) and a baseline of about 300 km it is expected to measure electron content to an absolute accuracy of about 10^{12} electrons /cm².

Interferometric Studies of Satellite Radio Signals—R. S. Lawrence, *National Bureau of Standards, Boulder Laboratories*, J. W. Warwick, *High Altitude Observatory, University of Colorado*, and E. R. Schiffmacher, *National Bureau of Standards, Boulder Laboratories*—Details are presented of a digital method for determination of satellite orbital parameters from a single passage through the lobes of a simple interferometer. Such an analysis is a necessary preliminary to studies of ionospheric effects on, for example, the angle of arrival of satellite radio signals.

As would be expected, the observed effects are greater for the 20-mc signal than for the 40-mc signal, and increase towards the

* The research described in this paper has been supported by the Army Ballistic Missile Agency under Contract DA-36-061-ORD-577.

* This work was sponsored by Rome Air Dev. Center of the Air Res. and Dev. Command under contract AF 30(602)-1762.

† This work is supported by a grant from the National Committee for the IGY under project 32.44. Acknowledgment is made of the cooperation of the University of Virginia and Ohio State University in providing receiver sites and other assistance. Acknowledgments are due also to Dr. S. A. Bowhill whose initial suggestion of a spaced receiver experiment led to the setting up of this program.

horizon. Furthermore, the refraction varies rapidly in localized ragions of the sky, in which patchy or wavy distributions of electrons may be present.

Finally, the peculiar advantage of a satellite is noted so far as measurements of the instantaneous state of the ionosphere are concerned. This feature appears to be a unique property of a satellite experiment.

Experimental Measurement of Electron Density in the Ionosphere Using Earth Satellite Radio Emissions—P. R. Arendt and H. P. Hutchinson, *U.S. Army Signal Engineering Laboratories*—This paper discusses the relationship of well-known ionospheric propagation effects caused by the polarization of the radiated CW waves through a dispersive medium with new effects caused by the velocity of a satellite and its time relationship to the constancy of ionization throughout the wave path from the satellite transmitter to the ground observer. By the introduction of a new and interesting concept, a differentially frozen ionosphere, it is possible to develop functional relationships between the short-time variations seen on signal amplitude recordings of these CW emissions with the ion density in the upper atmosphere and the radial velocity of the satellite along the path from satellite to ground observer. Furthermore, if data from two or more frequencies of emission are simultaneously available and the transmission paths to the observer can be assumed to be the same, then a simple relationship is derived for calculating the electron density in terms of the observed fading periods. Examples are given from recordings of Sputnik $\alpha 1957$ satellite which confirm the above hypothesis and allow these records to be read in an unambiguous manner.

Lunar Echo Investigations at Stanford, California, and College, Alaska*—L. T. Dolphin, R. I. Presnell, R. B. Dyce, M. R. Berg, R. L. Leadabrand and A. M. Peterson, *Stanford Research Institute*—Lunar radio echoes have been studied at Stanford on a frequency of 106.1 mc and at College, Alaska, at 398 mc. Polarization and fading rate data have been obtained.

At Stanford the rapid amplitude fluctuations have been studied at three receivers spaced a few kilometers apart.

Propagation of Electromagnetic Waves Through the Ionosphere into Cutter Space—W. Loreck, *The Martin Co., Denver, Colo.*—The ionosphere is idealized as a plane layer of a homogeneous and isotropic medium with a complex dielectric constant and a real permeability. The propagation of a ray through this layer is considered, which is incident at an arbitrary angle, and an expression is established for the transmission efficiency. This efficiency can be written as the product of the reflection effectivity at the boundaries of the ionosphere and of the propagation efficiency inside of it. For a sufficiently small electron density, the complex dielectric constant is computed as a function of the frequency, the temperature, the mean path length of the electrons, and of its variability with the temperature. The expression obtained for the dielectric constant is substituted in a formula for the efficiency which is studied as a function of the frequency with the other variables as parameters. Formulas are given for the optimum frequency and for the corresponding maximum efficiency. Numerical examples are computed for some specific ionospheric data.

A Swept-Lobe Interferometer at 515 Megacycles*—R. Fleischer and W. Redlich, *Observatory of Rensselaer Polytechnic Institute*, and R. Keevers, *Bell Telephone Laboratories*—A swept-lobe interferometer has been constructed at the Sampson Station of the Rensselaer Observatory, primarily to detect the motions across the line of sight of solar outbursts at 515 mc. The phase-sweeping is done electronically, at rates adjustable from 0 to 50 kc, by a method similar to the Armstrong method of frequency modulation. The amount of phase sweep is similarly adjustable, from zero (drift interferometer) to approximately 720°.

The Output Fluctuations of Radiometers—G. F. Mansur, *Collins Radio Co., Cedar Rapids, Iowa*—The theory of output fluctuations of a radiometer is extended to include the case of sinusoidal power modulation as well as square wave modulation for linear detection. The derivation of the temperature fluctuation is generalized to permit the modulating element to assume a temperature different from that of the receiver.

Based on mean squared error criteria, an equivalent white noise power spectrum is obtained for the fluctuations at the detector output to allow modern filter theory to be applied to the smoothing problem. Relative performance of several higher order filters is discussed.

The Prediction of Geomagnetic and Ionospheric Disturbances—T. R. Hartz, *Radio Physics Laboratory, Defence Research Board, Ottawa, Can.*—Some of the basic ideas on solar-terrestrial relations are examined in order to highlight the role played by solar particles. A system is outlined for predicing under what conditions and with what time delay particles ejected from the sun can reach the earth. Data for a two year period are examined to show the reliability of the system.

Evidence of the First, Second, and Third Harmonics of a Solar Radio Burst and a New Class of Dynamic Solar Spectrum—F. T. Haddock and M. Winsnes, *University of Michigan*—The sun has been observed at the University of Michigan since August 28 with a dynamic spectrometer. It consists of a 28-foot antenna and three receivers. Each receiver sweeps almost over an octave, giving complete coverage of the 100- to 600-mc frequency band every 0.3 second. Each receiver output is displayed as an intensity modulated line on a cathode-ray tube. This is photographed on a slowly moving (1 cm/sec) 35-mm film, producing a frequency-time record with solar intensity appearing as variations in photographic density. The combination of the film characteristic and the *logarithmic* response of the receivers permits the recording of a wide range of signal intensities in considerable detail.

On September 3 at about 12:15:10 UT three simultaneous bursts were recorded with "U-Type" spectra, having a duration of a few seconds, with their low-frequency "reversing" points at 130 mc, 250 mc and 375 mc. Between 130 mc and 125 mc there existed a continuous interfering signal which could have masked a few megacycles of the low-frequency limit of the "fundamental" frequency burst; the lowest frequencies could also have been attenuated in the sun, as suggested by Wild, Murry, and Rowe, when they presented evidence of the second harmonic. A Maxwell has reported evidence of two simultaneous "U-Type" bursts in a 2 to 3 frequency ratio but without evidence of a "fundamental" frequency.

Classical Type III burst groups associated with flare onsets have been recorded with, however, an unexpected broad-band, burst-free, continuum emission beginning 3 to 4 minutes after the Type III event and lasting from $1\frac{1}{2}$ to $2\frac{1}{2}$ hours, with a pronounced low frequency cut-off (above 300 mc), but showing a tendency to drift to somewhat lower frequencies. It is believed that this continuum emission is distinct from that associated with Type I noise storms observed at lower frequencies. It is similar in character, in occurrence following a Type III event, and in duration to the emission found by Boischot and called Type IV. Denisse has suggested that Type IV emission is due to synchrotron radiation, on the basis of its source being large and greatly elevated in the solar corona (4 or 5R).

The Slowly Varying Component of the Solar Radio Emission—G. Swarup, *Stanford University* and R. Parthasarathy, *National Physical Laboratory of India, New Delhi*—The localized radio bright regions on the sun that give rise to a slowly varying component of the solar radiation were studied at a wavelength of 60 cm, using a 32-antenna interferometer with a beamwidth of 8.7 minutes of arc. The observations were undertaken at Sydney from July, 1954 to March, 1955. The results concerning emission polar diagram, size, brightness temperature, and height of the source above photosphere are described.

The characteristics of the bright region observed at 60 cm are compared with those found by various workers at other decimeter-centimeter wavelengths. The emission polar diagram becomes narrower as the wavelength increases. The size of the radio bright regions corresponds approximately to that of the associated plages. The brightness temperature of the radio region increases with the wavelength. These results support the hypothesis of thermal origin of the radio emission from regions of very high electron density and temperature that tend to occur over sunspots. However, observations at 60 cm sometimes showed marked intensity fluctuations in periods of nearly a half hour. This suggests that a part of the slowly varying component at 60 cm has a nonthermal origin.

The Slowly Varying Component of Solar Radiation at 340 MC—J. W. Firor, *Department of Terrestrial Magnetism, Carnegie Institution of Washington*—The sun has been observed with a multiple fan beam antenna during much of 1957 and part of 1958. The

* This work was sponsored by Rome Air Dev. Center of the Air Res. and Dev. Command under Contract AF 30(602)-1762.

* This work has been supported by a grant from Research Corp.

antenna beams are 4'.8 wide to half power and the center frequency is 340 mc.

Persistent bright areas are found, similar to those found by Christiansen at 21 cm and associated, by him, with the slowly varying component of solar radio radiation. The bright areas seen at 340 mc are not, however, necessarily identical to the 21-cm bright areas, and furthermore, the 340-mc sun has some features of the meter wavelength sun, *e.g.*, noise storms, which are not entirely distinct from the persistent bright areas.

Limiting Accuracy of Open-Wire Transmission Lines in Positional Radio Astronomy—B. F. Burke and J. W. Firor, *Department of Terrestrial Magnetism, Carnegie Institution of Washington*—Open-wire transmission lines offer convenient and inexpensive means of feeding arrays that are to be used for accurate position measurements of radio sources, but such lines are affected by local atmospheric conditions, humidity and temperature, and secondary atmospheric effects like frost and dew. Most measurements described here were made on a line 1900 feet long, consisting of two parallel No. 6 copper wires, with a spacing of three inches, and supported every 50 feet by nylon filaments. Short circuits were placed at the ends, and at the center a 385-mc signal was fed into each half. By comparing the relative phases of the two reflected waves, the difference in electrical lengths of the two halves could be measured, assuming that all the reflected wave came from the short at the end. By replacing the shorts with matched terminations, it was possible to measure the reflected wave from irregularities, droplets of water on the line, and similar spurious effects. During the 228 hours of measurement, 64 per cent of the time the balance was better than 1/45,000, corresponding to an angular accuracy (when used in an array for measuring radio source positions) of about four seconds of arc. Seventy-five per cent of the time the balance was better than 1/12,000. The short-term stability was excellent, most of the periods of 1/45,000 stability being many hours long. It appears that open-wire lines can be expected to give many consecutive hours during which their phase stability should be sufficiently good to use in radio source positional measurements where the desired accuracy is of the order of one minute of arc.

Confusion Effects in Surveys of Radio Sources—B. F. Burke, *Department of Terrestrial Magnetism, Carnegie Institution of Washington*—In most existing surveys of radio sources, the effects of multiple-source blends, often referred to as "confusion," have usually been the limiting factor in the number of sources observed. A simple mathematical model has been used, assuming isotropic distribution of the sources in space, in order to estimate the useful resolving power of pencil-beam radio telescopes. If the intensity of eighty per cent of the source in a survey is to be accurate to within ten per cent, there should be no more than one source every 200 beamwidths. Even with the rough requirement that the measured source intensity be within a factor of two in eighty per cent of the cases, the limiting resolution is approximately one source every twenty beamwidths. Existing surveys of radio sources will be discussed in the light of these considerations.

Theory of Noisy Two-Port Networks—E. F. Bolinder, *Antenna Laboratory, Electronics Research Directorate, Air Force Cambridge Research Center, Bedford, Mass.*—This paper presents a new theory of noisy two-port networks. The theory is a straightforward generalization of transformation equations for noise-free two-port networks. It has the advantage of yielding immediate geometric interpretations of noise transformations.

The input voltage V' and the input current I' of a noise-free two-port network are linearly related to the output voltage V and the output current I, so that

$$\psi = \begin{pmatrix} V' \\ I' \end{pmatrix} = \begin{pmatrix} a & b \\ c & d \end{pmatrix} \begin{pmatrix} V \\ I \end{pmatrix} = T\psi. \quad (1)$$

The input impedance $Z = V'/I'$ is expressed in terms of the output impedance $Z = V/I$ by the linear fractional transformation:

$$Z' = \frac{aZ + b}{cZ + d}. \quad (2)$$

For a noise process, transformed by a noise-free two-port network, (1) and (2) are exchanged for

$$Q' = \begin{pmatrix} Q_1' \\ Q_2' \\ Q_3' \\ Q_4' \end{pmatrix} = \begin{pmatrix} \overline{V'V'^*} \\ \overline{V'I'^*} \\ \overline{V'^*I'} \\ \overline{I'I'^*} \end{pmatrix} = \begin{pmatrix} aa^* & ab^* & ba^* & bb^* \\ ac^* & ad^* & bc^* & bd^* \\ ca^* & cb^* & da^* & db^* \\ cc^* & cd^* & dc^* & dd^* \end{pmatrix} \begin{pmatrix} \overline{VV^*} \\ \overline{VI^*} \\ \overline{V^*I} \\ \overline{II^*} \end{pmatrix} = LQ \quad (3)$$

and

$$s'^2 = \frac{Q_1'}{Q_4'} = \frac{aa^* s^2 + ab^* Z_{cor} + ba^* Z^*_{cor} + bb^*}{cc^* s^2 + cd^* Z_{cor} + dc^* Z^*_{cor} + dd^*}$$

$$Z'_{cor} = \frac{Q_2'}{Q_4'} = \frac{ac^* s^2 + ad^* Z_{cor} + bc^* Z^*_{cor} + bd^*}{cc^* s^2 + cd^* Z_{cor} + dc^* Z^*_{cor} + dd^*}$$

$$Z'^*_{cor} = \frac{Q_3'}{Q_4'} = \frac{ca^* s^2 + cb^* Z_{cor} + da^* Z^*_{cor} + db^*}{cc^* s^2 + cd^* Z_{cor} + dc^* Z^*_{cor} + dd^*}. \quad (4)$$

An asterisk (*) indicates a complex-conjugate quantity and a bar indicates an ensemble average. Z_{cor} is a complex correlation impedance.

If the two-port network contains inner noise sources, (1) is modified. Thus we have

$$\psi' = T\psi + \psi_n, \qquad \psi_n = \begin{pmatrix} V_n \\ I_n \end{pmatrix} \quad (5)$$

and (3) is also modified

$$Q' = LQ + Q_n; \qquad Q_n = \begin{pmatrix} \overline{V_n V_n^*} \\ \overline{V_n I_n^*} \\ \overline{V_n^* I_n} \\ \overline{I_n I_n^*} \end{pmatrix}. \quad (6)$$

Eqs. (3) and (6) are the bases of a general theory of noisy two-port networks. The following topics are studied:

1) Wave representation of noisy two-port networks. The introduction of a complex correlation reflection coefficient.

2) Cascading of noisy two-port networks. The formulas of Dahlke are derived in a straightforward manner.

3) The equivalent noisy network of Rothe and Dahlke. The Q vector, expressed in the equivalent noise resistance r_n, the equivalent noise conductance g_n, and the complex correlation impedance Z_{cor}, is

$$Q = 4kT_0 \Delta f g_n \begin{pmatrix} \frac{r_n}{g_n} + |Z_{cor}|^2 \\ Z_{cor} \\ Z^*_{cor} \\ 1 \end{pmatrix}$$

where k is Boltzmann's constant, T_0 is the temperature, and Δf is the bandwidth.

4) The optimum noise factor.

5) Geometric representation of noise tuning and noise matching, a generalization of ordinary tuning and matching to three dimensions.

6) Geometric theory of transforming a noise process through a noise-free two-port network. A generalization of the author's isometric circle method to three dimensions. Simple examples.

Modular Sequential Circuits—B. Friedland, *Department of Electrical Engineering, Columbia University*—Sequential circuits comprising 1) modulo p (p=prime) summers, 2) amplifiers whose gains are integers $<p$ and 3) unit delays are considered in this paper which constitutes an extension of earlier work by D. Huffman. Such circuits are characterized in terms of the modular field $GF(p)$ and vectors and matrices defined thereover. A summary of the properties of $GF(p)$ is given.

A sequential circuit is defined in terms of

$$y(n) = F[s(n), x(n)]$$
$$s(n+1) = G[s(n), x(n)]$$

where $x(n)$, $y(n)$, and $s(n)$ are k-dimensional vectors defined over $GF(p)$ representing the input, output, and state of the circuit, respectively, at the nth observation, where F and G are arbitrary functions also defined over $GF(p)$, and where the equality is interpreted as congruence, modulo p. For a *linear* sequential circuit these equations reduce to

$$y(n) = Cs(n) + Dx(n)$$
$$s(n+1) = As(n) + Bx(n)$$

where A, B, C, and D are $k \times k$ matrices defined over $GF(p)$. The latter equations constitute a canonical representation of any circuit comprising the above listed components. It is shown that circuits of this type meet the usual additivity criterion of linear systems.

The behavior of the circuit is described by trajectories in a finite state space of k dimensions and p^k states. The autonomous (A, B, C, D=constant and $x(n)=0$, all n) circuit exhibits periodic trajectories of maximum period p^k-1. The trajectories are of shorter length, $q(p-1)$ if the characteristic polynomial $|A^q-\lambda I|$ has k incongruent roots.

It is shown that a linear sequential circuit may be treated by transform methods. The input and output are represented by their "transforms" and the circuit by its "transfer function." The output-transform is the product of the transfer function and the input-transform.

Several illustrative examples are included.

Gaussian-Response Filter-Design via Modern Network Theory—M. Dishal, *Federal Telecommunication Laboratories, Nutley, N. J.*—In recent years, a number of communication systems have been proposed for which the "optimum" system transfer function is Gaussian in shape.

The engineers involved in these systems must thus know how to design the various selective circuits involved to produce Gaussian response shapes, and this paper supplies these engineers with both a specific design procedure and the design data which result when this procedure is applied.

The equation for the shape of the magnitude of the perfectly Gaussian relative-attentuation is, of course

$$\frac{V_\rho}{V} = e^{0.3466}\left(\frac{\omega}{\omega}\,3\text{ db}\right)^2$$

and the equation for the (usually neglected) shape of the phase of the perfectly Gaussian relative attenuation is

$$\theta = \infty\left(\frac{\omega}{\omega_{3\text{db}}}\right)$$

i.e., the phase characteristic is perfectly linear vs frequency and has infinite slope (which means infinite time delay for signals passing through such a filter).

The impulse response of the perfectly Gaussian filter is

$$\left(\frac{v}{v_\rho}\right)\text{impulse} = e^{-0.721(\omega_{3\text{db}}\,\Delta t)^2}$$

where Δt is the difference in time (plus and minus) figured from the infinite delay existing at the center of the impulse response.

Finally, the step response of the perfectly Gaussian filter is

$$\left(\frac{v}{v_\rho}\right)\text{step} = 1/2 + \text{erf}\,(1.20\omega_{3\text{db}}\Delta t)$$

where Δt is the time difference (plus and minus) figured from the infinite delay existing halfway up the step response.

To produce perfectly the above characteristics would require an infinite number of network elements, and as soon as it is decided to *approximate* the Gaussian response with a *finite* number of elements, the engineer must decide whether to approximate the magnitude characteristic, or the phase characteristic, or the impulse response, or step response.

Once this decision has been made, the appropriate infinite series can be written for the desired characteristic, and in this paper, the problem of approximating the Gaussian response is considered to be the problem of satisfying as many terms of this series as possible with the number of network elements available. For example, if the magnitude of the Gaussian response is to be approximated, the appropriate infinite series is

$$\left(\frac{V_\rho}{V}\right)^2 = 1 + 2\left(\frac{\omega}{\omega}\right)_\beta^2 + 2\left(\frac{\omega}{\omega}\right)_\beta^4 + \frac{8}{6}\left(\frac{\omega}{\omega}\right)_\beta^6 + \frac{16}{24}\left(\frac{\omega}{\omega}\right)_\beta^8 + \frac{32}{120}\left(\frac{\omega}{\omega_\beta}\right)_\beta^{10} + \text{etc.}$$

The Darlington procedure is then applied to (NH) terms of this equation and the resulting design data for N-pole filters supplying up to 8 poles are obtained. Design data for stagger-tuned amplifiers are also supplied.

Corresponding design data for approximating the Gaussian *phase* characteristic are also supplied.

In both designs the important practical problem of using finite-Q elements in the filters is considered and is properly included in the design procedure.

Transistor Distributed Amplifier—B. J. Harper, *University of New Mexico*—The application of the principles of distributed amplification to transistor wideband amplifiers is described. This approach to transistor circuit design extends the usable bandwidth of the transistor by a factor of 70 per cent when used in certain configurations in the low-pass amplifier. Since the gain of each transistor section adds to produce the total gain of a stage, there is considerable freedom in the choice of transistor sections to be used. This degree of freedom permits the application of various feedback and neutralization techniques to the transistor section, thereby facilitating the achievement of prescribed responses or specified operational characteristics. Also, this mobility in the design criteria permits the use of many transistor circuit configurations which are ordinarily impractical for use in amplifiers. The fundamental theories, and some practical design considerations are presented, and the advantages and the limitations of the various transistor configurations are outlined.

Experimental data, verifying the feasibility of the transistor distributed amplifier, are discussed and are then compared to the results predicted by theory. The deviation of the experimental results from the theoretical predictions is investigated as to cause, and corrective measures for obtaining a more precise theoretical approach are recommended.

Cascade Directional Filters—O. Wing, *Department of Electrical Engineering, Columbia University*—A directional filter is a frequency selective 4-port which has the properties that 1) energy in a given band entering port 1 emerges in ports 2 and 3 but not at all in 4, 2) it is reflectionless. The directional filter considered in this paper consists of two sections of transmission line and two identical 2-ports which are connected transversely to the lines to form a 4-port. Let the 2-ports be characterized by its short-circuit admittances, y_{11}, y_{12}, and y_{22}. Then it is shown that the frequency characteristic of the filter is completely specified by y_{11}. In particular, the transfer voltage ratio from port 1 to port 2 is given by (constant) $(1+y_{11})-1$ and from 1 to 3 by (constant) $y_{11}(1+y_{11})-1$. Then if N such directional filters are connected in cascade, these ratios are of the identical form with y_{11} replaced by

$$Y = y_{11(1)} + y_{11(2)} + \cdots + y_{11(N)}.$$

It is clear then that if a given transfer voltage ratio can be written in the forms shown, the realization consists essentially of cascading as many directional filters as necessary to realize the partial fractions in the expansion of the reactance function of Y. In the special case of N identical filters in cascade, each having a band-pass characteristic of "Q"Q_0, the over-all Q is Q_0/N.

On the Fading and Attenuation of High-Frequency Radio Waves over a Long Path Crossing the Auroral Zone*—K. C. Yeh and O. G. Villard, *Radio Propagation Laboratory, Stanford University*—BBC short-wave transmissions can be received at Palo Alto, Calif. over the 8500-km great circle path even when the transmitting antenna is directed at other parts of the world. This path crosses the auroral zone twice, and signals traverseing it acquire a highly characteristic flutter fading which has a speed about ten times faster than fading on non-auroral paths of comparable length.

From July 24 to September 7, 1957, the fading rate and signal strength of the available transmission in the 9- 15- and 21-mc bands were sampled every half hour around the clock. 15-mc transmissions were available during roughly 19 out of the 24 hours. The two other frequencies were available about ¼ of the time. Carrier fluctuations were recorded by means of a paper tape recorder having an upper frequency limit of 70 cps.

The component of signal attenuation associated with auroral activity was investigated by comparing signal strength measured on disturbed days with measurements made during magnetically quiet days. At 15 mc, it was found that the auroral attenuation had a broad maximum centered about a time corresponding to midnight at the path midpoint.

The half-hourly median fading speed for disturbed days was found to have a value roughly twice that measured during quiet days, except for the hours between 1700 and 2200 midpoint time. During these hours the median fading speed was comparable to the quiet day value of 5 cps. This minimum in fading speed was also observed in 15-mc transmissions from Radio Netherlands.

A positive correlation was found between the auroral component of attenuation, fading speed, and magnetic activity along the path.

Comparisons with nonauroral paths were also made.

High Altitude 106.1-MC Radio Echoes from Auroral Ionization Detected at a Geomagnetic Latitude of 43 Degrees†—A. M. Peterson, R. L. Leadabrand, R. B. Dyce,

* This research was supported by the Geophysics Res. Directorate of the AF Cambridge Res. Center under Contract AF 19(604)-1830 with Stanford University.

† This work was sponsored by Rome Air Dev. Center of the Air Res. and Dev. Command under Contract AF 30(602)-1762.

L. T. Dolphin and J. C. Schlobohm, *Stanford Research Institute*—Radio echoes from auroral ionization at 300-km height have been obtained at a frequency of 106.1 mc at the unusually low geomagnetic latitude of 43 degrees. These auroral echoes are compared with auroral echoes seen on lower power HF radars operating as part of the IGY program. The results confirm previous indications that auroral ionization is formed at heights considerably in excess of 100 km.

High Latitude Observations of Radio Star Scintillations at VHF and UHF*—C. G. Little, R. P. Merritt and E. Stiltner, *Geophysical Institute, University of Alaska*—This paper describes the results of more than 12 months' observations at College, Alaska, of radio star scintillations at 223 mc and 456 mc. Diurnal, seasonal, and elevation angle effects are discussed for the Cygnus and Cassiopeia radio sources. Probability distributions for scintillations of different magnitude are given. Two hitherto unreported features of VHF–UHF radio star scintillations are described. These are the occurrence of radio star fades of period many minutes, and a significant difference between the scintillation amplitudes of the Cygnus and Cassiopeia radio sources. The amplitude scintillations are discussed in terms of a recent theoretical paper,† and certain modifications to the theory are proposed.

VHF Auroral Radar Observations from a Synchronized Radar Chain Across the Auroral Zone in Canada—A. G. McNamara, *National Council of Canada*—A chain of four identical auroral radar stations has been operating on a continuous basis during the IGY at Resolute, Baker Lake, Saskatoon, and Ottawa. The first two stations at geomagnetic latitudes of 83° and 73.7° are well inside the auroral zone, and the latter two at 60°.5 and 56°.8 are south of the zone. A quasi-rotating antenna system is employed, the rotation at all stations being maintained in synchronism in a mode which permits simultaneous observation from different aspects. The results of a preliminary synoptic analysis of the radar results will be presented. Of particular interest is the fact that auroral echoes are observed at all stations, and in the case of the two northern stations the echoes may occur in any direction, even the south.

The Polar Spur as Backscatter—E. Warren and E. E. Stevens, *Defence Research Board, Ottawa, Can.*—It has generally been assumed that polar spurs on vertical incidence ionospheric records are attributable to *F*-layer reflections from directions other than the vertical. A more adequate account of polar spurs is that they are a form of ionospheric backscatter occurring at, or near, vertical incidence. This mechanism has been proposed by Gallet as the explanation of a type of sporadic *E*. Because the detail of polar spurs in ionograms is greater than for sporadic *E*, it is possible to check the backscatter theory of the spurs as applied to the *F* layer in a manner which cannot be done for the *E* layer.

* This work was sponsored by the Rome Air Dev. Center, Air Res. and Dev. Command under Contract No. AF 30(635)-2887.

† H. G. Booker, "The use of radio stars to study irregular refraction of radio waves in the ionosphere," PROC. IRE, vol. 46, pp. 298–314; January, 1958.

Concerning the Phenomenon of Spread *F* in the Ionosphere—J. Renau, *Cornell University*—In order to shed some light upon the phenomenon of spread *F*, a thin scattering screen is postulated above the *E* region at a constant height and the delay time associated with a ray starting from the ionospheric sounder and scattered back to the sounder via the *F* region is calculated. It was found that the greater the height assumed for the scattering screen, the better is the agreement with observed ionograms exhibiting spread *F*. Best agreement is obtained when it is assumed that the scattering level is at the level of reflection. Even in this case, however, the agreement is not good.

Generation and Coupling of Radio Noise from Corona Discharges—R. L. Tanner, *Stanford Research Institute*—Radio interference from corona discharges occurs in many circumstances. It is particularly serious in aircraft, where it occurs because of turboelectric charging due to precipitation impingement, and is the principal source of "precipitation static." Under some circumstances it also occurs in ground installations.

This paper presents a coupling theorem by which this form of interference can be analyzed. The theorem enables important physical characteristics of the source discharges to be inferred from the electrical effects they produce in simple systems. It also permits prediction of the noise characteristics in terms of the properties of the discharges and the characteristics of the system in which they occur. Data on the characteristics of the discharges—their dipole moments and spectral characteristics—are given.

The function describing the strength of coupling from the discharges to the antenna terminals is described for systems of interest. These include a simple dipole, where the function can be derived by analytical methods, and the more complicated system presented by a typical aircraft, where experimental techniques are used.

The noise characteristics at the antenna terminals, which depend both on the source and the coupling function, are discussed in typical cases. It is shown that the noise in a particular antenna can be described in terms of an equivalent noise field. The equivalent noise field concept is particularly convenient in the quasistatic situation where the antenna system is small with respect to a wavelength. This case, together with the implications of the results for airborne communication and navigation, is discussed in some detail.

Error Probability in a Simulated Binary Communication System—F. Haber and J. T. Suss, *Moore School of Engineering, University of Pennsylvania*—The results of a continuing investigation of error probability in a binary communication system are presented. Theoretical studies covering modulated sine wave and random noise interference are discussed and some experimental results covering random noise and some types of man-made noise are presented.

The recognition principle employed in this communication system is such that errors are predictable through a knowledge of the first order probability distribution function of the noise. The theoretical work discussed describes the procedures used for translating probability density function into error probability. The experimental work is aimed, in part, at verifying these procedures and, in part, toward studying the characteristics of noise sources from their error generating propensities.

Attenuation at VLF Using Sferics—W. L. Taylor, *National Bureau of Standards, Boulder Laboratories*—Simultaneous observations have been made of the waveforms of sferics at distances from 100 km to 6500 km. The recording stations were located at Boulder, Colo.; Delta, Utah; Palo Alto, Calif., and Maui, T. H. The experiment consisted of recording the broad-band waveform from a vertical antenna and from crossed-loop antennas, the direction of arrival, and time. Interpretation of this data was limited to the vertical electric field during hours of darkness.

Spectral analysis was performed over a frequency range of 1–50 kc. Waveforms, amplitude spectra, and energy content are presented. The amplitude spectra are compared for each pair of the four-station net, and the results presented in the form of attenuation vs frequency.

Some Recent Noise Measurements and Comparisons with Predictions—W. Q. Crichlow and C. A. Samson, *National Bureau of Standards, Boulder Laboratories*—Measurements of atmospheric radio noise made at stations in the recording network supervised by the National Bureau of Standards have been compared with the latest predictions from CCIR Report No. 65. It appears that improvement in the accuracy of the predictions for the United States at certain seasons and time-blocks could be made by slight changes in noise grades and some modification in the prediction curves. In particular, the recorded noise in the early afternoon in summer has been much higher than predicted, and the observed diurnal variation of the noise at 20 mc is much different than the diurnal curve shown by the predictions. The ratio of the upper and lower decile to the median value of atmospheric noise shows considerably more variation with frequency, season, and time-block than is indicated in the CCIR report.

Regular measurements of the deviations of the mean voltage and the mean logarithm of the voltage during the past year indicate marked variation of these two parameters with frequency, season, and time of day.

Artificial Sferics Generation for Interference Reduction Researches—M. M. Newman, *Lightning and Transients Research Institute, Minneapolis, Minn.*—Compact small scale artificial sferics generators are described in application to duplicating natural sferics at radio receiver inputs for evaluation of system vulnerability to lightning atmospherics. On a larger scale, in studying change of wave shapes of propagated sferics, use is made of a mobile high-voltage generator in a sea-going schooner laboratory, pulsing a helicopter-supported wire system duplicating the lightning channel.

Wire lengths of 3000 feet were readily held vertical in preliminary tests, with 10,000 feet apparently readily attainable. One million-volt impulses were fired into the helicopter supported wire, using an insulat-

ing length of 200 feet of nylon rope between the helicopter and wire. Possible psychological pilot aversion to being at the receiving end of an artificial lightning discharge was avoided by the research director's coming along on the test flights. A condenser was also installed across the gas tank gage to prevent induced surges from exploding the fuel tanks. The high voltage safety precautions proved adequate.

Some typical lightning atmospherics were reproduced with the schooner generator. Since the source pulse is accurately known both as to exact radiated wave shape and original orientation, the high-power mobile sferics generator provides a decided advantage in continuing atmospherics propagation investigations.

Transmission of a Radio Frequency Ground Wave Pulse Around a Finitely Conducting Spherical Earth—J. R. Johler and L. C. Walters, *National Bureau of Standards, Boulder Laboratories*—The introduction of pulse techniques in radio navigation systems and the interest in thunderstorm spherics has naturally led in recent years to the theoretical problem of the reconstruction of radio-frequency pulses which have been propagated around the earth. The particular case of the ground wave is of primary interest in this paper; however, the extension of the method to an evaluation of the transient behavior of the sky-wave time-modes is also indicated. The theory of the Fourier integral for the ground wave is reduced to a procedure for numerical mastery of the problem. The results of this analysis are illustrated by a comparison with the independent results of the inverse Laplace transformation. The form of a ground wave pulse which has been propagated to great distance is illustrated for a general type on sinusoidal source dipole current.

Observations on Some Low-Frequency Propagation Paths in Arctic Areas—A. D. Watt and E. L. Maxwell, *National Bureau of Standards, Boulder Laboratories*—The very low ground conductivities encountered in arctic areas along with the particular ionospheric conditions prevailing at high latitudes, frequently lead to rather unusual radiation and propagation conditions. In order to determine the magnitude of these effects, field intensities from transmitters located in the Labrador and Greenland areas were measured both on the surface of the earth and during several aircraft flights over this area.

Under conditions where the initial portion of the propagation path is across ice cap or permafrost, the attenuation observed is very great, and when the propagation path extends out over sea water, the field intensity recovery taking place after the coast line is reached is very marked. The flight data contain dips in amplitude which appear to be caused by interference from sky waves, and estimates of sky wave field intensity based on the work of Belrose and others, appear to agree with the observed results provided the radiated field is suitably modified by the antenna vertical pattern. These vertical patterns based on work by Wait, along with the field intensity flight data, indicate that the siting of low-frequency stations several miles or more inland in arctic regions may result in very great increases in total transmission path loss.

Observed 8.7-MM Refraction as a Function of Surface Meteorological Conditions—G. R. Marner and W. R. Iliff, *Collins Radio Co., Cedar Rapids, Iowa*—Total atmospheric refraction of 8.7-mm solar radiation was measured over an extended period of time by the use of a radio sextant. The mean refraction and standard deviation from the mean are obtained as a function of altitude angle from these observations. Variation of the refraction is studied as a function of surface meteorological conditions and a refraction correction technique is applied to predict total refraction. An analysis of deviations from the predicted refraction values is presented. Applications to radio telescope guidance and precision position determination of celestial sources are pointed out.

Absorption, Refraction and Scintillation Measurements at 4700 MC with a Traveling-Wave Tube Radiometer—J. Castelli, C. Ferioli, J. Aarons, and J. Casey, *Propagation Laboratory, Electronics Research Directorate, AF Cambridge Research Center*—During the month of July, 1957, measurements were made at *C* band (4700 mc) on atmospheric absorption, refraction and scintilation using the sun as a source of radio frequency energy. The equipment used was a comparison type radiometer utilizing traveling wave tubes as a tuned radio frequency receiver and an altazimuth antenna mount. The average solar temperatures recorded for the period varied between 22,000°K at zero elevation and 26,000°K at 60° elevation. Individual readings ranged between 18,000°K and 30,000°K. The mean absorption based on average solar temperatures at the various elevations for the period was 0.00348 db/km. Refraction maxima were approximately the same as optical although deviations from the mean during any day were large. Atmospheric scintillation with periods ranging from one-half second to ninety seconds were recorded. Scintillation amplitudes ranged from 2 to 20 per cent of antenna signal temperature at low angles. At high elevations scintillations rarely reached 10 per cent and were generally less than 1 per cent.

Atmospheric Factors Affecting Precision Location of Celestial Radio Sources—W. H. Bellville, W. R. Iliff, and J. M. Holt, *Collins Radio Co., Cedar Rapids, Iowa*—The basic attenuation, radiation, and refraction phenomena of the atmosphere cause the apparent positions of celestial radio sources to deviate from their true positions. In order to evaluate these deviations it is necessary to specify an atmosphere model which defines temperature, pressure, and humidity variations with height.

Several atmosphere models are selected representative of various typical and extreme conditions. Total atmospheric attenuation, radiation, and refraction as functions of altitude angle are then computed for these models at various wavelengths. The resultant position errors for a radiometric tracker are analyzed for both point and extended sources. It is shown that for an extended source, proper choice of antenna parameters can, in some cases, result in cancellation of radiation and attenuation errors for all altitude angles. Comments are presented concerning the magnitude of these errors for precision location system other than the radiometric tracker.

Amplitude Scintillation of Extraterrestrial Radio Waves at UHF—H. C. Ko, *Ohio State University*—Fluctuations in the flux density of the intense radio star, Cygnus A, have been observed at an ultrahigh frequency of 915 mc using a steerable 40-foot parabolic antenna. Drift curves of Cygnus A were taken continuously, over a wide range of elevation angles, during the autumn and winter of 1957.

The amplitude of scintillation is strongest near the horizon and decreases very rapidly as the elevation angle is increased. Scintillation occurred at elevation angles less than about 5° on most nights. The scintillation characteristics have been noted to change from day to day. The amplitude of the fluctuations ranges from a few per cent to fifty per cent of the mean flux density of Cygnus A, while the fluctuation rate varies from ½ to 6 peaks per minute.

A comparison of the scintillation data with the 3-hour geomagnetic *K* index shows that the fluctuation rate is approximately proportional to the *K* index. The amplitude of the fluctuations is, however, relatively unaffected by the change of the *K* index.

It has also been observed that the scintillation was markedly affected by the presence of auroras. During the periods of auroral displays, the scintillation was observed both at low and high elevation angles, and was always characterized by a larger amplitude and a higher rate of fluctuation.

Atmospheric Radiation Received by Directional Antennas—G. R. Marner, *Collins Radio Co., Cedar Rapids, Iowa*—The general theory of radiation from semitransparent gases is sketched and the amount of power coupled into an antenna by a spherically stratified atmosphere with arbitrary attenuation constant is calculated. The attenuation constant as a function of height obtained from extinction observations is then used to calculate the antenna temperature as a function of altitude angle at 8.7-mm and 1.9-cm wavelengths. These results are compared with observed values of antenna temperature under different weather conditions. Estimates of atmospheric radiation throughout the microwave region are then made by use of the theoretical dependence of the attenuation constant upon wavelength.

New Determinations of Atmospheric Microwave Absorption by Radio-Astronomical Methods—G. R. Marner, *Collins Radio Co., Cedar Rapids, Iowa*—A brief description of a method for determination of atmospheric absorption is given. The 8.7-mm radiation from the sun is recorded throughout the afternoon by a combined radio sextant-radio telescope. The measured reduction of power during sunset is compared with that predicted from a model atmosphere which includes the effects of earth curvature and variation of attenuation with pressure, temperature, density, and humidity. Sea level values of the attenuation constant, as well as its variation with height, are thereby obtained.

Similar data taken at 1.9-cm wavelength are also presented. Comparison is made with previous theoretical and experimental values of atmospheric attenuation in the microwave region.

UHF Moon Reflections*—S. J. Fricker, R. P. Ingalls, W. C. Mason, and M. L. Stone, *Lincoln Laboratory, Massachusetts Institute of Technology*—A CW bistatic moon reflection experiment at 400 mc was conducted by Lincoln Laboratory for a period of approximately three weeks during August, 1957. Linearly polarized signals were transmitted, and two identical receiver channels were used to receive the orthogonal components of the returned signal. The receivers had narrow bandwidths (50, 100, and 300 cps) and were tracked to follow the Doppler-shifted frequency.

The system was operated from moon rise to moon set each day. The returned signal level on any one channel showed the effects of Faraday rotation, but the sum of the two components remained fairly steady throughout the entire period. The effect of libration on fading rates was quite marked, and some periods were noted when the fading rate approached zero. Computed libration rates agree with these observed variations in fading rate.

General Solution of the Luneberg Lens Problem—S. P. Morgan, *Bell Telephone Laboratories, Inc., Murray Hill, N. J.*—A Luneberg lens is a spherically symmetric refracting structure which will form perfect geometrical images of the points of two given concentric spheres on each other. The general solution is derived for the index of refraction of such a lens as a function of radius. One conjugate sphere is assumed to be outside the lens or at its surface, while the other may be either inside or outside the lens. If one of the spheres is of infinite radius, the lens will form a parallel beam perfectly at a point on the other sphere. Such a device has obvious potentialities as a wide-angle microwave scanner. It is shown that the index of refraction may be specified arbitrarily, subject to two simple conditions, in an outer shell of any desired thickness less than the radius of the lens. The index of the central portion is then expressed in terms of a tabulated function, and of an integral involving the index of the outer shell. Some properties of the general solution are discussed, and various special solutions are exhibited. In particular, the case in which the index of the outer shell varies as any power of radius is worked out completely.

Reflector Antenna Surface Errors—K. S. Kelleher and G. R. Lowrey, *Melpar Inc., Falls Church, Va.*—The purpose of this paper is to investigate theoretically, in as broad a manner as possible, the effect of variations in the surface of a reflector on its radiation pattern. The effects of random and systematic errors on the performance of a paraboloidal reflector are discussed, with regard to both gain and sidelobes; and various approximations to paraboloidal reflectors are also considered. Feeds of arbitrary taper are used.

Various simplified geometrical error distributions are treated exactly first. It turns out that the established formula for the reduction in gain caused by genuinely random surface errors gives quite an accurate estimate of the effect of most systematic errors too, with the exception of gross errors and certain very irregular distributions. This greatly extends the class of systematic error distributions whose effect can be accurately treated numerically; and some applications of this result are given. In addition the choice of manufacturing tolerances is discussed.

The approximations to a paraboloidal reflector which are considered include an approximating polyhedron and sections of a sphere and a parabolic torus. The authors hope to present also a discussion of methods of checking the figure of a reflector and the location of the focus. Wherever convenient the results are presented in the form of nomograms immediately useful in antenna engineering applications.

Resonant Slots Having Independent Control of Amplitude and Phase—B. J. Maxum, *Hughes Aircraft Co.*—The design of waveguide arrays requiring nonuniform phase distributions, such as those having shaped beam radiation patterns, would be greatly facilitated by development of slots with independent amplitude and phase control. A slot properly oriented on the broad wall of a rectangular waveguide makes it possible to control the coupling characteristics over a range in phase from zero to 2π and over a range in magnitude from zero to unity. Data have been obtained relating the complex amplitude of the voltage across the slot to the slot orientation. This complex voltage amplitude is also related to the coupling parameters used in common array design. A typical shaped beam array utilizing this type of slot is described. Radiation patterns are included which demonstrate the accuracy and usefulness of the design procedure.

The Design of Mirror-Lenses for Scanning—A. E. Marston and R. M. Brown, *Electronics Division, U. S. Naval Research Laboratory*—A study has been made of the scanning properties at microwave frequencies of the mirror-lens, which is a lens in direct contact with a reflecting surface. Rays from a point source are incident on the lens curve L and are refracted there, then reflected by the reflector curve R, and finally refracted a second time at L to form a collimated beam (if properly designed).

The only mirror-lens treated in classical optics is the Mangin mirror, for which both L and R are circles. Although they cannot focus perfectly, Mangin mirrors were designed here by a method of successive approximations and had phase errors small enough that radiation patterns showed sidelobes more than 25 db down. Unfortunately, for off-axis feed positions they suffered from coma and could not be used for scanning.

To better the scanning performance, two other types of mirror-lenses were designed. The first was made to satisfy the Abbe sine condition, which guarantees that the lens will be coma-free at least for infinitesimal displacements of the feed from the axis. Since no exact solution seemed possible, a design was evolved by requiring that L be a circle, R an ellipse, that the mirror-lens focus three rays perfectly and that these three rays also satisfy the Abbe sine condition. It was found experimentally that the Abbe sine mirror-lens was virtually coma-free and could scan a 1.5-degree beam over an angle of ± 12 degrees with sidelobes more than 19 db down.

By allowing both L and R to be ellipses and using a similar three-ray technique, bifocal mirror-lenses were designed. These had the property that three rays from an off-axis point were approximately focused at some angle α and so by symmetry the analogous rays from the point conjugate to the first were approximately focused at the angle $-\alpha$. These bifocal mirror lenses were, if anything, slightly better than the Abbe sine models, being able to scan a 1.1-degree beam over about ± 12 degrees with sidelobes more than 19 db down.

The scan angles that have been cited refer only to patterns in the plane in which the lens was designed. Actually, the models that were built were three-dimensional rotationally-symmetric lenses and for them, the aberration of astigmatism further limited the scan to about ± 8 degrees.

The Pattern of a Vertical Antenna on a Curved Lossy Surface—J. R. Wait and A. M. Conda, *National Bureau of Standards, Boulder Laboratories*—In 1946 V. A. Fock in in the U.S.S.R. disclosed a powerful method for the solution of the diffraction by a convex surface. He gave numerical results only for the surface currents excited by plane wave incident on a perfectly conducting body. In this paper, the extension of his work to the computation of the radiation pattern of a ground-based vertical antenna is described. The surface of the ground is represented by a smooth spherical surface of finite conductivity. Of particular interest is the radiation field at angles near grazing. The application of the results to the launching of sky waves is described. For example, at 100 kc at an angle of 3° below the horizon, and a ground conductivity of 5 milli-mhos/m, the radiation is reduced by 12 db from the ideal situation of a perfectly conducting flat ground plane.

Cross Sections of Large Cylinders by the Variational Method—E. S. Cassedy, Jr., *Radiation Laboratory, The Johns Hopkins University*—The electromagnetic field scattered by a conducting body large compared to wavelength may be computed with an accurate knowledge of the induced currents on the surface of the body. Work has been done by Logan and Rabinowitz on this basis using Fock's currents.

The variational method offers an alternative procedure for computing the far scattered field, in that computations may be made with only an approximate knowledge of the induced surface currents. Kodis has formulated the total scattering cross section of cylinders large compared to wavelength by this method. In the present work the differential scattering cross section vs angle of observation for large cylinders is found by the same method.

The trial functions used for the induced surface currents are the physical optics approximation on the surface of the cylinder plus a trial function on a hypothetical plane which intersects the body at the shadow line. The trial function on the plane is the unperturbed incident field plus a correction function which decays with increasing distance from the body.

* The research in this document was supported jointly by the Army, Navy, and Air Force under contract with the Mass. Inst. Tech.

Multiple Scattering of Electromagnetic Radiation and the Transport Equation of Diffusion—D. S. Bugnolo, *Columbia University*—Multiple scattering of electromagnetic radiation by atmospheric and ionospheric turbulence is of considerable importance in long line-of-sight paths. The usual single scatter or Born approximation is of questionable value in such cases. Higher order Born approximations usually lead to equations of unusual complexity incapable of exact solution.

Another possible method of solution is the transport equation of particle (photon) diffusion. The results of a single scatter or Born approximation can be used to construct an integral-differential equation in a six-dimensional phase space plus time. This method is of particular use in unbounded regions. The introduction of boundary conditions is usually untenable since the approximation is essentially scalar and the boundary conditions vector.

The transport equation will be reviewed briefly and applied to a number of rather interesting long line-of-sight problems.

Toward a Solution of the Tropospheric Multiple Scatter Problem—W. S. Ament, *Naval Research Laboratory*—Current theories of tropospheric scatter are single-scatter ray theories. The scattering blobs or wavy layers are regarded as converting a ray from the transmitter into a ray toward the receiver. Diffraction and ducting effects are ignored for lack of tractable solutions to the wave equation for points near the horizon ray, in even a standard atmosphere. The generally stratified average atmospheric refractive structure enters only through ray bending, allowing the illuminating and singly scattered rays to intersect at more or fewer scatterers at better or worse angles. On the other hand, multiple scatter is regarded as basic in current line-of-sight theories. Suggestions for the importance of multiple scatter in long-range propagation have hitherto been fruitless except in the qualitative interpretation of experimental data,* owing to the mathematical difficulties of even a ray treatment.

The commercially available ray-tracer can be modified by the insertion of appropriate noise voltages to trace multiply randomly scattered rays in stratified atmospheres. The authors describe the modifications necessary for this and for recording paths of 10^{-4} per cent of the rays, launched at the horizon, which reach low altitudes at scatter propagation ranges. The elementary theory of the analog calculation is given and some of the results conjectured.

Meanwhile, it is recommended that blob parameters be measured directly with refractometers rather than inferred via single-scatter ray theory from radio field measurements.

Scattering of Plane Waves by Locally Homogeneous Dielectric Noise†—R. A. Silverman, *Institute of Mathematical Sciences, New York University*—The scattering of acoustic and electromagnetic radiation by random refractive index fluctuations of the scattering medium (*e.g.*, the troposphere, the ocean) is a problem of considerable contemporary interest. For brevity, we shall refer to these refractive index fluctuations as *dielectric noise*. The purpose of this paper is to compare two approaches to the problem of the scattering of incident plane waves by a confined region of dielectric noise. In the first approach, which is the conventional one, the scattering dielectric noise is represented as a "section" of a homogeneous (*i.e.*, spatially stationary) random process. In the second approach, which is based on a recent generalization of the notion of stationarity,* the scattering dielectric noise is represented as a *locally homogeneous* random process. The advantage of representing the dielectric noise as a locally homogeneous process, rather than as a homogeneous process, is that one can thereby take into account in a natural way the spatial variation of the average noise power, without departing from the physically reasonable requirement that the process be approximately homogeneous in suitably restricted domains. When plane waves are scattered by locally homogeneous dielectric noise and observed in the Fraunhofer region, it is found that the local structure of the noise determines the average scattered power received at a fixed point, whereas the over-all structure of the noise determines the space correlations of the radiation received at two different points.

Calculation of the Fading Rate for Tropospheric Scatter Propagation—J. B. McGuire and A. D. Wheelon, *The Ramo-Wooldridge Corp., Los Angeles, Calif.*—The fading rate of the envelope of signals propagated beyond the horizon by scattering from refractive irregularities is discussed. The radio frequency and distance dependence of the fading rate is computed using the turbulent mixing-in-gradient scattering cross section†

$$\sigma(\theta,\lambda) = \frac{\pi^2}{\lambda^4}\left(\frac{dn_0}{dh}\right)^2\left[\frac{4\pi}{\lambda}\sin\frac{\theta}{2}\right]^{-5}$$

and single scattering theory. The fading is due to Doppler shifting of the waves by both the mean drift velocity of the atmosphere and the random self motion.‡ If the mean velocity is assumed to be horizontal, the principal contribution to the fading comes from volume elements which are far removed from the regions which contribute most to the scattered power. It is found that very high fading rates (10 to 100 cps) can be induced by these off-center elements. The fading rate due to drift is proportional to the radio frequency, while the self motion contribution has a frequency exponent which varies from 0.66 to 1.00. Estimations of the atmospheric properties are combined with these results and compared with experiments reported by the National Bureau of Standards and Lincoln Laboratories.

Measurements of the Bandwidth of Radio Waves Propagated by the Troposphere Beyond the Horizon*—J. H. Chisholm, L. P. Rainville, J. F. Roche, and H. G. Root, *Lincoln Laboratory, Massachusetts Institute of Technology*—It has been shown theoretically by S. O. Rice that radio waves scattered by an ensemble of point scatterers with a particular velocity distribution have instantaneous transmission characteristics as a function of frequency analogous to the transmission characteristics of a discrete frequency as a function of time. Experiments have been performed to investigate the "instantaneous" transmission characteristics of signals received over a 188-mile path between Round Hill, Mass. and Crawfords Hill, N. J. The transmitter frequency was swept over a 20-mc band centered about 2290-mc at a repetition rate of 100 cps. A broad-band receiver was utilized and each individual sweep was recorded photographically.

A representation of the "bandwidth" in a statistical form is given for these results as distributions of amplitude variations as a function of successive increments of frequency from 0.5 to 10 mc centered about the nominal carrier frequency of 2290 mc.

Diversity Reception in Scatter Communication with Emphasis on Angle Diversity—R. Bolgiano, Jr., N. H. Bryant, and W. E. Gordon, *Cornell University*—The angular separation of two receiving antenna beams provides a basis for a diversity system. The advantages (*e.g.*, reduction in number of antennas) and the problems (*e.g.*, design of antenna feeds) are presented in a comparison with a space-diversity system. Angular separations obtained in elevation or in azimuth are discussed on the basis of available theoretical models, quantitative estimates derived from pertinent experiments, and a derivation of diversity improvement as a function of correlation and inequality of average signal levels in the channels. This analysis indicates that angle diversity may play an important role in scatter circuits.

A Radar Terrain Return Model—I. Katz and L. M. Spetner, *Applied Physics Laboratory, The Johns Hopkins University*—A statistical model is proposed to explain the empirically-determined functional form of radar cross sections vs depression angle. The model is based, at large depression angles, on reflections from a large number of variously-oriented facets on the surface and at small depression angles on reflections from nearly vertical structures. The facet slopes and the heights and tilts of the vertical obtructions and their surface density become parameters which are used to simplify the description of the reflection properties of the terrain.

Comparison of Preliminary Results from Three Western United States IGY Fixed-Frequency Scatter Sounders—R. D. Egan and A. M. Peterson, *Stanford University*—Preliminary reduction of data from the International Geophysical Year Fixed-Frequency Backscatter program has yielded several interesting facts concerning sporadic-

* D. L. Ringwalt, W. S. Ament, and F. C. Macdonald, "Measurements of 1250-mc scatter propagation as function of meteorology," IRE TRANS. ON ANTENNAS AND PROPAGATION, vol. AP-6, pp. 208–209; April, 1958.

† The research reported in this article was supported by the Dept. of Defense under Contract No. DA49-170-sc-2253.

* R. A. Silverman, "Locally stationary random processes," IRE TRANS. ON INFORMATION THEORY, vol. IT-3, pp. 182–187; September, 1957.

† F. Villars and V. F. Weisskopf, "On the scattering of radio waves by turbulent fluctuations of the atmosphere," PROC. IRE, vol. 43, pp. 1232–1239; October, 1955, and A. D. Wheelon, *Phys. Rev.*, vol. 105, p. 1706; 1957.

‡ R. A. Silverman, *J. Appl. Phys.*, vol. 28, p. 506; 1957.

* The research in this document was supported jointly by the Army, Navy, and Air Force under contract with the Mass. Inst. Tech.

E and field-aligned ionization. Moving sporadic-*E* clouds have been tracked simultaneously on three sounders, located at Stanford, Calif.; Pullman, Wash.; and Boulder, Colo. A large-scale comparison of field-aligned ionization in the Western United States and Canada is also possible with these same sounders.

Characteristics of Solar Flares with Short-Wave Fadeouts—C. B. Warwick* and M. B. Wood, *National Bureau of Standards, Boulder Laboratories*—Occurrence of SWF's shows a strong relation to flare height. Among 144 limb flares, we find only 4 exceptions to the rule that a flare must be as high as 14,000 km to produce a SWF. Among flares over 14,000 km, *H*-alpha intensity of the flare is related to SWF occurrence.

Occurrence of SWF as a function of central distance of the associated flare is consistent with the interpretation of the SWF-height relation in terms of absorption of Lyman radiation. The results support an earlier conclusion, based on a small number of flares, that SWF's are caused by optical radiation rather than by soft X rays.

Temporal and Spatial Variation of Polar Es†—R. Penndorf and S. C. Coroniti, *Electronics Research Laboratory, Research and Advanced Development Division, AVCO Manufacturing Corp.*—The percentage of time $fEs>5$ and $fEs>7$ mc occurs, was investigated for all stations north of 60° geomagnetic latitude and for the years 1954 to 1957. The basic data are taken directly from the F series of CRPL. The following conclusions have been drawn:

1) There exist two distinct types of *Es* occurrence, the Thule and the aurora belt type. Some stations show a mixture of both types.

2) The Thule type is restricted to stations close to the geomagnetic pole. It shows a summer maximum occurring around geomagnetic noon for each station.

3) The auroral belt type occurs at all stations along the auroral belt. Here *Es* appear only at night, between about 18 LST and 7 LST. No seasonal or sunspot cycle variation is apparent.

4) The mixed type is found at Godhavn and Baker Lake. During some months, the Thule type prevails, whereas in other months, the auroral belt type prevails.

5) The above discussed effects show up for $fEs>5$ and also $fEs>7$ mc. No important difference between these two groups was found.

6) A longitudinal effect is most pronounced in the Thule type, but appears also in the auroral belt type. In the inner arctic, the diurnal maximum of *Es* occurrence coincides with the time when geomagnetic noon occurs at the station. Good agreement was found for the Russian ice island SP-3, Longyearbyen, Godhavn, Thule, Resolute, and Barrow. The time difference between geomagnetic noon and the diurnal maximum never exceeded two hours. Along the auroral belt the beginning and end of the nighttime *Es* shows a longitudinal effect.

7) The highest frequencies of *Es* in the inner arctic are 15–20 mc.

8) *Es* seems to be related to magnetic activity, more so along the auroral belt than near the pole and certain types of *Es* are reflections from overhead aurora. This correlation can only be interpreted as a direct or indirect influence of corpuscular radiation on the nighttime *Es* along the auroral belt, and on *Es* in general for the arctic region closer to the magnetic pole.

Time Constants in the Geomagnetic Storm Effect—C. O. Hines and L. R. O. Storey, *Defence Research Board, Ottawa, Can.*—It has been suggested that magnetic disturbances generated by a ring current could not penetrate the ionosphere to the earth's surface in any reasonable length of time to account for the main phase of a geomagnetic storm. The concepts on which this suggestion were based are shown to be invalid in a comparable idealized situation, and, by implication, in the case of the ring current itself. Instead, a time constant of the order of 10 minutes is found to characterize penetration through the ionosphere.

Typical geomagnetic storm effects are discussed in the light of this result.

The Ionosphere at High Southern Latitudes—R. W. Knecht, Y. Aono*, and R. E. McDuffie, *National Bureau of Standards, Boulder Laboratories*—A preliminary analysis of ionospheric data taken during the first six months of the IGY at the six U. S.-associated vertical soundings stations in the Antarctic has been made. The effects of geographic and geomagnetic latitude on the monthly median values of foF2 are discussed. Using the data from the South Pole station, it has been possible to study the behavior of the ionosphere under prolonged periods with the sun at a fixed elevation above (or below) the horizon. Observed diurnal trends in foF2 at the South Pole are presented with a possible explanation. Comparisons are made between the arctic and the antarctic ionospheres with particular reference to amount of spread echo, sporadic *E* and simultaneity of polar blackouts.

A Study of the Morphology of Ionospheric Storms—S. Matsushita, *National Bureau of Standards, Boulder Laboratories and High Altitude Observatory of the University of Colorado*, R. B. Norton, *National Bureau of Standards, Boulder Laboratories*, and M. Sugiura, *Geophysical Institute of University of Alaska*—Ionospheric F2 density variations in the ratio $(N_e - N_e \text{ median})/N_e$ median during strong and weak magnetic storms were studied, using the data collected during ten years (1946–1955) at 38 ionospheric stations between geomagnetic 60°N and 60°S. Fifty-one strong and fifty-eight weak storms occurred during that period.

Storm time variations (D_{st}) of F2 density in geomagnetic 60°–35° of both hemispheres showed a decrease (20–40 per cent during strong storms, and 10–20 per cent during weak storms) after an initial short increase of about 15 per cent for both strong and weak storms. In equatorial regions, however, storm time variations showed the opposite phase; generally an increase (about 20 per cent for strong storms and about 15 per cent for weak) after an initial short decrease (about 10 per cent for strong storms, and something less than 10 per cent for weak). The variations in both regions did not show any remarkable seasonal changes. The variations in the region between geomagnetic 35° and 10° were rather flat on the average; however, they seemed to have seasonal behavior.

The maximum of local time disturbed variations (D_s) of F2 density during strong storms occurred at 06–18^h, local time in geomagnetic 60°–50°N, at 18–06^h in 50°–10°N, and 03–09^h in 10°N–10°S.

Ionospheric behavior in high latitudes was studied during magnetic disturbances and storms using magnetograms and ionograms both made at the same station.

The Influence of the Solar Cycle and Magnetic Activity on the Lower Ionosphere and VHF Forward Scatter—H. I. Leighton, *National Bureau of Standards, Boulder Laboratories*, and C. D. Ellyett, *University of Canterbury, Christchurch, N. Z.*—A survey of the literature indicates that the electron concentration in the *D* region of the ionosphere undergoes a cyclic change of the order of eleven years. Such a change should also appear in VHF forward-scatter signal intensities. Analysis of the Cedar Rapids, Iowa to Sterling, Va. forward scatter paths on an annual basis indicates that the monthly median received intensities for daytime periods only follows the same general trend as that of the monthly sunspot number.

The effect is enhanced when the comparison is made in terms of the magnetic indices. However, if the comparison with magnetic indices is made in terms of three-hour periods (eliminating long term trends), no observable increase of signal intensity can be seen as magnetic conditions become disturbed. In addition it is found that the signal intensity increases moderately with rising magnetic index if only the midday period is considered.

It appears then that magnetic effects have a milder influence on VHF circuits at the middle as compared to higher latitudes, but that a clearly discernible effect is present in the midday period as can be seen by studying long term effects. This result is in conflict with the hypothesis that the whole of the VHF forward scatter signal is due to reflections from meteor trails.

UHF Auroral Observations*—S. J. Fricker, R. P. Ingalls, W. C. Mason and M. L. Stone, *Lincoln Laboratory, Massachusetts Institute of Technology*—Further results are reported of 400-mc radar and CW bistatic observations of aurora conducted by personnel of Lincoln Laboratory, M.I.T. Some knowledge was gained of the height dependence of the auroral echoing regions, and further information was gained of the perpendicularity requirement. The diurnal variation showed up in a well defined manner, with the peak occurring just before sunset. Maximum signals were obtained which corresponded to radar target cross sections of the order of 10^3 meter^2.

The frequency structure of the returned signals was examined in a crude way by

* Work done while at High Altitude Observatory of University of Colorado on a joint research program with CRPL.

† The research in this document was supported by AF Cambridge Res. Center under Contract AF 19(604)-2630.

* Guest worker; on staff of Radio Res. Labs., Tokyo, Japan.

* The research in this document was supported jointly by the Army, Navy, and Air Force under contract with the Mass. Inst. Tech.

determining the spectra of the returned pulses and comparing these with the transmitted pulse spectra. A more direct measurement was made with a CW bistatic system, in which a narrow band receiver (100 cps) was swept through the returned signal. All results analyzed to date point to an increased frequency for the returned signal, with the maximum occurring approximately 600 to 1000 cps higher than the transmitted frequency.

398-MC Auroral Echoes Obtained at College, Alaska*—R. I. Presnell, R. L. Leadabrand, R. B. Dyce, L. T. Dolphin and A. M. Peterson, *Stanford Research Institute*—Investigations of auroral echoes have been continued at College, Alaska, at a frequency of 398 mc. Comparison of auroral echoes at 398 mc and at 40 mc have been made.

Investigation of the polarization of 398-mc auroral echoes has been made by two methods:

1) Transmitting vertical linear polarization, receiving on vertical linear polarzation and horizontal linear polarization.
2) Transmitting horizontal linear polarization, receiving on horizontal linear polarization and vertical linear polarization.

Studies in the Off-Perpendicular Geometry of Aurora Reflections†—S. C. Wang, M. Loewenthal, P. A. Duffy, and J. N. Skenian, *Lincoln Laboratory, Massachusetts Institute of Technology*—For studying aurora reflections, a repertory of novel schemes have been prepared for a graphical representation of the geometry of the angle between the radar beam and the earth's magnetic field in the reflection of a signal. For any particular experimental arrangement or problem, there is in general a most suitable and useful set of charts of the geometry that will facilitate the tangible evaluation of the roles played by the values of the off-perpendicular angles and the heights of reflection centers, under the given experimental conditions of finite radar beamwidths and pulse length. To put computations for the charts on as solid a footing as possible, a procedure has been developed to base the field direction upon that given by the geomagnetic charts instead of the dipole approximation. Theoretical estimates are also made of the change of this field direction with the height above the earth's surface. The problem of treating actual radar data so as to infer useful information about the distribution of the reflecting ionization is considered and illustrated by example.

A New Theory of the Aurora—S. F. Singer, *Physics Department, University of Maryland*—A long-standing problem is to explain the energy of auroral protons. The author shows here that solar protons trapped in the earth's magnetic field‡ can be accelerated up to auroral energies. The mechanism does not use electric fields (*e.g.*, Martyn or Alfven). Instead some of the protons are accelerated by magnetohydrodynamic waves which are in turn produced by the bulk of the solar protons. In this acceleration process the earth's magnetic field acts as the energy transfer agent. There is additional empirical evidence supporting our proposed mechanism, namely geomagnetic micropulsations, the VHF emissions from the upper atmosphere, and the evidence that the auroral protons have a distribution of energies.

Whistler Paths in the Outer Ionosphere—I. Yabroff, *Stanford Research Institute*—Ray path equations are derived for a generalized inhomogeneous, anisotropic medium. A physical interpretation of these equations is discussed. The general equations are expressed in form suitable for computation of whistler mode propagation in the outer ionosphere. Several computed whistler paths are presented using simple models of electron density profile. Appreciable departures from the lines of force of the earth's field are found.

Comparison of Whistlers with Magneto-Ionic Duct Signals from Station NSS*—R. A. Helliwell and E. Gehrels, *Stanford University*—The time delays of one-hop whistlers and echoes from NSS (near Washington, D. C.). were measured at Cape Horn on 15.5 kc. They correlated closely, even though their day-to-day variations were large. The whistler variations could not, therefore, be attributed to changes in the location of the causative lightning flashes. At Washington, D. C., there were eighteen two-hop whistlers which were coincident at Cape Horn. Their dispersions were thirty per cent greater, on the average, than twice those at Cape Horn. If the propagation path had been the same for the Cape Horn and Washington whistlers, the dispersion ratio should have been exactly two.

These results are compared with NSS split-echo data and recent whistler data from the IGY program. The study provides new evidence that magneto-ionic duct signals are often restricted to discrete paths. Two possible models for such paths are compared. They are based on 1) columns of field-aligned ionization extending into the outer ionosphere and 2) irregularities in the *E* or F2 layer.

Tape recordings of whistlers at Washington, D. C., were kindly supplied by H. E. Dinger of the Naval Research Laboratory.

Whistler Propagation in Regions of Very Low Electron Densities—O. K. Garriott, *Stanford University*—The *Q-L* approximation to the Appleton-Hartree equation has found considerable utility in whistler analysis. From it the Eckersley dispersion law can be derived and many of the whistler characteristics understood.

More recently the analysis has been extended to regions in which the wave frequency approaches the local gyromagnetic frequency. At the higher frequencies the group velocity is found to decrease, resulting in a "nose" at roughly $\frac{1}{4}$ to $\frac{1}{2}$ the minimum gyro frequency. Experimental confirmation of this effect has been found in abundance.

Still another case has been found to be of interest. This is the case in which the wave frequency approaches the plasma frequency, while the gyro frequency is still much higher than either. The index of refraction now exhibits a pole at

$$X = \frac{1 - y_H^2}{1 - y_L^2}$$

and the group velocity again has a maximum at a frequency below the plasma frequency. This should be expected to result in a nose whistler. The frequency of minimum delay might be termed the "plasma nose" to distinguish the causative condition from that of a "gyro nose."

Calculations of the actual ray path at several frequencies for a particular model using the computer program developed by Yabroff are shown. A plot of time delay vs frequency reveals a "plasma nose" whistler.

Several published reports, notably by Dinger, have shown excellent whistlers with surprisingly low nose frequencies. It is suggested that these low nose frequencies may be due to unusually low electron densities for appreciable lengths along the whistler path. If correct, new information on minimum electron density as well as the general distribution is available.

Pulse Sky Wave Phenomena Observed at 100 KC—R. H. Doherty, *National Bureau of Standards, Boulder Laboratories*—Sky wave measurements made at 100 kc indicate that signals exist far beyond the geometrical optical limit for these signals. Data observed tend to support a theory that these waves are propagated partly as ground waves. The stability observed for these long range sky waves suggests that they may be utilized for relatively accurate navigational fixes.

The various phenomena observed on higher order multiple hops (third through seventh) are also discussed.

Diffraction by a Wide Slit and Complementary Strip—R. F. Millar, *Radio and Electrical Engineering Division, National Research Council, Ottawa, Can.*—A rigorous, asymptotic solution is obtained for the problem of the diffraction of a plane wave by the infinite slit separating two perfectly conducting half-planes of negligible thickness. Both *E* and *H* polarizations are considered. The solution in each case takes the form of a series in inverse power of the ratio of slit-width to wavelength of the incident wave, and is based on the solution by successive substitutions of a pair of integral equations and repeated applications of Watson's lemma on the asymptotic evaluation of integrals. The current densities induced on both halves of the screen are calculated, from which is deduced the electric field in the slit. The far-fields are determined from the aperture distribution, and asymptotic expressions are found for the transmission coefficients as functions of the angle of incidence and the ratio of slit width to wavelength.

By means of Babinet's principle, the solutions for diffraction by a strip are obtained.

A comparison is made with values of the transmission coefficients found previously and by the present method. It appears that this theory provides accurate information when the slit-width is greater than about a wavelength.

* This work was sponsored by Rome Air Dev. Center of the Air Res. and Dev. Command under Contract AF 30(602)-1762.

† The research in this document was supported jointly by the Army, Navy, and Air Force under contract with Mass. Inst. Tech.

‡ S. F. Singer, "A new model of magnetic storms and aurorae," *Trans. Am. Geophys. Union*, vol. 38, pp. 175–190; 1957.

* Supported in part under Contract Nonr 225 (27) and Contract AF 18(603)-126.

Properties of Long Slots in a Parallel-Plate Transmission Line—A. J. Simmons, *Technical Research Group, Cambridge, Mass.*—An array of many-wavelength-long slots cut in the top wall of a parallel-plate transmission line makes a potentially useful microwave radiator. As a first step in the design of such arrays, the theory has been worked out of a single infinitely long slot, cut in the top wall of a pair of infinite parallel plates, perpendicular to the direction of propagation of a TEM wave between the plates. The scattering matrix of the slot has been derived using an integral-equation variational method, which gives expressions involving the unknown electric field across the slot. A first-order assumption about this electric field permits calculation of the scattering coefficients, the results being invariant, to first order, to deviations of the assumed field from the actual field.

It is found that the radiation from the single slot can be controlled by varying slot width, d, plate spacing, a, and the dielectric constant of the material between the plates.

The theory may be easily generalized to the case of slots cutting the top plate at an angle α to the direction of propagation by substituting $\lambda \csc \alpha$ for λ in the theory. In this form the theory may be checked experimentally by measurements in rectangular waveguide. A slot is cut across the full width of the top wall of the waveguide and the waveguide side walls extended upward to form imaging planes. Precision measurements were made of the scattering matrices of some of the slots, using DesChamps' shorted-line method. Good agreement with the theory was obtained for values of slot width up to about quarter wavelength, which appears therefore to be the limiting value of d for which the approximations used in the theory apply.

The theory for single slots may be readily extended to include two narrow slots. The same equations are used but the values of field assumed across the region of the slots is that proper to two slots. A preliminary result gives the scattering matrix for the pair of slots; the terms involving mutual coupling may be readily separated out.

Propagation of Electromagnetic Waves in a Semi-Infinite, Flanged, Co-Axial Line with an Infinite Center Conductor—V. M. Papadopoulos, *Brown University, Providence, R. I.*—A solution is obtained for the problem of the propagation of electromagnetic waves in a semi-infinite, flanged, coaxial line with an infinite center conductor, in terms of an infinite set of coefficients which are determined by an infinite set of equations. The solution is discussed, in detail, in limiting cases which illustrate properties of a thin vertical antenna on a plane, perfectly conducting earth, and of a thick antenna fed by a low impedance line. The possibility of a solution for any excitation frequency also is discussed.

Radiation Field of an Elliptical Helical Antenna—J. Y. Wong and S. C. Loh, *National Research Council, Ottawa, Ont., Can.*—Rigorous expressions for the radiation field of a helical antenna of elliptical shape are derived on the assumption of a traveling-wave type of current distribution along the helix conductor. The analysis is valid for integral and nonintegral number of turns. These expressions for the general helix are employed to determine the fields for the limiting case of a circular helical antenna. The results are essentially the same as those derived by both Knudsen and Kornhauser. Allowing the ellipse to degenerate to the other limiting case, a solution for the radiation field is obtained for the planar or commonly known zig-zag antenna. Calculations are included to illustrate some of the salient features for each of the three cases considered.

Generalization of the Dolph-Tchebycheff Method—C. Schensted, *University of Michigan*—In the design of broadside and end-fire linear arrays, one can use the Dolph-Tchebycheff method or one of its modifications to obtain the minimum sidelobe level for a given beamwidth. In this paper this method is extended to much more general problems, such as arbitrary space arrays, arrays in which each element has a different radiation pattern from each other element, etc. Since the problem is so much more general, the results obtained are less specific. Once the direction of the sidelobe is obtained, the excitation coefficients are given explicitly. A rapidly convergent iterative process for determining the direction of the sidelobe is given.

Extension of Theory of Thin Wire Loop Antenna in Air and with a Spherical Ferrite Core—J. Herman, *Diamond Ordnance Fuze Laboratory, Washington, D. C.*—Complete and rigorous equations for the fields, input impedance, and radiated power and efficiency of a thin wire loop antenna in air and with a spherical ferrite core have been previously reported in DOFL Report TR-462. The solutions were based upon the assumption of a perfect conductor or zero internal impedance. They were expressed as independent families of TE and TM waves, each wave contributing to the over-all antenna characteristics.

The theory has been extended to the case of finite distributed internal impedance, and lumped internal impedances placed anywhere in the loop. Upon expressing the input admittance, input power, and radiated power as the sum of individual contributions from each current component summed over all wave modes, where the current has been derived in the form of a Fourier series in the ϕ coordinate, it is found that various desirable characteristics can be designed into the antenna. They are traveling-wave antenna, wide latitude in "tailoring" of input impedance, optimization of radiation efficiency with a lossy ferrite core, possibility of gain, directionality, and broad banding, and ability to deliver and radiate high power. These characteristics are obtainable irrespective of the electrical size of the loop. It is felt that the theory can have widespread application to practical antenna problems.

Frequency Conversion by Regenerative Modulation—D. M. Makow, *National Research Council, Radio and Electrical Engineering Division, Ottawa, Ont., Can.*—A feedback system is considered using three mixers $M1$, $M2$, and $M3$. An external input frequency f_1 and an internally generated frequency f_2 produce in $M1$ the difference $f_1-f_2=f_3$ which is applied to $M2$ and $M3$. Also, f_2 is applied to $M2$ which then generates f_1. This frequency in turn is fed to $M3$ and f_2 is obtained as a difference of f_1 and f_3. The frequency f_2 closes the loop providing the originally assumed inputs to $M1$ and $M2$. The output frequency of $M2$ is identical with f_1, while f_2 is determined by the zero-phase shift condition in the oscillatory loop formed by the branches connecting $M2$ and $M3$.

In a converter where f_3 is chosen much smaller than f_1 and f_2, f_3 can be thought to be the IF and f_2 the LO frequency. When certain design requirements are fulfilled, variations in the input frequency f_1 do not greatly affect f_3 or f_2. Also, an improvement in the stability of f_2 due to drifts in the circuit elements can be shown to be possible.

Canadian Standard of Frequency—S. N. Kalra, *National Research Council, Division of Applied Physics, Ottawa, Can.*, C. F. Pattenson, *National Research Council, Division of Radio and Electrical Engineering, Ottawa, Can.*, and M. M. Thomson, *Dominion Observatory, Division of Positional Astronomy, Ottawa, Can.*—Over the past three years, a frequency standard of very high precision has been installed in Canada. It is composed of equipment located in three different laboratories at Ottawa, Ontario, but separated by a few miles. Intercomparisons of frequency between these laboratories, which are done by sending signals over telephone lines and related techniques, are described briefly. Results indicate frequency stability of about $2:10^{10}$ over short and long periods. Absolute frequency is determined from astronomical observations. International intercomparison is carried out by phase measurement of standard frequency and by observations of time signals; some of the results are presented. A cesium-beam type of standard is under development and its progress is reported.

An Application of the Quasi—Peak Circuit to the Measurement of Probability Density Function—K. Yacoub, *The Moore School of Engineering, University of Pennsylvania*—Present-day noise meters are often equipped with a weighted detector called a quasipeak detector, whose output is within certain limits a function of the probability distribution of the applied voltage and the circuit time constants. This result is developed further, enabling procedures to be specified for converting quasipeak measurements into probability distribution function and vice versa. The former will require a variable time constant to obtain the result.

Examples of the application of these procedures are given. Direct application of quasipeak measurements to estimating error probabilities in some communication systems where, heretofore, the distribution function has had to be used is discussed.

In addition, a relation between detector measurements and distribution function is obtained by a different approach. Noting that noise passing through an infinitesimal bandwidth system has an output with a Gaussian distribution, for a finite bandwidth the output in general departs from the Gaussian distribution. This paper discusses this departure by making use of the Edgeworth series, whose coefficients involve the higher order moments of the random function. These moments are implied by appropriate weighted detector measurements; a procedure for finding the coeffi-

cients to a convenient accuracy using such measurements is described.

Improvement of Accuracy of Field Strength Meters at VHF and UHF—W. K. Roberts, *Laboratory Division, Office of Chief Engineer, Federal Communications Commission, Laurel, Md.*—VHF and UHF field strength measuring instruments commonly employ half-wave resonant dipole antennas, often in close proximity to various forms of balun devices which couple the antennas to the associated transmission lines. Calibration data furnished by the manufacturers may be based on theoretical assumptions as to antenna gain and impedance, balun performance, and the impedance match at the receiver input connector. This paper presents measurements of these characteristics of two commercial field strength meters in current use, and discusses measurement errors which may be avoided by taking into account the differences between actual and theoretical conditions. A new wide-band balun with an excellent impedance-transforming characteristic over at least a two-to-one frequency band is described.

Status Report CN NH_3 Maser Oscillator—S. Hopfer, *Polytechnic Research and Development Co., Inc., Brooklyn, N. Y.*—The present state of the art of NH_3 Maser oscillators is reviewed, starting with a presentation of the theory of the NH_3 Maser oscillator, its stability, and settability. Advantages derived from the use of $N^{15}H_3$ as well as others obtained by employing multicavity systems are discussed. Criteria for the optimum design of the various Maser components such as the beam forming assembly, the focuser, and the cavity are established and available performance characteristics of the various components presented. Special emphasis is placed on recent developments at the Polytechnic Research and Development Co. which have resulted in a truly sealed off Maser system.

A Wave Propagation Simulator—F. J. Tischer, *Department of Electrical Engineering, Ohio State University*—An electromechanical analog system is described for the simulation of wave propagation in statically magnetized ferrite material. Relations are derived which show the analogies mathematically. Phenomena such as the Faraday effect and nonreciprocal wave propagation a.o. can be simulated. Photographically recorded results are shown.

Twin-Feed Diversity Studies in Beyond-the-Horizon Propagation*—W. H. Kummer, *Bell Telephone Laboratories, Inc., Holmdel, N. J.*—This paper describes the characteristics of the signals received simultaneously by two adjacent feed horns on a high-gain paraboloid used in a 171-mile path beyond-the-horizon experimental circuit.

Two sets of experiments were conducted: in one, the feed horns were spaced horizontally so that each feed received the same median signal level; in the other, the feeds were placed one on top of the other, the upper feed being oriented to receive the maximum median signal. The experiments were conducted at both 460 mc and 4110 mc.

The theoretical diversity improvement was maintained substantially all the time at 4 kmc for both feed placements and at 460 mc for the vertical placement. For horizontal positioning of the horns at 460 mc, the diversity improvement was primarily a function of the fading rate.

The results are discussed with relation to fading rate, signal level, and structure of the atmosphere.

A Beam Swinging Experiment on a Short Tropospheric Path—A. W. Adey, W. J. Heikkila, C. A. May and S. Penstone, *Defence Research Telecommunications Establishment, Defence Research Board, Ottawa, Ont., Can.*—Equipment has been set up for a beam swinging experiment at 9400 mc on a 3.2 mile path. Two-foot parabolic reflectors are used, with beam widths of 4 degrees. An auxiliary link, excited by the same transmitter, provides a controlled reference signal for synchronous detection. The 4-degree antennas can be swung off the axis in both vertical and horizontal directions, to permit the study of atmospheric scattering over a wide range of scattering angles. The energy scattered in the common volume of the antenna beams can be separated from scattering occurring elsewhere in space, *e.g.*, on the reference link, on the basis of the Doppler shift in frequency due to the drift of the scatterers. The parameters of the system are such as to permit observation of scattering cross sections of 10^{-15} sq. cm/cm^3 or greater. Initial studies of scattering have been made, and further results will be reported, as available.

A Rapid Beam-Swinging Experiment—A. T. Waterman, Jr., *Stanford Electronics Laboratories, Stanford University*—Narrow beam antennas have been used very effectively as devices for probing the atmosphere in transhorizon propagation experiments. The unmanageable nature of the large physical structure required for a narrow beam is largely circumvented if a phased array is used and a mechanism provided for rapid variation of the phase of each radiating element.

The experiment described here utilizes such an array for the receiving antenna. A 3000-mc circularly polarized signal is transmitted, with sufficiently wide beamwidth to illuminate the pertinent portion of the atmosphere. The receiving antenna is a broadside array using for each element an offset section of parabolic reflector and a helical feed. Phase shifting is accomplished by physical rotation of each helix. By rotating the helices at multiple rates, the beam is made to swing in azimuth. Eight elements (each consisting of reflector and feed) are used so that the ratio of the width of a principal maximum (main beam) is six to seven times the interval between successive principal maxima, the width of the over-all pattern being determined by the extent of the array.

Design, construction, and operation of such an eight-element array are described in which a $\frac{1}{2}$-degree beam is swung at the rate of 40 degrees per second and successive beams pass through the great-circle bearing each tenth second. Thus the atmosphere is probed in rapid succession, so that beam-distorting effects can be studied in detail and their changes with time observed.

Tropospheric Refraction of Radio Waves at Low Angles to the Horizon*—J. R. Bauer, F. A. Wilson and W. C. Mason, *Lincoln Laboratory, Massachusetts Institute of Technology*—As a consequence of variations in the dependence of radio refractive index with height, $n(z)$, the heights of radio scatterers in the atmosphere (for which apparent slant range R and elevation ϵ_0 are specified) are known to fluctuate. The effect of these fluctuations is to render uncertain the heights of radar targets, stratified layers, turbulent blobs, and other dielectric irregularities. The fluctuations in height are naturally greatest and most troublesome at those low elevation angles of central interest in initial radar detection and scatter communications.

The integral

$$R[h_s, \epsilon_0, n(z)] = \int_0^{h_s} \left\{ 1 - \left[\frac{n(0)\cos\epsilon_0}{n(z)\left(1+\frac{z}{r_0}\right)} \right]^2 \right\}^{-0.12} n(z)dz,$$

which exactly relates the true height h_s of the scatterer with R, ϵ_0, and $n(z)$ in an assumed nondispersive spherically stratified atmosphere, has been evaluated by machine techniques for 353 refractive index soundings of the troposphere made at Riverhead, N. Y., throughout a full seasonal cycle. The results of this investigation are described in the form of probability curves for scattering heights and elevation angles of arrival in the height region 500–100,000 feet and angle region 0–4–$\frac{1}{2}$ degrees, respectively, at fixed slant ranges between 25 and 350 nautical miles. Diurnal and seasonal effects are noted.

Computation of Atmospheric Refraction by Ray-Tracing, and Comparison with Observed Results—W. L. Anderson, *University of New Mexico*, N. J. Beyers, *Missile Geophysics Division, White Sands Signal Agency, White Sands Proving Grounds, N. M.*, and B. M. Fannin, *University of New Mexico*—Ray tracing methods have been applied in the computation of atmospheric refraction at the White Sands Proving Grounds, N. M., for a range of approximately 54 miles and an elevation angle of about 15 mils. Good correlation between observed and computed angles is obtained.

Meteorological data consisted of surface observations, radiosonde, refractometer flight observations, and wiresonde. These normally were not all available on any one date, and were usually taken near the radar site only. The usual assumption of a horizontally stratified atmosphere has been made.

Radar observations were made in the X band, with a quoted accuracy of 0.25 mil or better. Day-to-day observed elevation angle varied over a range of about 1.7 mils, with rms deviation from mean of 0.34 mil. The rms deviation of computed from observed angles, to date, is in the range 0.17 to 0.37 mil, depending on the completeness of meteorological information used in preparing the refractive index profiles.

In comparing observed and computed results, a correlation coefficient of 0.95 was

* This work was supported in part by Contract AF 18(600)-572 with the U. S. Air Force, Air Res. and Dev. Command.

* The research in this paper was supported jointly by the U. S. Army, Navy, and Air Force under contract with Mass. Inst. Tech.

obtained when the best meteorological information was used, and 0.74 when all data were used. It is concluded that ray-tracing methods are reliable at this elevation angle, and that the assumption of horizontal stratification is quite valid in this locality.

Measurement of Atmospheric Humidity Fluctuations by the Attenuation of Lyman Alpha Radiation—J. M. Bologna, O. K. Lorison, D. L. Randall and D. L. Ringwalt, *U. S. Naval Research Laboratory*—The pure Lyman Alpha (1216.7A) line of hydrogen radiation is attenuated at the rate of 1700 db/cm in water vapor at NTP, and is relatively unaffected by other atmospheric constituents. Accordingly, a hygrometer consisting of a low pressure hydrogen glow tube illuminating an ultraviolet-senstitive NO photon counter across a short air gap appears promising as a light, swiftly responding humidity element for airborne and balloon-borne measurements. A developmental ultraviolet hygrometer has been assembled and flown in the NRL Flying Laboratory in the Florida/Nassau propagation link. The resulting humidity indications appeared to correspond well with the simultaneous refractive index as measured with a Texas refractometer. The ultraviolet hygrometer used in the measurements is described and the results given in detail. Only through the original development of the NO counter tubes by the Optics Division of NRL, and the division's continued assistance, has this work been possible.

Propagation at 36,000 MC in the Los Angeles Basin—W. L. Flock, R. C. Mackey and W. D. Hershberger, *Department of Engineering, University of California, Los Angeles*—A propagation study has been conducted at a frequency of approximately 36,000 mc, over a 11.4 mile path, in the Los Angeles basin. The basin is characterized by the presence of the persistent, low-level temperature inversion of the eastern edge of the Pacific anticyclone, and it is this temperature inversion which is responsible for the trapping of atmospheric pollutants. The index of refraction profile associated with the temperature inversion strongly influences propagation over the nearly horizontal, line-of-sight path. Large amplitudes of fading may occur when the elevation of the temperature inversion is near that of the transmitting and receiving antennas. Diurnal variations in the temperature inversion strength, height, and degree of tilting and corresponding diurnal variations in fading are observed.

The propagation mechanisms which may influence the signal variations include refraction, reflection, and scattering. The refraction mechanism more clearly indicates large amplitudes of fading, over a larger range of elevation of the inversion layer, than do the reflection or scattering mechanisms.

No positive indication of the effect of air pollutants has been observed, but it is shown that appropriately located microwave links provide information about index of refraction profiles and associated meteorological conditions. In particular, microwave links can indicate the proximity of temperature inversion layers when the inversion is accompanied by a sufficient variation in water vapor content.

Some Results from an Over-water Tropospheric Propagation Study—M. H. Latour, N. E. Rosier and W. F. Zetrouer, *Electrical Engineering Department, University of Florida*—Under ONR sponsorship, the University of Florida Engineering and Industrial Experiment Station has been operating an overwater forward scatter link at 1262 mc with the transmitter at Cape Canaveral, Fla., and the receiver located on New Providence Island, Bahamas. The path length is 260 nautical miles. Pulse transmission is employed; the received signal is sampled by automatic level sorting and read-out equipment. Distributions are printed out every five minutes, from which the median, 90 per cent and 10 per cent signal levels are plotted. Available meteorological data over the path are reduced for study in connection with variations in signal level.

On several occasions, continuous data were obtained for periods of several days. During these times refractometer soundings were taken frequently at several points along the path.

The data obtained are presented to show the variation of signal level, fluctuation rate, and the signal distribution as a function of the meteorology of the path.

Forward Scattering by Reflection from Meteor Trails of a UHF Signal over a 830 Mile Path*—M. Loewenthal, A. Teachman, L. P. Rainville, J. N. Pinkerton, W. J. Jones and H. H. Hoover, *Lincoln Laboratory, Massachusetts Institute of Technology*—Further results are reported for the scattering by reflections from meteor trails of a 412-mc signal over the 830-mile path between the M.I.T. field stations at Round Hill, Mass., and Elberton, Ga. Since the preliminary description previously given, considerably more data has been obtained. In addition the transmitting antenna assembly has been modified. Instead of employing the steerable az-el 60-foot parabolic dish, a fixed 60-foot parabola with multiple horn feeds has been erected. Any of the three horns may be used to feed the 40-kw signal by means of two high power switches. In the normal operation the beam is switched either side of the great circle path every fifteen minutes. At the receiving end, multiple feeds are used with a duplicate pair of sensitive narrow-band receivers and high speed recorders. Measurements of the antenna patterns of the receiving antenna system, made with the aid of a helicopter operated by the Air Force, are described. Various studies have been made of the path geometry and its effects on the expected rates. (Among these are some calculations by the group at the Experimental Field Station of the Georgia Institute of Technology.) Some future modifications of the system which are in progress are discussed.

A Theoretical Basis for Computing the Signal Rate in Meteor-Scatter Communication†—M. L. Meeks, *Georgia Institute of Technology*—An empirical distribution of sporadic meteor radiants is used as a basis for predicting the meteor-signal rates observed over forward-scatter radio links. For analysis, the smooth sporadic radiant distribution is replaced by various patterns composed of a number of discrete radiant points. The effect of each discrete radiant point is computed separately for the particular forward-scatter link under consideration, and the results are summed over the radiant points chosen to represent the empirical distribution. The relationship between the quantitative predictions of this approach and the number of discrete radiant points that are used is examined. The results are presented so that the problem of optimum antenna illumination can be studied.

A Comparison between Observed and Computed Meteor Signal Rates for Various Forward-Scatter Links*—J. C. James, *Georgia Institute of Technology*—The diurnal pattern of the meteor-signal rate observed over various forward-scatter radio links at various times of year are compared with predicted rates calculated on the basis of an approximate model of the empirical sporadic-radiant distribution. The forward-scatter data for which this comparison is made include published data for the Greenwood, Nova Scotia–Ottawa, Ont., Can., link and recently measured data for links between Boston, Mass., and Columbia, S. C.; between Boston, and Atlanta, Ga.; and between Knoxville, Tenn., and Atlanta, Ga. Generally good agreement is found between the mean observed rates and the calculated rates for various seasons and times of day.

The Geminid shower (1957) and the Quadrantid shower (1958) were observed on the Knoxville–Atlanta link, and a comparison is also made between calculated and observed signal rates for these showers.

An Experimental Study of Meteor Echoes at 200 MC—J. L. Heritage, S. Weisbrod and W. Fay, *Smyth Research Associates, San Diego, Calif.*—Using as source a high-power 200-mc transmitter with a high gain antenna, two portable receiving stations took simultaneous records of ionospheric forward scatter signals at locations on either side of the great circle path. Meteor bursts predominated, but occasional long lasting signals were observed, resembling sporadic *E* transmissions at low frequencies.

Six receiving sites were occupied, ranging from on the great circle to 40 degrees off the great circle. The transmission path was not symmetrical in that the distance from the *E*-layer "hotspot" to the transmitter was 850 km and to the receivers was 450 km. A comparison is made of the diurnal signal burst rate obtained at the several forward scatter sites and at the transmitter by backscatter. Some of the characteristic signal burst shapes are shown and discussed.

VHF Signal Level Measurements Along a 2000 Mile Path†—W. G. Abel, *Lincoln Laboratory, Massachusetts Institute of Technology*, A. S. Orange, *Massachusetts Institute of Technology and Air Force Cambridge Research Center* and T. F. Rogers, *Air Force Cambridge Research Center*—Signal level measurements at 50 mc were made in an aircraft flying at altitudes of 5000, 15,000, and

* The research in this paper was supported jointly by the U. S. Army, Navy, and Air Force under contract with Mass. Inst. Tech.

† This research was supported jointly by the Office of Naval Research and the Air Force Cambridge Research Center.

* This research was supported jointly by the Office of Naval Research and the AF Cambridge Res. Center.

† The research in this paper was supported jointly by the U. S. Army, Navy, and Air Force under contract with Mass. Inst. Tech.

25,000 feet over a great circle path out to a distance of 2000 miles from the transmitter. Flights were so scheduled that the aircraft reached the furthermost range at the time of day for either diurnal signal level maximum, diurnal signal level minimum or maximum meteor activity. Analysis of data has yielded information on the extent of the line-of-sight, diffraction, tropospheric scatter, tropospheric-to-ionospheric scatter transition, and ionospheric scatter regions. Signal level attenuation rates in the various regions and variation of fading rates with range were measured also. Some information on the frequency of occurrence of signal level enhancements due to reflections from ionized meteor trails was obtained.

The Influence of Continuous Meteoric Scattering on Long Distance VHF Communication Circuit Design—T. F. Rogers, *Air Force Cambridge Research Center*—Recent studies, including the experimental demonstration by Pineo that *E*-region scattering from off-path meteoric-induced ionization is the predominant mode of very long distance VHF propagation (at least for mid-latitudes)* make it important to reassess certain factors upon which the early design of ionospheric scatter communication circuits was based. In particular, with reference to data obtained using narrow beam antennas, it must now be appreciated that: 1) published values of path loss relative to the inverse distance squared attenuation† can imply much too high a transmission loss for wide angle antennas, 2) a major portion of the received signal level variation[2] is caused by departures from on-axis plane wave antenna gain rather than variations in wide angle scattered flux density, and 3) the space correlation coefficients measured by Sugar‡ are probably not (as he surmised) truly representative of the wide angle scattering mechanism. Consideration of these antenna propagation interactions in the design of antenna systems, and of certain other (technical) factors, encourages the prospect that communication circuits now can be designed to yield a much higher capacity-reliability product per radiated watt, and some relaxation in the requirement for spacious antenna sites.

50-MC Oblique Transmission Experiment Near the Magnetic Equator—R. S. Cohen and K. L. Bowles, *National Bureau of Standards, Boulder Laboratories*—The National Bureau of Standards is conducting an IGY experiment studying oblique transmission effects near 50 mc in the region of South America near the magnetic equator. Several paths similar to the Cedar Rapids-Sterling experiment, in length and instrumentation, have midpoints covering a zone centered on the magnetic equator near Huancayo. The spread of this zone is about 10 degrees of latitude and about 5 degrees of longitude. Another path, 2580 km long, with rhombic antennas directed at a zone above the horizon cut-off at 120 km, and centered on the magnetic equator, is also in operation. Interpretation of the observations during December, 1957, and January, 1958, leads to the following statements.

Daytime records over these paths are predominantly characterized by a trace representing a Rayleigh fading signal with a fading rate of several cycles per second. Onsets and occasional weakening of this trace, giving way to the kind of trace found on medium latitude paths with the same equipment, correlate in detail nearly 100 per cent of the time with similar onsets and diminutions of Equatorial *Es* observed on the C4 ionospheric sounder at Huancayo. During an appreciable percentage of the daytime hours variations of the median level of this characteristic trace correlate in detail on all six paths observed. When this is true, the variations of intensity of the H component of the terrestrial magnetic field correlate well with the variations of the radio field strength. These, and other features of the oblique path experiment, help to define the relation between Equatorial *Es* and the Equatorial Electrojet.

Nighttime records on the 2580-km path differ from the daytime records in that they rarely correlate in detail with those from the shorter paths. Some evidence has been found for associating enhanced nighttime signal strengths on the long path with Equatorial Spread *F* conditions observed with the C4 at Huancayo. Since the long path oblique scattering probably occurs somewhere in the height region 130 to 200 km, these results provide support for the belief that Equatorial Spread *F* may be due to scattering in that region.

Leaky Wave Contributions to Field of a Magnetic Line Source Above a Dielectric Slab—S. Barone, *Harvard University, Cambridge, Mass.; formerly at Polytechnic Institute of Brooklyn* and A. Hessel, *Microwave Research Institute, Polytechnic Institute of Brooklyn*—The asymptotic evaluation of the far field of a magnetic line source placed above and parallel to a grounded infinite dielectric slab is ordinarily expressed as the sum of a space wave plus surface waves. A more careful asymptotic evaluation indicates that leaky waves are present and should also be taken into account. These leaky waves are not discrete modes, as are surface waves, but are a portion of the continuous spectrum. Some of their characteristic features will be discussed. Because of their rapid decay with distance, these leaky waves do not contribute significantly to the total far field in the case of usual dielectric slab antennas; however, under certain circumstances, their contribution cannot be neglected. These conclusions are borne out by numerical calculations for a polystyrene slab.

Reflection and Transmission by a Class of Curved Dielectric Layers*—S. N. Karp, *Division of Electromagnetic Research, Institute of Mathematical Sciences, New York University*—The authors consider the reflection and transmission of electromagnetic waves by a special class of curved dielectric layers. The layers in question are bounded by two nonintersecting confocal parabolas, and between these boundaries, the dielectric constant, which may be complex, has a special form of space dependence. It is found that layers of this type have striking properties. If a plane wave is normally incident on such a layer, from the convex side, then the reflected field can be expressed as a product of two factors. The first factor is the field which would be reflected by a conducting parabola coincident with the surface of the layer. The second factor has no space dependence; it depends only upon the spacing of the shell boundaries, the frequency, and the special choice of dielectric constant. The transmitted wave has an especially simple form: it is a plane wave. The configuration thus has properties similar to those of a plane dielectric slab. In fact, the plane slab is a limiting case of the geometry we have described.

Two-Dimensional Model for Evaluation of Radome Analysis Approximations*—A. D. Jacobson, *Microwave Laboratory, Hughes Aircraft Co.*—Several methods in common use for analyzing antenna-radome errors involve two major assumptions: 1) The electric field that exists in the presence of the radome on a surface lying between the antenna and the radome can be approximated by the electric field measured over the surface in the absence of the radome, 2) the interior field can be transmitted through the radome wall using plane-wave-plane sheet transmission coefficients. The validity of these assumptions is evaluated by employing them to determine the field of a two-dimensional model consisting of offset electric and magnetic current line sources enclosed by circular cylindrical dielectric shell, all of infinite extent and comparing the results to the exact far field of this system. The exact far field is found by conventional boundary-value analysis. Comparison of the results indicates that both approximations, and, therefore, the quality of the approximate technique, are highly dependent on the intensity of the radome-antenna interaction. It is also shown that the intensity of the interaction increases as the sources approach the shell wall.

TE_{no} Surface Waves at a Ferrite Air Interface—A. D. Bresler, *Microwave Research Institute, Polytechnic Institute of Brooklyn*—It is shown that TE_{no} surface waves are guided along a plane interface separating two regions of a parallel plate waveguide, one empty, one filled with a lossless ferrite magnetized parallel to the interface and normal to the conducting plates. These surface waves represent a true surface phenomenon in that the fields decay exponentially away from both sides of the interface. The propagation constants of these surface waves are determined by an algebraic secular equation, the solutions of which are examined as functions of frequency, saturation magnetization, and dc magnetic field. It is found that two oppositely directed surface waves are guided along the interface. These two surface waves exist in different

* Bowles, *Ann. IGY*, vol. 3, pt. 4, p. 346; 1957.
L. A. Manning and V. R. Eshleman, *J. Geophys. Res.*, vol. 62, p. 367; September, 1957.

† D. K. Bailey, R. Bateman and R. C. Kirby, "Radio transmission at UHF by scattering and other processes in the lower ionosphere," PROC. IRE, vol. 43, pp. 1181–1231; October, 1955.
R. C. Kirby, "VHF propagation by ionospheric scattering—a survey of experimental results," IRE TRANS. ON COMMUNICATIONS SYSTEMS, vol. CS-4, pp. 17–27; March, 1956.

‡ G. R. Sugar, "Some fading characteristics of regular VHF ionospheric propagation," PROC. IRE, vol. 43, pp. 1432–1436; October, 1955.

* The research reported in this document has been sponsored by the AF Cambridge Res. Center, Air Res. and Dev. Command, under Contract No. AF 19(604)-1717

* This work has been partially supported by Wright Air Dev. Command, USAF, under Contract No. AF 33-038-28634.

finite ranges of the parameter values, which ranges may or may not overlap. Since these results are essentially unaffected by the introduction of conducting boundaries, they are employed in a discussion of that propagating mode of a slab-loaded rectangular waveguide which corresponds to the surface waves of the parallel plate structure. An examination of the power flow associated with the propagating modes of the rectangular waveguide structure reveals that the direction of power flow changes only at the poles of the derivative of the propagation constant. This result is then employed to show that the anomalous situation wherein there exists only a single propagating mode transporting power in only one direction is associated only with the surface wave mode referred to above.

The Application of the Reaction Concept to Cavities and Waveguides*—R. G. Kouyoumjian, *Electrical Engineering Department, The Ohio State University, Columbus, Ohio*—The reaction† is a quantity defined so that it may be used to express the reciprocity between a pair of electromagnetic sources. Since the stationary expressions for parameters such as impedance, scattering cross section, and frequency must satisfy the reciprocity theorem, it is convenient to use the reaction in deriving these expressions. In this presentation the reaction concept is used to obtain stationary expressions for the cavity resonant angular frequency ω and the waveguide propagation constant γ. If the total field in the cavity is used, a stationary expression for ω results; on the other hand, if the total field is considered as the superposition of two properly chosen fields, an expression for $\omega^2-\omega_0^2$ is obtained, where ω_0^2 is the known value for an empty or unperturbed cavity. Stationary expressions for γ and $\gamma^2-\gamma_0^2$ may also be derived in a similar fashion for the uniform waveguide. It is shown that these results can be extended to cavities and waveguides loaded with nonreciprocal media. This extension is particularly simple in the case of lossless gyrotropic media. The paper emphasizes the fact that a variety of stationary expressions appropriate for different problems may be obtained in a relatively-simple straightforward manner from a single quantity, the reaction.

On the Attenuation of Guided Waves in the Limit of High Frequencies—C. H. Papas, *California Institute of Technology, Pasadena, Calif.*—In the case of a lossy waveguide the first-order approximations employed in the computation of the attenuation constant due to wall losses cease to be valid at frequencies very large compared with the cut-off frequency.‡

It is the purpose of this paper to show that, contrary to the result of the first-order theory, the attenuation constant at very high frequencies reverses its upward trend and falls to zero with increasing frequency. The bearing that this new result has on the behavior of cavity resonators in the limit of high frequencies is discussed.

* This research was sponsored in part by the U. S. Army, Evans Signal Lab., Belmar, N. J.

† V. H. Rumsey, "Reaction concept in electromagnetic theory," *Phys. Rev.*, vol. 94, pp. 1483–1491; June, 1954; vol. 95, p. 1705; September, 1954.

‡ See, *e.g.*, F. E. Borgnis and C. H. Papas, "Encyclopedia of Physics," Springer-Verlag, Berlin, Ger., vol. 16, p. 310.

Magnified and Squared VSWR Responses in Microwave Impedance Measurements—R. W. Beatty, *National Bureau of Standards, Boulder Laboratories*—Starting with the analysis of MacPherson and Kerns of a 3-arm junction used in measuring the impedance of phasable loads, it is shown how it is possible to obtain magnified and squared VSWR responses using certain types of junction. These responses are of value in obtaining increased accuracy in the measurement of intermediate and small VSWR, and permit more accurate recognition of the minimum reflection condition when tuning or matching microwave systems.

Various types of suitable junctions are described and techniques for the accurate measurement of VSWR and reflection coefficient are developed. The accuracy of these techniques is discussed and observed data are presented.

The measurement of nonphasable loads by use of a line stretcher is discussed, and the design of suitable line stretchers is discussed and illustrated.

A Refined *X*-Band Microwave Microcalorimeter—G. F. Engen, *National Bureau of Standards, Boulder Laboratories*—The microcalorimetric method for evaluation of the efficiency and substitution error of a bolometer mount proposed by MacPherson and Kerns has been the object of further study and refinement at the Boulder Laboratories of the National Bureau of Standards, and an improved instrument based on this technique has been recently placed in operation.

The new microcalorimeter design features: 1) greatly improved ambient temperature control, permitting higher sensitivity and resolution, 2) improved dc instrumentation, 3) improved mechanical construction giving better repeatability, 4) relocation of the thermopile such that it is no longer attached directly to the bolometer mount, thus providing flexibility in the choice of termination, and 5) a more comprehensive treatment of this calorimetric substitution or equivalence error. These features permit the determination of the effective efficiency of a bolometer mount to an accuracy of better than 0.5 per cent.

A Bolometer Mount Efficiency Measurement Technique—G. F. Engen, *National Bureau of Standards, Boulder Laboratories*—The impedance method of measuring bolometer mount efficiency proposed by Kerns is one of the few basic techniques developed thus far for determining this parameter. As originally proposed, the accuracy which could be achieved was rather severely limited by the state of the impedance measuring art, and this led in turn to the development of a number of modifications of the technique with the objective of improving the over-all accuracy. However, most of these modifications involved mathematical approximations and restrictions in the generality of the method, and none of them has, thus far, come into widespread use.

Another variation of the impedance method has been recently proposed at the Boulder Laboratories of the National Bureau of Standards employing directional coupler techniques, which provides improved accuracy and simplified operational procedures, but unlike the earlier modifications, involves neither mathematical approximations nor restrictions in the generality. A particularly attractive feature of the new method is its independence (for practical purposes) of the impedance discontinuity which may be present at the input connector, which should prove particularly useful in measuring mounts with coaxial inputs. A preliminary implementation of the method in waveguide has given agreement of better than one-half per cent with result obtained by the microcalorimetric method.

Relative Voltmeter for VHF/UHF Signal Generator Attenuator Calibration—B. O. Weinschel, G. U. Sorger, and A. L. Hedrich, *Weinschel Engineering, Kensington, Md.*—A heterodyne type RF voltmeter for voltages in the range from 10 μv to 0.1 v, and in the frequency range of from 100 to 1000 mc is described.

The use of a precision intermediate frequency substitution attenuator allows voltage ratio measurements over a range of greater than 70 db, with an accuracy of 0.3 db without use of any corrections. With proper corrections for systematic errors this error can be reduced to 0.15 db. The system is described briefly, and the design considerations are discussed in detail with particular stress laid on those considerations most affecting the accuracy of the equipment.

Mixer linearity with methods of measurement, and accuracy of the piston attenuator law, are covered in detail.

The effect of each of these components and the possible errors contributed by each are discussed.

Half-Round Inductive Obstacles in Rectangular Waveguide as Standards of Impedance—D. M. Kerns, *National Bureau of Standards, Boulder Laboratories*—Accurate values have been calculated for the lowest-mode lumped-element representation of perfectly conducting half-round inductive obstacles in rectangular waveguide. These obstacles consist of either one or two opposed semicircular cyclindrical indentations extending across the narrow sides of the waveguide and seem especially suitable for use as independent, absolute standards of reflection or waveguide impedance. They can be fabricated by electroforming or by machining, do not require unduly close tolerances, and avoid a change in waveguide cross section.

Well known methods were used to obtain stationary expressions for the desired reactance elements as functionals of the obstacle currents. The Rayleigh-Ritz process, with one-term, two-term, and three-term Fourier expansions for the obstacle current as an "extremalizing" sequence, yielded rapidly convergent numerical results. A high-speed digital computer was used. Accuracy of the results is estimated at five figures or better for matched-termination VSWR's up to three; results are provided for $1.2<f/f_c<1.85$, where f is the operating frequency and f_c is the waveguide cutoff frequency.

A Recording Microwave Hygrometer*—C. M. Crain, *The Rand Corp., Santa Monica, Calif.*, J. B. Magee, *Tempco Aircraft, Dallas,*

* The development of this device at the University of Texas was sponsored by the Wright Air Dev. Center under Contract AF 33(616)-2842.

Texas, and J. R. Gerhardt, *Electrical Engineering Research Laboratory, University of Texas*—This paper describes a rapid response microwave hygrometer for continuously recording the water vapor pressure of atmospheric air over a wide ambient range. The principle used involves the measurement by means of a cavity resonator of the contribution of water vapor to the refractive index of atmosphere air. Typical results obtained with the instrument and simultaneously obtained temperature and refractive index data are presented. Other possible uses of the instrument such as the continuous measurement of the degree of contamination of one gas (or of gas mixtures) by another gas (or gases) or the contamination of one liquid by another liquid are discussed.

Simplified Method for Computing Knife-Edge Diffraction in the Shadow Region*—L. J. Anderson and L. G. Trolese, *Smyth Research Associates, San Diego, Calif.*—A simplified method of computing knife-edge diffraction in the shadow region is presented which is applicable to most obstacle-gain paths, that is, paths with a dominant mountain obstacle. The method has been worked out for 1) the four-ray model—specular reflection on each side of the obstacle, 2) the two-ray model—reflection on one side only, and 3) the single-ray model—no reflection on either side. The obstacle can be at any location along the path. The accuracy is within 2 db for path geometries such that the usual diffraction parameter v is greater than 1 and the two terminal heights are less than the obstacle height. Curves which further simplify the computation procedure are presented.

Radiometric Measurements at 4.3 Millimeter Wavelengths—C. W. Tolbert, C. O. Britt and A. W. Straiton, *The University of Texas*—This paper describes measurements made at 4.3-mm wavelengths with a Dicke type radiometer of the apparent temperature of some terrestrial materials and the sun. Since the apparent temperature of any object is a function of its reflectivity as well as its emissivity, the radiometric measurements were made as a function of viewing angle and of polarization.

Sky temperatures were measured and found to range from about 120°K at vertical incidence to approximately 300°K near the horizon for clear skies. Cloud coverage caused large increases in the apparent sky temperature.

Observation of the sun showed a temperature range between 10,000 and 12,000 degrees Kelvin based on optical disk size and showed total loss vertically through the atmosphere ranging from 1.6 to 2.3 db.

Apparent temperature measurements of sheet metal, asphalt and gravel roads, corrogated asbestos sheet, and plywood showed considerable variations which may be explained qualitatively by their surface characteristics and the portion of the sky reflected.

Smooth and rough water measurements are also reported. The water surface appeared cooler than all of the other materials except sheet metal and exhibited a temperature of 220°K for smooth water near normal incidence. The effects of the Brewster angle were noted for both smooth and rough surface.

Effects of Rainfall and Anomalous Propagation on Transmission over Short Paths at *X* Band—W. C. Jakes, Jr., *Bell Telephone Laboratories, Inc., Holmdel, N. J.*—During 1956 and 1957 propagation over short (5 to 7 mile) paths was studied in the 9–11 kmc band. The anticipated effects of interest were multipath fading, scattering, and attenuation by rainfall.

Very little fading attributable to multiple paths was observed during a 3-month period in 1956; fading was present about 3 per cent of the total time with the maximum fade about 8 db. In contrast to this, a 22-mile path at 4 kmc showed multiple-path fading 7 per cent of the total time with 40-db maximum fades during the same period.

An effort was made during 1957 to measure the forward scattering of rainfall. Calculations indicated it to be about 40 db below the direct transmission for the particular setup used and measurements did not indicate a level significantly higher than this.

The rainfall attenuation over the 7-mile path at 11.6 kmc was carefully measured and found to agree reasonably well with that predicted from the measured rainfall rate and the theory of Ryde. Distribution curves of rainfall attenuation show rather interesting correlation with average daily rainfall and type of rain; however, the data are probably too meager to warrant firm conclusions.

Reliability of Radio Propagation from 30 to 1000 Megacycles over Line-of-Sight Paths—J. S. Hill, *Hudson, Ohio*, and K. L. Huntley, *Air Force Armament Center, Eglin Field, Fla.*—This study has been conducted over a period of a year on a survey basis at Eglin Air Force Base on the Gulf Coast of Florida. Sampling was done on a 48-hour period basis over each of three line-of-sight paths representing rough terrain, smooth terrain, and overwater conditions. Five frequencies spaced on approximately an octave basis were used.

In the results of the survey a comparison is drawn between the three paths and the five frequencies as to diurnal and seasonal trend. Reliability is evaluated in terms of fadeouts of a duration of one minute or more for depth of fade levels up to 20 db.

The conclusions show that the long term or hour-to-hour fading is influenced more by terrain than path length and is reduced during the daytime. Short term or within-the-hour fading is influenced more by path length than terrain. The diurnal trend shows greater path loss in the daytime.

On the Climatology of Radio Ducts—B. R. Bean, *National Bureau of Standards, Boulder Laboratories*—An atmospheric duct is defined to occur when simple ray theory indicates that the radio ray is traveling parallel to the earth's surface. Three to five years of radiosonde data from locations typical of arctic, temperate, and tropical climates, are analyzed to determine the percentage incidence of ducts for radio rays starting from the earth's surface. Maximum observed incidence is 13 per cent in the tropics, 10 per cent in the arctic, and 5 per cent in the temperate zone. Annual maxima are observed in the winter for the arctic and in the summer for the tropics. The arctic ducts arise from ground based temperature inversions with the ground temperature less than −25°C while the tropical ducts are observed to occur with slight temperature and humidity lapse when the surface temperature is 30°C and greater.

Prediction of VHF, UHF Transmission Loss from an Exponential Model of the Earth's Atmosphere—P. L. Rice, *National Bureau of Standards, Boulder Laboratories*—A new radio standard atmosphere is described, where the radio refractive index decreases exponentially with height instead of linearly. The resulting modifications of previous four-thirds earth forward scattering theory shows much improved agreement with data. Theoretical effects of earth reflection are less frequency sensitive, and the theoretical reduction in realized antenna gain is reduced below previous estimates.

A new theory which allows for the scattering of energy diffracted into the region below the antenna horizons is also described. This theory gives different predictions for rough and smooth earth conditions.

Microwave Diffraction by Terrain Obstacles—F. J. Tischer, *Department of Electrical Engineering, Ohio State University*—Microwave diffraction by terrain obstacles is characterized by the wide range of the ratio of wavelength to obstacle dimensions. Treatment as boundary value problems and calculations by use of Huyghens' principle are discussed. New relations for non-line-of-sight obstacle transmission are presented.

Integral Equations for Long-Wave, Vertical Incidence Ionospheric Propagation and a Method of their Solution*—J. M. Tomlinson, *General Electric Co.; formerly with Ionosphere Research Laboratory, The Pennsylvania State University*—A pair of coupled scalar integral equations are obtained for the horizontal components of the electric field of a time-harmonic plane wave which is propagating vertically in an anisotropic, vertically-inhomogeneous, nonmagnetic stratum. A similar pair of coupled integral equations are obtained for the Forsterling-Rydbeck components of the same plane wave. For the practical cases (*e.g.*, the ionospheric lower *E*-layer *F-R* coupling and reflection regions) in which the stratum is bounded by strata where the *F-R* wave equations are practically uncoupled and WKB, the space derivatives are eliminated from the boundary condition terms in the integral equations.

The integrals are approximated by Simpson's rule to obtain a system of algebraic equations for the values of the components at evenly-spaced points in the stratum. Matrix manipulation almost completely diagonalizes this system, leaving, at the most, only three nonzero subdiagonals on each side of the main diagonal.

For the case of negligible coupling (*e.g.*, the lower *E*-layer *F-R* reflection region) the system of equations separates into two systems, having a matrix with one subdiagonal

* This work was partially supported by the Signal Communications Department, Army Electronic Proving Ground, Fort Huachuca, Ariz.

* The research reported in this paper has been sponsored by the Geophysics Research Directorate of the AF Cambridge Res. Center, Air Res. and Dev. Command, under Contract No. AF 19(604)-1304.

of −1's on each side of the main diagonal, and zero's elsewhere. The final triangularization of this matrix is accomplished with a repetitive-loop digital computer program having only 30 instructions and using only 5 additional words of computer storage, regardless of the matrix size. Computer triangularization of the 5×5, 9×9, 17×17, and 33×33 matrices for an *F-R* reflection region problem which has an exactly-known wave solution yield reflection coefficients which converge to within 0.5 per cent of the correct amplitude and 2° of the correct phase.

Coupling and Polarization Computations Approximated by a Single Discontinuity in the Medium*—J. J. Gibbons and A. J. Ferraro, *Ionosphere Research Laboratory, The Pennsylvania State University*—Following a suggestion by W. Becker that the coupling can be approximated by considering the medium as uniform around the coupling level, the problem has been further simplified by employing a step discontinuity at the N_c level. This gives a quick approximate method for computing the effect of coupling.

Coupling is concentrated by appropriately deforming the *N-h* and *ν-h* curves in a region around the level of N_c; the deformation is done in such a manner that the gradient of electron desnity and collision frequency is zero as one approaches the level of N_c from either below or above. At this level there is then a step discontinuity in the N and ν profiles. WKB solutions are used as the wave functions and the coupling between the ordinary and extraordinary modes is taken into account by solving a boundary value problem at the discontinuity.

Formulas have been developed for the polarization of the upgoing back scattered wave and the downgoing forward scattered wave. Results are compared with those obtained by presumably more accurate methods (Davids and Parkinson†). Even near critical coupling, the approximation gives fairly satisfactory results for the polarization of the main echo at 150 kc.

The Interpretation of Low-Frequency Ionograms—J. M. Watts, *National Bureau of Standards, Boulder Laboratories*—The availability of machine computation of group velocity index has made it possible to understand features of nighttime low-frequency ionograms covering the frequency range 50 kc to 2.0 mc which have no counterpart at high frequencies. The features can be used occasionally to measure the critical frequency of a layer from which no reflections are observed. Also, the total number of electrons below the *F* layer may be estimated by a single measurement from some of the records. The aspect of turbulence in the lower ionosphere as it affects the appearance of low-frequency ionograms is discussed.

Electron-Density-Height Profiles from Routine Ionograms‡—E. R. Schmerling, *Ionosphere Research Laboratory, The Pennsylvania State University*—As part of the IGY effort, a program is underway for the systematic reduction of routine ionograms to electron-density-height profiles by methods which include the effects of the earth's magnetic field, but are nevertheless rapid enough to be applied to many records. These are briefly discussed, and illustrated with examples.

Four stations have been selected for the U. S. program, in such a way that, together with the British program, reasonable coverage of low and medium magnetic latitudes is obtained. This is considered to be a first step towards obtaining world-wide coverage.

Actual profiles are presented, and preliminary interpretations given in terms of physical processes in region *F*.

Ionospheric Drifts Observed at Low Frequencies*—G. Sales, *Ionosphere Research Laboratory, The Pennsylvania State University*—This paper deals with the results of a study made on horizontal drift motions in the lower ionosphere using variations of amplitude pattern on the ground.

Previous work was done on a frequency of 75 kc, with receivers located at the vertices of a right triangle. Now a 60-kc transmitter is used with three receivers located at the vertices of an equilateral triangle with sides of 3 km. Drift velocities are obtained by a method of analysis similar to that proposed by Phillips and Spencer, which takes into account anisotropy at the amplitude pattern and random motions which are superimposed on the steady drift.

The results show diurnal variations and possible connection with solar and lunar tidal effects.

Application of a Method for Rapid Calculation of Group and Phase Heights and Nondeviative Absorption to 75 KC Sunrise Data†—A. C. Aikin and J. J. Gibbons, *Ionosphere Research Laboratory, The Pennsylvania State University*—With tables of the complex phase index $\mu+j\chi$ for a given frequency it is possible to construct curves of the group index as a function of N and ν. Group height, phase height, and nondeviative absorption can then be easily obtained by graphical methods. An atlas of plausible electron density height profiles is prepared with the three desired quantities for several frequencies appended to each profile.

The method is applied to sunrise data on 75 kc. The observed absorption remains relatively constant while group and phase heights are dropping most rapidly from nighttime levels. A series of profiles having about the desired constant absorption may be arranged in order of decreasing phase and group height. In this way the sunrise variation is exhibited as a series of changing electron density height profiles.

On the Earth Geometry—A Theorem—K. Toman, *Geophysics Research Directorate*—The angle of incidence of a radio beam originating at a point P above the surface of the earth and arriving at a spherical reflecting layer concentric to the earth, is shown to be smallest for radiation perpendicular to the diameter through P. These considerations disclose a minimum property of the circle which, with the advent of satellites and corresponding high antenna elevations, may prove valuable for ascertaining the existence of the reflection mode for radio signal returns.

Forward Scattering (Electromagnetic)—D. M. Raybin, T. B. A. Senior, K. M. Siegel, S. Stone and H. Weil, *The University of Michigan*—Several new results are presented for forward scattering from perfectly conducting bodies for the small wavelength region. Attention is directed primarily at the forward scattering function $g(\pi)$ which is the amplitude coefficient of the scattered field in the far zone. The squared modulus of $g(\pi)$ is, of course, proportional to the forward scattering cross section. The imaginary part of $g(\pi)$ is related to the total (*i.e.*, integrated) scattering cross section.

The asymptotic expansions of Re $g(\pi)$ and Im $g(\pi)$ are discussed for large ka, where a is a characteristic dimension of the body, and it is shown that the leading term in the expansion for Im $g(\pi)$ is always the Kirchhoff answer. For three-dimensional bodies the first correction term is always positive, which implies that the Kirchhoff result represents a lower bound.

The expansion for Re $g(\pi)$ is of the same form as that for Im $\{g(\pi)-[g(\pi)]$ optics$\}$, though the dependence of the terms on ka depends on the particular body under consideration. Thus, for a sphere or circular cylinder the terms are of order $(ka)^{-2n/3}$ $n=1,2,3,\cdots$, but this is not true of other bodies. It is also shown that for any given body Re $g(\pi)$ and Im $g(\pi)$ are related to one another and interpretations are provided for each part in terms of the fields near to the surface of the body.

Fock Theory Applied to an Infinite Cone—R. F. Goodrich, *The University of Michigan*—A semi-infinite perfectly conducting cone is considered to be illuminated by a plane electromagnetic wave such that part of the cone is shadowed. The methods of Fock* are generalized using an idea of Keller† to find the field induced on the surface in the shadow region.

Back Scattering from a Finite Cone—J. B. Keller, *Institute of Mathematical Sciences, New York University*—The back scattering of an electromagnetic wave from a perfectly conducting finite cone has been calculated. The calculation was based on the geometrical theory of diffraction. Cones with both flat and curved or rounded bases have been considered. The effect of the cone angle and of the shape of the base on the result have been examined. Resonances in the back scattering amplitude are found in the case of axial incidence on cones with flat bases when multiple diffraction is taken into account.

Measurement of Back-Scattering Cross Section of Circular Metallic Disks with a Space-Separation Method—H. J. Schmitt, *Gordon McKay Labroatory, Harvard Uni-*

* The research reported in this paper has been sponsored by the Geophysics Research Directorate of the AF Cambridge Res. Center, Air Res. and Dev. Command, under Contract No. AF 19(604)-1304.

† *J. Atmos. Terr. Phys.*, vol. 7, pp. 173–202; October, 1955.

‡ This work is supported by a grant from the Natl. Committee for the IGY under Project No. 6.9.

* The research reported in this paper has been sponsored, in part, by the National Science Foundation under Grant No. 1969 and, in part, by the AF Cambridge Res. Center under Contract No. AF 19(604)-1304.

† The research reported in this problem has been sponsored by the Geophysics Res. Directorate of the AF Cambridge Res. Center, Air Res. and Dev. Command, under Contract No. AF 19(604)-1304.

* V. A. Fock, *J. Phys. X*, p. 399; 1946.

† J. B. Keller, "Diffraction by a convex cylinder," IRE Trans. on Antennas and Propagation, vol. AP-4, pp. 312–321; July, 1956.

versity—A method for the experimental determination of the back-scattering cross section of arbitrarily shaped obstacles is described, which, in a manner analogous to the Michelson interferometer in optics, makes use of a semitransparent mirror in order to separate the incident wave and the reflected wave. An experimental setup for use with 3-cm and 1-cm waves is described and possible sources of error are discussed.

The accuracy of measurements is investigated by comparing the measured values of the back-scattering cross section of circular metallic disks with the results obtained from the exact theory.

Diffraction by a Smooth Object—B. Levy, *Institute of Mathematical Sciences, New York University*—This paper, on the diffraction of waves by smooth convex obstacles, consists of two parts. In Part I a new geometrical theory of wave propagation is explained and applied to the problem. In Part II the diffraction problem for various obstacles is formulated as a boundary value problem and solved by the usual separation of variables method. The solutions are then asymptotically expanded for large $ka=2\pi a/\lambda$ (a=obstacle dimension, λ=wavelength) and compared with the results of Part I. In all cases the geometric solution is found to agree with the asymptotic expansion of the exact solution.

The geometrical theory of Part I is developed for solutions of the time-reduced Maxwell's equations as well as the reduced wave equation. The diffracting objects are assumed to be of arbitrary convex shape and of any type (*e.g.*, acoustically hard or soft, perfect conductors, dielectrics). In addition to developing and applying the geometrical theory to variously shaped bodies in Part I, a certain feature of the self-consistency of the theory is demonstrated.

The exact solution of the diffraction problem associated with the reduced wave equation or the time reduced Maxwell's equations for the bodies considered in Part I are determined and asymptotically expanded in Part II. The problem of asymptotically expanding the electromagnetic field diffracted by an imperfectly conducting circular cylinder is treated as well as other vector and scalar diffraction problems associated with spheres and cylinders.

Diffraction by an Imperfectly Conducting Wedge—T. B. A. Senior, *The University of Michigan*—The problem of the diffraction of a plane electromagnetic wave by an imperfectly conducting wedge is solved subject only to the physical approximation implied by the usual impedance-type boundary conditions imposed on the faces of the wedge. The method is based on one which was originally proposed by A. S. Peters for the treatment of a problem in hydrodynamics and leads to a difference equation for the determination of a regular function related to the Laplace transform of the field with respect to the radial distance from the edge. This is solved exactly to give a closed-form expression for the total field valid for any angle of wedge. Several particular cases are examined and some ramifications of the theory are discussed.

CORRECTION

David C. Stickler, author of "Electromagnetic Diffraction by Dielectric Strips," which appeared on pages 148–151 of the January, 1958 issue of these TRANSACTIONS has requested that the following corrections be made to his paper.

Eq. (8), p. 149, should read

$$\bar{J} = -i\omega\epsilon\cdot[\mu_r\epsilon_r - 1]\bar{E}^i + \frac{\nabla\mu}{\mu_0}\times\bar{H}^i.$$

Eq. (9), on the same page, should read

$$\bar{E}^s(\bar{r}) = \frac{e^{ik_0r}}{4\pi r}[\hat{\theta}\hat{\theta}+\hat{\phi}\hat{\phi}]\cdot\left[k_0^2(\epsilon_r\mu_r-1)\int\bar{E}^i(\bar{r}')e^{-ik_0r'\cos\gamma}dv + i\omega\int\nabla u\times\bar{H}^i(\bar{r}')e^{-ik_0r'\cos\gamma}dv\right]$$

instead of

$$\bar{E}^s(\bar{r}) = \frac{k_0^2(\mu_r\epsilon_r-1)}{4\pi}\frac{e^{ik_0r}}{r}[\hat{\theta}\hat{\theta}+\hat{\phi}\hat{\phi}]\cdot\int\bar{E}^i(\bar{r}')e^{-ik_0r'\cos\gamma}dV + \frac{i\omega}{4\pi}\frac{e^{ik_0r}}{\Gamma}\int\nabla u\times\bar{H}^i(\bar{r}')e^{-ik_0r'\cos\gamma}dV.$$

Also, it has been found that the experimental points in Fig. 5, p. 151, may all be shifted laterally to the left, about $2\frac{1}{2}$ degrees. The apparent error was due to a mechanical slippage which would not affect the other patterns.

Contributors

L. J. ANDERSON

L. J. Anderson was born in Salt Lake City, Utah, in 1917. He received the A.B. degree in 1939 and the M.A. degree in 1942, both from the University of California at Los Angeles. He was a physicist at the U. S. N. Electronics Lab., San Diego, Calif., from 1942 to 1955, working on tropospheric propagation problems, particularly the effects of the lower atmosphere on propagation. He was responsible for developing methods of predicting radio-radar propagation from routine meteorological data, and was engaged in meteorological instrumentation for propagation purposes. Prior to 1955 he directed the Environment Studies Branch at NEL. In 1955 he joined colleages in forming Smyth Research Associates, where he is continuing work on tropospheric propagation and allied studies.

Mr. Anderson is a member of U. S. A. Commission II of URSI, the American Meteorological Society, and the American Chemical Society.

❖

J. T. BOLLJAHN

J. T. Bolljahn (A'43–SM'53) was born on June 10, 1918, in Oakland, Calif. He received the B.S. degree in 1941 and the Ph.D. degree in 1950, both in electrical engineering, from the University of California, Berkeley.

During World War II he was employed as a radio engineer at the Naval Research Laboratory in Washington, D. C. From 1946 to 1949 he was on the staff of the Navy Electronics Research Laboratory at the University of California. In 1949 he joined the Stanford Research Institute, where he is presently assistantant director of engineering research.

Dr. Bolljahn is a member of Tau Beta Pi, Eta Kappa Nu, and Sigma Xi.

❖

H. BREMMER

H. Bremmer was born on March 23, 1904, at The Hague, Netherlands. From 1922 to 1929, he studied at Leiden University. He was on the staff of Leiden Cyrogenic Laboratory from 1927 to 1934. Since 1934, he has been a senior physicist at Philips Research Laboratories, Eindhoven, Netherlands. His thesis on the conductivity of heat of superconductors was written in 1934.

Dr. Bremmer is a member of the Dutch Physical Society.

A. M. CONDA

Alyce M. Conda (M'57) was born in Leavenworth, Kan., on July 20, 1933. She received the B.S. degree in mathematics from Southwest Texas State College, San Marcos, Tex., in 1953, and remained there to teach mathematics from 1954 to 1955. She has been briefly associated with the University of Colorado, Boulder, Colo. where she also taught courses in mathematics.

Since 1956 Mrs. Conda has been employed as a mathematician with the Radio Propagation Engineering Division of the National Bureau of Standards, Boulder, Colo.

Mrs. Conda is an associate member of the Boulder Branch of RESA.

❖

C. M. CRAIN

C. M. Crain (S'42–M'49–SM'54–F'58) was born in Goodnight, Texas, on September 10, 1920. He received the B.S., M.S., and Ph.D. degrees from the University of Texas, Austin, Tex., in 1942, 1947, and 1952, respectively.

After graduation from the University of Texas in 1942 he worked on airborne radar developments with the Philco Corporation in Philadelphia, Pa. In 1943 he returned to the University of Texas as an instructor. In 1944 he was called to active duty in the Naval Reserve, where he served with the Bureau of Ordnance in the influence mine program and the Office of Research and Inventions. In 1946, he again returned to the University of Texas, where he was an assistant and later associate professor of electrical engineering and a member of the staff of the Electrical Engineering Research Laboratory. Since July, 1957, Dr. Crain has been at the Rand Corporation, Santa Monica, Calif., where he is a group leader in the Electronics Department.

Dr. Crain is a member of the AIEE, Sigma Xi, Tau Beta Pi, Eta Kappa Nu, and Commission II of URSI.

❖

W. C. Duesterhoeft (SM'56) was born in Austin, Texas, in 1921. He received the B.S.E.E. in 1943 and the M.S.E.E. in 1949 from the University of Texas, Austin, Texas, and his Ph.D. from the California Institute of Technology, Pasadena, Calif., in 1953.

From 1943 to 1946 he was employed by the General Electric Company, Schenectady, N. Y. Dr. Duesterhoeft was aerophysics engineer at the Fort Worth Division of Convair from 1952 to 1954. He held the position of instructor of electrical engineering at the University of Texas from 1946 to 1949 and at the California Institute of Technology from 1949 to 1952. He returned to the University of Texas as associate professor of electrical engineering and as radio research engineer at the Electrical Engineering Research Laboratory in 1954.

W. DUESTERHOEFT

Dr. Duesterhoeft is a member of AIEE, Sigma Xi, Tau Beta Pi, and Eta Kappa Nu.

❖

W. W. FAIN

William W. Fain (M'56) was born in Augusta, Ga., on April 23, 1927. He received the B.A., M.A. and Ph.D. degrees with a major in physics from the University of Texas in 1950, 1951, and 1955.

He was employed as a research engineer with Electro-Mechanics Company, Austin, Texas, from 1952 to 1955 participating in studies on spurious radiation and radio interference.

In the spring of 1956 he was with the Electrical Engineering Research Laboratory of the University of Texas for several months prior to joining the Engineering Department of Chance Vought Aircraft. During the 1956–1957 school year, Dr. Fain was on leave of absence as a student at the Université de Paris, Faculté des Sciences. He has returned to Chance Vought and is presently with the Aircraft Systems Analysis Group.

He is a member of Sigma Xi, Operations Research Society, American Institute of Physics, and Sigma Pi Sigma.

❖

R. F. HARRINGTON

Roger F. Harrington (S'48–A'53) was born in Buffalo, N. Y., on December 24, 1925. He received the B.E.E. degree in 1948 and the M.E.E. degree in 1950, both from Syracuse University, Syracuse, N. Y., and the Ph.D. degree in 1952 from The Ohio State University, Columbus, Ohio.

From 1945 to 1946, Dr. Harrington served as an instructor at the Naval Radio Materiel School, Dearborn, Mich., and from 1948 to 1950, he

was employed as an instructor and research assistant at Syracuse University. While studying at The Ohio State University, he served as a research fellow in the Antenna Laboratory. Since 1952, he has been on the faculty of Syracuse University, currently as associate professor of electrical engineering.

Dr. Harrington is a member of Tau Beta Pi, Sigma Xi, and the American Association of University Professors.

❖

Helen M. Johanson was born in Arlington, Mass., on June 8, 1930. She attended Arlington schools and Simmons College, Boston, Mass., from which she received the B.S. degree in 1951.

Mrs. Johanson joined the Antenna Laboratory of the Air Force Cambridge Research Center in 1951 and was associated with various projects there until 1955.

❖

Winston S. Lucke (SM'56) was born on July 23, 1921, in Loudon, Tenn. From Harvard University, Cambridge, Mass., he received the B.S. degree in 1943, M.A. and M.E.S. in 1947, and Ph.D. in physics in 1949.

W. S. Lucke

He was with the technical staff at Bell Telephone Laboratories from 1943 to 1946 and was a research associate at Cruft Laboratory, Harvard University, from 1948 to 1949. In May, 1949, he joined the staff of Stanford Research Institute, where he has been concerned with analytical problems in the fields of electromagnetic theory, information theory, and signal detection. Most recently he has participated in systems analysis and evaluation. He is presently technical program coordinator of the Weapons Systems Laboratory.

Dr. Lucke is a member of the Society of Industrial and Applied Mathematics and the Scientific Research Society of America.

❖

Richard B. Mack (A'55) was born in South Paris, Me., on September 18, 1928. He received the B.A. degree in physics from Colby College, Waterville, Me., in 1951 and the M.S. degree in applied physics from Harvard University in 1957. Mr. Mack joined the Antenna Laboratory of the Air Force Cambridge Research Center in 1951 and since that time has been associated with the Air Force Cambridge Research Center working on antenna research programs. He is a member of Sigma Pi Sigma.

R. B. Mack

❖

William G. Mavroides (M'57) was born in Newburyport, Mass., on March 5, 1925. He received the B.S. degree in mathematics in 1950 and the Master of Education degree in 1951, both from Tufts University, Medford, Mass. In 1957 he fulfilled requirements for the M.S. degree in mathematical physics at Northeastern University, Boston, Mass.

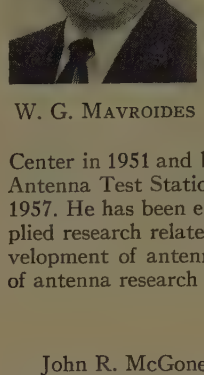

W. G. Mavroides

Mr. Mavroides joined the Air Force Cambridge Research Center in 1951 and became unit chief of the Antenna Test Station at Ipswich, Mass., in 1957. He has been engaged in basic and applied research related to the design and development of antennas and in the solution of antenna research problems.

❖

John R. McGonegal was born on February 10, 1933, in Washington, D. C. He received the B.E.E. degree from Catholic University of America, Washington, D. C. in 1953. From 1953 to 1956, he was in the graduate school of engineering at Johns Hopkins University, Baltimore, Md. and served as a laboratory instructor during 1955–1956.

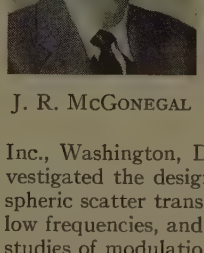

J. R. McGonegal

Since 1954, he has been employed by Jansky & Bailey, Inc., Washington, D. C., where he has investigated the design of antennas for ionospheric scatter transmission, propagation of low frequencies, and has carried out several studies of modulation and coding problems.

Mr. McGonegal is an associate member of Sigma Xi.

❖

Pierre Misme was born at Bourganeuf, Creuse, France, in 1920. After completing his studies in physics at the Science Faculty of Bordeaux in 1942, he was employed as an engineer at the Meteorologie Nationale. Until 1946 he was in charge of a radiosonde station.

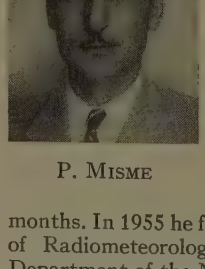

P. Misme

He then became chief forecaster of the Bourget Airport, and there directed meteorological research in the tropical Atlantic for several months. In 1955 he founded the Department of Radiometeorology at the Propagation Department of the National Center of Telecommunications Studies.

Since that time he has perfected a radiosonde to make fine measures in the lower layers of the troposphere. Mr. Misme is the author and co-author of monographs on the influence of meteorological fronts in broadcasting and radioclimatology, and the role of partial reflections in long distance broadcasting.

He is a member of the French Association of Radioelectricians.

❖

Ernest J. Moore (S'43–A'46–SM'51) was born on October 15, 1919, in Germany. He received the B.S. degree with honors in electrical engineering from the University of London, England, in 1940 and the M.S. and Ph.D. degrees in the same field from the University of California, Berkeley, Calif., in 1943 and 1950, respectively.

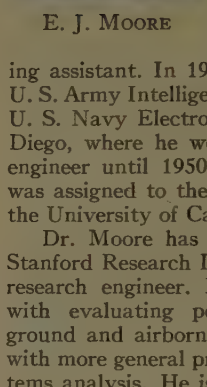

E. J. Moore

While at the University of California, he served as a teaching assistant. In 1946, after service in the U. S. Army Intelligence Corps, he joined the U. S. Navy Electronics Laboratory in San Diego, where he worked as an electronics engineer until 1950. Part of this time he was assigned to the Antenna Laboratory of the University of California.

Dr. Moore has been with the staff of Stanford Research Institute since 1950 as a research engineer. His work is concerned with evaluating performance of various ground and airborne antenna systems and with more general problems in weapons systems analysis. He is presently head of the Systems Evaluation Group of the Weapons Systems Laboratory.

He is a member of the Scientific Research Society of America, Sigma Xi, the Society for Industrial and Applied Mathematics, and an associate member of the Operations Research Society of America.

❖

Edward K. Proctor, for a photograph and biography, please see page 406 of the October, 1957, issue of these TRANSACTIONS.

❖

John W. Savage (M'56) was born on March 14, 1931, in Burlington, Vt. He received the B.E.E. degree from the George Washington University, Washington, D. C. in 1956.

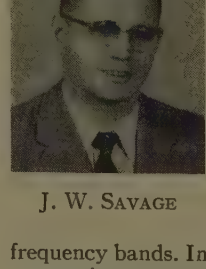

J. W. Savage

Since 1952 he has been employed by Jansky & Bailey, Inc., Washington, D. C., where he has worked on programs involving the evaluation of single sideband equipment and the measurement of radiation in various frequency bands. In 1956, he served as project engineer on a program investigating propagation phenomena involved in air-to-

air and air-to-ground transmissions under various conditions. He is currently working on the development of transistorized and miniaturized equipment.

❖

Carlyle J. Sletten (A'51–M'56) was born on January 13, 1922, in Wisconsin. He received the Bachelor of Science degree in physics in 1947 from the University of Wisconsin, Madison, Wis., where he was elected to Phi Beta Kappa, and the Master's degree in applied physics from Harvard University, Cambridge, Mass., in 1949.

C. J. Sletten

Mr. Sletten served for more than three years in the Air Corps during World War II as a meteorologist and radar weather officer. He has been with the Antenna Laboratory of the Air Force Cambridge Research Center since 1948. During that time he has published several papers on antennas and electromagnetic scattering.

Mr. Sletten is a member of the American Optical Society and the Scientific Research Society of America.

❖

Laszlo Solymar was born in Budapest, Hungary, in 1930. He received the Diploma of Electrical Engineering from Technical University of Budapest in 1952.

L. Solymar

He was assistant to the professor at Technical University during 1952 and 1953. He also worked as research engineer at the Research Institute of Telecommunication, Budapest from 1953 to 1956, where he was engaged in antenna theory and design. Since 1956, he has been research engineer at Standard Telecommunication Laboratories, Ltd., Enfield, Middlesex, England. His work there is concerned with various phases of microwave transmission.

❖

Robert L. Tanner (S'51–A'52–SM'56) was born on December 4, 1921, in Idaho Falls, Idaho. He received the B.S. degree in 1944, the M.S. degree in 1947, and the Ph.D. degree in 1953, all in electrical engineering from Stanford University, Stanford, Calif.

R. L. Tanner

From 1944 to 1946 he served in the Signal Corps, working with pulse modulated communication equipment and with voice coding equipment. In 1947, Dr. Tanner joined the electrical engineering faculty of the University of Washington. During 1950 he was employed by the Boeing Airplane Company, where he was engaged in antenna research. Since January, 1951, Dr. Tanner has been with Stanford Research Institute, where his interests have been largely in the field of aircraft antennas and related systems problems. In January, 1956 he became Group Head of the Antenna Research Group of the Antenna Systems Laboratory.

Dr. Tanner is a member of Phi Beta Kappa, Tau Beta Pi, Sigma Xi, and the Scientific Research Society of America.

❖

Louis G. Trolese (A'30–SM'47) was born in Sonora, Calif., on July 2, 1908. He received the B.S. degree in electrical engineering from the University of California, Berkeley, in 1930. His early engineering experience included one year with the RCA Victor Company, Camden, N. J. and five years with the General Air Conditioning Company, San Francisco, Calif. He also spent thirteen and one-half years at the Navy Electronics Laboratory, San Diego, Calif. where he was engaged in research on wave propagation problems and radar development, and held positions as head of the Atmospherics Studies Branch and the Radar Branch. In 1955 he helped form Smyth Research Associates, in San Diego, where he is now Vice-President.

L. G. Trolese

Mr. Trolese is a member of U.S.A. Commission II of URSI, and a licensed professional engineer in the state of California.

❖

Arthur Vassiliadis (A'57) was born on September 4, 1931, in French Cameroons, Africa. He received the B.S. degree in 1951 from Syracuse University, and the M.S. degree in June, 1952 from Stanford University, Stanford, Calif., both in electrical engineering. From 1952 to January, 1955, he attended Stanford University Graduate School while working at the University half time. His work at the University involved a study of the ionosphere, particularly the sporadic-*E* layer, and work on traveling wave tubes, specifically concerned with the magnetron amplifier.

A. Vassiliadis

Mr. Vassiliadis joined the staff of Stanford Research Institute, Menlo Park, Calif., in February, 1955. His work there has been mainly concerned with the optimum broadbanding of aircraft antennas, and precipitation static. He has had considerable experience in the programming and operation of electronic computers.

He is a member of Eta Kappa Nu, Pi Mu Epsilon, RESA, and Tau Beta Pi.

James R. Wait (SM'56) was born in Ottawa, Can., in January, 1924. He attended McGill University for a brief period before enlisting in the Canadian Army in 1942. By the end of the war he was in charge of a radar maintenance group at Kingston, Ontario.

J. R. Wait

He received the B.A.Sc. and M.A.Sc. degrees in engineering physics from the University of Toronto in 1948 and 1949, respectively. At this time he was employed as a junior research engineer at the Hydro Electric Power Commission of Ontario, where he assisted in the development of an infrared bolometer. Returning for further graduate work to the University of Toronto, he obtained the Ph.D. degree in electromagnetic theory in 1951.

From 1949 to 1952 Dr. Wait was associated with Newmont Exploration Ltd. of Jerome, Ariz., where he conducted theoretical and experimental research in electrical prospecting. From 1952 to 1955 he was a section leader in the Defence Research Telecommunications Establishment in Ottawa where he was mainly concerned with theoretical problems in radiation. He has been associated briefly with McGill University during 1954 and Colorado University in 1955 and 1957 where he taught graduate courses in antennas and propagation. At present he is a consulting theoretical physicist to the Radio Propagation Engineering Division of the National Bureau of Standards in Boulder, Colo.

Dr. Wait is a member of the Canadian Association of Physicists, the Society of Exploration Geophysicists, U.S.A. Commissions III and VI of URSI, and at present is president of the Boulder Chapter of RESA.

❖

C. A. Zielinski (A'47–M'53) was born in Holyoke, Mass., on December 5, 1920. He received the B.S. degree in biology from the University of Massachusetts, Amherst, Mass. in 1942 and served in the U. S. Signal Corps and the U. S. Air Force in World War II. He received the B.S. degree in electrical engineering from the University of California, Berkeley, in 1950.

C. A. Zielinski

From 1950–1956 he was with Jansky & Bailey, Inc., Washington, D. C., where he was engaged in the field testing of radar and hyperbolic navigation systems and in the development of countermeasures and radar-test equipment. In 1956 he joined the Light Military Electronic Equipment Department of the General Electric Company, Utica, N. Y., where he has worked principally on the development of Doppler navigation systems for aircraft.

Mr. Zielinski is a member of Eta Kappa Nu and Tau Beta Pi.

INSTITUTIONAL LISTINGS

The IRE Professional Group on Antennas and Propagation is grateful for the assistance given by the firms listed below, and invites application for Institutional Listing from other firms interested in the field of Antennas and Propagation.

ANDREW CORPORATION, 363 E. 75th St., Chicago 19, Ill.
Antennas, Antenna Systems, Transmission Lines, Development and Production.

ANTLAB, INC., 6330 Proprietors Rd., Worthington, Ohio
Antenna Pattern Range Systems—Recorders & Mounts.

BLAINE ELECTRONETICS, INC., 14757 Keswick St., Van Nuys, Calif.
Antennas, Paraboloids, Scale Models, Antenna Radiation Pattern Measurement Towers.

COMMUNICATION PRODUCTS COMPANY, INC., Marlboro, N. J.
Fixed Station and Vehicular Antennas and Associated Cable Systems

DEVELOPMENTAL ENGINEERING CORP., 1001 Conn. Ave. N.W., Washington, D. C. and Leesburg, V
Research, Development, Installation of Antennas and Antenna Equipment for Super Power Stations.

THE GABRIEL LABORATORIES, Div. of the Gabriel Co., 135 Crescent Road, Needham Heights 94, Mas
Research and Development of Antenna Equipment for Government and Industry.

HUGHES AIRCRAFT COMPANY, Culver City, Calif.
Research, Development, Mfr.: Radar, Missiles, Antennas, Radomes, Tubes, Solid State Physics, Computers.

I-T-E CIRCUIT BREAKER CO., Special Products Div., 601 E. Erie Ave., Philadelphia 34, Pa.
Design, Development and Manufacture of Antennas, and Related Equipment.

JANSKY & BAILEY, INC., 1339 Wisconsin Ave. N.W., Washington 7, D. C.
Radio & Electronic Engineering; Antenna Research & Propagation Measurements; Systems Design & Evaluatio

MARK PRODUCTS CO., 6412 W. Lincoln Ave., Morton Grove, Ill.
Multi Element Grid Parabolas, Antennas for Two-Way Communications, R & D.

MARYLAND ELECTRONIC MANUFACTURING CORPORATION, College Park, Md.
Antenna and System Development and Production for Civil and Military Requirements.

THE RAMO-WOOLDRIDGE CORPORATION, Los Angeles 45, Calif.

TRANSCO PRODUCTS, INC., 12210 Nebraska Ave., Los Angeles 25, Calif.
Res., Design, Dev., & Mfr. of Antenna Systems & Components for Missile, Aircraft & Ground Installations.

WHEELER LABORATORIES, INC., 122 Cutter Mill Road, Great Neck, N. Y.
Consulting Services, Research and Development, Microwave Antennas and Waveguide Components

WIND TURBINE COMPANY, West Chester, Pa.
Complete Antenna Systems and Towers

The charge for an Institutional Listing is $25.00 per issue or $75.00 for four consecutive issues. Application may be made to the Technical Secretary, The Institute of Radio Engineers, 1 East 79th Street, New York 21, N.Y.